Out-of-Equilibrium Phase Transitions in Nonlinear Optical Systems

Fabrizio Minganti

Université Sorbonne Paris Cité

université PARIS DIDEROT PARIS 7

MPQ

Thèse de Doctorat
de l'Université Sorbonne Paris Cité
Preparée à
l'Université Paris Diderot

École doctorale 564 : Physique en Ile-de-France

Laboratoire Matériaux et Phénomènes Quantiques
Équipe THEORIE

Out-of-Equilibrium Phase Transitions in Nonlinear Optical Systems

Thèse de doctorat de Physique par Fabrizio Minganti

Directeur : Cristiano Ciuti

Codirecteur : Giuliano Orso

JURY

DR	Denis Basko	Université Grenoble Alpes	Examinateur
PR	Cristiano Ciuti	Université Paris Diderot	Directeur de thèse
PR	Sebastian Diehl	University of Cologne	Rapporteur
DR	Pérola Milman	Université Paris Diderot	Président
DR	Anna Minguzzi	Université Grenoble Alpes	Rapporteur
MCF, HDR	Giuliano Orso	Université Paris Diderot	Co-directeur de thèse
Docteur	Davide Rossini	University of Pisa	Examinateur

Présentée et soutenue publiquement à Paris le 25/10/2018

Acknowledgements

This thesis is a scientific document and it will only present the results of my research, neglecting the process of trials and errors which lead, eventually, to resolution of the problems presented thereafter. Indeed, this manuscript contains none of the manifold emotions and humours which characterised the past three years: the pleasure of finding things out, the frustration of failure, the discourage after a negative referee report, the joy of a positive one. Even worse, it only partially acknowledges those who sustained me during these years. My gratitude goes to those many people, for their presence was the most indispensable part of my work.

The first thanks are doubtlessly for my PhD directors, Cristiano Ciuti and Giuliano Orso. In these years, they constantly helped me in my researches, transforming them into a challenging and amusing game. Their scientific culture and extraordinary physical intuition led us to investigate problems of extreme interest, and their availability in engaging in scientific discussions allowed me to grow as a scientist. Their human qualities contributed to create a working environment where it has been pleasant to spend time, facilitating the collaborations with my coauthors.

I am grateful to the members of the jury which took the time to examine my work; in particular, Anna Minguzzi and Sebastian Diehl who accepted to be the referees. I thank all the other examiners, Denis Basko, Davide Rossini and Pérola Milman, for the interest they took in my work and for the fruitful discussion which took place.

A special thanks goes to Carlo Sirtori, who was the director of the MPQ when I became a PhD student. What I esteem invaluable is that he dedicated time to discuss and connect with every PhD student, always verifying if everything was proceeding correctly during their thesis. I want also to acknowledge the extremely relevant suggestions he gave me about my future and my career. Moreover, I cannot thank enough all the administrative crew of the MPQ, Anne Servouze, Jocelyne Moreau and Sandrine Di Concetto. In this years, they helped me to extricate from the several complexities of the French bureaucracy.

This thesis has been a collective work under many aspects, and I will never be able to acknowledge enough the contributions of my collaborators. In all of the members of the équipe Théorie of MPQ I found interesting and competent people, but also friends with whom I shared these wonderful moments. In particular, I want to praise the numerical competences of Filippo Vicentini, which have been essential to achieve many of the results concerning extended lattice systems. I want to thank Wim Casteels for the most interesting discussions concerning both the methods and the physical models which we studied. I also have a huge debt of gratitude towards Jared Lolli, a friend with whom I shared part of my studies at the ENS and part of my PhD. Not only it was extremely funny to work with him, but his

creativity and intuition allowed us to explore several intriguing physical problems. I also acknowledge the many useful discussions with Vincenzo Savona from EPFL, Matteo Biondi from ETHZ, José Lebreuilly from ENS and Victor Albert from Caltech.

A separate section is needed for Nicola Bartolo, Alberto Biella and Riccardo Rota, who were postdocs during my PhD. They have been my closest collaborators and much of what I did and learned is a direct consequence of their outstanding scientific capability (and, even more, of their incredible endurance of me). Like in the fairy tales of old, to each of them I owe that something they taught me: to Nicola, the rigour in methods and the clarity in explanation; to Alberto, the necessary vision of clearely-defined underlying physical model; to Riccardo, the patience and regularity necessary to do numerical simulations. Even if I was a PhD student while they were postdocs, they never brought hierarchy in any scientific discussions we had, thus favouring the most ease in collaborating and exchanging ideas. Beyond that, I cannot praise enough their personal qualities, both inside and outside of the workplace. Our trips, for leisure and for scientific purpose, remain one of my best memories.

I am much obliged also to all the other people of the Théorie group, with whom, unluckily, I had no time to collaborate with. Florent Storme, with whom I had a excellent trip in Crete. Matthieu Labousse, for the precious encouragements. Alexandre Le Boité, for the many scientific initiatives he organised. Filippo Stellin for his kindness and availability. Cassia Naudet-Baulieu, for having transformed and improved the atmosphere of our office. Zakari Denis, for his dedication and for the many interesting ideas he provided. And even if, technically, he does not belong to the Theory group of MPQ, I want to thank here Simone Felicetti. Not only we engaged in many fruitful scientific discussions, but I also appreciated his sympathy and friendliness both in the working environment and outside of the laboratory.

I want to thank also all the people form MPQ, with whom I had the pleasure to share the corridors of the laboratory. In particular, my officemates, who endured a lot of noise: Nabeel Ahmad and Ouafi Mouhoub. The "old guard", who were there when I started my PhD, and with whom we rejoiced the many good news and endured the bad ones: Ian Aupiais, Adrian Chmielewski, Romain Grasset, Belhassen Jonathan, Dimitri Labat, and Bastien Loret. The companions of (objectively too many) coffees: Allegra Calabrese, Carlo Gigli, Valerio Flavio Gili, Giorgio Maletese, and Samantha Sbarra. And all those who engaged in the various activities and debates in MPQ: Zahra Asguari, Louis Garbe, Gaël Masse, and Jacko Rastikian.

This thesis, sometimes, has been stressful. And even if I had the chance to have an extremely pleasant working environment, I was even luckier to share an apartment (the glorious KB) with marvellous people, who constantly supported me during these years. Let me start by my oldest companions, Gabriele Rembado and Gabriele Montalbano. They were with me when we started our academic adventure almost 10 years ago in Bologna, and we shared most of our paths all along this years. They are people of extreme culture and generosity, without whom this period would have been far worse and boring. They enriched me in so many ways that it is impossible for me to think who would I be without them. We passed together through so many adversities and successes that now it seems strange that our ways are parting. I thank Martin Vogel, whose dedication to work stands as an example to be imitated. Beyond an excellent mathematician (and cook, and climber), a really funny guy to share the flat with. I am much obliged also to Marie Billy, and I will never be able to repay her kindness. The many evening spent playing games together would have relieved even the heaviest of workday. And last but not least, I thank Azzura Bigioli. On the one hand, a

colleague at MPQ, with whom I had the pleasure to indulge in remarkable discussions about our fields of study. On the other, a person of outstanding culture and amazing intelligence, whose eclecticism never ceased to amaze me.

A enormous debt of gratitude is also due to my family. Being far from home is never easy, but the limitless and unconditional support they provided me in the last years made this burden far less heavy. Thus I want to thank my cousins (and their spouses), as well as my uncles and aunties, for always having made me feel part of the family. Infinitely many thanks go to my mother and my grandmother, for they always helped me thorough these years, being always ready to welcome me home. In particular, I cannot express how much I appreciated the fact that my 87 years old grandmother took the plane for the first time to come and see my PhD discussion. I am also very grateful to my brother for the two marvellous voyages in New Zealand. During these years he always provided me with a different perspective on the many aspects of life, and he was always able to cheer me up. In this list, I want also to include Davide, Matteo and Riccardo, which I knew for more than 20 years, thus scoring *de facto* as the most patient people in the world. Their continuous friendship was a source of strength, even in the most difficult moments.

Finally, I am indebted to the many friends whose company made these years wonderful (and I am sorry for the many I will sure forget to mention). All those from Imola: Ally, Alice, Anna, Andro, Bond, Checco, Ciaccio, Fabrizio, Farfi, Fede, Fiasco, Gio, Lollo, Maria, Restone, Seve, Simo, Silvio, Tigre, Tommy and Zac; from Bologna: Betta, Calzo, Chiara, Ciampo, Dimitri, Dimitrii, Elisa, Enrica, Fara, Fede, Fulvia, Fra, Giulione, Leonardo, Laura, Luca, Martina, Mitch, Michele, Tejo; from the École Normale Supérieure: Aline, Andrea, Camilla, Daria, Donny, Dudo, Eckardt, Fabio, Federico (×2), Fréd, Giulio, Giulia, Laetitia, Leonardo, Madda, Mattia, Nils, Rita, Serena, Valerio; and the people from Cité Universitaire: Alessio, Alessia, Andrea, Elisa (×2), Laura, Lorenzo, Valentina.

This thesis is dedicated to the memory of my father and of my grandparents, Cesare and Carolina.

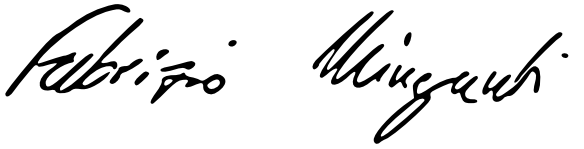

Summary

This thesis is a theoretical study of driven-dissipative nonlinear systems described by a Lindblad master equation, with particular focus on the emergence of criticality. In Chapter 3, we present a general and model-independent spectral theory relating first- and second-order dissipative phase transitions to the spectral properties of the Liouvillian superoperator. In the critical region, we determine the general form of the steady-state density matrix and of the Liouvillian eigenmatrix whose eigenvalue defines the Liouvillian spectral gap. We discuss the relevance of individual quantum trajectories to unveil phase transitions.

After these general results, we analyse the onset of criticality in several models. In Chapter 4, we study a nonlinear Kerr resonator in the presence of both coherent (one-photon) and parametric (two-photon) driving and dissipation. We present exact results for the steady-state density matrix, which allows us to study the "thermodynamic" regime with large photon density, where dissipative phase transitions take place.

We then explore in Chapter 5 the dynamical properties of a first-order dissipative phase transition in coherently driven Bose-Hubbard systems, describing, e.g., lattices of coupled nonlinear optical cavities. Via stochastic trajectory calculations based on the truncated Wigner approximation, we investigate the dynamical behavior as a function of system size for 1D and 2D square lattices in the regime where mean-field theory predicts nonlinear bistability. We show that a critical slowing down emerges for increasing number of sites in 2D square lattices, while it is absent in 1D arrays. We characterize the peculiar properties of the collective phases in the critical region.

We study dynamical properties of dissipative XYZ Heisenberg lattices where anisotropic spin-spin coupling competes with local incoherent spin flip processes in Chapter 6. In particular, we explore a region of the parameter space where a second-order magnetic phase transition for the steady state has been recently predicted by mean-field theories and exact numerical methods. We investigate the asymptotic decay rate towards the steady state both in 1D (up to the thermodynamic limit) and in finite-size 2D lattices, showing that critical dynamics does not occur in 1D, but it can emerge in 2D.

Finally, in Chapter 7 we investigate the physics of driven-dissipative resonators subject to engineered two-photon processes and one-photon losses. We demonstrate that the unique steady state is a statistical mixture of two photonic Schrödinger cat states, in spite of significant one-photon losses. By considering individual quantum trajectories, we find that the system intermittently jumps between two cats in photon-counting configurations, while the system jumps between two coherent states in a homodyne detection. We propose and study a feedback protocol to generate a pure cat-like steady state.

List of publications

- F. Minganti, A. Biella, N. Bartolo, and C. Ciuti,
Spectral theory of Liouvillians for dissipative phase transitions,
Physical Review A **98**, 042118 (2018).

- R. Rota [1], F. Minganti[1], A. Biella, and C. Ciuti,
Dynamical properties of dissipative XYZ Heisenberg lattices,
New Journal of Physics **20**, 045003 (2018).

- F. Vicentini, F. Minganti, R. Rota, G. Orso, and C. Ciuti,
Critical slowing down in driven-dissipative Bose-Hubbard lattices,
Physical Review A **97**, 013853 (2018).

- N. Bartolo[1], F. Minganti[1], J. Lolli, and C. Ciuti,
Homodyne versus photon-counting quantum trajectories for dissipative Kerr resonators with two-photon driving,
The European Physical Journal Special Topics **226**, 2705 (2017).

- N. Bartolo, F. Minganti, W. Casteels, and C. Ciuti,
Exact steady state of a Kerr resonator with one- and two-photon driving and dissipation: Controllable Wigner-function multimodality and dissipative phase transitions,
Physical Review A **94**, 033841 (2016).

- F. Minganti, N. Bartolo, J. Lolli, W. Casteels, and C. Ciuti,
Exact results for Schrödinger cats in driven-dissipative systems and their feedback control,
Scientific Reports **6**, 26987 (2016).

In the main text, these works are cited with the numbers [1–6].

1. Those authors contributed equally to this work.

Contents

Introduction

The foundation of quantum mechanics can be traced back to the statement that the electromagnetic field is made of photons [7, 8]. Following the revolutionary idea that the energy exchanges between light and matter were discrete, the whole building of quantum mechanics was constructed, making of it one of the most successful theories in human history. Historically, many of the first experimental and theoretical successes dealt with single quantum particles: the explanation of the photoelectric effect, the hydrogen atom, Stern–Gerlach experiment, and the lists goes on [9, 10]. Quantum physics becomes even more interesting when we consider systems made of several particles. When thermal effects do not destroy the quantum nature of the system, the fermionic or bosonic statistics can produce extraordinary effects. In bosonic systems at low temperature, a macroscopic fraction of particles starts to occupy the state of minimal single-particle energy, resulting in Bose-Eintein condensation [11–15]. For fermions, Pauli principle alone can easily explain the essential differences between conductors and insulators [16, 17]. The scenario becomes even richer when interaction-induced correlations combines with quantum degeneracy, producing phenomena such as superconductivity and superfluidity [15, 18–20].

In quantum mechanics, the unitary evolution of any closed system is described by the action of a Hamiltonian operator on a wavefunction [9, 10]. When we describe an isolated system we assume that none of its degrees of freedom is coupled to the rest of the universe. Obviously, this is only an approximation: any physical system interacts with its environment, exchanging energy, matter and information. Many physical systems, however, interact so weakly with their environment that it is possible to describe them as if they were *isolated*. This great simplification in the description of a phenomenon dates back to the very beginning of physics: Galileo's Leaning Tower of Pisa experiment on falling objects (and its interpretation) is nothing but neglecting air resistance for a body subject to gravitational attraction [21]. With the development of thermodynamics, it has also been possible to describe systems at thermal equilibrium with their environment. Indeed, the exchanges of both energy (canonical ensemble) and particles (grand canonical ensemble) can be described via the partition function of the system depending on two parameters: the temperature and the chemical potential [12]. There are systems for which, however, the condition of thermal equilibrium is not (or cannot be) satisfied, and therefore a thermodynamic description fails to capture the relevant phenomena. In those cases, one speaks of *open quantum systems* [22–24].

Historically, one of the first examples of open quantum systems is cavity Quantum Electrodynamics (cavity QED). In those systems, one or more atoms interact with the electromagnetic field confined between two high-quality mirrors [25]. Photon are, however, continuously lost to the environment [25–27]. Nowadays, light-matter interaction can be studied also in superconducting circuits [28, 29], semiconductor cavities [30] and optomechanical systems

[31]. When the interaction strength becomes larger than the dissipation, the system enters in the so-called strong light-matter coupling regime. For example, in semiconductors the interplay between the electronic degrees of freedom and the electromagnetic field can which gives rise to a new hybrid quasi-particle, the *polariton* [27, 32, 33]. The polariton can be seen as a photon dressed by matter excitations, thus permitting a finite effective photon-photon interaction. In order to compensate for particle losses, such photonic systems are often driven out of their equilibrium states. There are many ways to take a system out of equilibrium, such as applying a (periodic) driving field, or pumping energy and particles in the system through external reservoirs via quenches or sweeps [34, 35].

In the context of driven-dissipative systems, the characterisation of criticality is a timely subject. In thermodynamics, the occurrence of a phase transition has been understood in terms of thermodynamic potentials. Classical critical phenomena can be driven by a competition between the value of the system energy and the entropy produced by its thermal fluctuations [12]. A quantum system at zero temperature has zero entropy and it is in its ground state, which is the state minimizing the system energy [36]. However, critical phenomena can occur in the thermodynamic limit as the result of the competition between noncommuting terms of the Hamiltonian. A typical example is the Bose-Hubbard model, describing bosons living on a lattice with on-site interactions and nearest-neighbours hopping. As a function of the ratio between hopping and interaction, it presents a quantum phase transition from a strongly localised phase (Mott insulator), to a delocalised one (superfluid) [37, 38].

The intrinsic non-equilibrium nature of driven-dissipative systems does not allow a determination of the stationary state of the system via a free energy analysis [23–26]. At a quantum level, by properly designing the coupling with the environment and the driving mechanisms, it is possible to stabilize phases without an equilibrium counterpart [39, 40]. The reservoir engineering for complex many-body phases has been deeply explored in different contexts [41, 42]. As for criticality, in the thermodynamic limit, the competition between Hamiltonian evolution, pumping and dissipation processes can trigger a non-analytical change in the steady state [43]. The impressive experimental advances of the last decade provide the opportunity to explore non-equilibrium critical phenomena on a variety of platforms, such as lattices of superconducting resonators [44, 45], Rydberg atoms in optical lattices [46, 47], optomechanical systems [31, 48], and exciton-polariton condensates [27, 49]. Very recently, the critical properties have been investigated also experimentally in single superconducting cavities [50], semiconductor micropillars [51, 52], and large arrays of microwave cavities [45]. Dissipative phase transitions have been discussed theoretically for photonic systems [5, 53–64], lossy polariton condensates [65–67], and spin models [39, 40, 43, 68–73]. The interplay between classical and quantum fluctuations in triggering a nonequilibrium phase transition has been addressed by different methods, including renormalization group approaches based on the Keldysh formalism [65, 74, 75] and via extensive numerical analysis of lattice systems [2, 3, 71]. Our understanding of criticality in such systems is still in its infancy, even if some common paradigms have been identified [1, 43, 75].

For open quantum systems, the typical effect of the environment is to destroy quantum coherences, making a realisation of a macroscopic entangled state extremely difficult [76]. Even if the environment is often detrimental to the creation and preservation of quantum states, it can be also exploited to realise new quantum technologies. By manipulating the exchanges between a system and its environment, reservoir engineering aims to realise previously inaccessible quantum phases of matter [42, 77–82]. Recently, a photon-pair pumping

have been engineered for superconducting resonators [82], leading to the generation of so called photonic Schrödinger cats, characterised by a multi-modal Wigner function [6, 63, 83]. The possibility to control and protect such states is promising for the implementation of quantum computation protocols [84–88].

The structure of this thesis is the following. In Chapter 1 we introduce the field of Quantum Manybody physics with light, while in Chapter 2 we discuss the theoretical framework for driven-dissipative manybody physics. In Chapter 3, we explore fundamental properties of both first- and second-order dissipative phase transitions, the latter being associated to a symmetry breaking [1]. In Chapter 4 we present the analytic solution to the one- and two-photon driven-dissipative Kerr resonator, investigating the emergence of phase transitions in such models [5]. In Chapters 5 and 6 we discuss criticality in extended lattice models: the driven dissipative Bose-Hubbard model [3] and anisotropic Heisenberg XYZ model [2], respectively. Finally, in Chapter 7 we study the creation and preservation of photonic Schödinger cat states in quadratically driven-dissipative Kerr resonators subject to one photon losses [4, 6].

CHAPTER 1

Quantum Manybody Physics with Light

My thesis is devoted to the study of manybody interacting systems coupled in a non-negligible way to a memoryless environment. Even if a specific model is not necessary for such a general description, at the heart of my work there stands the pivotal example provided by Quantum Manybody Physics with Light [27]. Here, every word needs some explanation: *Quantum* means that classical physics does not fully capture the system complexity; *Manybody Physics* implies that we are interested in the collective phenomena of interacting particles; *Light* indicates that those particles are the elementary excitations of the Electro-Magnetic (EM) field. The aim of this Chapter is thus to review some fundamental properties of light and motivate the interest in studying interacting photons. The additional layer of complexity dictated by the dissipative nature of photonic systems will be treated in a general way in the next Chapter.

The plan of this Chapter is the following: in Sec. 1.1 we will briefly introduce the classical and quantum harmonic oscillator and we will provide an heuristic explanation about the concept of massive and interacting photons. In Sec. 1.2 we will discuss two paramount examples of experimental setups: the semiconducting micropillars and superconducting circuits.

Contents

1.1 Massive and interacting photons

In this section, we provide a simplified discussion about massive and interacting photons. Even if this description neglects much of the interesting features emerging from the light-matter coupling, it allows an easy and intuitive explanation of how confinement and nonlinear media generate mass and interaction. Since the Hamiltonian of the EM field in vacuum can be recast in term of a collection of harmonic oscillators, we start by briefly describing this model both in the classical and quantum-mechanical cases.

1.1.1 The harmonic oscillator

A classical Harmonic oscillator is described by the Hamiltonian [9, 89, 90]

$$H = \frac{p^2}{2m} + \frac{1}{2}m\omega x^2. \tag{1.1}$$

In accordance, the momentum and position functions evolve as

$$\begin{cases} \dfrac{\mathrm{d}}{\mathrm{d}t}p(t) = -m\omega^2 x(t), \\ \dfrac{\mathrm{d}}{\mathrm{d}t}x(t) = p(t)/m. \end{cases} \tag{1.2}$$

The solution to the previous equation can be found by introducing the complex dimensionless parameter $\alpha(t) = \left(x(t)\sqrt{m\omega} + \mathrm{i}p(t)/\sqrt{m\omega}\right)/\sqrt{2}$. Its equation of motion reads:

$$\frac{\mathrm{d}}{\mathrm{d}t}\alpha(t) = -\mathrm{i}\omega\alpha(t), \tag{1.3}$$

which has solution:

$$\alpha(t) = \alpha_0\, e^{-\mathrm{i}\omega t}, \tag{1.4}$$

where $\alpha_0 = \alpha(t=0)$ is the initial displacement. Accordingly, position and momentum evolve as:

$$\begin{cases} p(t) = -\dfrac{\mathrm{i}\sqrt{m\omega}}{\sqrt{2}}\left(\alpha_0 e^{-\mathrm{i}\omega t} - \alpha_0^* e^{\mathrm{i}\omega t}\right) = -\dfrac{\mathrm{i}\sqrt{m\omega}\,(\alpha(t) - \alpha^*(t))}{\sqrt{2}}, \\ x(t) = \dfrac{1}{\sqrt{2\,m\omega}}\left(\alpha_0 e^{-\mathrm{i}\omega t} + \alpha_0^* e^{\mathrm{i}\omega t}\right) = \dfrac{\alpha(t) + \alpha^*(t)}{\sqrt{2\,m\omega}}, \end{cases} \tag{1.5}$$

and the energy of the system is $H(t) = E = m\omega\left(x(t)^2 + p(t)^2\right)/2 = \omega\,|\alpha_0|^2$. The meaning of Eq. (1.5) is clear: by displacing the harmonic oscillator from its rest position (i.e. $x = 0$, $p = 0$) one induces a periodic motion, characterised by an exchange between potential and kinetic energy.

The Hamiltonian of a quantum Harmonic oscillator is of the form [9, 10, 25]

$$\hat{H} = \frac{\hat{p}^2}{2m} + \frac{1}{2}m\omega\hat{x}^2, \tag{1.6}$$

where $\hat{x}$ and $\hat{p}$ are the position and momentum operator, and $[\hat{x}, \hat{p}] = \mathrm{i}$ (in this manuscript, we will adopt the convention $\hbar = 1$). To solve this model, one introduces the so-called

annihilation and creation operators $\hat{a}$ and $\hat{a}^\dagger$, defined as

$$\hat{a} = \sqrt{\frac{m\omega}{2}}\left(\hat{x} + \frac{\mathrm{i}}{m\omega}\hat{p}\right), \tag{1.7a}$$

$$\hat{a}^\dagger = \sqrt{\frac{m\omega}{2}}\left(\hat{x} - \frac{\mathrm{i}}{m\omega}\hat{p}\right). \tag{1.7b}$$

It follows

$$\left[\hat{a}, \hat{a}^\dagger\right] = 1. \tag{1.8}$$

Eqs. (1.7) can be inverted, obtaining $\hat{x}$ and $\hat{p}$ as

$$\hat{x} = \sqrt{\frac{1}{2m\omega}}(\hat{a}^\dagger + \hat{a}), \tag{1.9a}$$

$$\hat{p} = \mathrm{i}\sqrt{\frac{m\omega}{2}}(\hat{a}^\dagger - \hat{a}). \tag{1.9b}$$

Inserting these expression into Eq. (1.6), and exploiting Eq. (1.8), one has

$$\hat{H} = \omega\left(\hat{a}^\dagger\hat{a} + \frac{1}{2}\right) = \omega\left(\hat{n} + \frac{1}{2}\right), \tag{1.10}$$

where $\hat{n} = \hat{a}^\dagger\hat{a}$. The solution of the Harmonic oscillator problem is therefore equivalent to the determination of the eigenvalues and eigenvectors of $\hat{n}$.

It can be shown [9, 10], that the spectrum of the operator $\hat{n}$ is non-degenerate and such that $\hat{n}\,|n\rangle = n\,|n\rangle$ with $n \in \mathbb{N}$. The states $|n\rangle$ are called the number or Fock states. Moreover, one has $\hat{a}\,|n\rangle = \sqrt{n}\,|n-1\rangle$ and $\hat{a}^\dagger\,|n\rangle = \sqrt{n+1}\,|n+1\rangle$. For this reason $\hat{a}$ and $\hat{a}^\dagger$ are said to be creation and annihilation operators: their action on an eigenvector $|n\rangle$ makes an energy quantum ω appear or disappear.

1.1.2 Photons in vacuum

The quantisation of the electromagnetic field was a milestone in the development of quantum field theory [91]. The idea, due to Dirac, Fock and Jordan allowed to introduce the theoretical machinery of second quantisation for the free fields: (i) one expands a classical Hamiltonian described via a scalar or vector field on a basis consisting of a complete set of functions; (ii) each of the coefficients in this expansion is interpreted as the classical counterpart of an operator: a creation or an annihilation one; (iii) Bose or Fermi statistics is imposed by requiring commutation or anti-commutation relations between the creation and annihilation operators.

This procedure for the $U(1)$ scalar field associated to the classical EM field is nowadays a textbook example [91, 92]: in the Coulomb gauge, one decomposes the vector potential of the EM field in its Fourier modes. The coefficients of this normal expansion are identified as the creation and annihilation operators of the photonic field. By applying this transformation to the classical Hamiltonian

$$H = \frac{\epsilon_0}{2}\iiint_V d^3\mathbf{r}\left(|E(\mathbf{r},t)|^2 + c^2|B(\mathbf{r},t)|^2\right) \tag{1.11}$$

one recovers the picture of the free electromagnetic field as an infinite collection of harmonic oscillators under the form:

$$\hat{H} = \sum_{\mathbf{k},\,\mu}\hbar\omega(\mathbf{k})(\hat{a}^\dagger_{\mathbf{k},\,\mu}\hat{a}_{\mathbf{k},\,\mu} + \frac{1}{2}), \tag{1.12}$$

where $\mathbf{k}$ is the momentum (whose value depends on the boundary conditions) and μ is the polarisation of the field, together with the canonical commutation relations for bosons $\left[\hat{a}_{\mathbf{k},\mu}, \hat{a}^\dagger_{\mathbf{k}',\mu'}\right] = \delta_{\mathbf{k},\mathbf{k}'}\delta_{\mu,\mu'}$. That is, the electromagnetic field can be understood in terms of an infinite collection of quantum harmonic oscillators.

In what follows, we will often be interested in studying the electromagnetic field confined inside optical cavities. The confinement (combined with the very good quality of the confining mirrors) results in a large frequency spacing between the $\omega(\mathbf{k})$ levels. In this case, one discerns the different modes of the field, so that most of the times it is possible to work in the approximation in which only one cavity mode of frequency ω determines the field dynamics:

$$\hat{H} = \hbar\omega\left(\hat{a}^\dagger\hat{a} + \frac{1}{2}\right). \tag{1.13}$$

1.1.3 Mass from confinement and interaction from nonlinearities

In the next Section, we will introduce two of the most important experimental platforms for the study of open quantum many-body systems, namely semiconductor micropillars and superconducting circuits. Here, in order to grasp the main ideas behind massive and interacting photons, we consider the simplified model of light propagating in a dielectric and confined between two mirrors. Confinement will give photons an effective mass, while the electronic degrees of freedom of the nonlinear medium will provide the effective interaction between the photons. For a more formal description of such a light-matter coupling, one can describe the response of the dielectric via a power series of the incoming electric field, recovering the various element of the susceptibility tensor [93]. This tensor can be then used to describe high-order photon-photon processes via a dielectric quantisation procedure [92].

Mass

Let us consider the EM field confined in between two mirrors at distance L in the z direction, and free in the xy plane (see Fig 1.1, left). Under the assumption of perfectly reflecting mirrors, the wave-vector k_z cannot have arbitrary values, but only $k_z = 2\pi n/L$, where n is an integer number. Now, let us suppose that the EM field in the cavity is almost completely parallel to the z direction. In this case the total wave vector k can be expressed as:

$$k = \sqrt{k_z^2 + k_\perp^2} = k_z\left(1 + \frac{k_\perp^2}{2k_z^2}\right) + \mathcal{O}\left(\frac{k_\perp^4}{k_z^4}\right) \tag{1.14}$$

where $k_\perp \ll k_z$ is the component of the field perpendicular to the z direction.

Since the particle we are considering are photons, their energy dispersion can be cast as:

$$E = \hbar ck = \hbar c\sqrt{k_z^2 + k_\perp^2} \simeq \frac{\hbar k_z}{c}c^2 + \frac{1}{2}\frac{k_\perp^2\hbar^2}{\hbar k_z/c} = m_{\text{eff}}c^2 + \frac{p_\perp^2}{2m_{\text{eff}}}, \tag{1.15}$$

where we have introduced the effective mass $m_{\text{eff}} = \hbar k_z/c$, and exploited the relativistic relation between momentum and wave vector $p_\perp = \hbar k_\perp$. Indeed, one finds the relativistic equation of a slow massive particle, where the value k_z plays, up to a constant, the role of an effective mass. We stress that, since $k_z = 2\pi n/L$, different values of n means different effective masses.

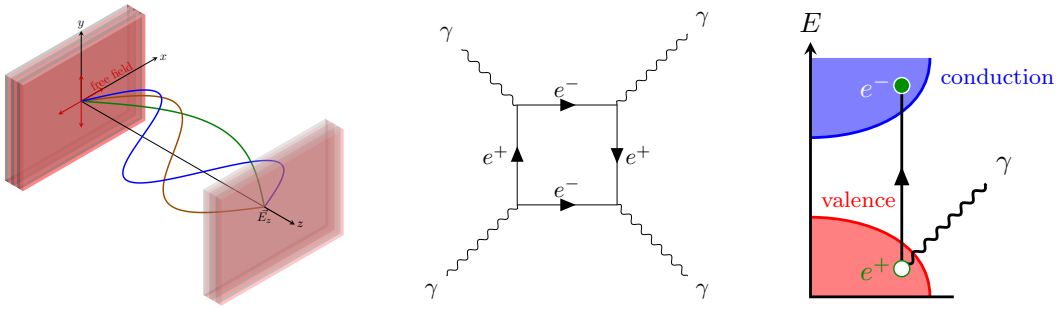

Figure 1.1 – Left panel: The EM field confined in region of space can be decomposed in a perpendicular component and a parallel one. Its energetic dispersion can be recast in the form of a non-zero mass term plus a kinetic one. Central panel: Heisenberg-Euler diagram of a photon-photon interaction in vacuum. Right panel: Creation of an electron-hole pair in a dielectric via the absorption of a photon.

Interaction

In order for photons to interact in vacuum, a creation of an electron-positron pair is necessary (cf. Fig. 1.1, middle). The energy of the electron-positron pair is $E_{\mathrm{e-p}} \simeq 1$ MeV, while for an optical photon $E_{\mathrm{ph}} \simeq 2$ eV. Since the cross section of this scattering process depends on the ratio between the energy of the photons and the one of the pair, this process can be neglected in experiments with optical photons. The situation is extremely different if we consider a dielectric material. In this case, instead of dealing with the virtual creation of an electron-positron pair, we can consider the creation of an electron-hole couple by excitation of an electron from the valence band to the conduction one (cf. Fig. 1.1, right). The diagram describing this process has the same form as in vacuum but the energy associated to the creation of an electron-hole pair is far smaller (e.g., for typical semiconductors $E_{\mathrm{e-h}} \simeq 1$ eV). In this regard, nonlinear media allows to introduce effective interaction between photons of the form

$$\hat{H}_{\mathrm{int}} = \frac{U}{2}\hat{a}^\dagger\hat{a}^\dagger\hat{a}\hat{a}. \tag{1.16}$$

Such interaction is often called a $\chi^{(3)}$ Kerr interaction, since it is the quantum counterpart of the classical Kerr effect stemming from the third order development of the electric susceptibility tensor χ.

1.2 Examples of physical systems

Having justified the rationale behind massive and interacting photons, in this section we present two of the most significant experimental platforms for the study of quantum many-body physics with light: semiconductor microstructures and superconducting circuits. Indeed, in those systems sizeable photon-photon interactions can be produced, and several resonators can be tailored to create lattices of photonic cavities [27]. In the following discussion, we will explicitly ignore the driven-dissipative nature of photonic systems (which will be addressed in Chapter 2) and we will mainly focus on the Hamiltonian properties.

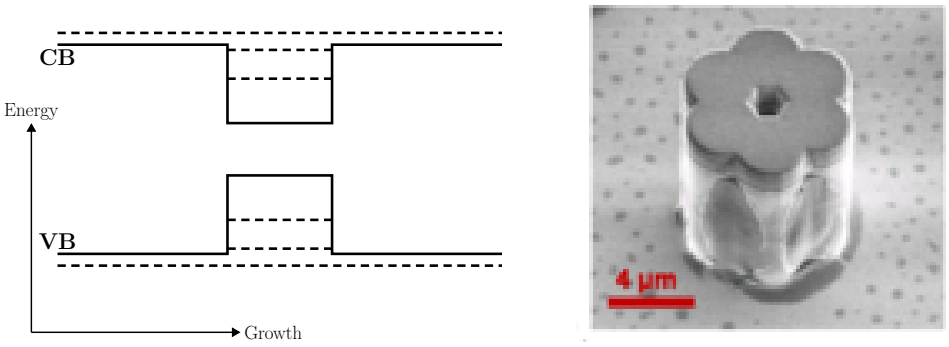

Figure 1.2 – Left: Energy bands of quantum states confined in a quantum well as a function of the position along the growth direction. VB is the valence band and CB the conduction band. The dashed lines represent the quantised energy levels of the system. Right: Scanning electron microscope image of the polaritonic molecule (from Ref. [94]).

1.2.1 Semiconducting cavities

In a pure semiconductor the valence band is separated from its conduction one by an energy gap. When light is shined on it, a significant number of electrons can be excited from the valence to the conduction band, creating electron-hole pairs. Due to Coulomb interaction, a pair can form a bound state called exciton, i.e. a bosonic quasiparticle associated to the lowest energy optical transition of the semiconductor. In order to increase the binding energy and favour the creation of excitons, one can confine the motion of electrons in a quantum well.

A quantum well consists of a localised confining potential which creates a discrete energy spectrum. In semiconductors, this can be achieved by growing a thin semiconductor layer on a second semiconductor (or by changing the doping of the semiconductor). The chemical composition of the well is then chosen to have the bottom of the conduction (the top of the valence) band at a lower (higher) energy than the surrounding material [27]. In this heterostructure, the electron and holes are then confined by the semiconductor-vacuum interface and by the "barrier material". The motion of carriers being confined in a plane, a quantum well acts as a two-dimensional structure (see Fig. 1.2 left).

If the confinement is sufficiently strong, the energy spacing between the confined modes is much larger then the spectral width, and it is safe to consider only one light mode interacting with a single excitonic level. The minimal-coupling Hamiltonian of such a exciton-photon system reads [95, 96]

$$\hat{H}_{\mathrm{ex-ph}} = \omega_{\mathrm{ph}}\hat{c}^\dagger\hat{c} + \omega_{\mathrm{ex}}\hat{d}^\dagger\hat{d} + \Omega(\hat{d}^\dagger\hat{c} + \hat{c}^\dagger\hat{d}) + \frac{\omega_{\mathrm{nl}}}{2}\hat{d}^\dagger\hat{d}^\dagger\hat{d}\hat{d}, \tag{1.17}$$

where ω_{ph} is the energy of one photon, ω_{ex} is that of an exciton pair, Ω quantifies the ligt-matter coupling strength and ω_{nl} is the nonlinear exciton-exciton interaction. The operators $\hat{c}$ and $\hat{d}$ annihilate a photon or an exciton, respectively. To enhance the light-matter coupling, one can embed one or more quantum wells in a Fabry-Pérot cavity with semiconducting Bragg mirrors.

The quadratic part of the Hamiltonian can be diagonalised via a Hopfield-Bogoliubov transformation [32], and the stemming elementary excitations are the so-called polaritons, hybrid light-matter (quasi-)particles [27, 33, 95]. For quasi-resonant excitation between the laser and the energy of such a quasi-particle, the micropillar can be considered as a single-

mode polariton cavity, characterised by the Hamiltonian:

$$\hat{H} = \omega \hat{a}^\dagger \hat{a} + \frac{U}{2} \hat{a}^\dagger \hat{a}^\dagger \hat{a} \hat{a}, \tag{1.18}$$

where the frequency of the polariton mode is

$$\omega = \frac{\omega_{\text{ph}} + \omega_{\text{ex}}}{2} - \sqrt{\Omega^2 + \left(\frac{\omega_{\text{ph}} + \omega_{\text{ex}}}{2}\right)^2}, \tag{1.19}$$

the strength of the non-linearity is

$$U = \frac{\omega_{\text{nl}}}{2\left[1 + \left(\frac{\Omega^2}{\omega_{\text{ph}} - \omega_{\text{ex}}}\right)^2\right]^2}, \tag{1.20}$$

and $\hat{a}$ is the polariton annihilation operator. Indeed, we find a Kerr interaction of the form given in Eq. (1.16).

Several semiconductor cavities can be arranged in a lattice configuration (see Fig. 1.2, right) resulting in an evanescent coupling between different sites. Keeping only the leading tunnelling terms, the Hamiltonian of this system reads

$$\hat{H}_{\text{coup}} = -J \sum_{\langle i,j \rangle} \hat{a}_i^\dagger \hat{a}_j + \hat{a}_j^\dagger \hat{a}_i, \tag{1.21}$$

where J quantifies the hopping strength and the sum runs over $\langle i, j \rangle$ nearest neighbours. This scheme has been implemented to realise artificial molecules [94], and extended lattice systems [97–99].

1.2.2 Circuits QED

In any electronic circuit, the flow of an electric current I can be characterised by a resistance R, an induction L, and a capacitance C. The resistance R describe the difficulty of current to pass through the circuit via the Ohm low $\Delta V = RI$, ΔV being the difference of potential between the two extremes of the circuit. The capacitance quantifies the potential energy stored in the electric field, i.e. $E_C = Q^2/2C$, Q being the charge cumulated. The induction, instead, quantifies the energy stored in the magnetic field as $E_L = \Phi^2/2L$, where $\Phi = LI$ is the magnetic flux.

Since $I = \mathrm{d}Q/\mathrm{d}t$, the magnetic flux and the charge can be seen as conjugate variables. Thus, for a circuit where the resistance is negligible, the classical Hamiltonian of a LC circuits is of the form

$$H = \frac{\Phi^2}{2L} + \frac{Q^2}{2C}. \tag{1.22}$$

The mechanical analogous to such a LC oscillator is a simple mass-spring system, the displacement playing the role of the charge and the momentum that of the flux. Accordingly, we can quantise the charge and flux in the electrical circuit as [1]

$$\hat{H} = \frac{\hat{\Phi}^2}{2L} + \frac{\hat{Q}^2}{2C} = \omega(\hat{a}^\dagger \hat{a} + \frac{1}{2}), \tag{1.23}$$

1. This procedure is known as mesoscopic quantisation. For more details see, e.g., [100].

where we introduce the canonically commutating variables $\left[\hat{\Phi}, \hat{Q}\right] = \mathrm{i}$, the frequency $\omega = 1/\sqrt{LC}$ and the annihilation operator

$$\hat{a} = \frac{1}{\sqrt{\omega}} \left(\frac{\hat{\Phi}}{\sqrt{2L}} - \mathrm{i} \frac{\hat{Q}}{\sqrt{2C}} \right). \tag{1.24}$$

The previous equation establishes the close parallelism between a superconducting LC circuit (where the resistance is zero) and a quantum harmonic oscillator. This formalism is quite general and describe a large class of systems, since transmission lines can be modeled by a chain of capacitors and inductors.

The nonlinear element of such a setup can be given, for example, by a Josephson junction [29, 100]. A Josephson tunnel junction is created by sandwiching a thin insulating layer between two superconductors [101], and the currents tunneling between the two superconductors obey the Josephson equations [19]. In particular, the current and voltage across the barrier are related to the phase difference between the two superconductors δ as

$$I = I_0 \sin(\delta), \tag{1.25a}$$

$$\frac{\mathrm{d}\delta}{\mathrm{d}t} = \frac{V}{\Phi_0} = 4\pi V e, \tag{1.25b}$$

where V is the voltage difference applied to the junction, I_0 is the critical intensity (depending on the superconductor energy gap and on the resistance of the junction) and $\phi_0 = 1/4\pi e$ is the flux quantum. A Josephson junction will introduce an additional inductance, whose form can be derived as

$$\frac{\mathrm{d}I}{\mathrm{d}t} = \frac{I_0 V}{\Phi_0} \cos(\delta) = \frac{V}{L_J} \cos(\delta), \tag{1.26}$$

where we have introduced the Josephson inductance $L_J = \Phi_0 / I_0$. Moreover, the junction will store a energy

$$H_J = \int_{-\infty}^{t} V(t') I(t') \mathrm{d}t' = -E_J \cos(\delta) = -E_J \left[1 + \frac{1}{2}\delta^2 + \frac{1}{24}\delta^4 + \mathcal{O}(\delta^6) \right], \tag{1.27}$$

where $E_J = I_0 \Phi_0$. Such a nonlinear element can be integrated in a LC circuit. The process to correctly quantise a Josephson junction is quite involved, and can be found, e.g., in the supplementary material of [102]. By expressing δ as a function of Φ, and by Taylor developing to the fourth order in the variable Φ, one obtains an effective quartic Hamiltonian of the form

$$\hat{H} = \frac{\Phi^2}{2L_t} + \frac{Q^2}{2C} - \frac{1}{24} \frac{L_J^3}{L_t^4 \Phi_0^2} \Phi^4, \tag{1.28}$$

where $L_t = L_J + L$. One can then quantise Q and Φ and rewrite them in terms of the creation and annihilation operators in Eq. (1.24). In one keeps only the energy-conserving terms with equal number of annihilation and creation operators, one obtains

$$\hat{H} = \omega \hat{a}^\dagger \hat{a} + \frac{U}{2} \hat{a}^\dagger \hat{a}^\dagger \hat{a} \hat{a}, \tag{1.29}$$

where $\omega = 1/\sqrt{L_t C}$ is the energy of one particle,

$$U = -\frac{e^2 \omega_0 \sqrt{L_t / C}}{2} \left(\frac{L_J}{L_t} \right)^3, \tag{1.30}$$

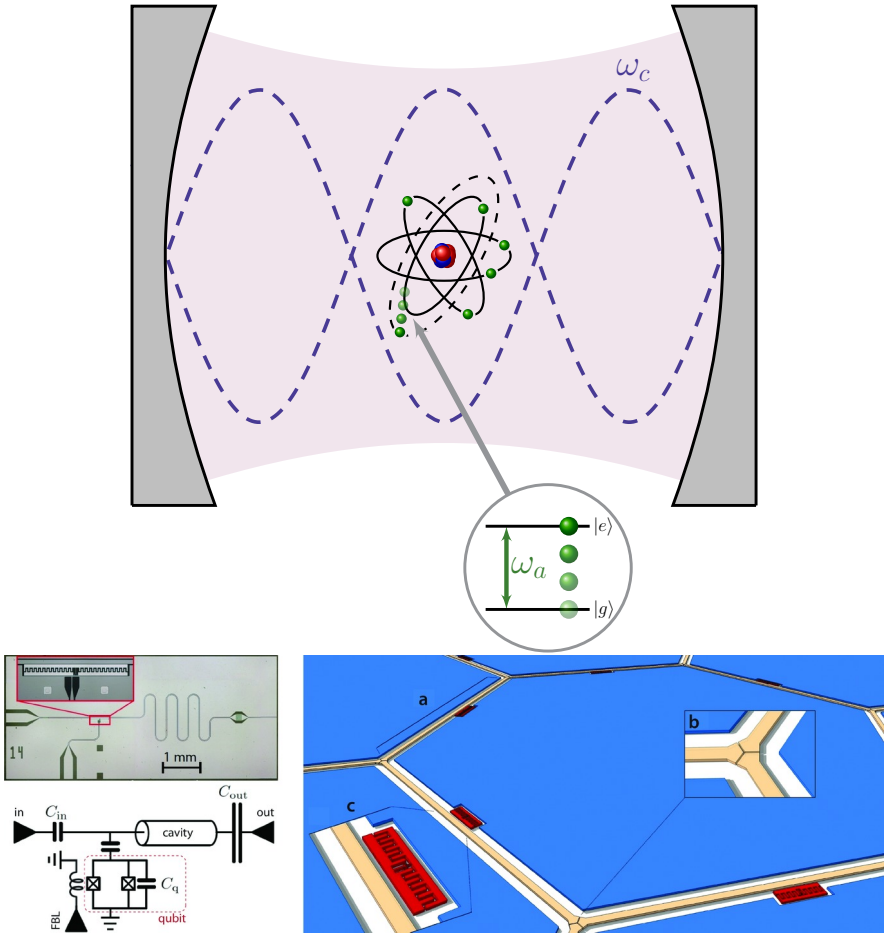

Figure 1.3 – Top: the Jaynes-Cummings model describes a two-level system interacting with a quantized mode of an optical cavity. It was originally developed to study the interaction of atoms with the quantized electromagnetic field. Bottom: Realization of the Jaynes-Cummings model and lattice in a circuit QED setup. Left: The device (top) and circuit scheme (bottom). A LC resonator is capacitively coupled to a qubit (realised via nonlinear superconducting circuit element). "In" and "out" ports connect the system to microwave drive and detection circuitry. Right: Circuit QED realization of the Jaynes-Cummings lattice. Transmission line resonators, "a", are coupled to each other via coupling capacitors, "b", and thus form a regular lattice in which photons can hop from site to site. Photon-photon interactions are induced by the presence of superconducting circuits such as the transmon qubit, "c". Bottom figures from Ref. [103].

is the effective interaction and $\hat{a}$ is the annihilation operator of a photon inside the circuit. Again, one finds a Kerr interaction as in Eq. (1.16).

Most of circuit-QED experiments focus on the interaction of microwave "cavity" photons shined on circuit elements (see Fig. 1.3, Bottom left). Given the extreme control achieved on the manipulation of electronic elements, there exists several ways to integrate and engineer nonlinear elements in a LC circuit [29, 103–106]. In particular, it is possible to realise circuits where presence of a single photon is able to effectively block the entrance of a second one. In this regime of *photon blockade* the circuit is an effective two-level system (qubit), and its physics is well capture by the Jaynes-Cummings model ([107] and Fig. 1.3, top):

$$\hat{H} = \omega_c \hat{a}^\dagger \hat{a} + \omega_\mathrm{a} \hat{\sigma}^+ \hat{\sigma}^- + g(\hat{a}^\dagger \hat{\sigma}^- + \hat{a}\hat{\sigma}^+), \tag{1.31}$$

where the operator $\hat{\sigma}^-$ is the lowering operator acting on the two level system and $\hat{a}$ is the annihilation operator for a cavity photon. The excited state of two level system has an of energy ω_a, a cavity photon has energy ω_c, and g is the Rabi coupling between the qubit and the cavity field. As it was the case for semiconducting micropillars, it is possible to evanescently couple different resonators in a lattice geometry (see, e.g. Fig. 1.3, Bottom right).

CHAPTER 2

Theoretical Framework for Open Quantum Systems

When considering open systems (e.g., dissipative photonic ones) one cannot neglect the effect of the environment. However, an exact treatment of the full problem is often impossible. Thus, in this Chapter we derive a reduced description of an open system dynamics by tracing out the environment. Describing the time evolution of a system weakly coupled to a memoryless environment, we obtain the so-called Lindblad master equation. By construction, the Lindblad master equation describes the average dynamics of a system, which can be interpreted as the effect of a continuous and unread measure. By "reading" the result of the measurement process, we determine the quantum trajectories associated to a stochastic Schrödinger equations. Finally, we introduce the coherent states and the phase-space representations of quantum mechanics, which allow to interpret the system density matrix in terms of quasiprobability distributions of semiclassical states.

The plan of this Chapter is the following. In Sec. 2.1 we derive the Lindblad master equation, while in Sec. 2.2 we investigate the physics of the stochastic Schrödinger equations. In Sec. 2.3 we derive the phase space representations of a photonic system.

Contents

2.1 The Lindblad master equation

A typical approach to simplify the description of an open system is to neglect the details about the system-environment interaction and only model the average effect of the environment on the system. To deal with such a problem, thus, one abandons a deterministic description (in terms of a wave function) and resort to a probabilistic one (in terms of a *density matrix* operator). Under the approximation of a weakly coupled and Markovian (i.e. memoryless) environment, we will obtain a very general and compact form for the evolution of the reduced density matrix of the system, called the (Gorini–Kossakowski–Sudarshan–)Linblad master equation [108, 109]. This equation of motion will not only contain a unitary Hamiltonian part, but will also describe *decoherence processes*, i.e., the dissipation of energy, particles and information into the environment. The following discussion was largely inspired by [23–26, 110, 111].

2.1.1 Density matrices and quantum maps

We consider the rather general problem of a quantum system S coupled to an environment E. By environment we mean a large collection of degrees of freedom, each one coupled to the system, with a continuous and wide spectrum of characteristic frequencies, in thermal equilibrium and at some temperature (possibly zero). The Hilbert space of $(S \oplus E)$ is $H_{SE} = H_S \otimes H_E$, where H_S is the Hilbert space of the system and H_E is the Hilbert space of the environment. The environment and system are, together, described by a wave function $|\Psi\rangle \in H_{SE}$. We are interested in describing S, neglecting what happens to E. To do so, one can build the reduced-density operator $\hat{\rho}_S$ by tracing $\hat{\rho}_{SE} = |\Psi\rangle\langle\Psi|$ over the degrees of freedom of E [24, 25, 111, 112], that is:

$$\hat{\rho}_S = \mathrm{Tr}_E\left[\hat{\rho}_{SE}\right] = \sum_{i,j} c_i c_j \left|\psi_i\right\rangle\left\langle\psi_j\right|, \tag{2.1}$$

where ψ_j is a wave function in H_S. The operator $\hat{\rho} \equiv \hat{\rho}_S$ (from now on we will drop the label S) contains all the information needed to describe the statistics of outcomes of any measurement performed only on the system. Moreover, $\hat{\rho}$ is a density matrix, since it is an Hermitian, positive definite and trace-one operator [9, 22, 24–26, 112]. Such a density matrix can describe the quantum system in a mixed state, that is, a statistical ensemble of several quantum states. Clearly, $\hat{\rho}$ can be diagonalised, obtaining

$$\hat{\rho} = \sum_i p_i \left|\psi_i\right\rangle\left\langle\psi_i\right|, \tag{2.2}$$

where the p_i can be interpreted as the probabilities of mutually excluding events associated to the states $|\psi_i\rangle$. Physically speaking, the probabilities p_i describe the likelihood to find the system in a certain state upon an appropriate measure.

General form of a quantum map

Having introduced the reduced density matrix $\hat{\rho}$, we are now interested in the most general equation for its time evolution. Such a quantum map $\mathcal{M}$ must transform a density matrix into another, i.e.

$$\hat{\rho}(t+\tau) = \mathcal{M}\hat{\rho}(t). \tag{2.3}$$

Therefore, $\mathcal{M}$ must to satisfy the following properties:

P1: $\mathcal{M}$ is linear:

$$\mathcal{M}(\alpha\hat{\rho}_1 + \beta\hat{\rho}_2) = \alpha\mathcal{M}(\hat{\rho}_1) + \beta\mathcal{M}(\hat{\rho}_2). \tag{2.4}$$

P2: $\mathcal{M}$ conserves the Hermiticity of $\hat{\rho}$.

$$(\mathcal{M}\hat{\rho})^\dagger = \mathcal{M}\hat{\rho}. \tag{2.5}$$

P3: $\mathcal{M}$ conserves the trace

$$\mathrm{Tr}[\mathcal{M}\hat{\rho}] = 1. \tag{2.6}$$

P4: $\mathcal{M}$ conserves the positivity [1]

$$\langle\psi|\mathcal{M}\hat{\rho}|\psi\rangle \geq 0 \qquad \text{for any } |\psi\rangle\,. \tag{2.7}$$

The quantum map $\mathcal{M}$ is a *superoperator*, since it transform an operator into another.

The conditions *P1-P4* severely limit the structure of the linear superoperator $\mathcal{M}$. Indeed, when $\mathcal{M}$ meets them, Choi's theorem on completely positive maps (see, e.g., [25, 112, 113]) guarantees that there exist a set of $\hat{M}_\mu$ Kraus operators such that

$$\mathcal{M}\hat{\rho}(t) = \sum_\mu \hat{M}_\mu\hat{\rho}(t)\hat{M}_\mu^\dagger, \tag{2.8}$$

with the normalization condition

$$\sum_\mu \hat{M}_\mu^\dagger\hat{M}_\mu = \mathbb{1}. \tag{2.9}$$

The number of Kraus operators is, at most, N^2, where N is the dimension of the Hilbert space H_S. We also stress that Kraus operators need not be unique: any linear unitary transformation mixing them leaves the quantum map unchanged. Kraus operators are an extremely powerful tool: indeed it is possible to compress the infinite complexity of the environment into the set of $\hat{M}_\mu$ operators.

2.1.2 A note about superoperators

In the following, we will often have to deal with superoperators, i.e. liner operators acting on the vector space of operators. That is, superoperators act on operators to produce new operators, just as operators act on vectors to produce new vectors.

An example of superoperator is the commutator $\mathcal{A} = \left[\hat{A}, \bullet\right] = \hat{A}\bullet - \bullet\hat{A}$. With this notation, we mean that $\mathcal{A}$ acting on $\hat{\xi}$ is such that $\mathcal{A}\hat{\xi} = \hat{A}\hat{\xi} - \hat{\xi}\hat{A}$. The dot simply indicates where the argument of the superoperator is to be placed. Moreover, we adopt the convention that the action is always on the operator to the immediate right of the dot. Superoperators can also "embrace" their operators, e.g., $\mathcal{A} = \hat{A}\bullet\hat{B}$ is such that $\mathcal{A}\hat{\xi} = \hat{A}\hat{\xi}\hat{B}$.

The dot-notation (i.e., $\bullet$) is particularly useful, since it allows for a nesting of superoperators. For example, consider $\mathcal{A} = \hat{A}\bullet\hat{B}$, $\mathcal{C} = \hat{C}\bullet\hat{D}$ and $\mathcal{E} = \hat{E}\hat{F}\bullet$. One has,

$$\begin{aligned}
\mathcal{A}\mathcal{C} &= (\hat{A}\bullet\hat{B})(\hat{C}\bullet\hat{D}) = \hat{A}\hat{C}\bullet\hat{D}\hat{B}, \\
\mathcal{E}\mathcal{A} &= \hat{E}\hat{F}\hat{A}\bullet\hat{B}, \\
\mathcal{A}\mathcal{E} &= \hat{A}\hat{E}\hat{F}\bullet\hat{B}.
\end{aligned} \tag{2.10}$$

1. To be more precise, $\mathcal{M}$ is completely positive. That is, not only does $\mathcal{M}$ map positive operators to positive operators, but so does the map for $\mathcal{M}\otimes\mathcal{I}$, where $\mathcal{I}$ is the idendity superoperator for an arbitrary second system S'. Indeed, $\mathcal{M}\otimes\mathcal{I}$ is a legitimate quantum map for a system $S\oplus S'$.

In this manuscript, we will systematically adopt the following notation: superoperators will be written in calligraphic characters (e.g., $\mathcal{A}$), operators will be denoted by hats (e.g., $\hat{A}$), states and their duals will be expressed in the Dirac notation ($|a\rangle$ and $\langle a|$). Since the operators form a vector space, it is possible to provide a vectorized representation to each element in $H \otimes H$. For an operator $\hat{A}$, it will be denoted by $\vec{A}$ or $|\hat{A}\rangle$. We choose the convention to convert the matrices into a column vectors as

$$\hat{A} = \begin{pmatrix} a & b \\ c & d \end{pmatrix} \longrightarrow \vec{A} = \begin{pmatrix} a \\ b \\ c \\ d \end{pmatrix}. \tag{2.11}$$

Consequently, to any *linear* superoperator $\mathcal{A}$ it is possible to associate its matrix representation $\bar{\bar{\mathcal{A}}}$.

Since there is no intrinsic definition of inner product in the operator space $H \otimes H$, we introduce the Hilbert-Schmidt one [2]:

$$\langle \hat{A} | \hat{B} \rangle = \mathrm{Tr}\left[\hat{A}^\dagger \hat{B}\right]. \tag{2.12}$$

Hence, the norm of an operator is:

$$\|\hat{A}\|^2 = \mathrm{Tr}\left[\hat{A}^\dagger \hat{A}\right]. \tag{2.13}$$

Most importantly, having introduced a inner product for the operators, it is possible to introduce the Hermitian adjoint [3] of $\mathcal{A}$, which by definition is $\mathcal{A}^\dagger$ such that:

$$\langle \hat{\xi} | \mathcal{A} \hat{\chi} \rangle = \langle \mathcal{A}^\dagger \hat{\xi} | \hat{\chi} \rangle. \tag{2.14}$$

The rules to obtain such adjoint, however, *are not* the same as in the case of operators. Consider the most general linear superoperator $\mathcal{A} = \hat{A} \bullet \hat{B}$. Exploiting the definition of Hermitian adjoint we have

$$\langle \hat{\xi} | \mathcal{A} \hat{\chi} \rangle = \mathrm{Tr}\left[\xi^\dagger \hat{A} \hat{\chi} \hat{B}\right] = \mathrm{Tr}\left[\hat{B} \xi^\dagger \hat{A} \hat{\chi}\right] = \mathrm{Tr}\left[(\hat{A}^\dagger \hat{\xi} \hat{B}^\dagger)^\dagger \hat{\chi}\right] = \mathrm{Tr}\left[(\mathcal{A}^\dagger \hat{\xi})^\dagger \hat{\chi}\right] = \langle \mathcal{A}^\dagger \hat{\xi} | \hat{\chi} \rangle. \tag{2.15}$$

We conclude that

$$\mathcal{A}^\dagger = \hat{A}^\dagger \bullet \hat{B}^\dagger. \tag{2.16}$$

We stress that

$$\left(\mathcal{A}\hat{\xi}\right)^\dagger = \left(\hat{A}\hat{\xi}\hat{B}\right)^\dagger = \hat{B}^\dagger \hat{\xi}^\dagger \hat{A}^\dagger \neq \mathcal{A}^\dagger \hat{\xi}^\dagger. \tag{2.17}$$

2. That is, given two matrices

$$\hat{A} = \begin{pmatrix} a & b \\ c & d \end{pmatrix}, \quad \hat{E} = \begin{pmatrix} e & f \\ g & h \end{pmatrix}$$

one has

$$\langle \hat{A} | \hat{E} \rangle = \begin{pmatrix} a^* & b^* & c^* & d^* \end{pmatrix} \begin{pmatrix} e \\ f \\ g \\ h \end{pmatrix} = a^* e + b^* f + c^* g + d^* h = \mathrm{Tr}\left[\hat{A}^\dagger \hat{E}\right].$$

3. There are several different notations in literature to indicate Hermitian conjugation, and the symbol † is used with different meanings. In particular, Carmichael in [110] uses the symbol $\hat{A}^\dagger$ to indicate a conjugate "associated" superoperator.

2.1.3 The Lindblad form

Having provided the general properties of any quantum map $\mathcal{M}$, we are now interested in the specific map describing the time evolution of the density matrix $\hat{\rho}$ of a system weakly coupled to its environment. First, we make the hypotheses that the environment is much "bigger" than the system, and therefore at all times it remains "close" to its equilibrium. That is, the system does not change the properties of the environment (*Born approximation*). Consequently, it is natural to assume that the Kraus operators are time independent. The density operator will evolve (smoothly) as

$$\hat{\rho}(t+\tau) = \mathcal{M}\hat{\rho}(t) = \sum_{\mu} \hat{M}_{\mu}^{\dagger}\hat{\rho}(t)\hat{M}_{\mu} = \hat{\rho}(t) + \tau\frac{\mathrm{d}\hat{\rho}(t)}{\mathrm{d}t} + \mathcal{O}(\tau^2). \tag{2.18}$$

If mathematically the time interval τ must be "infinitesimal", from a physicist perspective it should be handled with some care. It must be small at the scale of the system dynamics Δt_S (i.e. small compared to all characteristic timescales and relaxation times), so that the modification of $\hat{\rho}$ is only incremental. On the other hand, it must be much longer than the correlation time of the environment Δt_E, so that there are no remaining coherent effects in the system-reservoir interaction. In the limit in which $\Delta t_E \ll \Delta t_S$, the environment can be thought as memoryless, and we can assume that it is always in its thermal-equilibrium state, i.e., disentangled from the system. In other words, we are assuming that the environment is a *Markovian* bath for the system.

By considering the appropriate limit $\tau \to 0$, one can arrange the Kraus operators in Eq. (2.18) so that one is of the order of unity, while all the others are of order $\sqrt{\tau}$: [4]

$$\begin{cases} \hat{M}_0 = \mathbb{1} - \mathrm{i}\hat{K}\tau \\ \hat{M}_{\mu} = \sqrt{\tau}\hat{\Gamma}_{\mu} \qquad \text{for } \mu \neq 0 \end{cases} \tag{2.19}$$

The operator $\hat{K}$ can be split in an Hermitian part, $\hat{I} = (\hat{K} + \hat{K}^{\dagger})/2$, and an anti-hermitian one $\hat{J} = \mathrm{i}(\hat{K} - \hat{K}^{\dagger})/2$, so that $\hat{K} = \hat{I} - \mathrm{i}\hat{J}$. To the first order in τ one finds

$$\hat{M}_0^{\dagger}\hat{\rho}(t)\hat{M}_0 = \hat{\rho}(t) - \mathrm{i}\tau\left[\hat{I}, \hat{\rho}(t)\right] - \tau\left\{\hat{J}, \hat{\rho}(t)\right\} + \mathcal{O}(\tau^2), \tag{2.20}$$

where $[\bullet, \bullet]$ indicates the commutator and $\{\bullet, \bullet\}$ is the anticommutator. By using the normalisation condition of the Kraus operators, one has

$$\mathbb{1} = \sum_{\mu} \hat{M}_{\mu}^{\dagger}\hat{M}_{\mu} = \hat{M}_0^{\dagger}\hat{M}_0 + \tau\sum_{\mu\neq 0} \hat{\Gamma}_{\mu}^{\dagger}\hat{\Gamma}_{\mu} + \mathcal{O}(\tau^2) = \mathbb{1} - 2\tau\hat{J} + \tau\sum_{\mu\neq 0} \hat{\Gamma}_{\mu}^{\dagger}\hat{\Gamma}_{\mu} + \mathcal{O}(\tau^2). \tag{2.21}$$

Considering limit $\tau \to 0$, we conclude $\hat{J} = \sum_{\mu\neq 0} \hat{\Gamma}_{\mu}^{\dagger}\hat{\Gamma}_{\mu}/2$. Therefore, the dynamics of $\hat{\rho}(t)$ is dictated by an equation of the form

$$\hat{\rho}(t+\tau) = \hat{\rho}(t) - \mathrm{i}\tau\left[\hat{I}, \hat{\rho}(t)\right] + \tau\sum_{\mu\neq 0}\left(\hat{\Gamma}_{\mu}\hat{\rho}(t)\hat{\Gamma}_{\mu}^{\dagger} - \frac{1}{2}\hat{\Gamma}_{\mu}^{\dagger}\hat{\Gamma}_{\mu}\hat{\rho}(t) - \frac{1}{2}\hat{\rho}(t)\hat{\Gamma}_{\mu}^{\dagger}\hat{\Gamma}_{\mu}\right). \tag{2.22}$$

Eq. (2.22) means that $\hat{\rho}(t)$ evolves smoothly in time under the action of a completely-positive, trace-preserving linear map. Indeed, no assumptions have been made about the nature of the operators $\hat{I}$ and $\hat{\Gamma}_{\mu}$.

4. Indeed, one need a part of the quantum map $\mathcal{M}$ which is proportional to the identity, and the rest which is proportional to τ. Therefore, the most general form allowed for the Kraus operator is the one in Eq. (2.19).

To grasp their meaning, however, we can use the analogy with the isolated systems. In this case, the time evolution is dictated by

$$\hat{\rho}(t+\tau) = \hat{\rho}(t) - \mathrm{i}\tau \left[\hat{H}, \hat{\rho}(t)\right], \tag{2.23}$$

where $\hat{H}$ is the Hamiltonian of the isolated system. Comparing Eqs. (2.23) and (2.22), is clear that $\hat{I}$ plays the role of a coherent Hamiltonian evolution. As it will be clarified in Sec. 2.1.4, $\hat{\Gamma}_\mu$ are called jump operators and describe the coupling with the environment. If there are no coherent process linking the environment to the system and their interaction is purely dissipative, one has $\hat{I} = \hat{H}$. We finally obtain the master equation in the Lindblad form [23–27, 111, 114]

$$\frac{\partial \hat{\rho}(t)}{\partial t} = -\mathrm{i}\left[\hat{H}, \hat{\rho}(t)\right] + \sum_{\mu\neq 0}\left(\hat{\Gamma}_\mu \hat{\rho}(t)\hat{\Gamma}_\mu^\dagger - \frac{1}{2}\hat{\Gamma}_\mu^\dagger\hat{\Gamma}_\mu\hat{\rho}(t) - \frac{1}{2}\hat{\rho}(t)\hat{\Gamma}_\mu^\dagger\hat{\Gamma}_\mu\right). \tag{2.24}$$

Radiative damping in an optical cavity: an explicit example

The previous general derivation does not tell much about the operators $\hat{\Gamma}_\mu$. In Sec. 2.1.4, we will discuss a method allowing to guess the form of the jump operators. Here, instead, we derive the evolution equation starting from a microscopic description of the electromagnetic field in an optical cavity. We anticipate that we will recover the same form of the Linblad master equation (2.24).

Let us consider a one-mode optical cavity, where the EM field is confined between two high-quality mirrors. In first approximation, all photons inside the cavity have the same frequency ω_c. Thus, discarding the constant $\omega/2$ term, the Hamiltonian reads

$$\hat{H}_C = \omega_c \hat{a}^\dagger \hat{a}. \tag{2.25}$$

The environment, instead, is described as the collection of infinitely many harmonic oscillators, as discussed in Sec. 1.1.2. Therefore, its Hamiltonian is

$$\hat{H}_E = \int_0^\infty \mathrm{d}\omega\, \omega\, \hat{b}^\dagger(\omega)\hat{b}(\omega). \tag{2.26}$$

We suppose that the system and the environment are coupled via

$$\hat{H}_I = \int \mathrm{d}\omega\, g(\omega)(\hat{a} + \hat{a}^\dagger)(\hat{b}(\omega) + \hat{b}^\dagger(\omega)). \tag{2.27}$$

The evolution of the cavity coupled to the environment is

$$-\mathrm{i}\partial_t |\Psi\rangle = (\hat{H}_C + \hat{H}_E + \hat{H}_I)|\Psi\rangle, \tag{2.28}$$

where $|\Psi\rangle$ is the wave function describing the system and the environment.

To simplify the problem, we pass in the interaction picture, i.e. we introduce $|\tilde{\Psi}\rangle = \hat{U}(t)|\Psi\rangle$, where $\hat{U}(t) = \exp[\mathrm{i}(\hat{H}_C + \hat{H}_E)t]$. We have

$$-\mathrm{i}\partial_t |\tilde{\Psi}\rangle = \hat{\tilde{H}}|\tilde{\Psi}\rangle, \tag{2.29}$$

where the interaction Hamiltonian

$$\hat{\tilde{H}} = \hat{U}(t)\hat{H}_I\hat{U}^\dagger(t) = \int_0^\infty \mathrm{d}\omega g(\omega)\left(\hat{a}e^{-\mathrm{i}\omega_c t} + \hat{a}^\dagger e^{\mathrm{i}\omega_c t}\right)\left(\hat{b}(\omega)e^{-\mathrm{i}\omega t} + \hat{b}^\dagger(\omega)e^{\mathrm{i}\omega t}\right) \tag{2.30}$$

can be easily obtained exploiting $e^{\mathrm{i}\omega_c\hat{a}^\dagger\hat{a}t}\hat{a} = e^{-\mathrm{i}\omega_c t}\hat{a}e^{\mathrm{i}\omega_c\hat{a}^\dagger\hat{a}t}$ (a similar relation exists for $\hat{b}(\omega)$). When we expand the product of exponentials, we get two terms: one depending on $\omega_c - \omega$ and one on $\omega_c+\omega$. We can thus perform a secular approximation, that is, in the limit of small interactions we can neglect the fast oscillating terms. Intuitively, when integrating over a period $t = 2\pi/(\omega_c - \omega)$, the fast frequencies will average to zero in the Schrödinger equation. This simplification, known as rotating wave approximation, gives

$$\hat{\tilde{H}}(t) = \int_0^\infty \mathrm{d}\,\omega g(\omega)\left(\hat{a}\hat{b}^\dagger(\omega)e^{-\mathrm{i}(\omega_c-\omega)t} + \hat{a}^\dagger\hat{b}(\omega)e^{\mathrm{i}(\omega_c-\omega)t}\right). \tag{2.31}$$

Again, if $g(\omega)$ is small, in the previous integral the only terms which will be relevant are those for which $\omega_c - \omega \simeq 0$. Thus, we can send the integration limit towards $-\infty$. Moreover, we suppose a sufficiently regular $g(\omega)$, so that $g(\omega) \simeq g(\omega_c) \equiv \sqrt{\gamma/2\pi}$ if $\omega \simeq \omega_c$. Physically, γ represent the decay rate (i.e. the inverse of the lifetime) of a photon inside the cavity. Hence

$$\hat{\tilde{H}}(t) = \sqrt{\frac{\gamma}{2\pi}}\left(\hat{a}\hat{b}^\dagger(t) + \hat{a}^\dagger\hat{b}(t)\right), \tag{2.32}$$

where we define

$$\hat{b}(t) \equiv \int_{-\infty}^{+\infty} \mathrm{d}\omega\, \hat{b}(\omega)e^{\mathrm{i}(\omega_c-\omega)t}. \tag{2.33}$$

The definition of $\hat{b}(t)$ implies that $[\hat{b}(t), \hat{b}^\dagger(t')] = \delta(t - t')$. Indeed, we are assuming that the environment does not have memory about its previous states, i.e. it is *Markovian*.

We are now interested in computing the state of the system neglecting the environment. To do that, we introduce the density matrix $\hat{\tilde{\rho}}_{SE}(t) = |\tilde{\Psi}(t)\rangle\langle\tilde{\Psi}(t)|$. Formally, we obtain its time evolution as

$$\hat{\tilde{\rho}}_{SE}(t) = \hat{\tilde{\rho}}_{SE}(0) - \mathrm{i}\int_0^t \mathrm{d}t' \left[\hat{\tilde{H}}(t'), \hat{\tilde{\rho}}_{SE}(t')\right] \tag{2.34}$$

and therefore

$$\partial_t\hat{\tilde{\rho}}_{SE}(t) = -\mathrm{i}\left[\hat{\tilde{\rho}}_{SE}(0), \hat{\tilde{H}}(t)\right] - \int_0^t \mathrm{d}t' \left[\hat{\tilde{H}}(t), \left[\hat{\tilde{H}}(t'), \hat{\tilde{\rho}}_{SE}(t')\right]\right] \tag{2.35}$$

We assume that the interaction term $\hat{\tilde{H}}(t)$ is too weak to create a significant correlation between the system and the bath. Furthermore, we also assume that any excitation of the environment due to its interaction with the system is dispersed on the infinitely many environment degrees of freedom. These approximations, collectively known as the *Born approximation*, allow to consider that $\hat{\tilde{\rho}}_{SE}(t) \simeq \hat{\tilde{\rho}}_S(t) \otimes \hat{\rho}_E$, where $\hat{\rho}_E$ remain mostly unperturbed along the dynamics. If $\omega_c \ll k_B T$, where k_B is the Boltzmann constant and T is the temperature of the bath, we can assume that the environment has always zero excitations in those degrees of freedom which can effectively couple with the system. Hence, $\hat{\rho}_E = \bigotimes_\omega |0\rangle\langle 0|$, where $\bigotimes_\omega$ indicates the tensor product over all the frequencies ω. We can now take the partial trace over the degrees of freedom of the environment, obtaining

$$\partial_t\hat{\tilde{\rho}}_S(t) = \partial_t \mathrm{Tr}_E\left[\hat{\tilde{\rho}}_{SE}(t)\right] = \frac{\gamma}{2}\left(2\hat{a}\hat{\tilde{\rho}}_S(t)\hat{a}^\dagger - \hat{a}^\dagger\hat{a}\hat{\tilde{\rho}}_S(t) - \hat{\tilde{\rho}}_S(t)\hat{a}^\dagger\hat{a}\right). \tag{2.36}$$

Finally, by considering again the Schrödinger representation $\hat{\rho}_S = e^{-\mathrm{i}\hat{H}_c t}\hat{\tilde{\rho}}_S e^{\mathrm{i}\hat{H}_c t}$ we obtain the following master equation for a damped Harmonic oscillator:

$$\partial_t\hat{\rho}_S(t) = -\mathrm{i}\left[\hat{H}_c, \hat{\rho}_S(t)\right] + \frac{\gamma}{2}\left(2\hat{a}\hat{\rho}_S(t)\hat{a}^\dagger - \hat{a}^\dagger\hat{a}\hat{\rho}_S(t) - \hat{\rho}_S(t)\hat{a}^\dagger\hat{a}\right). \tag{2.37}$$

Indeed, Eq. (2.37) has the Linblad form presented in Eq. (2.24).

The driving

In the previous discussion, we made the hypotheses that the system is weakly coupled to the environment, and that the infinitely-many degrees of freedom of the environment remain unchanged by the system. If, instead, there exists a part of the environment which coherently exchanges excitations with the system, it will result in an additional effective term in the Hamiltonian.

For example, we can include a coherent driving term representing the excitation of the cavity mode by an external laser of frequency ω_0. This coupling is described via

$$\hat{H}_{\text{drive}} = g(\omega_0)(\hat{a}^\dagger \hat{d} + \hat{a}\hat{d}^\dagger), \tag{2.38}$$

where $\hat{d}$ is the annihilation operator of the Laser field at a frequency ω_0. If we suppose that the environment always remains in the coherent state $|\beta\rangle$ of the $\hat{d}$ operator [5], by partial tracing over the environment we have

$$\hat{H}_{\text{drive}} = F\hat{a}^\dagger + F^*\hat{a}, \tag{2.39}$$

where $F = g\beta$. In this regard, we will often encounter Hamiltonian operators describing a coherent drive.

More general drives can be introduced, as long as $\hat{H}_{\text{drive}}$ is weak compared to the system Hamiltonian $\hat{H}$. Indeed, if the drive is too strong, the Born and Markov approximations, necessary to obtain Eq. (2.24) may not be valid.

The Liouvillian superoperator and the steady-state solution

As we previously said, the Lindblad master equation (2.24) is linear in $\hat{\rho}(t)$. Hence, it is possible to associate to it the so-called Liouvillian superoperator $\mathcal{L}$, defined via

$$\partial_t \hat{\rho}(t) = \mathcal{L}\hat{\rho}(t) = -\mathrm{i}\left[\hat{H}, \hat{\rho}(t)\right] + \sum_{\mu\neq 0} \mathcal{D}[\hat{\Gamma}_\mu], \tag{2.40}$$

where $\mathcal{D}[\hat{\Gamma}_\mu]$ is the dissipator, acting as

$$\mathcal{D}[\hat{\Gamma}_\mu]\bullet = \hat{\Gamma}_\mu \bullet \hat{\Gamma}_\mu^\dagger - \frac{1}{2}\hat{\Gamma}_\mu^\dagger\hat{\Gamma}_\mu \bullet - \frac{1}{2}\bullet \hat{\Gamma}_\mu^\dagger\hat{\Gamma}_\mu. \tag{2.41}$$

The superoperator $\mathcal{L}$ is trace-preserving and generates a completely positive map, since it is associated to the Lindblad master equation. Accordingly, the formal solution of Eq. (2.24) is $\hat{\rho}(t) = e^{\mathcal{L}t}\hat{\rho}(0)$, for an initial condition $\hat{\rho}(0)$ [22, 24–26]. For a time-independent Liouvillian, there always exists at least one steady state (if the dimension of the Hilbert space is finite [22, 23]), i.e., a matrix such that

$$\mathcal{L}\hat{\rho}_{ss} = 0. \tag{2.42}$$

This equation means that the steady-state density matrix is an eigenmatrix of the superoperator $\mathcal{L}$ corresponding to the zero eigenvalue. The procedure to explicitly obtain $\bar{\bar{\mathcal{L}}}$ is presented in App. E.3. If the steady-state in unique, for any initial state $\hat{\rho}(0)$ we have that:

$$\hat{\rho}_{ss} = \lim_{t\to\infty} \hat{\rho}(t) = \lim_{t\to\infty} e^{\mathcal{L}t}\hat{\rho}(0). \tag{2.43}$$

5. The coherent state $|\beta\rangle$ can be defined as that state for which $\hat{d}\,|\beta\rangle = \beta\,|\beta\rangle$. See Sec. 2.3.1 and App. B.

2.1.4 Quantum jumps

Having provided a physical interpretation to the coherent evolution in terms of the Hamiltonian of the isolated system, one still has to determine the form of $\hat{\Gamma}_\mu$. To do that, we exploit the close analogy between the Kraus operators and the formalism of generalised measures.

Read and unread measurements

The framework to discuss generalised quantum measurement is provided by the formalism of positive-operator valued measures (POVM)[111, 113]. Consider a measure whose outcomes r are associated to a measure operator $\hat{M}_r$. Upon measuring the result r, the density matrix is modified as

$$\hat{\rho}_r = \frac{\hat{M}_r \hat{\rho} \hat{M}_r^\dagger}{\mathrm{Tr}\left[\hat{M}_r \hat{\rho} \hat{M}_r^\dagger\right]} \equiv \frac{\mathcal{M}_r \hat{\rho}}{\mathrm{Tr}[\mathcal{M}_r \hat{\rho}]}, \tag{2.44}$$

that is, the density matrix $\hat{\rho}_r$ is obtained by "projecting" $\hat{\rho}$ onto the measure operators associated to the outcome r. In this regard, the superoperator $\mathcal{M}_r = \hat{M}_r \bullet \hat{M}_r^\dagger$ describe the measure process having obtained the result r. Each one of those outcomes has a probability $p_r = \mathrm{Tr}\left[\hat{M}_r \hat{\rho} \hat{M}_r^\dagger\right]$. In order to assure $\sum_r p_r = 1$ we must require

$$\sum_r \hat{M}_r^\dagger \hat{M}_r = \mathbb{1}. \tag{2.45}$$

The POVM formalism generalises projective measures formalism [111, 113], allowing for a description of measurements associated to non self-adjoint operators.

In Eq. (2.44) we assumed to know which was the result of the measurement. If, however, we ignore the result but we know a measure took place, we can describe the density matrix after the measure as a statistical mixture of all the possible outcomes. That is, for an *unread measure* we have

$$\hat{\rho}' = \sum_r p_r \hat{\rho}_r = \sum_r \hat{M}_r \hat{\rho} \hat{M}_r^\dagger = \sum_r \mathcal{M}_r \hat{\rho}. \tag{2.46}$$

We also notice that the density matrix for an unread measure is identical to the one describing the mean result of several read measures.

Dissipation as a measure

Let us consider a system in which $\hat{H} = 0$ and there exist a unique dissipator $\hat{\Gamma}$. In this case, Eq. (2.19) is:

$$\begin{cases} \hat{M}_0 = \mathbb{1} - \dfrac{\tau}{2} \hat{\Gamma}^\dagger \hat{\Gamma}, \\ \hat{M}_1 = \sqrt{\tau} \hat{\Gamma}, \end{cases} \tag{2.47}$$

and Eq. (2.22) becomes:

$$\hat{\rho}(t+\tau) = \hat{M}_0 \hat{\rho}(t) \hat{M}_0^\dagger + \hat{M}_1 \hat{\rho}(t) \hat{M}_1^\dagger = \mathcal{M}_0 \hat{\rho}(t) + \mathcal{M}_1 \hat{\rho}(t), \tag{2.48}$$

where we recall $\mathcal{M}_\mu = \hat{M}_\mu \bullet \hat{M}_\mu^\dagger$. We notice that $\mathcal{M}_0 + \mathcal{M}_1$ can be interpreted as measure superoperators since $\hat{M}_\mu$ are POVM. Moreover, with a probability of order one, the quantum

state of the system is unchanged ($\hat{M}_0 \simeq \mathbb{1}$) or, with probabilities of order τ, the system undergoes a large evolution (described by $\hat{M}_1\hat{\rho}(t)\hat{M}_1^\dagger$). [6] We can therefore interpret the Linblad master equation as the the time evolution of a system subject to a *continuous and unread measure* [25].

We have, thus, a very simple path to guide us in writing the proper Lindblad master equation for any system, since this picture can be easily generalized both to a nonzero Hamiltonian and to several $\hat{\Gamma}_\mu$. Accordingly, the various $\hat{\Gamma}_\mu$ are *jump operators* describing a random (perhaps large) evolution of the system which suddenly changes under the influence of the environment. Of course, the density matrix $\hat{\rho}(t)$ evolves continuously, since the probability of a quantum jumps is finite and proportional to the time step τ.

The interest of the method is that, in many cases, the nature of the quantum jumps can be guessed from the mere nature of the system. Once again, we stress that the jump operators are not uniquely defined, since the same relaxation processes can be modelled in different ways, resulting in different unrevealing of the master equation. In some situations, the nature of the coupling to the environment may privilege one of these unravellings. For instance, for an atom completely surrounded by a photo-detector array, $\hat{\Gamma}$ correspond to a photodetection. As we will see, different unrevealing schemes may correspond to different ways of monitoring the environment (photon counters, homodyne recievers . . .). However, all the Lindblad master equations stemming from those different jump operators are equivalent one to the other.

Radiative damping in an optical cavity (again)

We saw previously that microscopic description of an optical resonator interacting with an environment at $T = 0$ leads to $\hat{\Gamma} = \hat{a}$ under the Born and Markov approximations. Here, according to the previous discussion, we consider the same system and we make the hypothesis that the environment is made of nothing but a perfect photodetector. First, the photodetector does not interact directly with the optical cavity, an therefore the Hamiltonian of the system is $\hat{H}_C$ defined in Eq. (2.25). We consider that, if a photon is emitted into the environment, it is destroyed. Thus, the operator $\hat{M}_1$ must be of the form $\hat{M}_1 = \sqrt{\tau}\sum_n c_n |n\rangle \langle n+1|$. Let us define $c_0 \equiv \sqrt{\gamma}$. If we consider a cavity with one photon inside, the operator $\hat{M}_1 |1\rangle \langle 1| \hat{M}_1^\dagger = \tau\gamma |0\rangle \langle 0|$ describes the probability that in a time τ a photon is emitted. We conclude that γ is the mean lifetime of one photon inside the cavity. Now, if we have n identical photons inside the cavity, we must require that this probability is n times bigger. We conclude that $c_n = \sqrt{\gamma}\sqrt{n}$. But, by definition, $\hat{a} = \sqrt{n}\sum_n \sqrt{n} |n\rangle \langle n+1|$. Hence, $\hat{M}_1 = \sqrt{\tau}\hat{a}$, and therefore $\hat{\Gamma} = \sqrt{\gamma}\hat{a}$. The time evolution of $\hat{\rho}(t)$ is thus

$$\partial_t\hat{\rho}(t) = -\mathrm{i}\left[\hat{H}_C, \hat{\rho}(t)\right] + \frac{\gamma}{2}(2\hat{a}\hat{\rho}(t)\hat{a}^\dagger - \hat{a}^\dagger\hat{a}\hat{\rho}(t) - \hat{\rho}(t)\hat{a}^\dagger\hat{a}). \tag{2.49}$$

Clearly, Eqs. (2.37) and (2.49) coincide.

2.2 The stochastic Schrödinger equation

In Sec. 2.1.4 we saw that the structure of the Lindblad master equation admits an interpretation in terms of a continuous and unread measure. The question now is which kind

6. In this sense, the factor $\tau\hat{\Gamma}^\dagger\hat{\Gamma}/2$ in $\hat{M}_0$ can be interpreted as the backaction of the measure, introducing a normalisation term needed to preserve the trace of the density matrix.

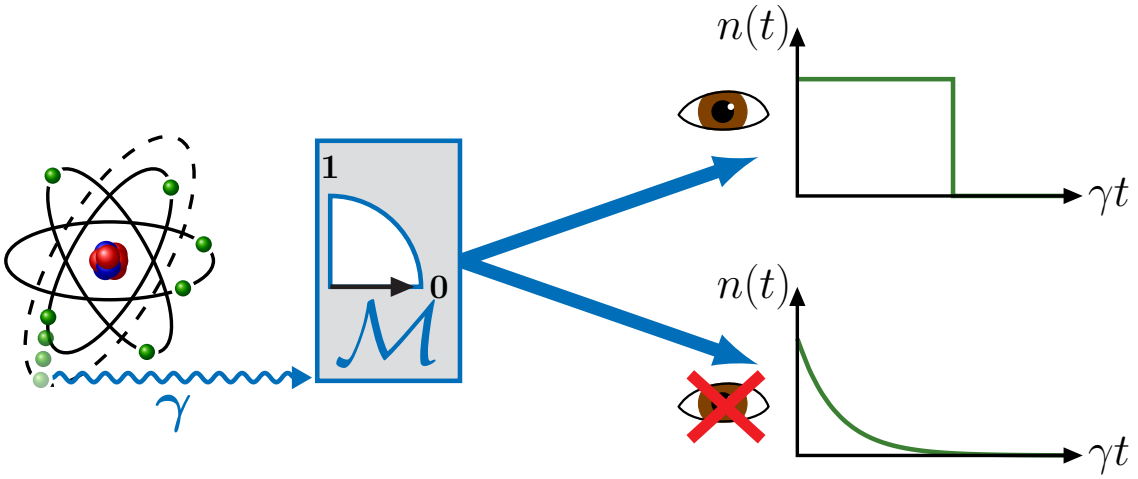

Figure 2.1 – Scheme of an apparatus measuring the spontaneous emission of an atom. The time evolution of $n(t)$ (defined in the main text) is due to a Linblad master equation (unread measure bottom) or to a stochastic process (read measure top).

of evolution does the system undergoes if we, instead, keep track of the results of such a measure.

To explain the qualitative difference between a read and an unread measure procedure, we consider the following example. An atom is prepared in an excited state $|e\rangle$. At any time, it may emit a photon into the environment, passing into its ground state $|g\rangle$. A perfect photodetector immediately signals such an event, thus destroying the photon (c.f. Fig. 2.1). The quantity $n(t) = \langle \hat{n}(t) \rangle$, where $\hat{n} = |e\rangle\langle e|$, indicates whether the system is in its excited or ground state. If we do not read the photodetector, we provide a probabilistic description of the system, so that $n(t)$ evolves smoothly towards 0 in accordance to Eq. (2.49). On the contrary, if the result of the measure is read, we are certain of the state of the atom: either in the excited state or in the ground one. The time evolution of $n(t)$ will therefore be of stochastic nature: at any moment the photon may be detected, corresponding to an abrupt jump of $n(t)$. The equation of motion for a system whose environment is continuously and perfectly probed is called a quantum trajectory [25, 110, 111, 115, 116].

2.2.1 Jump-counting trajectories

Suppose there exist a system whose coherent evolution is dictated by $\hat{H}$, and the environment can be modelled with a single jump operator $\hat{\Gamma}$. We continuously measure it at a rate τ with an instrument characterised by two possible outcomes: $r = 0$, associated to the superoperator $\mathcal{M}_0$, and $r = 1$, associated to $\mathcal{M}_1$. We recall $\mathcal{M}_\mu = \hat{M}_\mu \bullet \hat{M}_\mu^\dagger$ and

$$\begin{cases} \hat{M}_0 = \mathbb{1} - \tau \left(\mathrm{i}\hat{H} + \frac{1}{2}\hat{\Gamma}^\dagger\hat{\Gamma} \right), \\ \hat{M}_1 = \sqrt{\tau}\hat{\Gamma}. \end{cases} \tag{2.50}$$

The probability to obtain the result $r = 1$ is

$$p(t, r = 1) = \mathrm{Tr}[\mathcal{M}_1\hat{\rho}(t)] = \tau \mathrm{Tr}\left[\hat{\rho}(t)\hat{\Gamma}^\dagger\hat{\Gamma}\right], \tag{2.51}$$

and the one to obtain $r = 0$ is $p(t, r = 0) = 1 - p(t, r = 1)$. In the limit $\tau \to 0$, at almost all times the result of the continuous measurement will be $r = 0$, and the system will undergo a

smooth (but not unitary) evolution dictated by $\mathcal{M}_0$. At random times, whose mean rate is $p(t, r = 1)$ the system will, instead, experience a finite evolution due to the jump operator $\hat{\Gamma}$ in $\hat{M}_1$. This abrupt change in $\hat{\rho}(t)$ is called a *quantum jump*.

For sake of simplicity, let us suppose the system is in a pure state $|\psi(t)\rangle$, so that $\hat{\rho}(t) = |\psi(t)\rangle \langle\psi(t)|$ (the generalisation to mixed states can be done exploiting the linearity of any quantum map). To keep track of the continuous measure, let us define the parameter $N(t)$, which counts the number of quantum jumps which have occurred up to the time t. Accordingly, $N(t = 0) = 0$. If a quantum jumps occur between time t and $t + \tau$, the result of the measure is $r = 1$ and $N(t + \tau) = N(t) + 1$. Otherwise, if $r = 0$, $N(t + \tau) = N(t)$. Thus, we can introduce the (Itô) stochastic increment $\mathrm{d}N(t) = N(t + \tau) - N(t)$. It obeys:

$$\mathrm{d}N(t)^2 = \mathrm{d}N(t) \tag{2.52a}$$

$$E[\mathrm{d}N(t)] = p(t, r = 1) = \tau \mathrm{Tr}\left[\hat{\rho}(t)\hat{\Gamma}^\dagger\hat{\Gamma}\right] = \tau \langle\psi(t)|\hat{\Gamma}^\dagger\hat{\Gamma}|\psi(t)\rangle\,, \tag{2.52b}$$

where $E[\mathrm{d}N(t)]$ indicates the expected value of the stochastic variable $\mathrm{d}N(t)$, and the last equality follows from the hypothesis of a pure state. From the two previous conditions, it follows also $\tau \mathrm{d}N(t) = 0$.

Let us recall that a measure whose result is r transforms $\hat{\rho}(t)$ as

$$\hat{\rho}_r(t + \tau) = \frac{\hat{M}_r\hat{\rho}(t)\hat{M}_r^\dagger}{\mathrm{Tr}\left[\hat{M}_r\hat{\rho}(t)\hat{M}_r^\dagger\right]} = \frac{\hat{M}_r\,|\psi(t)\rangle\,\langle\psi(t)|\,\hat{M}_r^\dagger}{\langle\psi(t)|\hat{M}_r^\dagger\hat{M}_r|\psi(t)\rangle}, \tag{2.53}$$

where the last follows from the hypothesis of a pure state and the denominator ensures the condition $\mathrm{Tr}[\hat{\rho}(t + \tau)] = 1$. From Eq. (2.53) follows that, given an initial pure state, $\hat{\rho}(t)$ will always remain pure. Therefore, it is sufficient to consider the wave function $|\psi(t)\rangle$ to fully describe the evolution of the system.

The time evolution of $|\psi(t)\rangle$ is, thus, the following. If $\mathrm{d}N(t) = 1$, i.e., a quantum jump happens,

$$|\psi(t + \tau, \mathrm{d}N(t) = 1)\rangle = \frac{\hat{M}_0\,|\psi(t)\rangle}{\sqrt{\langle\psi(t)|\hat{M}_0^\dagger\hat{M}_0|\psi(t)\rangle}} = \frac{\hat{\Gamma}\,|\psi(t)\rangle}{\sqrt{\langle\hat{\Gamma}^\dagger\hat{\Gamma}\rangle}}, \tag{2.54}$$

where we denoted $\langle\hat{\Gamma}^\dagger\hat{\Gamma}\rangle = \langle\psi(t)|\hat{\Gamma}^\dagger\hat{\Gamma}|\psi(t)\rangle$. Otherwise, if there is no detection, $\mathrm{d}N(t) = 0$, and

$$\begin{aligned}
|\psi(t + \tau, \mathrm{d}N(t) = 0)\rangle &= \frac{\hat{M}_1\,|\psi(t)\rangle}{\sqrt{\langle\psi(t)|\hat{M}_1^\dagger\hat{M}_1|\psi(t)\rangle}} = \frac{\left[\mathbb{1} - \tau\left(\mathrm{i}\hat{H} - \frac{1}{2}\hat{\Gamma}^\dagger\hat{\Gamma}\right)\right]|\psi(t)\rangle}{\sqrt{\langle\psi(t)|\mathbb{1} - \tau\hat{\Gamma}^\dagger\hat{\Gamma} + \mathcal{O}\left(\tau^2\right)|\psi(t)\rangle}} \\
&= \left[\mathbb{1} - \tau\left(\mathrm{i}\hat{H} - \frac{1}{2}\hat{\Gamma}^\dagger\hat{\Gamma}\right)\right]\left[\mathbb{1} + \frac{\langle\hat{\Gamma}^\dagger\hat{\Gamma}\rangle}{2} + \mathcal{O}\left(\tau^2\right)\right] \\
&= \left[\mathbb{1} - \tau\left(\mathrm{i}\hat{H} + \frac{\hat{\Gamma}^\dagger\hat{\Gamma}}{2} - \frac{\langle\hat{\Gamma}^\dagger\hat{\Gamma}\rangle}{2}\right)\right]|\psi(t)\rangle\,.
\end{aligned} \tag{2.55}$$

Finally, one obtains a nonlinear stochastic Schrödinger equation of the form

$$\begin{aligned}
|\psi(t + \tau)\rangle &= \mathrm{d}N(t)\,|\psi(t + \tau, \mathrm{d}N(t) = 1)\rangle + [1 - \mathrm{d}N(t)]\,|\psi(t + \tau, \mathrm{d}N(t) = 0)\rangle \\
&= \mathrm{d}N(t)\frac{\hat{\Gamma}\,|\psi(t)\rangle}{\sqrt{\langle\hat{\Gamma}^\dagger\hat{\Gamma}\rangle}} + [1 - \mathrm{d}N(t)]\left[\mathbb{1} - \tau\left(\mathrm{i}\hat{H} + \frac{\hat{\Gamma}^\dagger\hat{\Gamma}}{2} - \frac{\langle\hat{\Gamma}^\dagger\hat{\Gamma}\rangle}{2}\right)\right]|\psi(t)\rangle\,,
\end{aligned} \tag{2.56}$$

which in its differential form becomes

$$\mathrm{d}\,|\psi(t)\rangle = \left[\mathrm{d}N(t)\left(\frac{\hat{\Gamma}}{\sqrt{\langle\hat{\Gamma}^\dagger\hat{\Gamma}\rangle}} - \mathbb{1}\right) + -\mathrm{i}\tau\hat{H}_{\text{eff}}\right]|\psi(t)\rangle\,, \tag{2.57}$$

where we used $\mathrm{d}N(t)\tau = 0$ and we introduced the effective Hamiltonian

$$\hat{H}_{\text{eff}} = \hat{H} - \mathrm{i}\frac{\hat{\Gamma}^\dagger\hat{\Gamma}}{2} + \mathrm{i}\frac{\langle\hat{\Gamma}^\dagger\hat{\Gamma}\rangle}{2}. \tag{2.58}$$

We will call Eq. (2.57) a counting stochastic Schrödinger equation, since it is a purity-preserving equation which depends on the "counting" stochastic parameter $N(t)$. We will call a solution to this equation a *counting quantum trajectory* for the system. The algorithm to numerically integrate a counting quantum trajectory, known in literature as wave function Monte Carlo [115], is detailed in App. E.4.1.

2.2.2 Homodyne trajectories

Clearly, Eq. (2.57) is not the only possible stochastic Schrödinger equation which one can obtain from a Lindblad equation: different choices of the Kraus operators would lead to different evolutions. Consider a system described by an Hamiltonian $\hat{H}$ and subject to only one jump operator $\hat{\Gamma}$. The following transformation does not modify the structure of the Lindblad master equation

$$\hat{\Gamma} \to \hat{\Gamma} + \beta, \qquad \hat{H} \to \hat{H} - \frac{\mathrm{i}\beta}{2}\left(\hat{\Gamma} - \hat{\Gamma}^\dagger\right), \tag{2.59}$$

where β is a real number. Under this transformation the measure operators of Eq. (2.50) become

$$\begin{cases} \hat{M}_0 = \mathbb{1} - \tau\left[\mathrm{i}\hat{H} + \dfrac{\beta}{2}(\hat{\Gamma} - \hat{\Gamma}^\dagger) + \dfrac{1}{2}(\hat{\Gamma}^\dagger + \beta)(\hat{\Gamma} + \beta)\right], \\ \hat{M}_1 = \sqrt{\tau}(\hat{\Gamma} + \beta). \end{cases} \tag{2.60}$$

From a physical point of view, the parameter β can be thought as a constant coherent field which is continuously measured together with the dissipated particles of our system.

One injects Eq. (2.59) into Eq. (2.57), obtaining a stochastic equation of the form

$$\begin{aligned} \mathrm{d}\,|\psi(t)\rangle = \Bigg[&\mathrm{d}N(t)\left(\frac{\hat{\Gamma} + \beta}{\sqrt{\langle(\hat{\Gamma}^\dagger + \beta)(\hat{\Gamma} + \beta)\rangle}} - \mathbb{1}\right) \\ &+\tau\left(-\mathrm{i}\hat{H} - \beta\hat{\Gamma} - \frac{\hat{\Gamma}^\dagger\hat{\Gamma}}{2} + \frac{\langle\hat{\Gamma}^\dagger\hat{\Gamma}\rangle}{2} + \frac{\beta\,\langle\hat{\Gamma}^\dagger + \hat{\Gamma}\rangle}{2}\right)\Bigg]|\psi(t)\rangle\,, \end{aligned} \tag{2.61}$$

The ideal limit of homodyne detection is when the coherent field amplitude goes to infinity. We stress that, in this limit, the number of detections per time unit is infinite, and a stochastic Schrödinger equation based on $\mathrm{d}N(t)$ is ill defined. Thus, some care needs to be taken in order to derive the appropriate limit $\beta \to \infty$. From a physical point of view, the condition $\beta \gg 1$ implies that quantum jumps will occur more frequently, but at the same time their effect on the evolution of $|\psi(t)\rangle$ is smaller. Indeed, the detected field is almost entirely due to

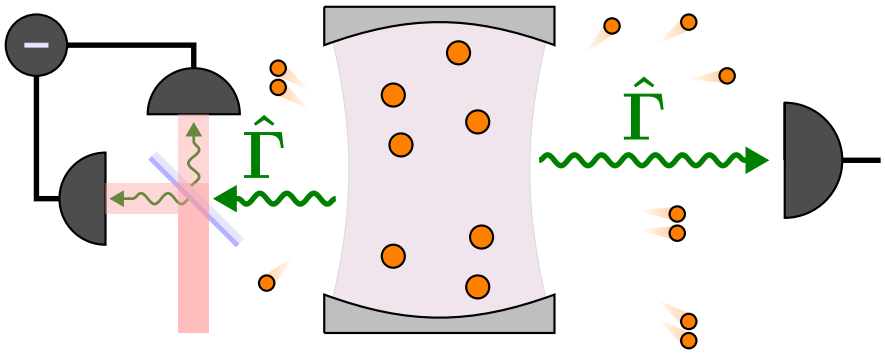

Figure 2.2 – Sketch of the two schemes of detection on a photonic cavity. On the right side, the photon counting mechanism. Every time a perfect photodetector "clicks", an observer knows that a photon has been lost by the cavity. Homodyne detection on the left. Before the measure by a perfect photodetector, the output filed of the cavity is mixed (e.g., with a beamsplitter) with a strong local filed. The statistics of "clicks" allows an observer to follow the state of the cavity.

the coherent field, and thus the measure backaction on the system must be extremely small. Here, we report only the final result (the formal derivation is provided in App. A):

$$\mathrm{d}\,|\psi(t)\rangle = \left[\mathrm{d}W(t)\left(\hat{\Gamma} - \frac{\langle\hat{\Gamma}^\dagger + \hat{\Gamma}\rangle}{2}\right) + \tau\left(-\mathrm{i}\hat{H} - \frac{\hat{\Gamma}^\dagger\hat{\Gamma}}{2} + \hat{\Gamma}\frac{\langle\hat{\Gamma}^\dagger + \hat{\Gamma}\rangle}{2} - \frac{\langle\hat{\Gamma}^\dagger + \hat{\Gamma}\rangle^2}{8}\right)\right]|\psi(t)\rangle\,, \tag{2.62}$$

where $\mathrm{d}W(t)$ is a Wiener process of variance τ and mean 0 [24, 117]. We call a solution of this equation a *homodyne quantum trajectory*. The algorithm to numerically integrate such a trajectory is detailed in App. E.4.2.

2.2.3 Physical interpretation of a quantum trajectory

A natural question is what is the relation between Eq. (2.57) and Eq. (2.24). In agreement with the previous discussion, one can think of the Linblad master equation as a continuous unread measure performed on the system, while in Eq. (2.57) one keeps track of the measure results. In the same way in which the mean over an infinite number of read measures must coincide with the expectation value of an unread one, it is possible to recover the result of the Lindblad master equation by averaging over an infinite number of quantum trajectories [24, 25, 110, 116].

Furthermore, one may try to provide some meaning to individual trajectories. Indeed, a single quantum trajectory corresponds to the simulation of an ideal experiment, in which the environment is continuously monitored by perfect instruments. In this regard, single quantum trajectories can account for actually observed features. However, the result obtained along a single quantum trajectory can strongly depend upon the choice of Kraus operators, and some care should be taken about which properties can be inferred.

Consider, for instance, the counting trajectory derived in Sec. 2.2.1 in the specific case of an optical cavity, where $\hat{\Gamma} = \sqrt{\gamma}\hat{a}$ (Fig. 2.2). Indeed, suppose we are able to build a perfect photodetector which continuously *measures the environment* and "clicks" every time it registers a photon. If we hear a "click", we know for sure that a jump has occurred and the cavity wave function has undergone a quantum jump. If no jump has occurred, instead,

the system evolves under the effective Hamiltonian $\hat{H}_{\text{eff}} = \hat{H} - \mathrm{i}\gamma\hat{a}^\dagger\hat{a}/2$.[7] Remarkably, the absence of a quantum jump does not mean that the system evolves under the effect of the Hamitonian alone, but knowing that a jump has not occurred gives us information about the state of the cavity. Indeed, the imaginary term $-\mathrm{i}\gamma\hat{a}^\dagger\hat{a}$ is the backaction of the continuous measurement of the photodetector.

Consider now Eq. (2.61) in the limit $\beta \gg 1$. Due to the fact that the cavity output field is mixed to a local reference oscillator, the detector measures a superposition of the two fields. Since the local laser is extremely strong, the detector continuously "click", and the field inside the cavity undergoes a quantum jump. However, as it stems from Eq. (2.61), the effect of such a quantum jump is minimal:

$$\frac{\hat{\Gamma}+\beta}{\sqrt{\langle(\hat{\Gamma}^\dagger+\beta)(\hat{\Gamma}+\beta)\rangle}} - \mathbb{1} = \frac{\hat{\Gamma}}{\beta} - \frac{\langle\hat{\Gamma}+\hat{\Gamma}^\dagger\rangle}{2\beta} + \mathcal{O}(\beta^{-2}). \tag{2.63}$$

Indeed, the detection will be almost entirely due to the local oscillator, and therefore the cavity wavefunction remains almost unaffected by the measure.

From an information theory perspective, the difference between the two types of trajectories reduces to the way an observer acquires information about the state of the cavity. In the counting case, the state is abruptly and randomly modified due to the great amount of information gained by one detection. In the homodyne case, instead, the state is continuously randomly changed due to the high number of detections. However, the information gained about the state of the cavity is minimal since every registered photons is in a superposition of the cavity output field and of the local oscillator.

To visualize this differences in the procedures, we simulate the radiative damping described in Sec. 2.1.3 and Sec. 2.1.4. We consider a resonator, described by an Hamiltonian $\hat{H} = \omega\hat{a}^\dagger\hat{a}$, ω being the energy of one photon in the cavity and $\hat{a}$ the annihilation operator. The coupling to the environment is via the single jump operator $\hat{\Gamma} = \sqrt{\gamma}\hat{a}$, where γ is the mean-lifetime of one photon inside the resonator. At $t = 0$, we initialise the cavity is the Fock state with ten photons, i.e. $|\psi(t=0)\rangle = |n=10\rangle$. In Fig. 2.3 we plot the mean number of photons $\langle\hat{a}^\dagger\hat{a}(t)\rangle$ along five counting and five homodyne quantum trajectories[8]. In the case of a counting trajectory [panel (a)], the evolution of the parameter $\langle\hat{a}^\dagger\hat{a}(t)\rangle$ is smooth, except in a finite number of points, where a quantum jump happens. As for the homodyne [panel (b)], instead, there are no abrupt jumps, but the evolution is a noisy one. Both procedures, once the average is taken, recover the same result [panel (c)], which coincides with the one obtained via integration of the Linblad master equation [inset of panel (c)].

2.3 Phase-space representations

In Sec. 1.1.1 we saw that it is possible to describe the state of a classical harmonic oscillator via a complex variable $\alpha(t)$ [c.f. Eqs. (1.4) and (1.5)]. Therefore, the state of a system, i.e., the set $\{x(t), p(t)\}$, is a point in the phase space $\{\mathbb{R}\mathrm{e}\left[\alpha(t)\right], \mathbb{I}\mathrm{m}\left[\alpha(t)\right]\}$.

A phase-space formulation of quantum mechanics has the same purpose. One wants to describe the density matrix of a quantum system as a superposition of "semiclassical states" $|\alpha\rangle$, i.e., those states which in the limit of many quanta recover the behaviour of the classical

7. In this discussion, we will neglected the terms ensuring the normalisation of the wave function.

8. We recall that the numerical techniques necessary to numerically simulate a quantum trajectory are detailed App. E.4.

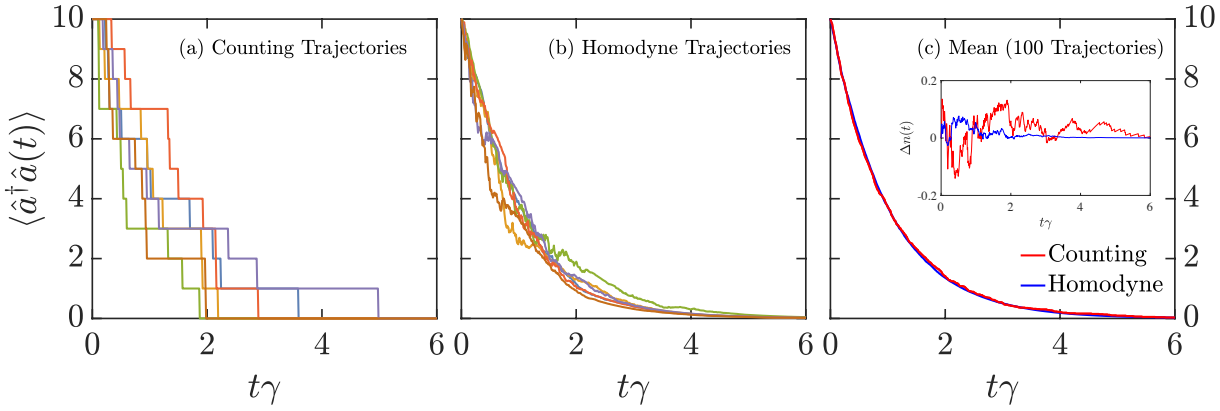

Figure 2.3 – Mean number of photon $\langle \hat{a}^\dagger \hat{a}(t) \rangle$ as a function of time for a resonator subject to dissipation. Panel (a): Counting trajectories. The wave function changes abruptly under the effect of a quantum jump. Panel(b): Homodyne trajectories. The evolution of the wave function is a noisy one. Panel (c): Average $\langle \hat{a}^\dagger \hat{a}(t) \rangle$ over 100 trajectories. The two procedures recover the same results. Inset: $\Delta n(t) = n(t) - \langle \hat{a}^\dagger \hat{a}(t) \rangle$ as a function of time, where $n(t)$ is the mean number of photons obtained via direct integration of the master equation with a cutoff of 30 photons (see App. E.1). Parameters: $\omega/\gamma = 1$.

harmonic oscillator. In this way, the system density matrix can be described in a quantum phase space $\{\mathbb{R}\mathrm{e}[\alpha], \mathbb{I}\mathrm{m}[\alpha]\}$. Instead of having a point in such a phase space, however, the density matrix of the system becomes a distribution $W_\kappa(\alpha, t)$. The index κ indicates which kind of representation are we considering, since there exists several different ones. From a quantum optics point of view, much of the interest in this approach lies in the ability to map the quantum dissipation onto a classical noise [24, 117].

2.3.1 Coherent states

As discussed in Sec. 1.1.1, the eigenstates of the harmonic-oscillator Hamiltonian are the Fock states, such that $\hat{a}^\dagger \hat{a} |n\rangle = n |n\rangle$. The number state $|n\rangle$ does not correspond at all to the classical picture of a harmonic oscillator: under the action of the Hamiltonian the state $|n\rangle$ does not oscillate. Moreover, those states have *always* zero expectation value for the displacement $\hat{x} \propto \hat{a}^\dagger + \hat{a}$ and for the momentum $\hat{p} \propto \hat{a}^\dagger - \hat{a}$. We conclude that $|n\rangle$ can never become qualitatively as a classical states, even for very big n. Intuitively, we rather visualize the harmonic oscillator has evolving in time by periodically changing its position and its momentum. Thus the question: can we construct quantum mechanical states which, in the "semiclassical" limit of many quanta, recover the same physical prediction as in classical mechanics?

The solution of the classical harmonic oscillator is a function of the form $\alpha(t) = (\sqrt{m\omega}x(t) + \mathrm{i}p(t)/\sqrt{m\omega})/\sqrt{(2)}$ which evolves according to Eq. (1.4). The phase-space representation $\alpha(t)$ is equivalent to a displacement of the harmonic oscillator from its rest position $x = p = 0$ into $x(\alpha) = (\alpha + \alpha^*)\sqrt{2}$ and $p(\alpha) = -\mathrm{i}(\alpha - \alpha^*)\sqrt{2}$. A very educated guess to retrieve the semiclassical state comes from trying the same procedure in the quantum case. [9] In quantum mechanics, the spatial translation operator, sending the vacuum $|0\rangle$ into $|x(\alpha)\rangle$, has the form $\exp[-\mathrm{i}x(\alpha)\hat{p}]$. Similarly, one can transform the ground state of the harmonic oscillator $|0\rangle$

9. There exists several other way to obtain a definition of the coherent state, for instance in [9, 24, 25].

into a state with momentum $|p(\alpha)\rangle$ via the operator $\exp[\mathrm{i}p(\alpha)\hat{x}]$. Therefore, let us call the displacement operator [10]

$$\begin{aligned}\hat{D}(\alpha) &= \exp[-\mathrm{i}x(\alpha)\hat{p} + \mathrm{i}p(\alpha)\hat{x}] = \exp[-\frac{\mathrm{i}}{\sqrt{2m\omega}}(\alpha+\alpha^*)\hat{p} + \sqrt{\frac{m\omega}{2}}(\alpha-\alpha^*)\hat{x}] \\ &= \exp[\alpha\sqrt{\frac{m\omega}{2}}\left(\hat{x} - \frac{\mathrm{i}\hat{p}}{m\omega}\right) - \alpha^*\sqrt{\frac{m\omega}{2}}\left(\hat{x} + \frac{\mathrm{i}\hat{p}}{m\omega}\right)] = \exp[\alpha\hat{a}^\dagger - \alpha^*\hat{a}].\end{aligned} \tag{2.64}$$

In analogy to classical mechanics, where α is the displacement from the rest position $x = p = 0$, we define the coherent state $|\alpha\rangle$ as the displacement operator acting on the vacuum, i.e.,

$$|\alpha\rangle = \hat{D}(\alpha)\,|0\rangle\,. \tag{2.65}$$

The coherent state plays a fundamental role in the description of many quantum systems. We report some of its most relevant properties, as well as the demonstration that the coherent states recover the classical prediction, in App. B.

2.3.2 Quasiprobability distributions

The density matrix operator can be represented with respect to a "complete" orthonormal basis, e.g., the Fock one:

$$\hat{\rho} = \sum_{m,n} \langle m|\hat{\rho}|n\rangle\,|m\rangle\,\langle n| = \sum_{m,n} p_{m,n}\,|m\rangle\,\langle n|\,. \tag{2.66}$$

Given this representation, the density matrix can be diagonalised, obtaining:

$$\hat{\rho} = \sum_i p_i\,|\Psi_i\rangle\,\langle\Psi_i|\,. \tag{2.67}$$

where $|\Psi_i\rangle$ are the eigenvectors of $\hat{\rho}$ and p_i can be interpreted as the probability of the system to be found in the state $|\Psi_i\rangle$ upon an appropriate measure.

As we proved in Eq. (B.20), any operator can be expressed as analytic function of two complex parameters, α and β. In particular,

$$\hat{\rho} = \frac{1}{\pi^2}\iint d^2\alpha e^{-\frac{|\alpha|^2}{2}}\iint d^2\beta e^{-\frac{|\beta|^2}{2}}\rho(\alpha^*,\beta)\,|\alpha\rangle\,\langle\beta|\,, \tag{2.68}$$

This equation closely resembles Eq. (2.66), where, instead of having a matrix of coefficient $p_{m,n}$ one has a function $\rho(\alpha^*,\beta)$. What we will show is that it is possible to obtain a diagonal form of $\hat{\rho}$ on the overcomplete basis of coherent states, that is

$$\hat{\rho} = \int \mathrm{d}^2\alpha W_\kappa(\alpha)\,|\alpha\rangle\,\langle\alpha|\,, \tag{2.69}$$

where $W_\kappa(\alpha)$ is called a phase-space representation of the density matrix [118–121]. While Eq. (2.68) is unique, there exists several different forms of $W_\kappa(\alpha)$ in Eq. (2.69). While the

10. The symmetric choice of ordering in $\hat{D}(\alpha)$ seems quite arbitrary. However, exploiting the commutation relations of creation and annihilation operators, one can show that all the choices are proportional:

$$\exp[-\mathrm{i}x(\alpha)\hat{p} + \mathrm{i}p(\alpha)\hat{x}] \propto \exp[-\mathrm{i}x(\alpha)\hat{p}]\exp[\mathrm{i}p(\alpha)\hat{x}] \propto \exp[\mathrm{i}p(\alpha)\hat{x}]\exp[-\mathrm{i}x(\alpha)\hat{p}].$$

The definition we gave has the advantage that $\hat{D}(\alpha)$ is a unitary operator, i.e., $\hat{D}^\dagger(\alpha)\hat{D}(\alpha) = \mathbb{1}$.

coefficients p_i in Eq. (2.67) are probability coefficients, $W_\kappa(\alpha)$ *cannot* be interpreted as the probability to find the system in the state $|\alpha\rangle$. Indeed, we will show that W_κ has the features of a *quasiprobability* distribution.

The advantage of this framework is that, when we consider a Lindblad master equation, the time evolution of $\hat{\rho}(t)$ becomes a differential equations for the distribution $W_\kappa(\alpha, t)$.

The characteristic functions

We define the symmetrically-ordered characteristic function $\chi_0(\alpha)$ as

$$\chi_0(\alpha) = \mathrm{Tr}\left[\hat{D}(\alpha)\hat{\rho}\right], \tag{2.70}$$

so that

$$\hat{\rho} = \int \mathrm{d}^2\alpha \chi_0(\alpha)\hat{D}^\dagger(\alpha). \tag{2.71}$$

The previous equation can be proved exploiting the so-called Fourier-Weil relation (a demonstration can be found in App. C). We notice that $\chi_0(\alpha)$ plays (almost) the role of the characteristic function of a probability distribution. Indeed, consider any symmetrically-ordered correlator $(\hat{a}^{\dagger\, m}\hat{a}^n)_0$, defined as the normalised sum of products of $\hat{a}^\dagger$ and $\hat{a}$ in all possible orders (which is therefore symmetric under the exchange of $\hat{a}^\dagger$ and $\hat{a}$). [11] We have

$$\begin{aligned}\langle(\hat{a}^{\dagger\, m}\hat{a}^n)_0\rangle &= \mathrm{Tr}\left[(\hat{a}^{\dagger\, m}\hat{a}^n)_0\hat{\rho}\right] = \mathrm{Tr}\left[(\hat{a}^{\dagger\, m}\hat{a}^n)_0\hat{D}(0)\hat{\rho}\right] \\ &= \left(\frac{\partial}{\partial\alpha}\right)^m\left(-\frac{\partial}{\partial\alpha^*}\right)^n \mathrm{Tr}\left[\hat{D}(\alpha)\hat{\rho}\right]_{\alpha=0} = \left(\frac{\partial}{\partial\alpha}\right)^m\left(-\frac{\partial}{\partial\alpha^*}\right)^n \chi_0(\alpha)\Big|_{\alpha=0}\end{aligned} \tag{2.72}$$

The characteristic function can be easily generalised for normally or antinormally ordered operators. Consider the following characteristic function

$$\chi_\kappa(\alpha) = \mathrm{Tr}\left[\hat{D}(\alpha)\hat{\rho}\right] e^{\kappa|\alpha|^2/2}, \tag{2.73}$$

the previous symmetrically-ordered characteristic function having $\kappa = 0$. By exploiting $\hat{D}(\alpha) = e^{-|\alpha|^2/2}e^{\alpha\hat{a}^\dagger}e^{\alpha^*\hat{a}} = e^{|\alpha|^2/2}e^{\alpha^*\hat{a}}e^{\alpha\hat{a}^\dagger}$, we have

$$\langle(\hat{a}^{\dagger\, m}\hat{a}^n)_\kappa\rangle = \left(\frac{\partial}{\partial\alpha}\right)^m\left(-\frac{\partial}{\partial\alpha^*}\right)^n \chi_\kappa(\alpha)\Big|_{\alpha=0}, \tag{2.74}$$

where $\kappa = \pm 1$ indicates the normal or antinormal ordering: $(\hat{a}^{\dagger\, m}\hat{a}^n)_1 = \hat{a}^{\dagger\, m}\hat{a}^n$ and $(\hat{a}^{\dagger\, m}\hat{a}^n)_{-1} = \hat{a}^n\hat{a}^{\dagger\, m}$, respectively.

Normal, antinormal and symmetric quasi-probability distributions

In analogy with probability theory, we can associate to the characteristic function a distribution via a complex Fourier transform, i.e.

$$W_\kappa(\alpha) = \int \frac{\mathrm{d}^2\beta}{\pi^2}\chi_\kappa(\beta)e^{\alpha\beta^* - \alpha^*\beta}. \tag{2.75}$$

11. For example,

$$(\hat{a}^{\dagger\, 2}\hat{a})_0 = \frac{\hat{a}^{\dagger\, 2}\hat{a} + \hat{a}^\dagger\hat{a}\hat{a}^\dagger + \hat{a}\hat{a}^{\dagger\, 2}}{3}.$$

The function $W_\kappa(\alpha)$ plays the role of a quasi-probability distribution, since $\int \mathrm{d}^2\alpha W_\kappa(\alpha) = 1$ but $W_\kappa(\alpha) \not> 0$. Importantly, we have

$$\begin{aligned}\langle(\hat{a}^{\dagger\,m}\hat{a}^n)_\kappa\rangle &= \left(\frac{\partial}{\partial\beta}\right)^m\left(-\frac{\partial}{\partial\beta^*}\right)^n\chi_\kappa(\beta)\bigg|_{\beta=0} = \int \mathrm{d}^2\beta\delta^2(\beta)\left[\left(\frac{\partial}{\partial\beta}\right)^m\left(-\frac{\partial}{\partial\beta^*}\right)^n\chi_\kappa(\beta)\right]\\ &= \iint\frac{\mathrm{d}^2\alpha\mathrm{d}^2\beta}{\pi}e^{\alpha\beta^*-\alpha^*\beta}\left[\left(\frac{\partial}{\partial\beta}\right)^m\left(-\frac{\partial}{\partial\beta^*}\right)^n\chi_\kappa(\beta)\right]\\ &= \iint\frac{\mathrm{d}^2\alpha\mathrm{d}^2\beta}{\pi}\alpha^{*\,m}\alpha^n e^{\alpha\beta^*-\alpha^*\beta}\chi_\kappa(\beta) = \int\mathrm{d}^2\alpha W_\kappa(\alpha)\alpha^{*\,m}\alpha^n.\end{aligned} \tag{2.76}$$

For historical reasons, the symmetritcally ordered $W_0(\alpha) \equiv W(\alpha)$ is called the Wigner function, while $W_1(\alpha) \equiv P(\alpha)$ is the Glauber–Sudarshan P-representation and $W_{-1}(\alpha) \equiv Q(\alpha)$ is the Husimi Q-function. From their definition it follows that

$$\hat{\rho} = \int \mathrm{d}^2\alpha P(\alpha)\,|\alpha\rangle\,\langle\alpha|\,, \tag{2.77}$$

while

$$Q(\alpha) = \langle\alpha|\hat{\rho}|\alpha\rangle\,. \tag{2.78}$$

The time evolution of the quasi-probability distribution $W_k(\alpha, t)$ is instead determined via the following mapping [120]:

$$\hat{a}\hat{\rho} \longrightarrow \left(\alpha + \frac{1-\kappa}{2}\frac{\partial}{\partial\alpha^*}\right)W_k(\alpha) \tag{2.79a}$$

$$\hat{a}^\dagger\hat{\rho} \longrightarrow \left(\alpha^* - \frac{1+\kappa}{2}\frac{\partial}{\partial\alpha}\right)W_k(\alpha) \tag{2.79b}$$

$$\hat{\rho}\hat{a}^\dagger \longrightarrow \left(\alpha^* + \frac{1-\kappa}{2}\frac{\partial}{\partial\alpha}\right)W_k(\alpha) \tag{2.79c}$$

$$\hat{\rho}\hat{a} \longrightarrow \left(\alpha - \frac{1+\kappa}{2}\frac{\partial}{\partial\alpha^*}\right)W_k(\alpha) \tag{2.79d}$$

Indeed, Eqs. (2.79) maps the Linblad master equation for the density matrix onto differential equation for the quasiprobabilities distributions.

CHAPTER 3

Phase Transitions in Driven-Dissipative Systems

One of the firsts efforts in understanding criticality in driven-dissipative systems exploiting the spectral properties of the Liouvillian is due to Kessler *et al.*. In Ref. [43], the authors present a direct and insightful analogy between thermal/quantum phase transitions in Hamiltonian systems and dissipative phase transitions in Markovian systems. In this Chapter, we extend to a general framework the seminal ideas of Ref. [43], in order to provide a common theoretical framework to describe the emergence of critical behaviour in Markovian open quantum systems, analysing both first- and second-order phase transitions. Namely, we prove the intimate connection between the spectral properties of the Liouvilllian superoperator and the emergence of criticality.

First, in Sec. 3.1 we recall some fundamental properties of classical and quantum phase transitions. We also stress why the driven-dissipative case can be profoundly different from its equilibrium counterpart. In Sec. 3.2 we introduce the theoretical framework, pointing out some general key properties of the Liouvillian superoperator and of density matrices. In Sec. 3.3 we consider first- and second-order dissipative phase transitions. We show the general form of the steady-state density matrix in the vicinity of the critical point. We determine also the form of the eigenmatrix of the Liouvillian superoperator corresponding to the non-zero eigenvalue with the smallest modulus of the real part (the so-called Liouvillian spectral gap or asymptotic decay rate). When the transition is of the first order, we show that the gap closes only at the critical point, where the stationary state is bimodal. Concerning second-order phase transitions associated to a symmetry-breaking, we provide a general spectral description proving that the Liouvillian gap remains closed in the whole region of broken symmetry. In this context, we highlight the connection between the structure of the eigenmatrices and the symmetry properties of the Lindblad master equation. Finally, in Sec. 3.4.2, we discuss why and how quantum trajectories can be used to unveil criticality.

Contents

3.1 Introduction to driven-dissipative phase transitions

Here, we briefly revise two examples of phase transitions at equilibrium, one triggered by temperature and one depending on the non-commutativity of two Hamiltonian terms. We then discuss in which aspects the driven-dissipative case is different.

3.1.1 Thermal phase transitions

Thermal "classical" phase transitions are characterised by the competition between the minimisation of energy and the maximisation of entropy [12]. This variational constraint can lead to the emergence of criticality in the thermodynamic limit. A classical example is the paramagnetic-to-ferromagnetic phase transition in the Ising model [122]. This model describes a metal as a lattice of magnetic moments (spin) which can assume only two orientations: $\sigma_i = \pm 1$, where i indicates the lattice site. Nearest-neighbours spins interact, so that two parallel spins have an energy $-J$, while two antiparallel have energy J. An external magnetic field h may be present, so that the Hamiltonian reads:

$$H = -J \sum_{\langle i,j \rangle} \sigma_i \sigma_j - h \sum_i \sigma_i. \tag{3.1}$$

The study of this textbook problem provides several insight on the nature of thermal phase transitions.

In absence of an external magnetic field, the lattice presents a Z_2 symmetry , i.e., the transformation $\sigma_i \to -\sigma_i$ for all i leaves the Hamiltonian unchanged. We conclude that, for any finite lattice, the expectation value $\langle \sigma_i \rangle = 0$. Instead, if we consider the thermodynamic limit of an infinite lattice system, we have [12, 122]:

1. For 2D (or higher dimensional) lattices, below a critical temperature $T < T_c$, there exists a spontaneous magnetisation of the lattice: a second-order transition between a paramagnetic and a ferromagnetic phase takes place.
2. Such transition is associated with the spontaneous symmetry breaking of the Z_2 symmetry of the lattice.
3. Dimensionality plays a fundamental role: in 1D chains a ferromagnetic order exists only for $T = 0$.

If there is an external magnetic field, instead:

1. For 2D (or higher dimensional) lattices, a first-order phase transition, associated to an abrupt change of the magnetisation, can take place.
2. This transition is caused by the competition between two states minimizing the thermodynamic potential.
3. The phase transition is associated to *metastability* and *hysteresis*.
4. The external magnetic field h breaks the Z_2 invariance, and therefore this phase transition is not a spontaneous symmetry breaking.

3.1.2 Quantum phase transitions

We consider now a quantum transverse Ising model at $T = 0$ [36]. Its Hamiltonian reads:

$$\hat{H} = -J \sum_{\langle i,j \rangle} \hat{\sigma}_i^z \hat{\sigma}_j^z - h \sum_i \hat{\sigma}_i^x, \tag{3.2}$$

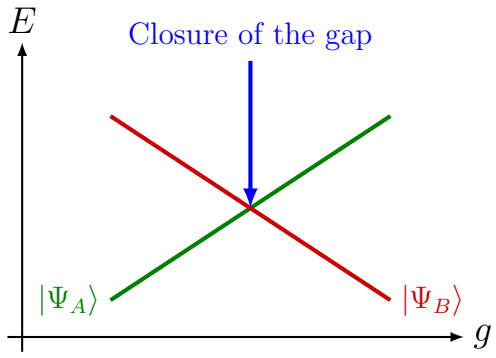

Figure 3.1 – Low-lying spectrum of a Hamiltonain depending on a parameter g. A transition describes an abrupt change in the ground state due to an exchange between two eigenvectors.

where $\hat{\sigma}_i^{x,z}$ are the Pauli matrices of the ith spin. This system has a $\hat{Z}_2$ symmetry, since the transformation $\hat{\sigma}_i^z \to -\hat{\sigma}_i^z$ leaves the Hamiltonian unchanged. We conclude that, for any finite system with $h \neq 0$, the magnetisation along z must be zero, i.e. $\sum_i \langle \hat{\sigma}_i^z \rangle = 0$. For $h = 0$, the Hamiltonian contains only the $\hat{\sigma}_i^z$ terms, and the ground state must aligned along the z direction. Conversely, in the limit $J = 0$, the ground state must be an eigenstate of $\hat{\sigma}_i^x$. Since $[\hat{\sigma}_i^x, \hat{\sigma}_i^z] \neq 0$, their competition in the determination of the ground state triggers a phase transition [36].

In this regard, quantum phase transitions present several differences with respect to their equilibrium counterparts. A classical system has zero entropy at $T = 0$, and therefore no phase transition can occur. Indeed, quantum phase transitions can only be accessed via the competition between noncommuting terms of the Hamiltonian. While thermally-driven phase transitions signal a reorganization of the system (e.g., from randomly oriented spin to a collectively ordered phase in the Ising model), quantum phase transitions describe an abrupt change in the *ground state* of the many-body system. In this regard, the Hamiltonian spectrum must present a closure of the energy gap at the critical point (see Fig. 3.1).

3.1.3 Why is driven-dissipative different?

The previous discussion about classical and quantum phase transition begs the question of why is necessary to develop a different theory for driven-dissipative critical phenomena [75]. Indeed, when considering a system of infinite size, one expects to recover the statistical mechanics paradigm: the infinitely many degrees of freedom of the environment should fix both the temperature and the chemical potential of the system.

The answer to this question is in the form of the driving and dissipation. Indeed, the system may have reached its steady state, but part of the environment may be in a non-thermal state, and remain in such state forever. In this regard, an effective current may continuously flow throughout the system, and therefore, $\hat{\rho}_{ss}$ may not be $e^{-\beta \hat{H}}$. [1] For example, consider the following configuration. A laser exciting a cavity is connected to a battery,

1. We notice that, however, any thermal state $\hat{\rho} \propto e^{-\beta \hat{H}}$ can be obtained as the steady-state of a Linblad master equation (for a specific case see, for example, Ref. [114]). Indeed, consider a system characterised by an Hamiltonian $\hat{H}$, whose eigenvectors are $|\Psi_i\rangle$ and eigenenergies E_i, such that $E_i \leq E_{i+1}$. Consider the operators

$$\hat{A} = \sum_i k_i \, |\Psi_i\rangle \langle \Psi_{i+1}| \, ,$$

which provides the necessary power. Once we switch it on, the photons enter the cavity and, thanks to the dissipation, the resonator rapidly converges towards a stationary state. The electric current of the battery, however, continuously flow, and the emitted field remains in a coherent state. That is, until the battery is decharged, thermal equilibrium cannot be reached. In the limit of an everlasting battery (i.e., the Liouvillian is time-independent), $\hat{\rho}_{ss}$ needs not obey Boltzmann statistics.

Much of the interest in studying driven-dissipative phase transitions comes from the fact that there are several terms which can compete in determining the steady state: Hamiltonian noncommuting operators, dissipation-induced fluctuations and the driving. This further enriches the panorama with respect to the equilibrium case, permitting the realisation of new phases without any equilibrium counterpart [39–42]. From a theoretical point of view, dissipative phase transitions have been discussed in a variety of systems, such as nonlinear photonic resonators [5, 53–64], exciton-polariton condensates [65–67], and spin lattices [39, 40, 43, 68–73]. The interplay between quantum fluctuations and dissipative phenomena in the determining the steady state has been addressed in [65, 74, 75] using a Keldysh formalism renormalisation approach, and via extensive numerical analysis of lattice systems [2, 3, 71].

Experimentally, the onset of criticality have been discussed in few key articles. In Ref. [50], the authors observe in a single superconducting cavity the photon-blockade breakdown phase transition predicted in Ref. [53]. The onset of a first-order phase transition associated to a bistable behaviour, predicted in Refs. [57, 59], has been addressed in Refs. [51, 52] using a semiconductor micropillars. In particular, in Ref. [51] the authors explore the dynamical optical hysteresis of a semiconductor microcavity as a function of the sweep time, demonstrating that the hysteresis area exhibit a power law decay characterising a dissipative phase transition. In Ref. [52], instead, it is proven that the asymptotic decay rate towards the steady state can be determined by measuring photon correlations in a Hanbury Brown and Twiss set-up. Using such a measure, the authors demonstrate the presence of a critical slowing down in such a system. Finally, in Ref. [45], the authors study a large arrays of microwave cavities (72 superconducting resonators). They find evidence of a dissipative phase transition, since the steady state properties dramatically change as a function of the driving strength.

The lack of a "free energy" minimisation principle for driven-dissipative systems [23–26], however, makes a general characterisation of phase transition extremely interesting, and sparks some natural questions: given the intrinsic quantum origin of drive and dissipation, what are the parallels and differences to quantum phase transitions? And to which extent can dissipative phase transitions be assimilated to thermal ones? Even if several examples of driven dissipative phase transition have been studied, a common theoretical background describing the onset of criticality is still missing. Some pioneering works managed to identify common characteristics in these phase transitions, and in what they differ from their equilibrium counterparts [43, 65, 75]. In the following, we detail the emergence of criticality in a general and model-independent framework. One of the goal of the present Chapter is to identify a general spectral mechanism which can explain these phenomena regardless to the nature of the system (bosons, fermions or spins) and dimensionality.

$$\hat{B} = \sum_i k'_i \left|\Psi_{i+1}\right\rangle \left\langle\Psi_i\right|,$$

with $k_i^2 = k_i'^2 e^{-\beta(E_i - E_{i+1})}$. The Linblad Master Equation with dissipators $\mathcal{D}[\hat{A}]$ and $\mathcal{D}[\hat{B}]$ is such that $\hat{\rho}_{ss} = e^{-\beta \hat{H}}$.

3.2 Spectral properties of Liouvillian superoperators

As we saw in Sec. 2.1.3, it is possible to associate a superoperator $\mathcal{L}$ to a Linblad master equation. In this regard, the steady state $\hat{\rho}_{ss}$ is the eigenmatrix of $\mathcal{L}$ with zero eigenvalue. However, to fully determine the dynamics of the system, the knowledge of the steady-state density matrix $\hat{\rho}_{ss}$ is not enough. Indeed, one has to know all the spectrum of the Liouvillian superoperator $\mathcal{L}$, whose eigenmatrices and eigenvalues are defined via the relation

$$\mathcal{L}\hat{\rho}_i = \lambda_i \hat{\rho}_i. \tag{3.3}$$

Equivalently, in the vector-representation, $\vec{\rho}_i$ (or $|\hat{\rho}_i\rangle$) is a right-eigenvector of the superoperator matrix $\bar{\bar{\mathcal{L}}}$. Having introduced a norm, we require the eigenstates to be normalised: $\|\hat{\rho}_i\|^2 = 1$ [2]. Since $\mathcal{L}$ is not Hermitian, its eigenvectors need not be orthogonal: $\vec{\rho}_i \cdot \vec{\rho}_j \neq 0$. Generally, the Liouvillian has an holomorphic dependence on the system parameter(s) ζ. Therefore, there might exist values of ζ for which $\mathcal{L}(\zeta)$ is not diagonalizable: this implies the existence of a degenerate eigensubspace. The eigenvalues $\lambda_i(\zeta)$ of $\mathcal{L}(\zeta)$ can be obtained via the resolution of the characteristic equation $\det\left(\bar{\bar{\mathcal{L}}}(\zeta) - \lambda_i(\zeta)\mathbb{I}\right) = 0$. A well-known result of function theory [123] guarantees that the roots of this equation are branches of analytic functions of ζ with, at most, algebraic singularities. Therefore, the number s of distinct eigenvalues of $\mathcal{L}(\zeta)$ is a constant except in a countable number of points. This ensures that if the Liouvillian has a simple spectrum on a finite region of the parameter space, it will be diagonalizable for any ζ, except the countable exceptional points. For all the systems we will consider, this condition is fulfilled far from the thermodynamic limit.

If the Liouvillian is diagonalizable, we can conveniently use the eigenstates of $\mathcal{L}$ as a basis of the Liouville space (apart from the exceptional points) [124]. Under this hypothesis, for any operator $\hat{A}$ there exists a unique decomposition

$$\hat{A} = \sum_i c_i \hat{\rho}_i. \tag{3.4}$$

It can be proved [22, 23] that $\mathbb{R}\mathrm{e}\,[\lambda_i] \leq 0, \forall i$. The real part of the eigenvalues is responsible for the relaxation towards the steady-state, $\hat{\rho}_{ss} = \lim_{t\to+\infty} e^{\mathcal{L}t}\rho(0)$. For convenience, we sort the eigenvalues in such a way that $|\mathbb{R}\mathrm{e}\,[\lambda_0]| < |\mathbb{R}\mathrm{e}\,[\lambda_1]| < \ldots < |\mathbb{R}\mathrm{e}\,[\lambda_n]|$. From this definition it follows that $\lambda_0 = 0$ and $\hat{\rho}_{ss} = \hat{\rho}_0/\mathrm{Tr}[\hat{\rho}_0]$. We can also identify another relevant quantity: the Liouvillian gap $\lambda = |\mathbb{R}\mathrm{e}\,[\lambda_1]|$, which is also called asymptotic decay rate [43], determining the slowest relaxation dynamics in the long-time limit.

For any Liouvillian, the following lemmas hold:

Lemma 3.1. *Given Eq.(3.3),* $e^{\mathcal{L}t}\hat{\rho}_i = e^{\lambda_i t}\hat{\rho}_i$.

Lemma 3.2. $\mathrm{Tr}[\hat{\rho}_i] = 0$ *if* $\mathbb{R}\mathrm{e}\,[\lambda_i] \neq 0$.

Proof. Indeed, the Liouvillian evolution conserves the trace [22, 24–26] and if $\mathbb{R}\mathrm{e}\,[\lambda_i] \neq 0$ for $t \to +\infty$ we have $e^{\mathcal{L}t}\hat{\rho}_i = e^{\lambda_i t}\hat{\rho}_i \to 0$.

■

2. The steady-state density matrix $\hat{\rho}_{ss}$ is thus proportional to the eigenstate of $\mathcal{L}$ whose eigenvalue is zero, since $\hat{\rho}_{ss}$ must satisfy $\mathrm{Tr}[\hat{\rho}_{ss}] = 1$, which may not correspond to a state with norm one.

Lemma 3.3. *If $\mathcal{L}\hat{\rho}_i = \lambda_i\hat{\rho}_i$ then $\mathcal{L}\hat{\rho}_i^\dagger = \lambda_i^*\hat{\rho}_i^\dagger$.*
This implies that, if $\hat{\rho}_i$ is Hermitian, then λ_i has to be real. Conversely, if λ_i is real and of degeneracy 1, $\hat{\rho}_i$ is Hermitian. If λ_i has geometric multiplicity n and $\mathcal{L}$ is diagonalizable, it is always possible to construct n Hermitian eigenmatrices of $\mathcal{L}$ with eigenvalue λ_i [3].

Proof.
Thanks to the master equation (2.24) we have:

$$\begin{aligned}\mathcal{L}\hat{\rho}_i^\dagger &= -\mathrm{i}\left[\hat{H},\hat{\rho}_i^\dagger\right] + \frac{\gamma}{2}\left(2\hat{a}\hat{\rho}_i^\dagger\hat{a}^\dagger - \hat{a}^\dagger\hat{a}\hat{\rho}_i^\dagger - \hat{\rho}_i^\dagger\hat{a}^\dagger\hat{a}\right)\\ &= \left(-\mathrm{i}\left[\hat{H},\hat{\rho}_i\right] + \frac{\gamma}{2}\left(2\hat{a}\hat{\rho}_i\hat{a}^\dagger - \hat{a}^\dagger\hat{a}\hat{\rho}_i - \hat{\rho}_i\hat{a}^\dagger\hat{a}\right)\right)^\dagger \\ &= (\mathcal{L}\hat{\rho}_i)^\dagger = \lambda_i^*\hat{\rho}_i^\dagger.\end{aligned} \tag{3.5}$$

If $\hat{\rho}_i$ is Hermitian, we have $\lambda_i\hat{\rho}_i = \mathcal{L}\hat{\rho}_i = \mathcal{L}\hat{\rho}_i^\dagger = \lambda_i^*\hat{\rho}_i^\dagger = \lambda_i^*\hat{\rho}_i$. Thus, we can conclude $\lambda_i = \lambda_i^*$. Conversely, in case $\lambda_i \in \mathbb{R}$ is a simple eigenvalue (i.e. with degeneracy 1), we can conclude that $\hat{\rho}_i = \hat{\rho}_i^\dagger$, and thus $\hat{\rho}_i$ is Hermitian. If the eigenvalues have geometric multiplicity n, it may happen that for some eigenmatrices $\hat{\rho}_i^\dagger \neq \hat{\rho}_i$. From Eq. (3.5) it follows $\mathcal{L}\hat{\rho}_i^\dagger = \lambda_i\hat{\rho}_i^\dagger$. In this case, we can consider the matrices $\left(\hat{\rho}_i + \hat{\rho}_i^\dagger\right)/2$ and $\mathrm{i}\left(\hat{\rho}_i - \hat{\rho}_i^\dagger\right)/2$, which are Hermitian by construction, and whose eigenvalue is λ_i.

■

Lemma 3.4. *If $\lambda_i = 0$ has degeneracy n, then there exist n independent eigenvectors of the Liouvillian (the algebraic multiplicity is identical to the geometrical one). Therefore, there exist n different steady states towards which the system can evolve, depending on the initial condition.*

Proof. We will prove this lemma by contradiction. Let us suppose that the algebraic multiplicity is greater than the geometrical one. Since the dimension of the reduced space is n, we can write the Liouvillian as a matrix acting on a basis of vector in this reduced space, i.e. the invariant space of λ_0 has a finite dimension. Since we can write the Liouvillian as a matrix, this means that we can put in its canonical Jordan form. In other words the Liouvillian acting on the vectors of this subspace can be decomposed in a diagonal part $\bar{\bar{\Lambda}}_0$ and a nilpotent matrix $\bar{\bar{N}}$ via a similarity transformation S:

$$\bar{\bar{\mathcal{L}}}_{\lambda_0} = S^{-1}\left(\bar{\bar{\Lambda}}_0 + \bar{\bar{N}}\right)S = S^{-1}\begin{bmatrix}\lambda_0 & 1 & 0 & \cdots & 0 & 0\\ 0 & \lambda_0 & 1 & \cdots & 0 & 0\\ \vdots & \ddots & \ddots & \ddots & \vdots & \vdots\\ 0 & 0 & 0 & \cdots & \lambda_0 & 1\\ 0 & 0 & 0 & \cdots & 0 & \lambda_0\end{bmatrix}S. \tag{3.6}$$

Of course, the new basis of vectors obtained by the non-unitary transformation S may not be orthonormal. The time evolution of the system is given by $e^{\bar{\bar{\mathcal{L}}}t}$, and since $\bar{\bar{\Lambda}}_0$ and $\bar{\bar{N}}$ commute,

3. The algebraic multiplicity of λ is defined as the number of times λ appears as a root of the characteristic equation. The geometric multiplicity, instead, is the maximum number of linearly independent eigenvectors associated with λ.

one has

$$
\begin{aligned}
e^{\bar{\bar{\mathcal{L}}}_{\lambda_0} t} &= S^{-1} e^{\bar{\bar{\Lambda}}_0 t} e^{\bar{\bar{N}} t} S \\
&= S^{-1} e^{\lambda_0 t} (\mathbb{1} + \bar{\bar{N}} t + \frac{(\bar{\bar{N}} t)^2}{2} + \dots \frac{(\bar{\bar{N}} t)^n}{n!}) S \\
&= S^{-1} e^{\lambda_0 t} \begin{bmatrix} 1 & t & \frac{t^2}{2} & \cdots & \frac{t^{n-1}}{(n-1)!} & \frac{t^n}{n!} \\ 0 & 1 & t & \cdots & \frac{t^{n-2}}{(n-2)!} & \frac{t^{n-1}}{(n-1)!} \\ \vdots & \ddots & \ddots & \ddots & \ddots & \ddots \\ 0 & 0 & 0 & \cdots & 1 & t \\ 0 & 0 & 0 & \cdots & 0 & 1 \end{bmatrix} S.
\end{aligned}
\tag{3.7}
$$

Since $\lambda_0 = 0$, the previous expression clearly will cause the dynamics to diverge, proving the absurd. We stress that this reasoning can not be directly extended to $\lambda_i \neq 0$ nor to infinite degeneracies $n \to \infty$.

■

3.2.1 Spectral decomposition of eigenmatrices

Let us consider a system admitting a unique steady state. To be physical, its $\hat{\rho}(t)$ must be a Hermitian, positive-definite matrix with trace equal to one. Hence, from Lemma 3.2, to ensure $\mathrm{Tr}[\rho(t)] = 1$ at every time, we must have:

$$
\hat{\rho}(t) = \frac{\hat{\rho}_0}{\mathrm{Tr}[\hat{\rho}_0]} + \sum_{i \neq 0} c_i(t) \hat{\rho}_i = \hat{\rho}_{ss} + \sum_{i \neq 0} c_i(0) e^{\lambda_i t} \hat{\rho}_i. \tag{3.8}
$$

The case of a real Liouvillian eigenvalue λ_i

When λ_i is real, $\hat{\rho}_i$ can be constructed to be Hermitian (see Lemma 3.3). Thus, it can be diagonalized, obtaining the spectral decomposition [22]

$$
\hat{\rho}_i = \sum_n p_n^{(i)} \left| \psi_n^{(i)} \right\rangle \left\langle \psi_n^{(i)} \right|, \tag{3.9}
$$

where all the $p_n^{(i)}$ must be real and $\langle \psi_n^{(i)} | \psi_m^{(i)} \rangle = \delta_{n,m}$. Moreover, since $\hat{\rho}_i$ is traceless (see Lemma 3.2 of Sec. 3.2), some of the $p_n^{(i)}$ must be positive and the others negative. We can order them in such a way to have $p_n^{(i)} > 0$ for $n \leq \bar{n}$ and $p_n^{(i)} < 0$ for $n > \bar{n}$. Thus, we have:

$$
\hat{\rho}_i \propto \hat{\rho}_i^+ - \hat{\rho}_i^-, \tag{3.10}
$$

where

$$
\begin{aligned}
\hat{\rho}_i^+ &= \sum_{n \leq \bar{n}} p_n^{(i)} \left| \psi_n^{(i)} \right\rangle \left\langle \psi_n^{(i)} \right|, \\
\hat{\rho}_i^- &= -\sum_{n > \bar{n}} p_n^{(i)} \left| \psi_n^{(i)} \right\rangle \left\langle \psi_n^{(i)} \right|
\end{aligned}
\tag{3.11}
$$

and where the $\{p_n\}$ have been normalized to ensure $\mathrm{Tr}\left[\hat{\rho}_i^+\right] = \mathrm{Tr}\left[\hat{\rho}_i^-\right] = 1$. With this definition, $\hat{\rho}_i^\pm$ are density matrices. Consequently, a state of the form $\hat{\rho}(0) = \hat{\rho}_{ss} + A\,\hat{\rho}_i$ will evolve in time as [124]

$$
\hat{\rho}(t) = \hat{\rho}_{ss} + A e^{\lambda_i t} (\hat{\rho}_i^+ - \hat{\rho}_i^-). \tag{3.12}
$$

The case of a complex Liouvillian eigenvalue λ_i

Let us now consider an eigenmatrix $\hat{\rho}_i$ with a complex eigenvalue λ_i. As it stems from Eq. (3.8), to ensure an Hermitian $\hat{\rho}(t)$ such an eigenmatrix must always appear in combination with its Hermitian conjugate $\hat{\rho}_i^\dagger$, which is also an eigenmatrix of $\mathcal{L}$ (Lemma 3.3). Thus, one can simply consider the Hermitian combinations $\hat{\rho}_i + \hat{\rho}_i^\dagger$ and $\mathrm{i}\,(\hat{\rho}_i - \hat{\rho}_i^\dagger)$. For example, given an initial condition $\hat{\rho}(0) = \hat{\rho}_{ss} + A(\hat{\rho}_i + \hat{\rho}_i^\dagger)$ with A real, one has [124]:

$$\begin{aligned}\hat{\rho}(t) &= \hat{\rho}_{ss} + A\left(e^{\lambda_i t}\hat{\rho}_i + e^{\lambda_i^* t}\hat{\rho}_i^\dagger\right) = \hat{\rho}_{ss} + A\, e^{\mathbb{R}\mathrm{e}[\lambda_i]t}\left(\hat{\rho}_i e^{\mathrm{i}\mathbb{I}\mathrm{m}[\lambda_i]t} + \hat{\rho}_i^\dagger e^{-\mathrm{i}\mathbb{I}\mathrm{m}[\lambda_i]t}\right)\\ &= \hat{\rho}_{ss} + 2A\, e^{\mathbb{R}\mathrm{e}[\lambda_i]t}\left[\left(\hat{\rho}_i + \hat{\rho}_i^\dagger\right)\cos(\mathbb{I}\mathrm{m}\left[\lambda_i\right]t) + \mathrm{i}\left(\hat{\rho}_i - \hat{\rho}_i^\dagger\right)\sin(\mathbb{I}\mathrm{m}\left[\lambda_i\right]t)\right].\end{aligned} \tag{3.13}$$

3.3 Definition and properties of dissipative phase transitions

Let us consider a system where a thermodynamic limit is obtained when a parameter $N \to +\infty$. For example, in a lattice of spins, N would be the number of lattice sites. For any finite N, the system always admits a unique steady-state solution. In the thermodynamic limit $N \to +\infty$, a transition between two different phases is characterized by the nonanalytical behavior of some ζ-independent observable $\hat{o}$ when the parameter ζ tends to the critical value ζ_c. Formally, we say that there is a phase transition of order M if

$$\lim_{\zeta\to\zeta_c}\left|\frac{\partial^M}{\partial\zeta^M}\lim_{N\to+\infty}\mathrm{Tr}[\hat{\rho}_{ss}(\zeta,N)\hat{o}]\right| = +\infty. \tag{3.14}$$

Since $\hat{o}$ does not depend on ζ, the discontinuity in Eq. (3.14) is due to a discontinuous behavior in $\hat{\rho}_{ss}(\zeta, N\to\infty)$. As proved in [123], a discontinuity of an eigenmatrix is to be associated with a level crossing in the spectrum of the Liouvillian. Since $\hat{\rho}_{ss}$ is associated to $\lambda_0 = 0$, the phase transition must coincide with the closure of the Liouvillian gap [43, 125] (indeed, in this case, is more correct to talk about *level touching*). Therefore, dissipative phase transitions are intimately connected to the emergence of multiple steady states in the thermodynamic limit $N \to +\infty$.

3.3.1 Analogies and differences with respect to the equilibrium case

The idea that a level crossing is a necessary condition in order to observe a phase transition can be traced back to perturbation theory. Indeed, in his seminal work about perturbation theory of linear operators (Ref. [123]), Kato provided a simple necessary condition to observe non-analiticitical behaviour. Consider, for example, a Hamiltonain $\hat{H}$, depending on a parameter ζ, whose eigenvalues are the energies $E_i(\zeta)$ and eigenvectors are $|\Psi_i(\zeta)\rangle$, i.e.

$$\hat{H}(\zeta) = \sum_i E_i\,|\Psi_i(\zeta)\rangle\langle\Psi_i(\zeta)|\,. \tag{3.15}$$

We are interested in the ground state $|\Psi_0(\zeta)\rangle$ whose energy is E_0. For sufficiently small perturbation $\Delta\zeta$, the state $|\Psi_0(\zeta+\Delta\zeta)\rangle$ can *always* be expressed as an power series of $\Delta\zeta$, *except if* $E_0(\zeta) = E_1(\zeta)$. In this regard, quantum phase transitions must be accompanied

by a closure of the Hamiltonian gap (cf. Fig. 3.1). Criticality can be then thought as an exchange (or mixing) between two wavefunctions.

One would be tempted to extend this interpretation to a Liouvillian system, and simply say that a phase transition is associated to an exchange between $\hat{\rho}_0(\zeta^-)$ and $\hat{\rho}_1(\zeta^-)$. However, Lemma 3.2 proves that $\mathrm{Tr}[\hat{\rho}_1(\zeta^-)] = 0$. We conclude that this simple description in terms of an exchange (or mixing) of eigenmatrices is not sufficient to capture the emergence of a phase transition in dissipative systems. On top of the theory developed by Kato, we must require that the steady-state remains *always* physically meaningful. The formalisation of this simple intuition is the key idea of this Section.

3.3.2 First-order phase transitions

In this section we consider the emergence of a first-order dissipative phase transition at $\zeta = \zeta_c$ in the thermodynamic limit $N \to +\infty$. Such a transition must be associated to the existence of two different and steady states, one for $\zeta < \zeta_c$ and the other for $\zeta > \zeta_c$, which implies that for $\zeta \neq \zeta_c$ the gap is finite:

$$\lambda_1(\zeta, N \to +\infty) \neq \lambda_0 = 0 \quad \text{for} \quad \zeta \neq \zeta_c. \tag{3.16}$$

According to our definition, a first-order dissipative phase transition occurs when Eq. (3.14) is satisfied for $M = 1$, which also corresponds to

$$\lim_{\zeta \to \zeta_c^+} \lim_{N \to +\infty} \hat{\rho}_{ss}(\zeta, N) = \hat{\rho}^+ \neq \hat{\rho}^- = \lim_{\zeta \to \zeta_c^-} \lim_{N \to +\infty} \hat{\rho}_{ss}(\zeta, N), \tag{3.17}$$

which defines ρ^+ (ρ^-) as the steady state in the thermodynamic limit right after (before) the critical point. From Eq. (3.17) we can write that $\hat{\rho}_{ss}(\zeta) = \theta(\zeta - \zeta_c)\hat{\rho}^+ + \theta(\zeta_c - \zeta)\hat{\rho}^-$ for $\zeta \neq \zeta_c$, where $\theta(x)$ is the Heaviside step function. Assuming the continuity of the Liouvillian, we can state that $\mathcal{L}(\zeta_c)\hat{\rho}^\pm = 0$ (we drop the explicit dependence on N when assuming the thermodynamic limit). This implies that $\lambda_1(\zeta_c) = \lambda_0 = 0$ and hence $\hat{\rho}_{ss}(\zeta_c)$ and $\hat{\rho}_1(\zeta_c)$ belong to the kernel spanned by $\hat{\rho}^\pm$. It is worth stressing that, in the thermodynamic limit and for $\zeta = \zeta_c$, *both* the real and imaginary part of λ_1 must vanish. Furthermore, in a first-order dissipative phase transition, the condition $\mathbb{I}\mathrm{m}\,[\lambda_1] = 0$ must hold in a finite domain of $\zeta = \zeta_c$, as a consequence of Lemma 3 [4].

Lemma 3.2 ensures that $\mathrm{Tr}[\hat{\rho}_1(\zeta)] = 0$ if $\lambda_1(\zeta) \neq 0$ (i.e., $\zeta \neq \zeta_c$). Moreover, as discussed in [123], $\lambda_1(\zeta)$ must be continuous in a domain of the parameter space around $\zeta = \zeta_c$ (c.f. Fig. 3.2). By analogy, we want also $\hat{\rho}_1(\zeta)$ to be continuous around ζ_c, and to extend the zero-trace condition we must set

$$\hat{\rho}_1(\zeta_c) \propto \hat{\rho}^+ - \hat{\rho}^-. \tag{3.18}$$

The above equation allows the identification of the states $\hat{\rho}_1^\pm$ obtained with the eigendecomposition (3.10) with the two phases $\hat{\rho}^\pm$ [Eq. (3.17)] emerging in the thermodynamic limit. Together with the continuity requirement, this allows to interpret $\hat{\rho}_1^\pm(\zeta) \simeq \hat{\rho}^\pm$ in a domain around $\zeta = \zeta_c$. In this region, since the Liouvillian gap is finite, we also have $\hat{\rho}_0(\zeta) \propto \hat{\rho}_{ss}(\zeta)$. Using that $\theta(0) = 1/2$, we can infer

$$\hat{\rho}_0(\zeta_c) \propto \hat{\rho}^+ + \hat{\rho}^-. \tag{3.19}$$

4. Since if λ_1 belongs to the spectrum of $\mathcal{L}$ so it does λ_1^*, if $\mathbb{I}\mathrm{m}\,[\lambda_1]$ vanishes only at $\zeta = \zeta_c$ there would be three zeros in the Liouvillian spectrum at $\zeta = \zeta_c$. This is in contrast with the present theory of first-order dissipative phase transitions.

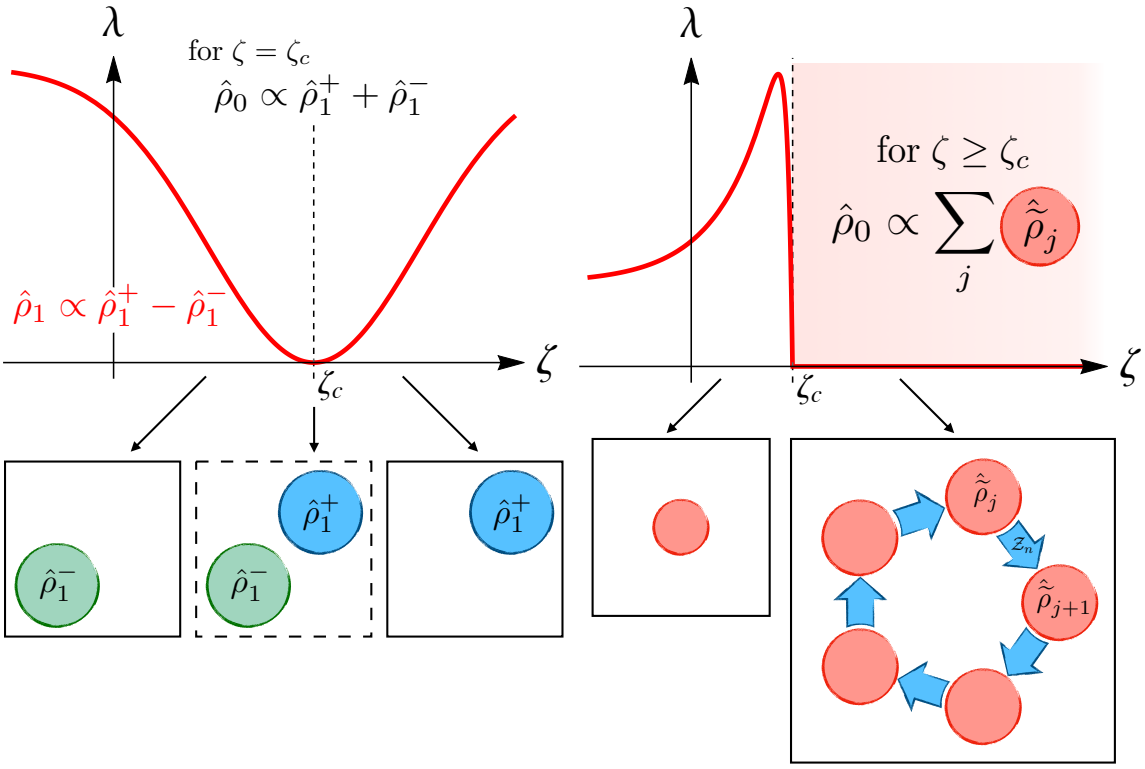

Figure 3.2 – Left: Sketch depicting the paradigm of a first-order dissipative phase transition, formally described in Sec. 3.3.2. In the thermodynamic limit, the Liouvillian gap $\lambda = |\mathbb{R}\mathrm{e}\,[\lambda_1]|$ closes when the parameter ζ of the Liouvillian assumes the critical value ζ_c. We note that, for $\zeta \simeq \zeta_c$, we must also have $\mathbb{I}\mathrm{m}\,[\lambda_1] = 0$. Just before (after) the critical point, the steady-state density matrix $\hat{\rho}_{ss} \simeq \hat{\rho}_1^-$ ($\hat{\rho}_{ss} \simeq \hat{\rho}_1^+$), which represents one of the two different phases of the system. At the critical point $\zeta = \zeta_c$, $\hat{\rho}_{ss}$ is bimodal: the steady state is a statistical mixture of $\hat{\rho}_1^+$ and $\hat{\rho}_1^-$. Right: Schematic representation of a second-order dissipative phase transition (cf. Sec. 3.3.3), associated to the breaking of a $\mathcal{Z}_n$ symmetry (in the sketch $n = 5$). In the thermodynamic limit, the Liouvillian gap λ closes over the whole region $\zeta \geq \zeta_c$, being ζ the critical parameter triggering the transition. Moreover, one has that $\lambda_0, \cdots, \lambda_{n-1} = 0$ for $\zeta \geq \zeta_c$. When $\lambda \neq 0$ (here for $\zeta < \zeta_c$), the steady-state density matrix $\hat{\rho}_{ss}$ is mono-modal. In the symmetry-broken phase ($\lambda = 0$ and $\zeta \geq \zeta_c$), $\hat{\rho}_{ss}$ is an n-modal statistical mixture of density matrices $\hat{\tilde{\rho}}_j$, which are mapped one into the other under the action of the symmetry superoperator $\mathcal{Z}_n$. Figure from Ref. [1].

Accordingly, $\hat{\rho}_0(\zeta_c)$ and $\hat{\rho}_1(\zeta_c)$ are orthogonal, since $\langle \hat{\rho}_0(\zeta_c), \hat{\rho}_1(\zeta_c) \rangle \propto \mathrm{Tr}\left[(\rho^+)^2\right] - \mathrm{Tr}\left[(\rho^-)^2\right] = 0$.

For large but finite N, provided that $|\mathbb{R}\mathrm{e}\,[\lambda_2]\,| \gg |\mathbb{R}\mathrm{e}\,[\lambda_1]\,| > 0$, Eqs. (3.18) and (3.19) are asymptotic good approximations and, since $\hat{\rho}^\pm = \hat{\rho}_1^\pm(\zeta_c, N)$, we get the asymptotic expression

$$\hat{\rho}_{ss}(\zeta_c, N) \simeq \frac{\hat{\rho}_1^+(\zeta_c, N) + \hat{\rho}_1^-(\zeta_c, N)}{2}, \tag{3.20}$$

which ensures Hermiticity and unit trace of the $\hat{\rho}_{ss}(\zeta_c, N)$. Let us note that Eq. (3.20) has a clear physical interpretation: at the critical point, for a finite-size system, the steady state is the equiprobable mixture of the two phases, which are encoded in the spectral decomposition of $\hat{\rho}_1(\zeta_c, N)$. Remarkably, in a small region at the left (right) of the critical point, $\hat{\rho}_1^+$ ($\hat{\rho}_1^-$) are metastable. This means that if the system is initialized in one of these two states it will

remain stuck, for a time proportional to $1/\lambda$, before reaching the steady-state [124]. This can gives rise to hysterical behaviour, typical of first-order phase transitions [51].

Conversely, if the Liouvillian gap closes in a point, there is criticality, i.e., $\lim_{\zeta\to\zeta_c}\lambda_1(\zeta)=0$ implies a first-order phase transition. We will prove this statement by contradiction. Let us suppose that even if $\lambda_1=0$ there is no phase transition. From the definition (3.14), we deduce that for any operator $\hat{o}$ in $\mathcal{H}\otimes\mathcal{H}$, $\langle\hat{o}(\zeta)\rangle$ is continuous in ζ_c. Hence, we have that also $\hat{\rho}_0(\zeta)$ is continuous. From Lemma 3 and 4 of Sec. 3.2, the eigenstate $\hat{\rho}_1(\zeta_c)$, being associated to $\lambda_1(\zeta_c)=0$, exists and is Hermitian. By exploiting its spectral decomposition, we can write $\hat{\rho}_1(\zeta_c)=(\hat{\rho}_1^+(\zeta_c)-\hat{\rho}_1^-(\zeta_c))/\sqrt{2}$ (we stress that here we have $\|\hat{\rho}_1^\pm(\zeta_c)\|=1$, and $\langle\hat{\rho}_1^+(\zeta_c)|\hat{\rho}_1^-(\zeta_c)\rangle=0$ by construction).

The first part of the proof is to show that, $\hat{\rho}_0(\zeta_c)=(\hat{\rho}_1^+(\zeta_c)+\hat{\rho}_1^-(\zeta_c))/\sqrt{2}$. Indeed, $\|\hat{\rho}_1(\zeta_c)\|=1$ and $e^{\mathcal{L}t}\hat{\rho}_1=\hat{\rho}_1$. Thus, exploiting the triangular inequality, we have:

$$\begin{aligned}1=\|\hat{\rho}_1(\zeta_c)\|^2=\left\|e^{\mathcal{L}t}\hat{\rho}_1(\zeta_c)\right\|^2&=\left\|e^{\mathcal{L}t}\frac{\hat{\rho}_1^+(\zeta_c)-\hat{\rho}_1^-(\zeta_c)}{\sqrt{2}}\right\|^2\\&\leq\frac{\left\|e^{\mathcal{L}t}\hat{\rho}_1^+(\zeta_c)\right\|^2+\left\|e^{\mathcal{L}t}\hat{\rho}_1^-(\zeta_c)\right\|^2}{2}\leq 1.\end{aligned}\tag{3.21}$$

It follows $\left\|e^{\mathcal{L}t}\hat{\rho}_1^\pm(\zeta_c)\right\|=1$ for every time t. Hence, $\hat{\rho}_1^\pm(\zeta_c)$ must be a linear superposition of eigematrices of the Liouvillian with zero eigenvalue. Considering that $\hat{\rho}_1(\zeta_c)=(\hat{\rho}_1^+(\zeta_c)-\hat{\rho}_1^-(\zeta_c))/\sqrt{2}$, $\|\hat{\rho}_0(\zeta_c)\|=1$, and $\langle\hat{\rho}_1^+(\zeta_c)|\hat{\rho}_1^-(\zeta_c)\rangle=0$, we obtain $\hat{\rho}_0(\zeta_c)=(\hat{\rho}_1^+(\zeta_c)+\hat{\rho}_1^-(\zeta_c))/\sqrt{2}$.

Having proved the first part, let us consider the eigendecomposition of $\hat{\rho}_1(\zeta)$ around ζ_c. Except at the critical point, we have $\lim_{t\to\infty}e^{\mathcal{L}t}\hat{\rho}_1^\pm(\zeta)=\hat{\rho}_0(\zeta)/\mathrm{Tr}\left[\hat{\rho}_1^\pm\right]$. But, by hypothesis, all function are continuous, hence:

$$\begin{aligned}\hat{\rho}_1^\pm(\zeta_c)=\lim_{\zeta\to\zeta_c}\lim_{t\to\infty}e^{\mathcal{L}t}\hat{\rho}_1^\pm(\zeta)&=\lim_{\zeta\to\zeta_c}\hat{\rho}_0(\zeta)/\mathrm{Tr}\left[\hat{\rho}_1^\pm\right]\\&=\frac{\hat{\rho}_1^+(\zeta_c)+\hat{\rho}_1^-(\zeta_c)}{2}.\end{aligned}\tag{3.22}$$

Consequently, we find that at the critical point, $\hat{\rho}_1^+(\zeta_c)=\hat{\rho}_1^-(\zeta_c)$. This statement would require that at $\zeta=\zeta_c$ $\hat{\rho}_1(\zeta_c)=0$. This statement is absurd, since proposition 4 of Sec. 3.2 guarantees that $\hat{\rho}_1(\zeta_c)$ is a well-defined eigenvector of the Liouvillian. Therefore, by contradiction, we deduce that the function $\hat{\rho}_0(\zeta)$ can not be continuous at $\zeta=\zeta_c$.

3.3.3 Second-order phase transitions with symmetry breaking

In this section, we will consider second-order dissipative phase transitions associated to a symmetry breaking. A symmetry of an open quantum system is described by a unitary superoperator $\mathcal{U}=\hat{V}\bullet\hat{V}^{-1}$ (with $\hat{V}$ unitary) [126], such that

$$\mathcal{U}^{-1}\mathcal{L}\mathcal{U}=\mathcal{L},\tag{3.23}$$

or, equivalently, $[\mathcal{L},\mathcal{U}]=0$. It follows that the matrix representations $\bar{\bar{\mathcal{U}}}$ of $\mathcal{U}$ and $\bar{\bar{\mathcal{L}}}$ of $\mathcal{L}$ can be simultaneously diagonalised. From now on, we will call the symmetry sector L_u the subspace of the Liouville space L spanned by the eigenmatrices of $\mathcal{U}$ with eigenvalue u.

The existence of a symmetry means that the Lindblad master equation cannot mix different symmetry sectors. Therefore $\bar{\bar{\mathcal{L}}}$ can be cast in a block-diagonal form:

$$\bar{\bar{\mathcal{L}}} = \begin{bmatrix} \bar{\bar{\mathcal{L}}}_{u_0} & 0 & \dots & 0 \\ 0 & \bar{\bar{\mathcal{L}}}_{u_1} & \dots & 0 \\ \vdots & \vdots & \ddots & \vdots \\ 0 & 0 & \dots & \bar{\bar{\mathcal{L}}}_{u_n} \end{bmatrix}. \tag{3.24}$$

Consider an arbitrary density matrix $\hat{\rho}$ which is an eigenmatrix of $\mathcal{U}$: $\mathcal{U}\hat{\rho} = u\hat{\rho}$. Taking the trace of both sides of the previous identity, and given the form of $\mathcal{U}$, one finds $u = 1$. If $\hat{\rho}_{ss}$ is the only eigenmatrix with zero eigenvalue of $\mathcal{L}$ (unique steady state), it must also be an eigenmatrix of $\mathcal{U}$. From a physical perspective, this tells us that the symmetry sector to which $\hat{\rho}_{ss}$ (and therefore $\hat{\rho}_0$) belongs is *always* $L_{u=1}$.

A symmetry-breaking dissipative phase transition is associated to the emergence of multiple eigenmatrices of $\mathcal{L}$ with $\lambda = 0$, each of them belonging to a different symmetry sector L_{u_i}. The structure imposed by Eq. (3.24) is preserved and the previous considerations still hold. Therefore, $\hat{\rho}_0$ (belonging to the symmetry sector $L_{u=1}$) is still the only eigenmatrix of $\mathcal{L}$ with nonzero trace.

The block-diagonal structure of the Liouvillian (see Eq. (3.24)), together with the previous observations, can play a fundamental role in reducing the complexity of the problem. Indeed, by properly exploiting spatial and/or internal symmetries, one can explicitly construct the reduced subspace in which the steady-state density matrix belongs. This can give a substantial speed-up for algorithms based on Montecarlo strategies [127], cluster expansions [128, 129], corner methods [130] and tensor-network ansatz [131–133].

$\mathcal{Z}_2$ symmetry

Let us consider at first a system which has a discrete Z_2 symmetry represented by the superoperator $\mathcal{Z}_2 = \hat{Z}_2 \bullet \hat{Z}_2^\dagger$. Later, we will deal with the general case of a Z_n symmetry. The symmetry superoperator $\mathcal{Z}_2$ admits two eigenvalues, namely ± 1. For $\zeta < \zeta_c$ (ζ being the critical parameter) there exists a unique steady state associated to the eigenvalue $\lambda_0 = 0$, and $\mathcal{Z}_2\hat{\rho}_{ss} = \hat{\rho}_{ss}$. For $\zeta \geq \zeta_c$, a phase transition with a symmetry breaking takes place. Consequently, $\lambda_0 = \lambda_1 = 0$ while $\hat{\rho}_0$ and $\hat{\rho}_1$ belong to two different symmetry sectors (cf. Fig. 3.2). From these properties, it follows that $\hat{\rho}_0$ and $\hat{\rho}_1$ are orthogonal, since

$$\langle \hat{\rho}_0 | \hat{\rho}_1 \rangle = \langle \mathcal{Z}_2 \hat{\rho}_0 | \hat{\rho}_1 \rangle = \langle \hat{\rho}_0 | \mathcal{Z}_2 \hat{\rho}_1 \rangle = - \langle \hat{\rho}_0 | \hat{\rho}_1 \rangle , \tag{3.25}$$

where we exploited the hermiticity of $\mathcal{Z}_2$. Similarly, $\langle \hat{\rho}_0^\dagger | \hat{\rho}_1 \rangle = 0$. Since $\lambda_1 = 0$ is real and $\hat{\rho}_1^\dagger \neq \hat{\rho}_0$, the eigenmatrix $\hat{\rho}_1$ is Hermitian (Lemmas of Sec. 3.2). Hence, the density matrices

$$\hat{\rho}^\pm = \frac{\hat{\rho}_0 \pm \hat{\rho}_1}{\mathrm{Tr}[\hat{\rho}_0]} \tag{3.26}$$

are steady states of the master equation breaking the symmetry, as $\mathcal{Z}_2\hat{\rho}^\pm = \hat{\rho}^\mp$. From Eq. (3.25) it follows that $\hat{\rho}^+$ and $\hat{\rho}^-$ are orthogonal as well. So that we have:

$$\hat{\rho}_0 \propto \hat{\rho}^+ + \hat{\rho}^-, \tag{3.27a}$$
$$\hat{\rho}_1 \propto \hat{\rho}^+ - \hat{\rho}^-. \tag{3.27b}$$

Thus, we can conclude that the two symmetry-broken states $\hat{\rho}^{\pm}$ are the two matrices stemming from the spectral decomposition of $\hat{\rho}_1$, i.e., $\hat{\rho}_1^{\pm}$ [c.f. Eq (3.10)]. For a finite-size system, where the steady state is unique,

$$\hat{\rho}_{ss}(\zeta \geq \zeta_c, N) \simeq \frac{\hat{\rho}_1^{+}(\zeta_c, N) + \hat{\rho}_1^{-}(\zeta_c, N)}{2}. \tag{3.28}$$

Since we are considering a second-order phase transition, we must ensure that the unique steady state in ζ_c^- coincides with both the simmetry-breaking steady states in ζ_c^+: $\hat{\rho}_{ss}(\zeta_c^-) = \hat{\rho}^{+}(\zeta_c^+) = \hat{\rho}^{-}(\zeta_c^+)$. Consequently, according to this discussion, $\hat{\rho}_1(\zeta_c) = 0$. Therefore, a second-order phase transition is characterised by the coalescence of two eigenvectors of the Liouvillian, which may give rise to a Jordan form of the Liouvillian (see App. D).

In order to unveil the symmetry breaking in a finite-size system (where the symmetry is always preserved) one can resort to different strategies. To identify the critical point, one can use an external weak probe which breaks the symmetry (see for example Refs. [71, 128]) and look for divergences in the associated susceptibility.

$\mathcal{Z}_n$ symmetry

Consider now a generic symmetry superoperator $\mathcal{Z}_n = \hat{Z}_n \bullet \hat{Z}_n^{\dagger}$. In this case, the Liouvllian can be partitioned in n blocks, each characterised by an eigenvalue $z_j = \exp[2\,\mathrm{i}\,\pi j/n]$, with $j = 0, 1 \ldots n-1$ (i.e. the eigenvalues must satisfy the equation $z_j^n = 1$). In the symmetry-broken phase, in each of those blocks there exists an eigenmatrix $\hat{\rho}_j$ such that $\mathcal{L}\hat{\rho}_j = 0$ and $\mathcal{Z}_n\hat{\rho}_j = z_j\hat{\rho}_j$. Lemma 3 of Sec. 3.2 imposes $\mathcal{L}\hat{\rho}_j^{\dagger} = 0$. Moreover, $\hat{\rho}_j^{\dagger}$ is also an eigenmatrix of $\mathcal{Z}_n$ of eigenvalue z_j^*, since

$$\mathcal{Z}_n\hat{\rho}_j^{\dagger} = \left(\hat{Z}_n\hat{\rho}_j^{\dagger}\hat{Z}_n^{\dagger}\right) = \left(\hat{Z}_n\hat{\rho}_j\hat{Z}_n^{\dagger}\right)^{\dagger} = z_j^*\hat{\rho}_j^{\dagger}. \tag{3.29}$$

Note that, by definition $z_j^* = z_{n-j}$, and hence $\hat{\rho}_j^{\dagger} = \hat{\rho}_{n-j}$. As a particular case, if $z_j = z_j^*$ then $\hat{\rho}_j = \hat{\rho}_j^{\dagger}$.

To construct a basis of the degenerate subspace made of density matrices, consider the operator

$$\hat{\tilde{\rho}}_0 = \sum_{j=0}^{n-1} \frac{\hat{\rho}_j}{\mathrm{Tr}[\hat{\rho}_0]} = \sum_{j=0}^{n-1} \frac{\hat{\rho}_j + \hat{\rho}_{n-j}}{2\,\mathrm{Tr}[\hat{\rho}_0]} = \sum_{j=0}^{n-1} \frac{\hat{\rho}_j + \hat{\rho}_j^{\dagger}}{2\,\mathrm{Tr}[\hat{\rho}_0]}. \tag{3.30}$$

With this choice, $\hat{\tilde{\rho}}_0$ is a density matrix, since it is Hermitian and it has trace 1 ($\mathrm{Tr}[\hat{\rho}_j] = \mathrm{Tr}[\hat{\rho}_0]\,\delta_{j,0}$). For $\hat{\tilde{\rho}}_1 = \mathcal{Z}_n\hat{\tilde{\rho}}_0$, one has

$$\hat{\tilde{\rho}}_1 = \sum_{j=0}^{n-1} \frac{z_j\hat{\rho}_j + z_j^*\hat{\rho}_j^{\dagger}}{2\,\mathrm{Tr}[\hat{\rho}_0]}, \tag{3.31}$$

which is still Hermitian and of unitary trace, and therefore a density matrix. By iterative application of the symmetry operator $\mathcal{Z}_n$, and since $\hat{\tilde{\rho}}_i \neq \hat{\tilde{\rho}}_j$ for $i \neq j$, one obtains a basis $\{\hat{\tilde{\rho}}_i\}$ of density matrices, with $i = 0, \cdots, n-1$. In compact notation, one has

$$\hat{\tilde{\rho}}_l = \mathcal{Z}_n^l \sum_{j=0}^{n-1} \frac{\hat{\rho}_j}{\mathrm{Tr}[\hat{\rho}_0]} = \sum_{j=0}^{n-1} \frac{z_j^l(i)\hat{\rho}_j}{\mathrm{Tr}[\hat{\rho}_0]}. \tag{3.32}$$

Eq. (3.32) can be inverted to obtain $\hat{\rho}_k$ as a function of $\hat{\tilde{\rho}}_l$:

$$\begin{aligned}\sum_{l=0}^{n-1}(z_k^*)^l\,\hat{\tilde{\rho}}_l &= \sum_{l=0}^{n-1}\sum_{j=0}^{n-1}\frac{(z_k^* z_j)^l\,\hat{\rho}_j}{\mathrm{Tr}[\hat{\rho}_0]} = \sum_{l=0}^{n-1}\sum_{j=0}^{n-1}\frac{z_{j-k}^l\hat{\rho}_j}{\mathrm{Tr}[\hat{\rho}_0]}\\ &= \frac{n}{\mathrm{Tr}[\hat{\rho}_0]}\sum_{j=0}^{n-1}\delta_{j,k}\hat{\rho}_j = \frac{n}{\mathrm{Tr}[\hat{\rho}_0]}\hat{\rho}_k,\end{aligned} \tag{3.33}$$

where we used the identity

$$\sum_{l=0}^{n-1} z_{j-k}^l = \sum_{l=0}\left(e^{\frac{2\mathrm{i}\pi(j-k)}{n}}\right)^l = n\,\delta_{k,j}. \tag{3.34}$$

We conclude that

$$\hat{\rho}_k \propto \sum_{l=0}^{n-1}\frac{(z_k^*)^l\hat{\tilde{\rho}}_l}{n}. \tag{3.35}$$

Summarising, we have constructed a basis of $\{\hat{\tilde{\rho}}_i\}$ of the kernel of the Liouvillian made of density matrices such that $\mathcal{Z}_n\hat{\tilde{\rho}}_i = \hat{\tilde{\rho}}_{\mathrm{mod}(i+1,n)}$, as depicted in Fig. 3.2. This construction ensures that $\mathcal{Z}_n\hat{\rho}_0 = \hat{\rho}_0$. Again, for large enough but finite N, where the steady state is unique also for $\zeta \geq \zeta_c$, we get the asymptotic expression

$$\hat{\rho}_{ss}(\zeta \geq \zeta_c, N) \simeq \sum_{l=0}^{n-1}\frac{\hat{\tilde{\rho}}_l(\zeta \geq \zeta_c, N)}{n}. \tag{3.36}$$

3.4 Quantum trajectories to observe a phase transition

The previous discussion clarifies that, in order to prove the emergence of criticality, one needs $\hat{\rho}_{ss}$, and all those $\hat{\rho}_i$ such that $\lambda_i \simeq 0$. For many systems, however, an exact solution of the steady state does not exist, and the exponentially growing size of the Hilbert space makes an exact numerical diagonalisation of the Liouvillian often impossible. In those cases, however, one can use *single* quantum trajectories to characterise the emergence of a phase transition, the main idea being the following. Consider a finite-size system with a unique steady state and whose slowest timescale is $\tau = 1/\lambda_1$. That is, given any initial state $\hat{\rho}(0)$, for $t \gg \tau$ we have $\hat{\rho}(t) \simeq \hat{\rho}_{ss}$. As we discussed in Sec. 2.2, we can interpret $\hat{\rho}(t)$ as the average over many quantum trajectories $|\Psi(t)\rangle$. Therefore, even if the density matrix is stationary, the quantum trajectory can still change in time, and thus explore all the states compounding $\hat{\rho}_{ss}$. In formulas, for $t \gg \tau$, we have that $|\Psi(t)\rangle \in \{|\Psi_i^{\mathrm{ss}}\rangle\}$, where $\{|\Psi_i^{\mathrm{ss}}\rangle\}$ indicate the set of wave function such that $\hat{\rho}_{ss} = \sum_i p_i\,|\Psi_i^{\mathrm{ss}}\rangle\langle\Psi_i^{\mathrm{ss}}|$. [5]

3.4.1 First-order phase transition

According to our general theory, at the critical point ζ_c, the steady state is the sum of two density matrices, i.e. $\hat{\rho}_{ss} = (\hat{\rho}_1^+ + \hat{\rho}_1^-)/2$. For finite-size systems, however, we expect this "phase coexistence" in a finite region $\zeta \simeq \zeta_c$ around the critical point. Consequently, we

5. We stress that the wavefunctions $\{|\Psi_i^{\mathrm{ss}}\rangle\}$ need not be orthogonal, and the form of the wavefunction *depends* on the type of quantum trajectory considered. Moreover, the probabilities p_i are not those obtained via spectral decomposition of the density matrix.

expect that $\hat{\rho}_{ss}(\zeta)$ to be a statistical mixture of $\hat{\rho}_1^{\pm}(\zeta)$. Each one of them is a metastable state, decaying towards $\hat{\rho}_{ss}$ on a timescale of order $\tau = 1/\lambda_1$. Let us call $|\Psi_i^{\pm}\rangle$ the wavefunction compounding the matrices $\hat{\rho}_1^{\pm}$, i.e.

$$\hat{\rho}_1^{\pm} = \sum_i p_i^{\pm} |\Psi_i^{\pm}\rangle \langle\Psi_i^{\pm}| . \tag{3.37}$$

If at a time $t \gg \tau$ the wave function is $|\Psi(t)\rangle \in \{|\Psi_i^-\rangle\}$, at which time t' we expect to have $|\Psi(t')\rangle \in \{|\Psi_i^+\rangle\}$? Since the typical relaxation time for a system in $\hat{\rho}_1^-$ to relax to $\hat{\rho}_{ss}$ is $\tau = 1/\lambda$, we deduce that $t' - t \simeq \tau$.

Consider, instead, a region where $\zeta > \zeta_c$ but, still, $\lambda_1 \ll \gamma$ (the case $\zeta < \zeta_c$ is clearly equivalent). In this case, $\hat{\rho}_{ss}(\zeta) \simeq \hat{\rho}_1^+(\zeta)$. Hence, for $t \gg \tau$, we expect that the system will almost always be in a state $|\Psi(t)\rangle \in \{|\Psi_i^+\rangle\}$. In other words, the fact that the gap is very small is not associated to a random switch between two density matrices, and there is no bistable behaviour emerging in this case. However, if one can guess the form of one of the $|\Psi_i^-\rangle$, τ can be obtained by initialising the system in $|\Psi(0)\rangle = |\Psi_i^-\rangle$.

3.4.2 Second-order phase transition

The case of a second-order phase transition requires a separate discussion. Consider a generic symmetry $\mathcal{Z}_n = \hat{Z}_n \bullet \hat{Z}_n^\dagger$. For finite size system, if $\lambda_1 \ll \gamma$, in the symmetry-broken phase the steady state is multimodal and can be approximated by $\hat{\rho}_{ss} \simeq \sum_k \hat{\tilde{\rho}}_k$, where $\hat{\tilde{\rho}}_k$ are the matrices in Eq. (3.32). According to our previous discussion, there are no difficulties in observing the multimodal character of $\hat{\rho}_{ss}$.

What can be difficult, instead, is to observe the symmetry-breaking states and the emergence of a critical slowing down. Indeed, along a quantum trajectory one wants to explore states $|\Psi_i^k\rangle$ such that

$$\hat{\tilde{\rho}}_k = \sum_i p_i^k |\Psi_i^k\rangle \langle\Psi_i^k| . \tag{3.38}$$

Therefore, to have $|\Psi(t)\rangle \in \{|\Psi_i^k\rangle\}$, $|\Psi(t)\rangle$ cannot be an eigenstate of $\hat{Z}_n$.[6]

Theorem 3.5. *Suppose that $\hat{Z}_n$ is a symmetry of the Hamiltonian, i.e. $\left[\hat{H}, \hat{Z}_n\right] = 0$ and, for every jump operator $\hat{\Gamma}_\mu$, $\hat{Z}_n\hat{\Gamma}_\mu = z_\mu \hat{\Gamma}_\mu \hat{Z}_n$, where z_μ is an eigenvalue of $\hat{Z}_n$.*[7] *Given a counting quantum trajectory such that $\hat{Z}_n |\Psi(0)\rangle = z(0) |\Psi(0)\rangle$, at any time t we have*

$$\hat{Z}_n |\Psi(t)\rangle = z(t) |\Psi(t)\rangle , \tag{3.39}$$

where $z(t)$ is an eigenvalue of $\hat{Z}_n$.

Proof. Let us call the times in which quantum jumps happens $\{T_1, T_2, T_3, \ldots\}$. Consequently, the corresponding jump operators are $\{\hat{\Gamma}(T_1), \hat{\Gamma}(T_2), \hat{\Gamma}(T_3) \ldots\}$. Accordingly, we have $\hat{Z}_n\hat{\Gamma}(T_i) = z(T_i)\hat{\Gamma}(T_i)\hat{Z}_n$. In between any two quantum jumps, the system evolves according to the effective Hamiltoanian in Eq. (2.58). The operator $\hat{Z}_n$ commutes with $\hat{H}_{\text{eff}}$,

6. Since $\mathcal{Z}_n\hat{\tilde{\rho}}_k \neq \hat{\tilde{\rho}}_k$, we have $\hat{Z}_n |\Psi_i^k\rangle \langle\Psi_i^k| \hat{Z}_n^\dagger \neq |\Psi_i^k\rangle \langle\Psi_i^k|$. We deduce that $|\Psi_i^k\rangle$ is not an eigenstate of $\hat{Z}_n$.

7. This is explicitly the case for any

$$\mathcal{Z}_n = e^{\mathrm{i}\pi\hat{a}^\dagger\hat{a}/n} \bullet e^{-\mathrm{i}\pi\hat{a}^\dagger\hat{a}/n}$$

and $\hat{\Gamma}_\mu \propto \hat{a}$.

since $\left[\hat{Z}_n, \hat{H}\right] = 0$ and $\left[\hat{Z}_n, \hat{\Gamma}_\mu^\dagger \hat{\Gamma}_\mu\right] = \hat{Z}_n \hat{\Gamma}_\mu^\dagger \hat{\Gamma}_\mu - z_\mu^* z_\mu \hat{Z}_n \hat{\Gamma}_\mu^\dagger \hat{\Gamma}_\mu = 0$ (we recall $z_\mu^* z_\mu = 1$). Thus, for $T_i < t < T_{i+1}$ we have

$$
\begin{aligned}
\hat{Z}_n |\Psi(t)\rangle &= \hat{Z}_n e^{-\mathrm{i}\hat{H}_{\mathrm{eff}}(t-T_i)} |\Psi(T_i)\rangle = e^{-\mathrm{i}\hat{H}_{\mathrm{eff}}(t-T_i)} \hat{Z}_n |\Psi(T_i)\rangle \\
&= e^{-\mathrm{i}\hat{H}_{\mathrm{eff}}(t-T_i)} \hat{Z}_n \hat{\Gamma}(T_i) e^{-\mathrm{i}\hat{H}_{\mathrm{eff}}(T_i-T_{i-1})} |\Psi(T_{i-1})\rangle \\
&= e^{-\mathrm{i}\hat{H}_{\mathrm{eff}}(t-T_i)} \hat{\Gamma}(T_i)(z(T_i)\hat{Z}_n) e^{-\mathrm{i}\hat{H}_{\mathrm{eff}}(T_i-T_{i-1})} |\Psi(T_{i-1})\rangle \\
&= z(T_i) e^{-\mathrm{i}\hat{H}_{\mathrm{eff}}(t-T_i)} \hat{\Gamma}(T_j) e^{-\mathrm{i}\hat{H}_{\mathrm{eff}}(T_i-T_{i-1})} \hat{Z}_n |\Psi(T_{i-1})\rangle \\
&= z(T_i) e^{-\mathrm{i}\hat{H}_{\mathrm{eff}}(t-T_i)} \left(\prod_{j=1}^{i-1} z(T_j) e^{-\mathrm{i}\hat{H}_{\mathrm{eff}}(T_j-T_{j-1})} \hat{\Gamma}(T_j) \right) e^{-\mathrm{i}\hat{H}_{\mathrm{eff}} T_1} \hat{Z}_n |\Psi(0)\rangle . \qquad (3.40) \\
&= \prod_{k=0}^{i} z(T_k) \left[e^{-\mathrm{i}\hat{H}_{\mathrm{eff}}(t-T_i)} \left(\prod_{j=1}^{i-1} e^{-\mathrm{i}\hat{H}_{\mathrm{eff}}(T_j-T_{j-1})} \hat{\Gamma}(T_j) \right) e^{-\mathrm{i}\hat{H}_{\mathrm{eff}} T_1} |\Psi(0)\rangle \right] \\
&= \prod_{k=0}^{i} z(T_k) |\Psi(t)\rangle
\end{aligned}
$$

That is, $|\Psi(t)\rangle$ is an eigenstate of $\hat{Z}_n$, whose eigenvalue $z(t) = \prod_{k=0}^{i} z(T_k)$ changes at every quantum jump.

■

We conclude that, performing a counting quantum trajectory, the system explore only eigenstates of the operator $\hat{Z}_n$. Therefore, such a trajectory can never explore metastable states. A homodyne trajectory, instead, allows to access those states. Indeed, in Eq. (2.61), the pseudo-Hamiltonian terms contains a term proportional to $\hat{\Gamma}_\mu$. Thus $\left[\hat{H}_{\mathrm{eff}}, \hat{Z}_n\right] \neq 0$. That is, in order to observe second-order phase transition associated to the spontaneous symmetry breaking of $\mathcal{Z}_n$, we should use homodyne detection.

3.5 Conclusions

In this Chapter, we have presented theoretical results for first- and second-order dissipative phase transitions. Within a general formalism, we have determined the structure of the density matrix in the vicinity of a critical point. In particular, due to the closure of the Liouvillian gap at the critical point, we have shown how the the steady-state density matrix is directly related to the eigenmatrix of the Liouvillian superoperator corresponding to the eigenvalue λ_1 (the one with the smallest absolute value of the real part). Our work provides a general insight into dissipative phase transitions, allowing for a clear analysis of criticality via quantum trajectories. Moreover, it gives precise constraints for variational methods [54, 134] to describe critical phenomena in open quantum systems, whose corresponding ansatz matrices must satisfy the relations derived in this Chapter.

CHAPTER 4

The One- and Two-Photon Kerr Resonators

An exact solution of a driven-dissipative model is of particular interest, since it allows the exploration of any range of system parameters, rather than the limiting regimes of small or high photon densities. An example of a solvable model is the driven-dissipative Kerr resonator, for which Drummond and Walls derived the steady-state solution via the complex P-representation [135]. Beyond the single resonator case, analytic solutions proved to be very useful for an efficient implementation of Gutzwiller mean-field decoupling for arrays of coupled cavities [61, 136–142].

In the present Chapter, we use the complex P-representation to provide an exact solution for the steady state of a general class of driven-dissipative nonlinear resonators. More precisely, we consider a standard driven-dissipative Kerr model (subject to the usual coherent pumping and one-photon dissipation) driven by an additional parametric two-photon pump and subject to two-photon losses. Recently, these processes have been engineered for superconducting resonators [82] and have been discussed for optomechanical setups [55, 64]. By performing a Bogoliubov-like approximation, we show that the Liouvillian of a uniform lattice of Kerr resonators obeys the same equation of a single nonlinear cavity with a different photon-photon interaction strength. Thus, we use the exact solution derived in this Chapter to capture the emergence of dissipative phase transitions and to test the theory derived in Chapter 3.

This Chapter is organised as follows. In Sec. 4.1 we introduce the driven-dissipative Kerr resonator. Following the seminal paper of Drummond and Walls [135], we derive the analytic solution for the steady-state of this model using the formalism of the complex P-representation [143]. In Sec. 4.2 we solve the general model of a one- and two-photon driven-dissipative Kerr resonator. Having benchmarked our solution against numerical resolution of the Linblad master equation, we study the interplay between the one- and two-photon driving in determining the steady state. In Sec. 4.3, we study the emergence of phase transitions in Kerr resonators. Finally, in Sec. 4.4 we study quantum trajectories in these critical systems.

Contents

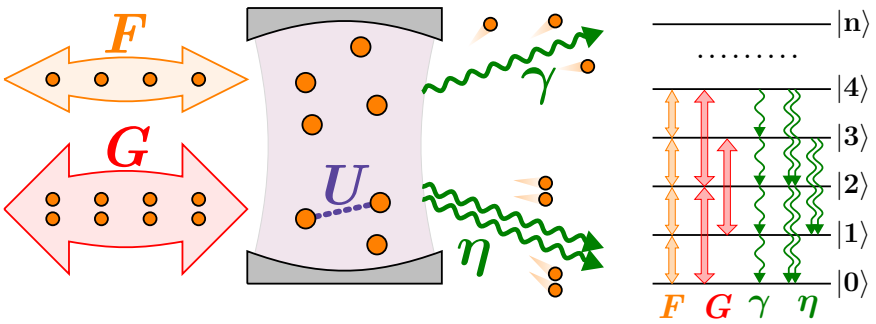

Figure 4.1 – A sketch of the considered class of systems. The picture represents a photon resonator subject to one-photon losses with rate γ, and coherently driven by a one-photon pump of amplitude F. The resonator is also subject to a coherent two-photon driving of amplitude G and two-photon losses with rate η. The strength of the photon-photon interaction is quantified by U. On the right, we sketch the effects of these physical processes on the Fock (number) states $|n\rangle$. Figure from Ref. [5].

4.1 The analytic solution for the one-photon pump

Let us introduce the general model of a driven-dissipative Kerr nonlinear resonator, (sketched in Fig. 4.1 for $G = \eta = 0$). In the absence of pumping we get (we recall $\hbar = 1$)

$$\hat{H}_0 = \omega_c \, \hat{a}^\dagger \hat{a} + \frac{U}{2} \hat{a}^\dagger \hat{a}^\dagger \hat{a} \hat{a}, \tag{4.1}$$

where $\hat{a}$ and $\hat{a}^\dagger$ are, respectively, the annihilation and creation operator for photons inside the resonator. In the the Hamiltonian, ω_c is the cavity-mode frequency and U the strength of the Kerr nonlinearity, quantifying the photon-photon interaction (see Chapter 1). A coherent drive with amplitude F and frequency ω_p can be described by

$$\hat{H}_{1\text{ph}} = F \, e^{-i\omega_p t} \hat{a}^\dagger + F^* \, e^{i\omega_p t} \hat{a}. \tag{4.2}$$

From now on we will denote this mechanism as one-photon pumping. To remove the time-dependence from the Hamiltonian, we perform the unitary transformation $e^{-i\omega_p t \hat{a}^\dagger \hat{a}}$, describing the system in the reference frame rotating at the coherent pump frequency ω_p. The full Hamiltonian, hence, becomes

$$\hat{H} = -\Delta \hat{a}^\dagger \hat{a} + \frac{U}{2} \hat{a}^\dagger \hat{a}^\dagger \hat{a} \hat{a} + F \hat{a}^\dagger + F^* \hat{a}, \tag{4.3}$$

where $\Delta = \omega_p - \omega_c$ is the pump-cavity detuning. For the considered system, photons are typically lost individually to the environment and the jump operator is the annihilation operator $\hat{a}$ [25–27]. The resulting Lindblad master equation describing the evolution of the the system density matrix $\hat{\rho}$ is

$$\frac{\partial \hat{\rho}}{\partial t} = -\mathrm{i} \left[\hat{H}, \hat{\rho} \right] + \frac{\gamma}{2} \mathcal{D}[\hat{a}] \, \hat{\rho} \tag{4.4}$$

where γ is the one-photon dissipation rates and $\hat{H}$ is the one given in Eq. (4.3).

4.1.1 Complex P-representation solution

The exact solution to the steady-state of the Kerr resonator was find by Drummond and Walls in [135] exploiting the complex P-representation, defined as

$$\hat{\rho} = \iint_{\mathcal{C},\mathcal{C}'} \mathrm{d}\alpha\, \mathrm{d}\beta\, P(\alpha,\beta)\hat{\Lambda}(\alpha,\beta), \tag{4.5}$$

where $\hat{\Lambda}(\alpha,\beta) = |\alpha\rangle \langle\beta^*| \,/\, \langle\beta^*|\alpha\rangle$ is the projector on the coherent overcomplete basis. $\mathcal{C}$ and $\mathcal{C}'$ are, instead, appropriate closed contours in the complex plane encircling all the singularities of the P-function (for a detailed discussion about this method, see App. E.5). Substituting the operators in Eq. (4.4) according to the rules given in Eq. (E.17), we find the integro-differential equation:

$$\begin{aligned}\int_{\mathcal{C}} \mathrm{d}\alpha \int_{\mathcal{C}'} \mathrm{d}\beta \hat{\Lambda}(\alpha,\beta)\frac{\partial}{\partial t}P(\alpha,\beta) = -\mathrm{i} \int_{\mathcal{C}} \mathrm{d}\alpha \int_{\mathcal{C}'} \mathrm{d}\beta \\ \hat{\Lambda}(\alpha,\beta)\left[-\frac{\partial}{\partial\alpha}\left(-\alpha\Delta + U\alpha^2\beta + F - \frac{\mathrm{i}\gamma}{2}\alpha\right)\right. \\ \left. -\frac{\partial}{\partial\beta}\left(\beta\Delta - U\alpha\beta^2 - F - \frac{\mathrm{i}\gamma}{2}\beta\right) + \frac{U}{2}\left(\frac{\partial^2}{\partial\alpha^2}\alpha^2 - \frac{\partial^2}{\partial\beta^2}\beta^2\right)\right] P(\alpha,\beta),\end{aligned} \tag{4.6}$$

where

$$\hat{\Lambda}(\alpha,\beta) = \frac{|\alpha\rangle \langle\beta^*|}{\langle\beta^*|\alpha\rangle} = |\alpha\rangle \langle\beta^*| \, e^{\frac{|\alpha|^2+|\beta|^2}{2} - \alpha\beta}, \tag{4.7}$$

and $\mathcal{C}$ and $\mathcal{C}'$ are closed path in the complex plane encircling all the poles. Since both sides of the equation involve the same integral, we can ask that the two integrands to be equal. By calling $\delta = \Delta + \mathrm{i}\frac{\gamma}{2}$ we obtain the Fokker-Plank equation

$$\frac{\partial P(\alpha,\beta)}{\partial t} = -\mathrm{i}\sum_i \frac{\partial}{\partial x_i}\left[-A^i P(\alpha,\beta) + \sum_j \frac{\partial}{\partial x_j}\left(\frac{D^{ij}}{2}P(\alpha,\beta)\right)\right], \tag{4.8}$$

where $x_i = \alpha, \beta$,

$$\vec{A} = \begin{bmatrix} -\delta\alpha + U\alpha^2\beta + F \\ \delta^*\beta - U\alpha\beta^2 - F^* \end{bmatrix}, \tag{4.9}$$

and

$$\mathbb{D} = \begin{bmatrix} U\alpha^2 & 0 \\ 0 & -U\beta^2 \end{bmatrix}. \tag{4.10}$$

We are interested in the steady-state solution $\partial_t P_{\mathrm{ss}}(\alpha,\beta) = 0$. Eq. (4.8) satisfies the potential conditions defined in Eq. (E.23). Hence, one can introduce a scalar potential ϕ, such that $P_{\mathrm{ss}}(\alpha,\beta) = e^{-\phi}$, with

$$\phi = \int_0^{x^i} dx^i (D^{-1})^{ii}\left(2A^i - \frac{\partial}{\partial x_i}D^{ii}\right). \tag{4.11}$$

By direct integration on the path $\Gamma := \{0,0\} \to \{\alpha,0\} \to \{\alpha,\beta\}$, we obtain, up to a multiplicative constant:

$$\phi = 2\alpha\beta - 2\left[\log(\alpha)\left(1 + \frac{\delta}{U}\right) + \frac{F}{U\alpha}\right] - 2\left[\log(\beta)\left(1 + \frac{\delta^*}{U}\right) + \frac{F^*}{U\beta}\right] \tag{4.12}$$

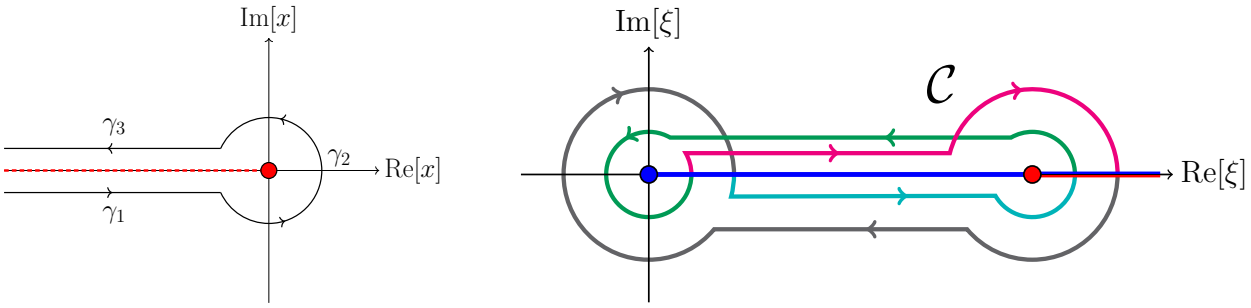

Figure 4.2 – Integration path for the computation of the momenta of the P-function on the complex plane. The dots represent the poles of the integrand , while the coloured lines are the branch cuts. Left: One-photon keyhole path encircling the branch cuts. The path encircles the pole in zero and it closes at infinity. Right: Two-photon Prochhammer's path. It crosses each of the cuts an equal number of times in one direction and in the opposite, hence, for any starting point, it begins and ends on the same Riemann sheet. The change in the path colour emphasizes the passage to a different Riemann surface. Right figure from Ref. [5].

and therefore

$$P_{\rm ss}(\alpha,\beta) = e^{-\phi} = e^{2\alpha\beta}\alpha^{-2(c+1)}e^{-2f/\alpha}\beta^{-2(c^*+1)}e^{-2f^*/\beta}. \tag{4.13}$$

where we have introduced the rescaled parameters

$$f \equiv \frac{F}{U} \qquad\qquad c \equiv \frac{\delta}{U} = \frac{\Delta + \mathrm{i}\gamma/2}{U}. \tag{4.14}$$

Having obtained the solution for $P_{\rm ss}(\alpha,\beta)$, we are now interested in the expectation values of any operator $\hat{O}$, which in terms of the P-representation is

$$\langle\hat{O}\rangle = \mathrm{Tr}\big[\rho\,\hat{O}\big] = \frac{\mathrm{Tr}\big[\hat{O}\int_{\mathcal{C}}\mathrm{d}\alpha\int_{\mathcal{C}'}\mathrm{d}\beta\;\hat{\Lambda}(\alpha,\beta)P_{\rm ss}(\alpha,\beta)\big]}{\mathrm{Tr}\big[\int_{\mathcal{C}}\mathrm{d}\alpha\int_{\mathcal{C}'}\mathrm{d}\beta\;\hat{\Lambda}(\alpha,\beta)P_{\rm ss}(\alpha,\beta)\big]}. \tag{4.15}$$

4.1.2 Integrating the P-function

Since any operator can be expressed as a combination of creation and annihilation operators, our main task is the computation of

$$\langle\hat{a}^{\dagger\,i}\hat{a}^{j}\rangle = \frac{\mathrm{Tr}\big[\int_{\mathcal{C}}\mathrm{d}\alpha\int_{\mathcal{C}'}\mathrm{d}\beta\;\hat{a}^{j}\hat{\Lambda}(\alpha,\beta)\hat{a}^{\dagger\,i}P_{\rm ss}(\alpha,\beta)\big]}{\mathrm{Tr}\big[\int_{\mathcal{C}}\mathrm{d}\alpha\int_{\mathcal{C}'}\mathrm{d}\beta\;\hat{\Lambda}(\alpha,\beta)P_{\rm ss}(\alpha,\beta)\big]} = \frac{\int_{\mathcal{C}}\mathrm{d}\alpha\int_{\mathcal{C}'}\mathrm{d}\beta\;\alpha^{j}\beta^{i}P_{\rm ss}(\alpha,\beta)}{\int_{\mathcal{C}}\mathrm{d}\alpha\int_{\mathcal{C}'}\mathrm{d}\beta\;P_{\rm ss}(\alpha,\beta)}. \tag{4.16}$$

That is, we are interested in computing the momenta of the $P_{\rm ss}(\alpha,\beta)$ distribution. The crucial and missing point is the identification of a convenient path $\mathcal{C}$, which has to encircle all the branches and poles of the P function. The idea is to bring all the poles and branch cuts along the real axis, so to allow an easy identification of $\mathcal{C}$.

At first, we consider the normalisation factor:

$$N = \int_{\mathcal{C}}\mathrm{d}\alpha\int_{\mathcal{C}'}\mathrm{d}\beta\;P_{\rm ss}(\alpha,\beta) = \int_{\mathcal{C}}\mathrm{d}\alpha\int_{\mathcal{C}'}\mathrm{d}\beta\;e^{2\alpha\beta}\alpha^{-2(c+1)}e^{-2f/\alpha}\beta^{-2(c^*+1)}e^{-2f^*/\beta}. \tag{4.17}$$

Due to the symmetry of the P-function, we will choose $\mathcal{C} = \mathcal{C}'$. If we expand in series $e^{2\alpha\beta}$ and perform the change of variable $x = -1/\alpha$, $y = -1/\beta$, we obtain

$$\begin{aligned} N &= \iint_{\mathcal{C},\mathcal{C}} \mathrm{d}x\mathrm{d}y \sum_n \frac{2^n}{n!} x^{2c-n} y^{2c^*-n} e^{2(fx+f^*y)} = \sum_n \frac{2^n}{n!} \int_{\mathcal{C}} \mathrm{d}x\; x^{2c-n} e^{2fx} \int_{\mathcal{C}} \mathrm{d}y\; y^{2c^*-n} e^{2f^*y} \\ &= \sum_n \frac{2^n}{n!} I(c, f, n) I(c^*, f^* n). \end{aligned} \tag{4.18}$$

Let us focus on the integral on x, i.e.,

$$I(c, f, n) = \int_{\mathcal{C}} \mathrm{d}x\; x^{2c-n} e^{2fx}. \tag{4.19}$$

Since x^{2c-n} is not uniquely determined, we introduce a branch cut in the complex plane from 0 to $-\infty$. We can now identify $\mathcal{C}$ as the keyhole path. The path can be divided in γ_1 (a straight line from $-\infty - \mathrm{i}\epsilon$ to $0 - \mathrm{i}\epsilon$), γ_2 (a circle around zero of radius ϵ), and γ_3 (another straight line from $0 + \mathrm{i}\epsilon$ to $-\infty + \mathrm{i}\epsilon$)(c.f. left panel of Fig. 4.2). One can write

$$I(c, f, n) = \left(\int_{\gamma_1} + \int_{\gamma_2} + \int_{\gamma_3} \right) \mathrm{d}x\; x^{2c-n} e^{2fx}. \tag{4.20}$$

To evaluate Eq. (4.20), one consider $2c - n > 0$, where all the integrals are well defined. Then, by analytic extension, one can define this integral almost-everywhere. All together, one has

$$I(c, f, n) = 2\pi i \, (2f)^{-2c+n-1} \frac{1}{\Gamma(n - 2c)}. \tag{4.21}$$

Therefore, the normalisation N reads

$$N = -4\pi^2 \sum_n \frac{2^n}{n!} \frac{(4|f|^2)^{-c-c*+n-1}}{\Gamma(n - 2c)\Gamma(n - 2c^*)}. \tag{4.22}$$

Once the normalisation integral is known, we still need to compute $\langle \hat{a}^{\dagger\, i} \hat{a}^j \rangle$ But, following the same technique as before, we can easily write the numerator of Eq. (4.16) as

$$\begin{aligned} \langle \hat{a}^{\dagger\, i} \hat{a}^j \rangle &= \frac{1}{N} \int_{\mathcal{C}} \mathrm{d}\alpha \int_{\mathcal{C}'} \mathrm{d}\beta\; \alpha^j \beta^i P_{\mathrm{ss}}(\alpha, \beta) \\ &= \frac{1}{N} \int_{\mathcal{C}} \mathrm{d}\alpha \int_{\mathcal{C}'} \mathrm{d}\beta\; e^{2\alpha\beta} \alpha^{-2(c+1)+j} e^{-2f/\alpha} \beta^{-2(c^*+1)+i} e^{-2f^*/\beta} \\ &= \frac{(-1)^{i+j}}{N} \iint_{\mathcal{C},\mathcal{C}} \mathrm{d}x\mathrm{d}y \sum_n \frac{2^n}{n!} x^{2c-j-n} y^{2c^*-i-n} e^{2fx+2f^*y} \\ &= \frac{(-1)^{i+j}}{N} \sum_n \frac{2^n}{n!} I(c + \frac{j}{2}, f, n) I(c^* + \frac{i}{2}, f^*, n) \\ &= (-2f)^i (-2f^*)^j \frac{\sum_n \frac{2^n}{n!} (4|f|^2)^n / \Big(\Gamma(-2c + n + j)\Gamma(-2c^* + n + i)\Big)}{\sum_n \frac{2^n}{n!} (4|f|^2)^n / \Big(\Gamma(-2c + n)\Gamma(-2c^* + n)\Big)}. \end{aligned} \tag{4.23}$$

This sum of Γ-functions can be recast as

$$\langle \hat{a}^{\dagger\, i} \hat{a}^j \rangle = (-2f)^i (-2f^*)^j \frac{\Gamma(-2c)\Gamma\left(-2c^*\right)}{\Gamma(-2c + j)\Gamma\left(-2c^* + i\right)} \frac{{}_0F_2\left(\{\}; -2c + j, -2c^* + i; 8\,|f|^2\right)}{{}_0F_2\left(\{\}; -2c, -2c^*; 8\,|f|^2\right)}, \tag{4.24}$$

where ${}_pF_q$ denotes a generalized hypergeometric function [144, 145], defined by the analytic extension of

$$ {}_pF_q(a_1,\cdots,a_p;\,b_1,\cdots,b_p;\,z)=\sum_{k=0}^{\infty}\frac{\prod_{n=1}^{p}(a_n)_k}{\prod_{m=1}^{q}(b_m)_k}\frac{z^k}{k!}, \tag{4.25} $$

with $(a)_k=\Gamma(a+k)/\Gamma(a)$.

In a very similar way, one obtains

$$ \begin{aligned}\langle m|\hat{\rho}_{ss}|n\rangle &= \frac{\int_{\mathcal{C}}\mathrm{d}\alpha\int_{\mathcal{C}'}\mathrm{d}\beta\ \langle m|\hat{\Lambda}(\alpha,\beta)|n\rangle\,P_{\rm ss}(\alpha,\beta)}{\int_{\mathcal{C}}\mathrm{d}\alpha\int_{\mathcal{C}'}\mathrm{d}\beta\,P_{\rm ss}(\alpha,\beta)}=\frac{1}{\sqrt{m!n!}}\frac{\int_{\mathcal{C}}\mathrm{d}\alpha\int_{\mathcal{C}'}\mathrm{d}\beta\,\frac{P_{\rm ss}(\alpha,\beta)\alpha^m\beta^n}{\langle\beta^*|\alpha\rangle}}{\int_{\mathcal{C}}\mathrm{d}\alpha\int_{\mathcal{C}'}\mathrm{d}\beta\,P_{\rm ss}(\alpha,\beta)}.\\ &=(-2f)^m(-2f^*)^n\frac{{}_0F_2\left(\{\};-2c+m,-2c^*+n;4\,|f|^2\right)}{\Gamma(-2c+m)\Gamma(-2c^*+n)}.\end{aligned} \tag{4.26} $$

and the Wigner function of the steady state $W_{\rm ss}(z)$ reads

$$ \begin{aligned}W_{\rm ss}(z) &= \frac{2}{\pi}\,\mathrm{Tr}\left[\hat{D}(z)\,e^{i\pi\hat{a}^\dagger\hat{a}}\,\hat{D}(z)^\dagger\,\hat{\rho}_{ss}\right]=\frac{2\,e^{-2|z|^2}}{\pi}\int_{\mathcal{C}}\mathrm{d}\alpha\int_{\mathcal{C}'}\mathrm{d}\beta\,\frac{P_{\rm ss}(\alpha,\beta)}{e^{2\alpha\beta}}\,e^{2\alpha z^*}e^{2\beta z}\\ &=\frac{2e^{-2|z|^2}}{\pi}\frac{\left|\left(2\sqrt{fz^*}\right)^{1+2c}\right|^2}{\left|J_{-2c-1}\left(4\sqrt{fz^*}\right)\right|^2}\frac{\left|J_{-2c-1}\left(4\sqrt{fz^*}\right)\right|^2}{{}_0\tilde{F}_2\left(\{\};-2c,-2c^*;8\,|f|^2\right)},\end{aligned} \tag{4.27} $$

where $\hat{D}(z)$ is the displacement operator [cf. Eq. (2.64)], $J_n(x)$ is the Bessel function of first kind and ${}_p\widetilde{F}_q$ are the regularized hypergeometric functions, defined as

$$ {}_p\widetilde{F}_q(a_1,\cdots,a_p;\,b_1,\cdots,b_p;\,z)=\frac{{}_pF_q(a_1,\cdots,a_p;\,b_1,\cdots,b_p;\,z)}{\prod_{m=1}^{q}\Gamma(b_m)}. \tag{4.28} $$

4.2 The two-photon pump

We consider now the general model of a one- and two-photon driven-dissipative Kerr resonator. Similarly to the previous case, we consider a system whose bare Hamiltonian is $\hat{H}_0$ introduced in Eq. (4.1). Photons are exchanged one at the time via an Hamiltonian process of the form $\hat{H}_{\rm 1ph}$. Moreover, a parametric process coherently adds photons pairwise via

$$ \hat{H}_{\rm 2ph}=\frac{G}{2}\,e^{-i\omega_2 t}\hat{a}^\dagger\hat{a}^\dagger+\frac{G^*}{2}\,e^{i\omega_2 t}\hat{a}\hat{a}, \tag{4.29} $$

where G is the pump amplitude and ω_2 its frequency. Such a two-photon pumping mechanism can be obtained by engineering the exchange of photons between the cavity and the environment. The Hamiltonian $\hat{H}_{\rm 2ph}$ can emerges from an adiabatic elimination in parametric downconversion processes [110], occurring, e.g., in birifrangent crystals [114]. Moreover, it has been studied in optomecanical setups [55] and it has been experimentally realised in superconducting circuits by engineering the coupling between two superconducting resonators via a Josephson junction [82].

In order to get a time-independent Hamiltonian, we consider $\omega_2=2\omega_p$. By passing in the frame rotating at the pumps frequency via the unitary transformation $e^{i\omega_p t\hat{a}^\dagger\hat{a}}$, we obtain the Hamiltonian

$$ \hat{H}=-\Delta\hat{a}^\dagger\hat{a}+\frac{U}{2}\hat{a}^\dagger\hat{a}^\dagger\hat{a}\hat{a}+F\hat{a}^\dagger+F^*\hat{a}+\frac{G}{2}\hat{a}^\dagger\hat{a}^\dagger+\frac{G^*}{2}\hat{a}\hat{a}. \tag{4.30} $$

In addition, we also consider two-photon losses, which naturally emerge together with the engineered two-photon pumping [82, 110]. These losses are included through the dissipator $\mathcal{D}[\hat{a}^2]$. Finally, the Linblad master equation for the one- and two-photon driven-dissipative Kerr resonator (c.f. Fig 4.1) is

$$\mathcal{L}\hat{\rho}(t) = -\mathrm{i}\left[\hat{H}, \hat{\rho}(t)\right] + \frac{\gamma}{2}\mathcal{D}[\hat{a}]\hat{\rho}(t) + \frac{\eta}{2}\mathcal{D}[\hat{a}^2]\hat{\rho}(t). \tag{4.31}$$

In the case $F = 0$, this model has a discrete Z_2 symmetry, resulting from the invariance under the transformation $\hat{a} \to -\hat{a}$. The corresponding superoperator $\mathcal{Z}_2$ is:

$$\mathcal{Z}_2 = e^{\mathrm{i}\pi\hat{a}^\dagger\hat{a}} \bullet e^{-\mathrm{i}\pi\hat{a}^\dagger\hat{a}}, \tag{4.32}$$

with $\mathcal{Z}_2\hat{\rho}_{ss} = \hat{\rho}_{ss}$.

4.2.1 Complex P-representation

In order to find the analytic solution, we proceed as in Sec. 4.1.1. The Fokker-Planck equation for the present case will be the same as Eq. (4.8), but with the addition of the terms related to two-photon pump and dissipation. Inserting all those other terms and introducing $\delta = \Delta + \mathrm{i}\frac{\gamma}{2}$ and $W = U - \mathrm{i}\frac{\eta}{2}$, we obtain the following Fokker-Planck equation

$$\frac{\partial P(\alpha,\beta)}{\partial t} = -\mathrm{i}\sum_{x_i}\frac{\partial}{\partial x_i}\left[-A^i P + \sum_{x_j}\frac{\partial}{\partial x_j}\left(\frac{D^{ij}}{2}P(\alpha,\beta)\right)\right], \tag{4.33}$$

where $x_i = \alpha, \beta$,

$$\vec{A} = \begin{pmatrix} -\delta\alpha + W\alpha^2\beta + F + G\beta \\ \delta^*\beta - W^*\alpha\beta^2 - F^* - G^*\alpha \end{pmatrix}, \tag{4.34}$$

and

$$\mathbb{D} = \begin{bmatrix} W\alpha^2 + G & 0 \\ 0 & -W^*\beta^2 - G^* \end{bmatrix}. \tag{4.35}$$

Again, this equation satisfies the potential conditions introduced in Eq. (E.23). Thus, we can compute the function ϕ to obtain $P_{\mathrm{ss}}(\alpha,\beta) = e^{-\phi}$, obtaining

$$\begin{aligned}\phi &= \int_0^{x^i} dx^i (D^{-1})^{ii}\left(2A^i - \frac{\partial}{\partial x_i}D^{ii}\right) \\ &= \log\left(G + W\alpha^2\right)^{1+c} + \log\left(G^* + W^*\beta^2\right)^{1+c^*} - 2\alpha\beta \\ &\quad - \frac{2F\tan^{-1}\left(\frac{\alpha\sqrt{W}}{\sqrt{G}}\right)}{\sqrt{G}\sqrt{W}} - \frac{2F^*\tan^{-1}\left(\frac{\beta\sqrt{W^*}}{\sqrt{G^*}}\right)}{\sqrt{G^*}\sqrt{W^*}}.\end{aligned} \tag{4.36}$$

Exponentiating and collecting the terms depending on W, we obtain:

$$P_{\mathrm{ss}} = \left(g + \alpha^2\right)^{-1-c}\left(g^* + \beta^2\right)^{-1-c^*}\exp\left[2\alpha\beta + \frac{2f\tan^{-1}\left(\frac{\alpha}{\sqrt{g}}\right)}{\sqrt{g}} + \frac{2f^*\tan^{-1}\left(\frac{\beta}{\sqrt{g^*}}\right)}{\sqrt{g^*}}\right], \tag{4.37}$$

for $f = \frac{F}{W}$, $g = \frac{G}{W}$, and $c = \frac{\delta}{W}$.

An important check on this result consist in recovering Eq. (4.13) for $G, \eta \to 0$, i.e. $g \to 0$ and $W \to U$. Let us start by considering the limit $g \to 0$. In this case, the exponential

in Eq. (4.37) is divergent. To solve this apparent problem, we recall that P can always be defined up to a normalisation constant. It is worth stressing that, in virtue of Eq. (4.15), any constant prefactor is irrelevant for the evaluation of an operator mean value. Thus,

$$\exp\left[2f\frac{\tan^{-1}\left(\frac{\alpha}{\sqrt{g}}\right)}{\sqrt{g}}\right]\xrightarrow{g\to 0}\exp\left[2f\frac{\frac{\pi}{2}-\sqrt{g}/\alpha}{\sqrt{g}}\right]=\exp\left[\frac{2f}{\sqrt{g}}\frac{\pi}{2}\right]\cdot\exp\left[-\frac{2f}{\alpha}\right]. \tag{4.38}$$

Neglecting the constant terms, i.e., those independent of α and β, we obtain

$$P_{\rm ss}(\alpha,\beta)=\alpha^{-2-2c}\beta^{-2-2c^*}\exp\left[2\alpha\beta-\frac{2f\alpha+2f^*\beta}{\alpha\beta}\right], \tag{4.39}$$

which immediately returns Eq. (4.13) for $W\to U$. We stress that, however, Eq. (4.39) is valid also for $\eta\neq 0$. That is, it allows to consider the case of a one-photon driven Kerr resonator subject to one- and two-photon dissipation.

4.2.2 Computation of the moments

Let us now focus on the evaluation of the momenta for a two photon pump. Even if the computation will be more involved, the procedure is similar to the one introduced in Sec. 4.1.2.

Due to the symmetry between α and β we choose $\mathcal{C}=\mathcal{C}'$. The moments of the P-function reads

$$\begin{aligned}\langle\hat{a}^{\dagger\,n}\hat{a}^m\rangle&=\iint_{\mathcal{C},\mathcal{C}}\frac{{\rm d}\alpha{\rm d}\beta}{N}P_{\rm ss}(\alpha,\beta){\rm Tr}\left[\hat{a}^m\hat{\Lambda}(\alpha,\beta)\hat{a}^{\dagger\,n}\right]\\&=\frac{1}{N}\iint_{\mathcal{C},\mathcal{C}}{\rm d}\alpha{\rm d}\beta\,\frac{\alpha^m}{(g+\alpha^2)^{1+c}}\frac{\beta^n}{(g^*+\beta^2)^{1+c^*}}e^{2\alpha\beta}\\&\qquad\exp\left[\frac{2f\tan^{-1}\left(\frac{\alpha}{\sqrt{g}}\right)}{\sqrt{g}}+\frac{2f^*\tan^{-1}\left(\frac{\beta}{\sqrt{g^*}}\right)}{\sqrt{g^*}}\right],\end{aligned} \tag{4.40}$$

where the normalisation integral is

$$\begin{aligned}N=\iint_{\mathcal{C},\mathcal{C}'}{\rm d}\alpha{\rm d}\beta\,P_{\rm ss}(\alpha,\beta)=\iint_{\mathcal{C},\mathcal{C}'}{\rm d}\alpha{\rm d}\beta\,&\left(g+\alpha^2\right)^{-1-c}\left(g^*+\beta^2\right)^{-1-c^*}e^{2\alpha\beta}\\&\exp\left[\frac{2f\tan^{-1}\left(\frac{\alpha}{\sqrt{g}}\right)}{\sqrt{g}}+\frac{2f^*\tan^{-1}\left(\frac{\beta}{\sqrt{g^*}}\right)}{\sqrt{g^*}}\right].\end{aligned} \tag{4.41}$$

Again, we expand in series the term $e^{2\alpha\beta}$ so that we can separate N in the sum of the product of two integrals, namely

$$\langle\hat{a}^{\dagger\,n}\hat{a}^m\rangle=\frac{\sum_k\frac{2^k}{k!}\mathcal{F}_{m+k}(f,g,c)\mathcal{F}_{n+k}(f^*,g^*,c^*)}{\sum_k\frac{2^k}{k!}\mathcal{F}_k(f,g,c)\mathcal{F}_k(f^*,g^*,c^*)}, \tag{4.42}$$

where

$$\mathcal{F}_j(f,g,c)=\int_{\mathcal{C}}{\rm d}\alpha\frac{\alpha^j}{(g+\alpha^2)^{1+c}}\exp\left[\frac{2f}{\sqrt{g}}\arctan\left(\frac{\alpha}{\sqrt{g}}\right)\right]. \tag{4.43}$$

We notice that $\mathcal{F}_j(f^*, g^*, c^*) = \mathcal{F}_j^*(f, g, c)$.

As already done in the previous section, the objective is now to bring all the poles and branches on the real axis. First we use the following change of variable: $x = -\mathrm{i}\alpha/\sqrt{g}$ and the identity $\arctan(z) = 1/2\mathrm{i}[\ln(1-\mathrm{i}z) - \ln(1+\mathrm{i}z)]$, obtaining

$$\begin{aligned}\mathcal{F}_j(f,g,c) &= \int_{\mathcal{C}} \mathrm{d}x\, (\mathrm{i}\sqrt{g})^{j+1} x^j (g - gx^2)^{-1-c} \exp\left[\frac{2f}{\sqrt{g}} \arctan(\mathrm{i}x)\right] \\ &= \frac{(\mathrm{i}\sqrt{g})^{j+1}}{g^{1+c}} \int_{\mathcal{C}} \mathrm{d}x\; x^j (1+x)^{-1-c}(1-x)^{-1-c} \exp\left[-\frac{\mathrm{i}f}{\sqrt{g}} \ln\left(\frac{1+x}{1-x}\right)\right] \\ &= \frac{(\mathrm{i}\sqrt{g})^{j+1}}{g^{1+c}} \int_{\mathcal{C}} \mathrm{d}x\; x^j (1+x)^{\varphi-1-c}(1-x)^{-\varphi-1-c},\end{aligned} \tag{4.44}$$

where $\varphi = -\frac{\mathrm{i}f}{\sqrt{g}}$. By performing the second change of variable $2z = 1 + x$ we obtain

$$\mathcal{F}_j(f,g,c) = \frac{(\mathrm{i}\sqrt{g})^{j+1}}{g^{1+c}} 2^{-1-2c} \int_{\mathcal{C}} dz (1-2z)^j (z)^{\varphi-1-c}(1-z)^{-\varphi-1-c}. \tag{4.45}$$

We will neglect the constant term 2^{-1-2c}, as well as the g^{-1-c}, since they will appear both in the numerator and in the denominator with the same power in every integral. To explicitly compute this integral, we could use the same contour as in Sec. 4.1.2. This procedure, even if perfectly doable, leads to a very non-compact form.

Let us focus on a second possible method, involving a more elaborate path. The path $\mathcal{C}$ must encircle both the poles at $\xi = 0$ and $\xi = 1$. Furthermore, for $\mathcal{C}$ to be properly closed one must take into account the presence of two branch cuts going from each pole to $|\xi| \to \infty$. A convenient choice is the Pochhammer contour [146], which is sketched in the right panel of Fig. 4.2. Such a path correctly encircles the poles and crosses the branch cuts an equal number of times in one sense and in the opposite one (a property which does not depend on the cut orientations). Hence, the path is closed since it begins and ends on the same Riemann sheet. We have

$$\begin{aligned}\mathcal{F}_j(f,g,c) &= (\mathrm{i}\sqrt{g})^j \int_{\mathcal{C}} dz (1-2z)^j (z)^{\varphi-1-c}(1-z)^{-\varphi-1-c} \\ &= (\mathrm{i}\sqrt{g})^j \int_{\mathcal{C}} \sum_{l=0}^{j} dz \binom{j}{l} (-2)^l (z)^{\varphi-1-c+l}(1-z)^{-\varphi-1-c} \\ &= -4(\mathrm{i}\sqrt{g})^j \sum_{l=0}^{j} \binom{j}{l} (-2)^l \sin(\varphi - 1 - c + l) \times \\ &\qquad \times \sin(\varphi + 1 + c) B(\varphi - 1 - c + l, -\varphi - 1 - c) \\ &= (\mathrm{i}\sqrt{g})^j (1 - e^{2\pi i(\varphi - c)}) B(\varphi - c, -\varphi - c)\; {}_2F_1(-j, -\varphi - c, -2c, 2) \\ &= \mathrm{const}(c, \varphi)\; (i\sqrt{g})^j\; {}_2F_1(-j, -\varphi - c, -2c, 2),\end{aligned} \tag{4.46}$$

where ${}_2F_1$ is the Gaussian Hypergeometric function [145, 146]. Since we can neglect the constants independent of j, we eventually obtain

$$\langle \hat{a}^{\dagger\, n} \hat{a}^m \rangle = \frac{\sum_k \frac{2^k}{k!} (\mathrm{i}\sqrt{g})^{m+n+2k}\; {}_2F_1(-m-k, -\varphi - c, -2c, 2)\; {}_2F_1(-n-k, \varphi^* - c^*, -2c^*, 2)}{\sum_k \frac{2^k}{k!} (\mathrm{i}\sqrt{g})^{2k}\; {}_2F_1(-k, -\varphi - c, -2c, 2)\; {}_2F_1(-k, \varphi^* - c^*, -2c^*, 2)}. \tag{4.47}$$

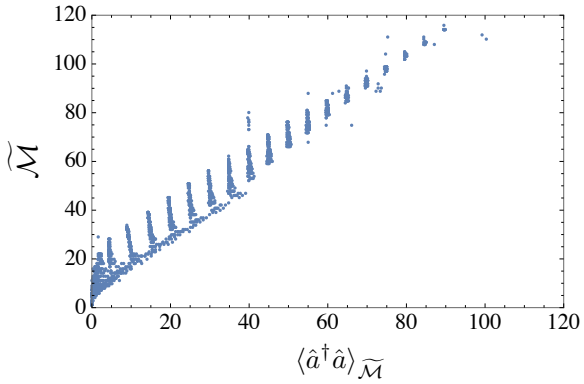

Figure 4.3 – Numerical cutoff $\widetilde{\mathcal{M}}$ as a function of the corresponding mean photon density $\langle \hat{a}^\dagger \hat{a} \rangle_{\widetilde{\mathcal{M}}}$ [Eq. (4.50)] for different system parameters. The plot has been obtained setting the convergence criterion as explained in the main text. Each point of the diagram corresponds to $\gamma = \eta = 0.1U$, while we varied $\Delta/U \in [-30, 30]$ and $F/U, G/U \in [0, 60]$. From Ref. [5].

Similarly, we have

$$\begin{aligned} \langle p|\hat{\rho}_{\rm ss}|q\rangle =& \int_{\mathcal{C}} \mathrm{d}\alpha \int_{\mathcal{C}'} \mathrm{d}\beta \, \frac{P(\alpha,\beta)}{\langle \beta^*|\alpha\rangle} \frac{\alpha^p \beta^q}{\sqrt{p!q!}} \\ =& \frac{1}{N\sqrt{p!q!}} \sum_{m=0}^{\infty} \frac{1}{m!} \mathcal{F}_{m+p}\left[f,g,c\right] \mathcal{F}^*_{m+q}\left[f,g,c\right], \end{aligned} \tag{4.48}$$

and the Wigner function of the steady state $W_{\rm ss}(z)$ reads

$$\begin{aligned} W_{\rm ss}(z) =& \frac{2}{\pi} \mathrm{Tr}\left[\hat{D}(z)\, e^{i\pi \hat{a}^\dagger \hat{a}}\, \hat{D}(z)^\dagger\, \hat{\rho}_{ss}\right] = \frac{2\, e^{-2|z|^2}}{\pi} \int_{\mathcal{C}} \mathrm{d}\alpha \int_{\mathcal{C}'} \mathrm{d}\beta \, \frac{P_{\rm ss}(\alpha,\beta)}{e^{2\alpha\beta}} \, e^{2\alpha z^*} e^{2\beta z} \\ =& \frac{2}{\pi\, N} \left| \sum_{m=0}^{\infty} \frac{(2z^*)^m}{m!} \mathcal{F}_m\left[f,g,c\right] \right|^2 e^{-2|z|^2}. \end{aligned} \tag{4.49}$$

Therefore, the Wigner function given in Eq. (4.49) is real and positive over the whole complex plane for *any* choice of the system parameters.

4.2.3 Series convergence and closed forms

The analytic results for the one- and two-photon driven-dissipative nonlinear resonator given in Eqs. (4.46), (4.48), and (4.49), contain infinite summations which, in the general case $F, G \neq 0$ must be estimated numerically. First, we take as an example the photon number $\langle \hat{a}^\dagger \hat{a} \rangle$ to show that such series converge rapidly in a wide range of parameters. Having proved the computational efficiency of the introduced formulæ, we benchmark them against exact diagonalisation of the Liouvillian superoperator. Finally, we give the exact closed forms of $\langle \hat{a}^{\dagger\, i} \hat{a}^j \rangle$, ρ_{pq}, and $W(z)$ for the case $F = 0$.

Convergence of the series in the general case

To investigate the convergence of the series defined by Eq. (4.46), let us consider the mean photon number $\langle \hat{a}^\dagger \hat{a} \rangle$. In this expression there are two sums to evaluate: the one explicitly expressed in Eq. (4.46), and a second one implicitly contained in the normalization N. The

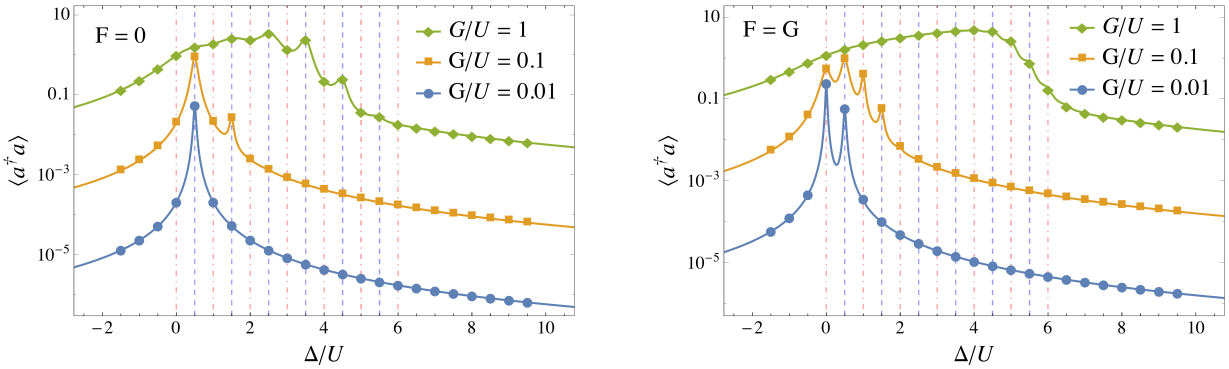

Figure 4.4 – Mean photon number $\langle \hat{a}^\dagger \hat{a} \rangle$ as a function of the pump-cavity detuning Δ normalized by the photon-photon interaction strength U. Different curves and data sets correspond to different pump intensities (cf. legend). Solid lines represent the analytic solution while the points are the numerical results obtained by diagonalization of the Liouvillian superoperator on a truncated Fock basis (see App. E.3). Left: results in the absence of one-photon pumping, i.e. $F = 0$ [Eq. (4.53) for $i = j = 1$]. Right: results in the presence of both one- and two-photon pumping with $F = G$ [Eq. (4.46)]. In both panels, vertical dot-dashed red (dashed blue) lines mark the position of odd (even) photonic resonances. One- and two-photon dissipation rates were set to $\gamma = \eta = 0.03U$. From Ref. [5].

convergence of $\langle \hat{a}^\dagger \hat{a} \rangle$ can be examined in terms of a single parameter $\mathcal{M}$, the cutoff of both sums. Hence, we introduce

$$\langle \hat{a}^\dagger \hat{a} \rangle_{\mathcal{M}} = \frac{\sum_{m=0}^{\mathcal{M}} \frac{2^m}{m!} \left| \mathcal{F}_{m+1}(f,g,c) \right|^2}{\sum_{m=0}^{\mathcal{M}} \frac{2^m}{m!} \left| \mathcal{F}_{m}(f,g,c) \right|^2}. \tag{4.50}$$

In what follows, we checked the convergence by verifying that the addition of two further elements does not affect the result beyond the 6$^{\text{th}}$ relevant digit. In other words, we chose the smallest $\widetilde{\mathcal{M}}$ ensuring that $\left| \langle \hat{a}^\dagger \hat{a} \rangle_{\widetilde{\mathcal{M}}} - \langle \hat{a}^\dagger \hat{a} \rangle_{\widetilde{\mathcal{M}}-2} \right| < 10^{-6} \langle \hat{a}^\dagger \hat{a} \rangle_{\widetilde{\mathcal{M}}}$. In Fig. 4.3, we show the required cutoff $\widetilde{\mathcal{M}}$ as a function of the corresponding value of the mean photon number for different system parameters. It turns out that $\widetilde{\mathcal{M}}$ grows roughly linearly with $\langle \hat{a}^\dagger \hat{a} \rangle_{\widetilde{\mathcal{M}}}$. We verified that similar convergence criteria efficiently applies to the other quantities defined by Eqs. (4.46), (4.48), and (4.49), in a wide range of system parameters. In general, the numerical evaluation of the exact solution can be performed with arbitrary precision. Such a computation is faster and much less memory demanding than numerical approaches, in particular for high-density regimes.

Benchmarking in the low-density regime

In order to benchmark the analytic solution with numerical approaches, we study it in the low-density regime. The two panels of Fig. 4.4 show the results obtained in the presence of only two-photon pumping (left) and for both one- and two-photon driving (right). The agreement with numerics is excellent, thus corroborating the validity of the analytic solution. The parameters have been chosen to clearly visualize the photonic resonances. Those are expected to appear when the energy of n pump photons is equal to that of n photons inside the resonator. Thus, in the regime of weak pumping, the energy of the empty cavity become comparable to that of a state with n photons, and thus the pump struggles *only* against the

dissipation in order to populate the resonator. In the frame rotating at the pump frequency, this condition reads:

$$-\Delta n + \frac{U}{2} n(n-1) = 0. \tag{4.51}$$

Thus, beside the one-photon resonance ($n = 1$, thus occurring for $\Delta = 0$), the multi-photon resonances are due to the competition between detuning and interaction, and arise when $\Delta/U = (n-1)/2$. For $F = 0$ only resonances with an even number of photons appear, while all of them are observed in the presence of a one-photon pumping. For very weak pumping, the dissipation prevent the system from populating states with high number of photons. Therefore, in case $F = 0$ the main resonance is for $n = 2$ and $\Delta/U = 1/2$, while if $F \neq 0$ the main resonance is for $n = 1$ and $\Delta = 0$ (c.f. Fig. 4.4 left and right, respectively). For moderate pumping, also other resonances starts to appear, and the resonances progressively merge in a continuum by increasing the pump intensities.

Closed forms for $F = 0$

The general model described by the master equation (4.31) can be specialized to many different cases. Among them, a case of particular interest is the one in which the one-photon pumping is absent, that is when $F = 0$ [6, 82, 147, 148]. Remarkably, in this case one finds that

$$\mathcal{F}_{2m+1}(0, g, c) = 0, \tag{4.52a}$$

$$\begin{aligned}\mathcal{F}_{2m}(0, g, c) &= \left(\mathrm{i}\sqrt{g}\right)^{2m} {}_2\widetilde{F}_1(-2m, -c; -2c; 2) \\ &= (-g)^m \frac{1}{\sqrt{\pi}} \frac{\Gamma\left(\frac{1}{2} - c\right)}{\Gamma(-2c)} \frac{\Gamma\left(\frac{1}{2} + m\right)}{\Gamma\left(\frac{1}{2} + m - c\right)} = (-g)^m \frac{\Gamma\left(\frac{1}{2} + m\right)}{\Gamma\left(\frac{1}{2} + m - c\right)},\end{aligned} \tag{4.52b}$$

where, in the last identity, we dropped further m-independent factors which would be naturally absorbed in the normalization.

Making use of Eqs. (4.52), we derived the following closed forms for the correlators:

$$\begin{aligned}\langle \hat{a}^{\dagger\,(2i)} \hat{a}^{(2j)} \rangle =& (-g)^j (-g^*)^i \frac{\Gamma\left(\frac{1}{2} + j\right)\Gamma\left(\frac{1}{2} + i\right)}{\sqrt{\pi}} \\ & \frac{{}_2\widetilde{F}_3\left(\frac{1}{2} + j, \frac{1}{2} + i; \frac{1}{2}, \frac{1}{2} + j - c, \frac{1}{2} + i - c^*; |g|^2\right)}{{}_1\widetilde{F}_2\left(\frac{1}{2}; \frac{1}{2} - c, \frac{1}{2} - c^*; |g|^2\right)},\end{aligned} \tag{4.53a}$$

$$\begin{aligned}\langle \hat{a}^{\dagger\,(2i+1)} \hat{a}^{(2j+1)} \rangle =& (-g)^{j+1} (-g^*)^{i+1} \frac{\Gamma\left(\frac{3}{2} + j\right)\Gamma\left(\frac{3}{2} + i\right)}{\sqrt{\pi}} \\ & \frac{{}_2\widetilde{F}_3\left(\frac{3}{2} + j, \frac{3}{2} + i; \frac{3}{2}, \frac{3}{2} + j - c, \frac{3}{2} + i - c^*; |g|^2\right)}{{}_1\widetilde{F}_2\left(\frac{1}{2}; \frac{1}{2} - c, \frac{1}{2} - c^*; |g|^2\right)},\end{aligned} \tag{4.53b}$$

$$\langle \hat{a}^{\dagger\,(2i)} \hat{a}^{(2j+1)} \rangle = \langle \hat{a}^{\dagger\,(2i+1)} \hat{a}^{(2j)} \rangle = 0, \tag{4.53c}$$

For the matrix elements we find

$$\langle 2p|\hat{\rho}|2q\rangle = (-g)^p(-g^*)^q \frac{\Gamma\left(\frac{1}{2}+p\right)\Gamma\left(\frac{1}{2}+q\right)}{\sqrt{\pi(2p)!(2q)!}} \frac{{}_2\widetilde{F}_3\left(\frac{1}{2}+p,\frac{1}{2}+q;\frac{1}{2},\frac{1}{2}+p-c,\frac{1}{2}+q-c^*;\left|\frac{g}{2}\right|^2\right)}{{}_1\widetilde{F}_2\left(\frac{1}{2};\frac{1}{2}-c,\frac{1}{2}-c^*;|g|^2\right)}, \tag{4.54a}$$

$$\langle 2p+1|\hat{\rho}|2q+1\rangle = (-g)^{p+1}(-g^*)^{q+1} \frac{\Gamma\left(\frac{3}{2}+p\right)\Gamma\left(\frac{3}{2}+q\right)}{2\sqrt{\pi(2p+1)!(2q+1)!}} \frac{{}_2\widetilde{F}_3\left(\frac{3}{2}+p,\frac{3}{2}+q;\frac{3}{2},\frac{3}{2}+p-c,\frac{3}{2}+q-c^*;\left|\frac{g}{2}\right|^2\right)}{{}_1\widetilde{F}_2\left(\frac{1}{2};\frac{1}{2}-c,\frac{1}{2}-c^*;|g|^2\right)}, \tag{4.54b}$$

$$\langle 2p|\hat{\rho}|2q+1\rangle = \langle 2p+1|\hat{\rho}|2q\rangle = 0, \tag{4.54c}$$

Finally, for the Wigner function we obtain:

$$W(z) = \frac{2}{\pi} \frac{\left|{}_0F_1\left[\frac{1}{2}-c;-g(z^*)^2\right]\right|^2}{{}_1F_2\left[\frac{1}{2};\frac{1}{2}-c,\frac{1}{2}-c^*;|g|^2\right]} e^{-2|z|^2}. \tag{4.55}$$

In the equations above, we stress that ${}_p\widetilde{F}_q$ are the regularized hypergeometric functions

$${}_p\widetilde{F}_q(a_1,\cdots,a_p;\,b_1,\cdots,b_p;\,z) = \frac{{}_pF_q(a_1,\cdots,a_p;\,b_1,\cdots,b_p;\,z)}{\prod_{m=1}^{q}\Gamma(b_m)}. \tag{4.56}$$

The closed forms presented above are computationally much more efficient than the corresponding implicit forms (4.46), (4.48), and (4.49).

4.2.4 Properties of the steady state

The exact analytic solution of the Lindblad equation (4.31) allows us to compute the average steady-state quantities of the considered system in any physical regime, from low- to high-density phases, passing through the nontrivial mesoscopic regime. In this section, we investigate how the properties of the steady state evolve through these different regimes.

Quantum *vs* semiclassical behaviour

When the resonator has a small population, the solution of the master equation (4.31) can be obtained numerically. For instance, by integrating the master equation on a truncated Fock basis or by diagonalizing the Liouvillian super-operator (see App. E.1 and E.3). On the other hand, for high photon number the cavity field can be typically approximated by a coherent state $|\alpha\rangle$. Thus, the master equation reduces to a differential equation for the complex amplitude α (see App. E.2). This corresponds to the so-called semiclassical approximation [27]. In this case, however, all quantum correlations are neglected, which makes our exact analytic solution a precious tool. The differential equation for the complex amplitude α can be easily derived from $\partial_t \langle\hat{a}\rangle = \mathrm{Tr}[\hat{a}\,\partial_t\rho]$ as in Eq. (E.2), namely:

$$\partial_t\alpha = (\mathrm{i}\Delta - \gamma/2)\alpha - \mathrm{i}F - \mathrm{i}G\alpha^* - (\mathrm{i}U+\eta)\alpha^*\alpha^2. \tag{4.57}$$

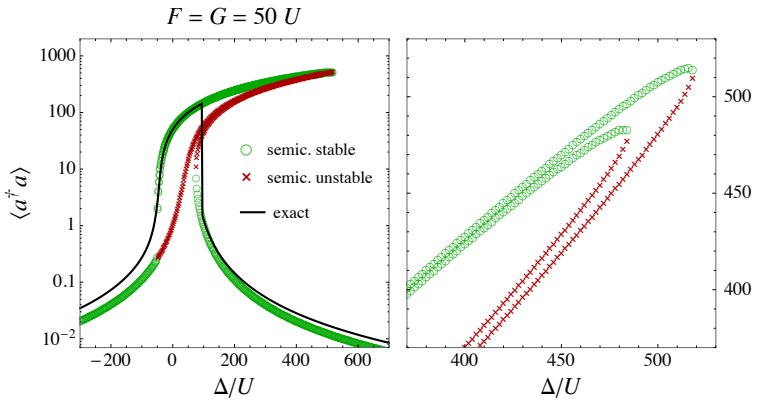

Figure 4.5 – Left: mean steady-state photon number $\langle \hat{a}^\dagger \hat{a} \rangle$ as a function of the dimensionless detuning parameter Δ/U. The green circles (red crosses) mark the stable (unstable) semiclassical steady-state solutions. The black line is the analytic solution given by Eq. (4.46) ($i = j = 1$). One- and two-photon dissipation rates were set to $\gamma = \eta = 0.1U$. Right: zoom-in on the region in which the almost-degenerate high-density semiclassical solutions get unstable. From Ref. [5].

Note that the latter equation is coupled to the one for the conjugate variable α^*. Solving for the steady state $\partial_t \alpha, \partial_t \alpha^* = 0$ one can get, depending on the system parameters, up to five solutions, of which at most three are dynamically stable [148, 149]. In quantum optics, this condition of multiple semiclassical solutions is known bistability and has been observed in a broad range of experimental realizations for a one-photon pumping [150–155].

In left panel of Fig. 4.5 we show the semiclassical prediction for the mean photon number according to the semiclassical analysis. For large and negative detuning, Eq. (4.57) predicts a single low-density steady-state solution. By increasing Δ, the low-density solution gets unstable and two high-density ones emerge. The corresponding values of $\langle \hat{a}^\dagger \hat{a} \rangle$ are almost equal, but the phases of their complex amplitudes differ approximatively by π. Eventually, a third low-density stable solution appears, coexisting with the two high-density ones until a parameter-dependent threshold is reached (see right panel in Fig. 4.5). Then, only the low-density stable state is present. By comparing these results with the exact one given by Eq. (4.46) (also plotted in Fig. 4.5), we note that the multi-stable behavior does not appear in the analytic solution. We point out that the quantum solution is unique, while the semiclassical approach gives multiple dynamically stable solutions. However, the exact and unique quantum solution can display a multimodal mixed-state behavior.

The presence of one (or more) semiclassical solution(s) in the steady state can be visualized by the Wigner function $W(z)$, whose analytic expression is in Eq. (4.49). The case $F = 0$ has already been discussed in [148], in particular the evolution of $W(z)$ across the density drop. We present, in Fig. 4.6, the results for the general case $F, G \neq 0$. In the multiple-solution regime, even for $F/G \ll 1$, the one-photon driving prevents the system from being in a balanced mixture of coherent states, which is the case for $F = 0$ [6, 82, 86, 148, 149]. By looking at the bottom panel of Fig. 4.6, one notes that a bimodal Wigner function only exists nearby the transitions from low- to high-density regimes. Elsewhere, $W(z)$ always exhibits a single peak. In the low-density regimes, we recover a squeezed-vacuum steady state as the one observed for $F = 0$ [148, 149]. This squeezing of the state can be seen by looking at the elongated elliptic shape of the corresponding Wigner function in the bottom panels of Fig. 4.6.

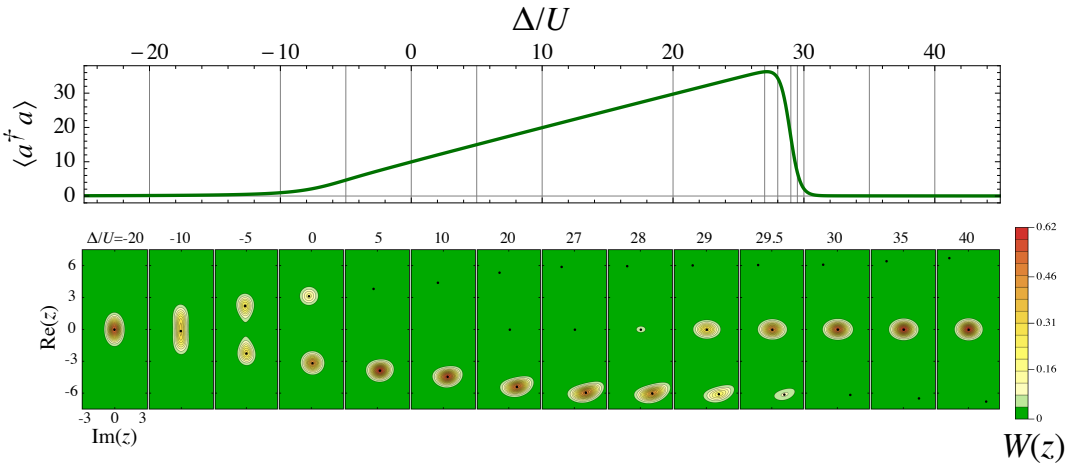

Figure 4.6 – Top: steady-state photon number $\langle \hat{a}^\dagger \hat{a} \rangle$ as a function of the dimensionless detuning parameter Δ/U for $F = U$, $G = 10U$, $\gamma = \eta = 0.1U$. The results have been obtained through the exact solution (4.46) for $i = j = 1$. The vertical grid lines mark the values of Δ/U for which we evaluated the steady-state Wigner function (cf. bottom panels). Bottom: steady-state Wigner functions $W(z)$ calculated according to Eq. (4.49) for the same parameters as in the top panel and for different values of Δ/U (see frame labels). The black dots mark the position of the corresponding stable semiclassical solutions. From Ref. [5].

Interferences effect and competition between the one- and two-photon pumps

We investigate now the interplay between one- and two-photon pumping in determining the full quantum solution. For this purpose, we plot in the left panel of Fig. 4.7 the steady-state photon density as a function of G/U for different values of F. Overall, as expectable, the number of photons increases with F but, interestingly, adding a small two-photon pump $G \ll F$ decreases the photon density. In this regime, an insight on the physical origin of this counter-intuitive effect can be found through a perturbative expansion in G. At the lowest order, indeed, $F\hat{a}^\dagger + G/2\,(\hat{a}^\dagger)^2 \approx (F + G\,\langle \hat{a}^\dagger \rangle_0)\hat{a}^\dagger$, where $\langle \hat{a}^\dagger \rangle_0$ is the mean value for $G = 0$. When $\Delta, \gamma \ll F$ (which is the case for all the curves in Fig. 4.7) and $U \geq 0$, one finds that $\mathbb{I}\mathrm{m}\left[\langle \hat{a}^\dagger \rangle_0\right] \simeq 0$ and $\mathbb{R}\mathrm{e}\left[\langle \hat{a}^\dagger \rangle_0\right] < 0$, hence a small G effectively reduces the one-photon driving amplitude.

The effects of the competition between F and G not only affects the photon number, but also the whole steady-state properties. Remarkably, as shown in the right panel of Fig. 4.7, the dominant peak in the multi-modal Wigner function is selected by the relative phase of F and G. For this analysis, we took the same parameters as in Fig. 4.6, setting the detuning around the threshold value. In the outer panels we have varied the relative phase $\phi = \arg(F/G)$, changing the relative weight of the Wigner-function peaks. The central panel (e) shows the case $F = 0$, for which the three peaks have comparable heights. This property can be a valuable tool for the control of two-photon driven resonators for quantum computation based on quasi-orthogonal coherent states [87, 88]. Indeed the relative phase ϕ could be experimentally controlled and adjusted at will. In this direction, it is worth stressing that expression (4.49) allows to predict precisely the shape of the multi-modal Wigner function even in highly populated regimes, where a numerical approach would be extremely demanding.

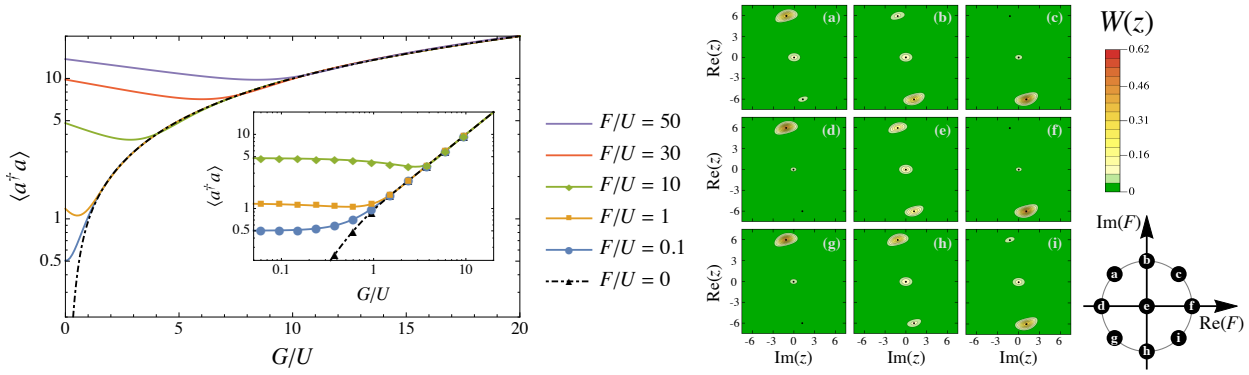

Figure 4.7 – Left: On a Log-linear scale, behaviour of $\langle \hat{a}^\dagger \hat{a}\rangle$ [Eqs. (4.46) or (4.53) for $i = j = 1$] as a function of the two-photon driving amplitude G normalized over the nonlinear interaction strength U. Different curves (colours) correspond to different normalized values of the one-photon driving F/U coexisting with the two-photon one (cf. legend to the right). Inset: On a Log-Log plot, zoom-in on the low-density regime which shows the agreement of the analytic solution (solid lines) with numerical results (markers). The latter have been obtained via numerical diagonalization of the Liouvillian superoperator matrix with Fock-basis cutoff $n_{\max} = 40$. Parameters: $\Delta = 0$, $\gamma = \eta = 0.05U$. Right: Steady-state Wigner functions $W(z)$ calculated according to Eq. (4.49) for $\Delta = 28U$, $G = 10U$, $\gamma = \eta = 0.1U$ and for different complex values of F. For panel (e) we took $F = 0$. In the others, $F/U = e^{i\phi}$ and the phase ϕ changes as sketched in the bottom-right scheme. Right figure from Ref. [5].

4.3 Emergence of a phase transition in the steady state

Having found the analytic solutions to the one- and two-photon Kerr resonator, we are interested in using this model to study dissipative phase transitions.

4.3.1 The "thermodynamic" limit

Let us consider a lattice of N Kerr resonators described via the following Hamiltonian:

$$\hat{H} = \sum_{i=1}^{N} \hat{H}_i - J \sum_{\langle i,j\rangle} \hat{a}_i^\dagger \hat{a}_j \tag{4.58}$$

where J is the coupling strength and

$$\hat{H}_i = -\Delta \hat{a}_i^\dagger \hat{a}_i + \frac{U}{2} \hat{a}_i^\dagger \hat{a}_i^\dagger \hat{a}_i \hat{a}_i + F(\hat{a}_i^\dagger + \hat{a}_i) + \frac{G}{2}(\hat{a}_i^{\dagger\,2} + \hat{a}_i^2), \tag{4.59}$$

where, in the following, we will assume F and G real. The dissipation acts locally via $\mathcal{D}[\hat{a}_i]$ and $\mathcal{D}[\hat{a}_i^2]$, so that the Lindblad master equation becomes

$$\mathcal{L}\hat{\rho}(t) = -\mathrm{i}[\hat{H}, \hat{\rho}(t)] + \frac{\gamma}{2} \sum_{i=1}^{N} \mathcal{D}[\hat{a}_i]\hat{\rho}(t) + \frac{\eta}{2} \sum_{i=1}^{N} \mathcal{D}[\hat{a}_i^2]\hat{\rho}(t). \tag{4.60}$$

One can transform the previous equation by passing to the Fourier space $\mathbf{k}$, so that

$$\hat{a}_{\mathbf{k}} = \frac{2\pi}{N} \sum_i e^{-\mathrm{i}\mathbf{k}\mathbf{x}_i} \hat{a}_i. \tag{4.61}$$

Accordingly, Eq. (4.58) becomes:

$$\hat{H} = \sum_{\mathbf{k}} -(\Delta + 2J\cos(\mathbf{k}))\hat{a}^\dagger_{\mathbf{k}}\hat{a}_{\mathbf{k}} + \frac{G}{2}(\hat{a}^\dagger_{\mathbf{k}}\hat{a}^\dagger_{\text{-}\mathbf{k}} + \hat{a}_{\mathbf{k}}\hat{a}_{\text{-}\mathbf{k}}) + \frac{U}{2N}\sum_{\mathbf{k},\mathbf{k'},\mathbf{q}} \hat{a}^\dagger_{\mathbf{k'}-\mathbf{q}}\hat{a}^\dagger_{\mathbf{k}+\mathbf{q}}\hat{a}_{\mathbf{k'}}\hat{a}_{\mathbf{k}} + F\sqrt{N}\hat{a}^\dagger_0\hat{a}_0, \tag{4.62}$$

where $\cos(\mathbf{k}) = \cos(k_x \cdot e_x) + \cos(k_y \cdot e_y) + \ldots$, and $\hat{a}_0$ is the creation operator of the uniform mode $\mathbf{k} = 0$. The dissipators transform instead as

$$\frac{\gamma}{2}\sum_{i=1}^{N}\mathcal{D}[\hat{a}_i] = \frac{\gamma}{2}\sum_{\mathbf{k}}\mathcal{D}[\hat{a}_{\mathbf{k}}], \tag{4.63a}$$

$$\frac{\eta}{2}\sum_{i=1}^{N}\mathcal{D}[\hat{a}_i^2] = \frac{\eta}{2N}\sum_{\mathbf{k},\mathbf{k'},\mathbf{q}}\left(2\hat{a}^\dagger_{\mathbf{k}+\mathbf{q}}\hat{a}^\dagger_{\mathbf{k'}-\mathbf{q}}\bullet\,\hat{a}_{\mathbf{k'}}\hat{a}_{\mathbf{k}} - \hat{a}^\dagger_{\mathbf{k}+\mathbf{q}}\hat{a}^\dagger_{\mathbf{k'}-\mathbf{q}}\hat{a}_{\mathbf{k'}}\hat{a}_{\mathbf{k}}\bullet - \bullet\,\hat{a}^\dagger_{\mathbf{k}+\mathbf{q}}\hat{a}^\dagger_{\mathbf{k'}-\mathbf{q}}\hat{a}_{\mathbf{k'}}\hat{a}_{\mathbf{k}}\right). \tag{4.63b}$$

In the limit of a lattice of high dimensionality, we imagine that the fluctuation are suppressed, and therefore the only relevant mode must be $\mathbf{k} = 0$. Thus, the model reduce to

$$\mathcal{L}_0\hat{\rho}_0(t) = -\mathrm{i}\left[\hat{H}_0, \hat{\rho}_0(t)\right] + \frac{\gamma}{2}\mathcal{D}[\hat{a}_0] + \frac{\eta}{2N}\mathcal{D}[\hat{a}_0^2], \tag{4.64}$$

where

$$\hat{H}_0 = -(\Delta + 2zJ)\hat{a}^\dagger_0\hat{a}_0 + \frac{U}{2N}\hat{a}^\dagger_0\hat{a}^\dagger_0\hat{a}_0\hat{a}_0 + F\sqrt{N}(\hat{a}^\dagger_0 + \hat{a}_0) + \frac{G}{2}(\hat{a}^{\dagger\,2}_0 + \hat{a}^2_0), \tag{4.65}$$

z being the coordination number.

That is, thanks to this Bogoliubov-like approximation, we can investigate the physics of high-dimensional lattices exploiting the analytic solution of the single cavity. The thermodynamic limit corresponds to the case $N \to \infty$, and, therefore, $\langle\hat{a}^\dagger\,\hat{a}\rangle \to +\infty$ [53, 59].

4.3.2 One-photon pumping: a first-order phase transition

Let us start by considering the case in which the resonator is subject only to a coherent drive (i.e., $G = 0$). Since its Liouvillian has no symmetry which can be broken we expect to observe, at most, a first-order phase transition. This can be triggered by the competition between the detuning Δ and the interaction U. Indeed, the energy cost to add one photon $-\Delta\hat{a}^\dagger\hat{a}$ can be counterbalanced by $U\hat{a}^\dagger\hat{a}^\dagger\hat{a}\hat{a}$. Thus, it may happen that a phase with n photons inside the cavity have the same energy of one with fewer photons. In this case, the pump of strength F struggles against the dissipation of rate γ in determining which state is selected.

Detuning vs Interaction

Having understood that the ratio Δ/U is the triggering parameter for the transition, we begin our investigation exploiting the analytic solution to obtain the steady state as a function of the detuning for different driving amplitudes F. Accordingly, in the left top panel of Fig. 4.8 we plot the mean number of photons $\langle\hat{a}^\dagger\hat{a}\rangle$, which should witness the transition. For a small drive amplitude $F \lesssim U$, the photon number shows well-resolved multi-photon resonances. In the intense-pumping regime $F \gg U$, instead, these resonances are replaced by a continuous and monotonous increase of the photon density, up to a sharp transition from a high- to a low-density phase. Corresponding to the drop in $\langle\hat{a}^\dagger\,\hat{a}\rangle$, the normalized

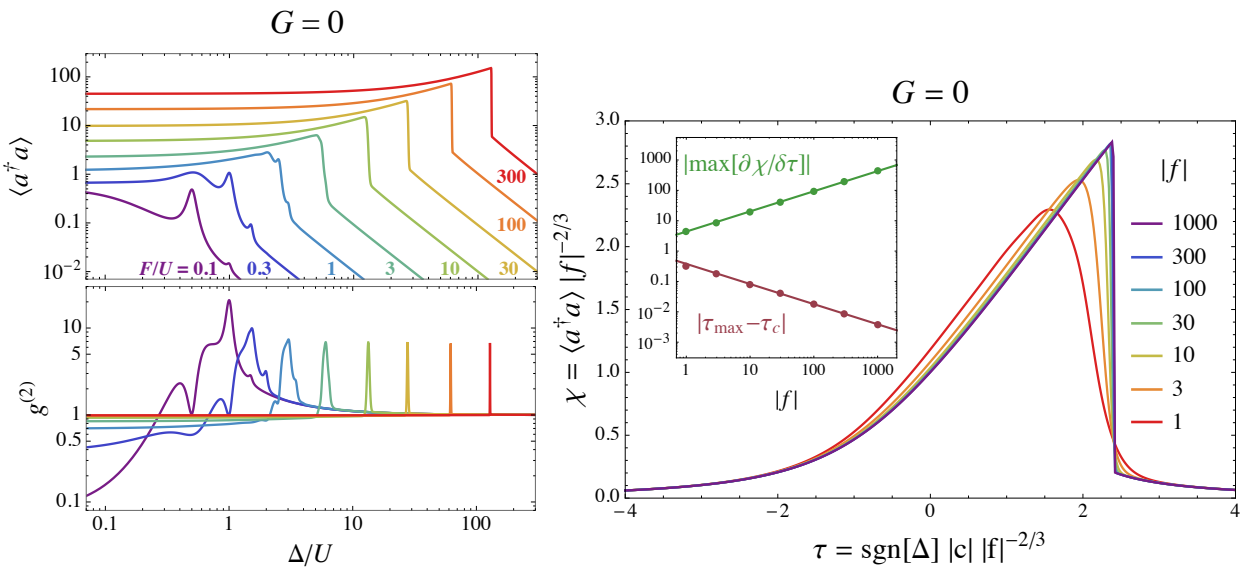

Figure 4.8 – Left: Mean photon number $\langle \hat{a}^\dagger \hat{a} \rangle$ (top panel) and normalized second-order correlation function $g^{(2)}$ (bottom panel) as a function of the pump-cavity detuning Δ normalized by the photon-photon interaction strength U for a resonator subject only to one-photon coherent driving ($G = 0$, $F \neq 0$). Different curves (and colors) correspond to different pumping intensities F/U, varied between 0.1 and 300 (as indicated in the top panel). One- and two-photon dissipation rates were set to $\gamma = \eta = 0.03U$. Right: rescaled mean photon density $\chi = \langle \hat{a}^\dagger \hat{a} \rangle / |f|^{2/3}$ as a function of the dimensionless parameter $\tau = \mathrm{sgn}[\Delta]|c|/|f|^{2/3}$ for different values of the dimensionless coherent drive intensity $|f|$ (see legend). The points in the inset mark height and position of the peak in $\partial\chi/\partial\tau$ as a function of $|f|$. The solid lines are power-law fits with exponents $\pm 2/3$, performed on the last four points. Figure from Ref. [5].

second-order correlation function $g^{(2)}$ exhibits a sharp peak, shown in the Left bottom panel of Fig. 4.8. This quantity is defined as $g^{(2)} = \langle \hat{a}^{\dagger\,2} \hat{a}^2 \rangle / \langle \hat{a}^\dagger \hat{a} \rangle^2$. At the transition, photons have a highly super-Poissonian distribution ($g^{(2)} \gg 1$).

We conclude that the abrupt change in the density is the expected precursor of a driven-dissipative phase transition which would occur in the thermodynamic limit. As previously discussed, we can reach the thermodynamic limit by considering a parameter $N \to \infty$. Thus, in order to further characterize the transition, we consider a scaling of $\chi = \langle \hat{a}^\dagger \hat{a} \rangle |f|^{-2/3}$, which leads to an universal behavior in the thermodynamic limit. [1] In the Left panel of Fig. 4.8, we saw that the high-to-low density transition is triggered by the detuning Δ. In a more general description, we expect the phase transition to be controlled by the dimensionless complex detuning $c = (\Delta + i\gamma/2)/(U - i\eta)$. Hence, in the right panel of Fig. 4.8 we show the behavior of $\chi(\tau)$ for $\tau = \mathrm{sgn}[\Delta]|c||f|^{-2/3}$. In the thermodynamic limit $|f| \to \infty$, $\chi(\tau)$ shows a discontinuous first-order phase transition. For finite values of $|f|$, the derivative $\partial\chi/\partial\tau$ is peaked at the transition point. We find that the height and position of this peak follow the power-law behaviors $\max[\partial\chi/\partial\tau] \propto |f|^{2/3}$ and $|\tau_{\max} - \tau_c| \propto |f|^{-2/3}$ [cf. inset of Fig. 4.8 (right)]. For the selected parameters, we find $\tau_c \sim 2.41$.

1. One can obtain the same result starting from the semiclassical equation (4.57), where one finds that for a large photon number $\langle \hat{a}^\dagger \hat{a} \rangle \propto |f|^{2/3}$ [as a reminder, $f = F/(U - i\eta)$].

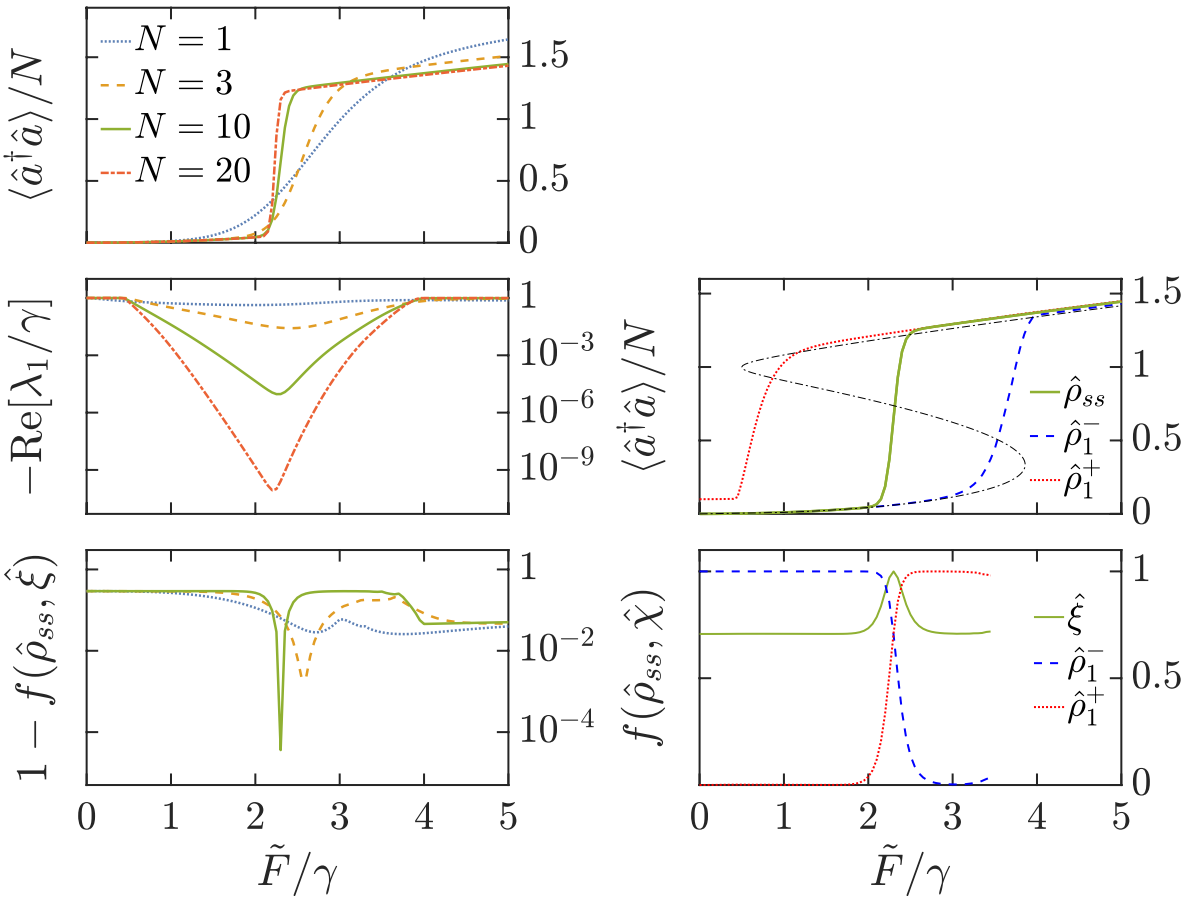

Figure 4.9 – Left: Numerical results for the driven-dissipative Kerr model. Top panel: rescaled number of photons $\langle \hat{a}^\dagger \hat{a} \rangle / N$ as a function of the rescaled driving $\tilde{F}/\gamma$ for different values of N. Middle panel: -Re$[\lambda_1/\gamma]$ (Liouvillian gap) for different values of N. Bottom panel: The error $1 - f$, where f is the fidelity between the steady-state density matrix $\hat{\rho}_{ss}$ and the one reconstructed via the eigendecomposition of the first eigenstate $\hat{\xi} = (\hat{\rho}_1^+ + \hat{\rho}_1^-)/2$. Right: study of the metastable states obtained via the spectral decomposition of $\hat{\rho}_1$. Top panel: average number of photons according to $\hat{\rho}_{ss}$ and $\hat{\rho}^\pm$ as a function of the rescaled driving $\tilde{F}/\gamma$ for $N = 10$ (see definitions in the main text). The dotted line indicates the Gross-Pitaevskii prediction. Bottom panel: fidelity f between the steady-state density matrix $\hat{\rho}_{ss}$ and a density matrix $\hat{\chi} = \hat{\rho}_1^+, \hat{\rho}_1^-, \hat{\xi}$ (for $\hat{\xi} = (\hat{\rho}_1^- + \hat{\rho}_1^+)/2$) as a function of the rescaled driving $\tilde{F}/\gamma$. The transition can be seen as a switching from a region where $\hat{\rho}^-$ describes the system to one where the physics is dominated by $\hat{\rho}^+$. Even if the region of phase coexistence in $\hat{\rho}_{ss}$ is very narrow, $\hat{\rho}_1$ describes the physics in a larger region. Parameters: $\Delta/\gamma = 10$, $\tilde{U}/\gamma = 10$. From Ref. [1].

Applying the general theory

Having proved the onset of a first-order phase transition, we consider now the spectral properties of $\mathcal{L}$ detailed in Chapter 3. We adopt the convention to express the nonlinearity and driving amplitude in the following form:

$$U = \tilde{U}/N, \qquad F = \tilde{F}\sqrt{N}, \tag{4.66}$$

and let change (we recall, the thermodynamic limit is $N \to +\infty$). In Fig. 4.9 we study numerically the emergence of the first-order phase transition by increasing N. The top panel shows the mean value of $\langle \hat{a}^\dagger \hat{a} \rangle / N = \mathrm{Tr}\left[\hat{\rho}_{ss} \hat{a}^\dagger \hat{a}\right] / N$ as a function of $\tilde{F}/\gamma$. The middle panel shows the rescaled Liouvillian gap $-\mathbb{R}\mathrm{e}\left[\lambda_1\right]/\gamma$ as a function of the rescaled driving amplitude. Such Liouvillian gap tends to zero in the thermodynamic limit $N \to +\infty$. The bottom panel of Fig. 4.9 presents a study of the fidelity between the steady state $\hat{\rho}_{ss}$ and the matrix $\hat{\xi} = (\hat{\rho}_1^+ + \hat{\rho}_1^-)/2$, obtained by the spectral decomposition of $\hat{\rho}_1$ [Eq. (3.10)]. We recall that the fidelity is defined as $f(\hat{\rho}, \hat{\xi}) = \mathrm{Tr}\left[\sqrt{\sqrt{\hat{\rho}}\, \hat{\xi} \sqrt{\hat{\rho}}}\right]$. A fidelity equal to 1 indicates that the two states are identical. As the thermodynamical parameter N increases, we notice two important effects: (i) in the region in which the Liouvillian gap is minimal the fidelity is maximal; (ii) the region in which $\hat{\rho}_{ss}$ and $\hat{\xi}$ are close becomes narrower and narrower. This is consistent with our general results which are exact in the thermodynamic limit.

It is interesting now to connect our findings with the results predicted by mean-field theories. A Gross-Pitaevskii-like mean-field approximation for the driven-dissipative Kerr model is known to exhibit bistability, while the full quantum solution is always unique [135]. In the same way, a Gutzwiller-mean-field theory predicts multiple solutions [61, 138, 139]. In Fig. 4.9, we investigate the properties of the exact steady state $\hat{\rho}_{ss}$ and of the density matrices $\hat{\rho}_1^+$ and $\hat{\rho}_1^-$ for a system with $N = 10$ as a function of the rescaled driving amplitude $\tilde{F}/\gamma$. In the top panel, we plot the mean photon density $\langle \hat{a}^\dagger \hat{a} \rangle / N = \mathrm{Tr}\left[\hat{a}^\dagger \hat{a}\, \hat{\chi}\right] / N$, for $\hat{\chi} = \hat{\rho}_{ss}$, $\hat{\rho}_1^+$, $\hat{\rho}_1^-$ as indicated in the legend. To further characterize the nature of $\hat{\rho}_1^\pm$ in the phase transition, in the bottom panel we plot the fidelity between $\hat{\rho}_{ss}$ and $\hat{\chi} = \hat{\xi}$, $\hat{\rho}_1^+$, $\hat{\rho}_1^-$ (where $\hat{\xi} = (\hat{\rho}_1^+ + \hat{\rho}_1^-)/2$). For $\tilde{F} < \tilde{F}_c$, $\hat{\rho}_{ss}$ is almost exactly $\hat{\rho}_1^-$. Around the critical point $F \simeq F_c$, $\hat{\rho}_{ss}$ becomes an equal mixture of $\hat{\rho}_1^+$ and $\hat{\rho}_1^-$. The maximal mixed character occurs for $\tilde{F} = \tilde{F}_c$. Finally, for $\tilde{F} > \tilde{F}_c$, the density matrix becomes very close to $\hat{\rho}_1^+$. This analysis allows us to interpret the two stable solutions predicted by the mean-field approach in terms of the metastable states which compose $\hat{\rho}_1$.

4.3.3 Two-photon pumping: a first- and a second-order phase transition

A similar discussion about the role of the detuning can be performed in the presence of two-photon pumping. That is, if Δ and U compete in determining the number of photons, a first-order phase transition can take place. This time, however, also a second-order phase transition can take place, since the $\mathcal{Z}_2$ symmetry can be broken. Again, we start by analysing the effect of Δ on the steady-state solution.

Detuning vs Interaction

The results obtained for different values of G/U are presented in the Left panel of Fig. 4.10. In the top panel, we observe a similar behavior of the photon density as in Fig. 4.8. Note that the analytic solution allows us to reach very high values of $\langle \hat{a}^\dagger\, \hat{a} \rangle$ (up to ~ 1300 photons for $G = 300U$). The behavior of the second-order correlation function $g^{(2)}$ dramatically differs from the case $G = 0$ considered in Fig. 4.8. For $G \geqslant 10U$, we find a sub-Poissonian statistics ($g^{(2)} < 1$) for small Δ and a strong peak corresponding to the drop in density. After the peak, in the low-density phase, $g^{(2)}$ drops but stays considerably larger than one and, furthermore, it keeps growing roughly quadratically. This high probability of observing photons pairwise

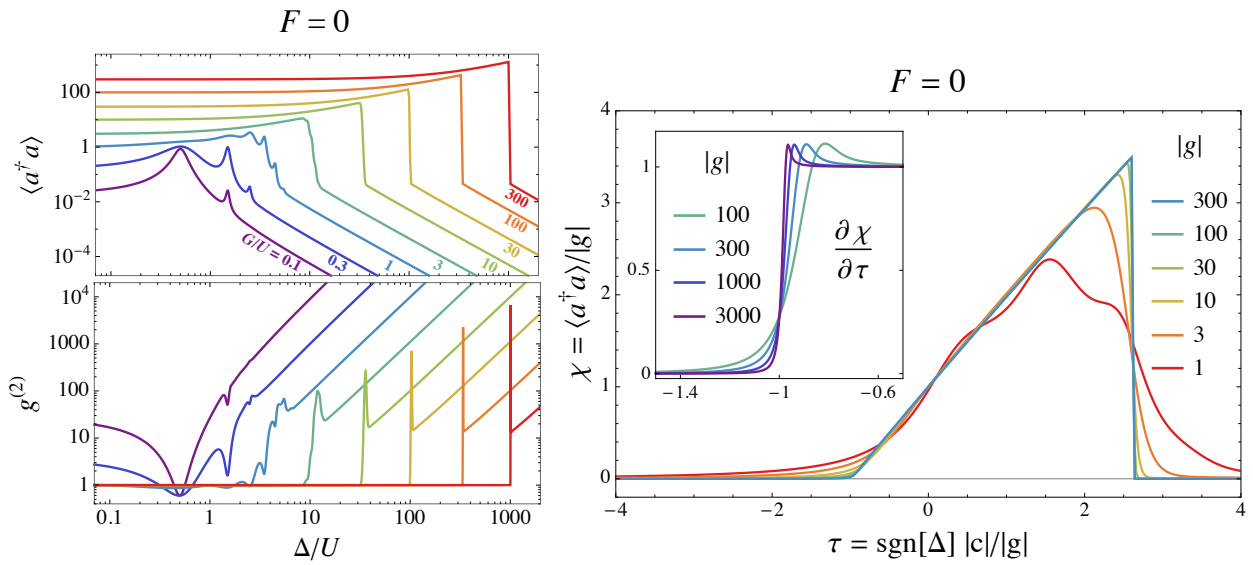

Figure 4.10 – Left: Same as Fig. 4.8, but in the presence of two-photon driving only, i.e. $F = 0$ and $G \neq 0$. Different curves (and colors) correspond to different pumping strengths G/U, spanning from 0.1 to 300. One- and two-photon dissipation rates were set to $\gamma = \eta = 0.03U$. Right: rescaled mean photon density $\chi = \langle \hat{a}^\dagger \hat{a} \rangle / |g|$ as a function of $\tau = \mathrm{sgn}[\Delta]|c|/|g|$ for different values of $|g|$ (see legend). In the inset we show the rapid growth in the derivative $\partial\chi/\partial\tau$ around $\tau = -1$, which tends to a discontinuity increasing $|g|$. Overall, dissipations have been set to $\eta = 0.1U$ and $\gamma = 0.1|\Delta|$. From Ref. [5].

is a clear consequence of the two-photon pumping mechanism. Again, we conclude that the abrupt change in the density is the result of the first-order driven-dissipative phase transition stemming from the competition between U and Δ.

We now perform the same scaling analysis we did in Sec. 4.3.2, for which, in the thermodynamic limit, one expects $\langle \hat{a}^\dagger \hat{a} \rangle \propto |g|$ [with $g = G/(u - i\eta)$]. In the right panel of Fig. 4.10 we plot, for different values of $|g|$, the function $\chi(\tau)$ where we defined $\chi = \langle \hat{a}^\dagger \hat{a} \rangle / |g|$ and $\tau = \mathrm{sgn}[\Delta]|c|/|g|$. Once again, the behavior becomes universal for $|g| \gg 1$, with a sharp transition at positive detuning. The critical-exponent analysis of the derivative is compatible with $\max[\partial\chi/\partial\tau] \propto |g|$ and $|\tau_{\max} - \tau_c| \propto 1/|g|$ for $\tau_c \sim 2.62$. The divergent behavior of the derivative in the thermodynamic limit signals the first-order nature of this phase transition. The latter has the same character of the one observed for $G = 0$ and both occur in the regime for which the semiclassical solution predicts optical multistability. Remarkably, we can identify another phase transition, taking place for $\tau \simeq -1$. Although χ stays continuous in the thermodynamic limit, its derivative, shown in the inset of Fig. 4.10 (right), acquires a discontinuity. In this case, there is no competition between Δ and U in the determination of the steady state. This second-order phase transition has no counterpart in the driven-dissipative Kerr model without the two-photon processes, and thus it strongly suggest the presence of a spontaneous symmetry breaking. Moreover, it takes place around the semiclassical bifurcation point, i.e. when the Wigner function acquires a bi-modal character.

In order to better understand the nature of the first- and second-order phase transition in the two-photon Kerr resonator, we resort to our general theory.

Applying the general theory

The thermodynamic limit of this model is obtained by expressing U and η as

$$U = \tilde{U}/N, \qquad \eta = \tilde{\eta}/N, \tag{4.67}$$

and considering the limit $N \to +\infty$. In this way the ratio U/η is kept constant.

In Fig. 4.11 we show the emergence of a second-order phase transition for $\Delta < 0$ by increasing the value of N. The top panel shows $\langle \hat{a}^\dagger \hat{a} \rangle / N = \mathrm{Tr}\left[\hat{\rho}_{ss} \hat{a}^\dagger \hat{a}\right] / N$ as a function of G/γ. In the middle panel we show the rescaled Liouvillian gap $-\mathbb{R}\mathrm{e}\left[\lambda_1\right]/\gamma$ as a function of the rescaled pump amplitude. The abrupt change in the behavior of λ_1 indicates the onset of the phase transition. In the whole region of broken symmetry, the gap is much smaller than γ and λ_1 is real, while $\hat{\rho}_1$ is a traceless Hermitian matrix which belongs to the odd symmetry sector of $\mathcal{Z}_2$ ($\mathcal{Z}_2 \hat{\rho}_1 = -\hat{\rho}_1$). The states $\hat{\rho}_1^+$ and $\hat{\rho}_1^-$ obtained via the spectral decomposition of $\hat{\rho}_1$ are such that $\mathcal{Z}_2 \hat{\rho}_1^+ = \hat{\rho}_1^-$. As it has been shown in Sec. 3.3.3, in the symmetry-broken region, $\hat{\rho}_{ss}$ can be constructed as a symmetric mixture of $\hat{\rho}_1^+$ and $\hat{\rho}_1^-$. As shown in the bottom-left panel of Fig. 4.11, this gives an excellent approximation for the finite-sized systems considered here. Remarkably, this expression for $\hat{\rho}_{ss}$ remains very accurate even quite far from the thermodynamic limit.

In order to characterize the abrupt change in the behavior of λ_1, which becomes discontinuous for $N \to +\infty$, we plot part of the full spectrum of $\bar{\bar{\mathcal{L}}}$ for $N = 20$ across the critical point. In the top of the right panel in Fig. 4.12, we show the real part of the spectrum, while the bottom one reports the imaginary part. Starting from the imaginary part, we clearly see that there is a point in which two complex-conjugate eigenvalues (highlighted by the red line) become real. We call $G_B(N)$ the point in which this bifurcation happens. Looking at the top panel, this merging is associated to a change in the behavior of the real part of those eigenvalues, which split and bifurcate. The one approaching zero is responsible for the phase transition and its associated eigenvector becomes $\hat{\rho}_1 = \hat{\rho}_1^+ - \hat{\rho}_1^-$ for $G > G_B(N)$. As we saw in Fig 4.11, it is not clear where the gap starts to close, but one might guess that it happens when the two eigenvalues bifurcate. To test this conjecture, in the inset we plot, as a function of N, the scaling of the bifurcation point $\Delta G = G_B(N) - G_c$, where G_c is the critical point extrapolated via the study of the analytic solution for $N = 1000$. Indeed, the clear power-law decay of this quantity demonstrates that the onset of this transition can be understood in terms of a merging of two eigenvalues. The emergence of criticality is thus to be associated with a crossing of two eigenvalues in the complex plane. This fact, together with the emergence of a discontinuity in λ_1 for $N \to \infty$, implies that, at the bifurcation point, the Liouvillian becomes not diagonalizable, resulting in a Jordan structure. This leads to a non-exponential relaxation dynamics at criticality. To better understand this behavior, in App. D we study an exactly-solvable two-level system which admits a Jordan-block structure for a specific choice of parameters.

We have previously shown that for $\Delta > 0$ there is a first-order phase transition associated to a symmetry broken phase, example which seems in contrast with our general theory. Up to now, however, we considered the case in which only an eigenvalue of the symmetry sector L_{-1} approaches zero and gives rise to a symmetry breaking without inducing first-order discontinuities in $\hat{\rho}_{ss}$. Indeed, together with the emerging of a zero in L_{-1}, for $\Delta > 0$ the symmetry sector L_1 acquires two zero eigenvalues: one associated to $\hat{\rho}_{ss}$, the other to an eigenmatrix whose eigenvalue touches zero only at the critical point. This allows a discontinuous behavior of $\hat{\rho}_{ss}$ with symmetry breaking. In Fig. 4.12 we plot the behavior of

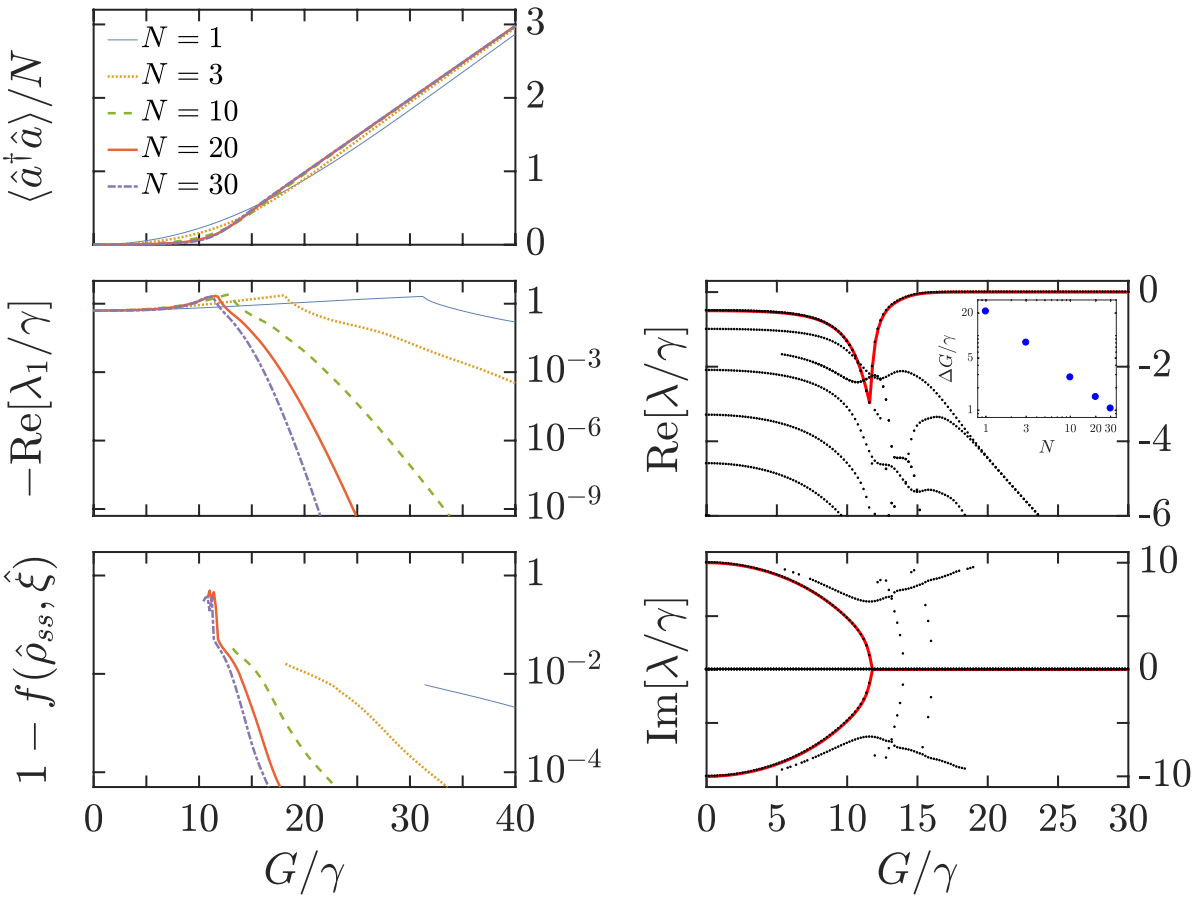

Figure 4.11 – Left: Numerical results for the driven-dissipative two-photon Kerr model. Top panel: rescaled number of photons $\langle \hat{a}^\dagger \hat{a} \rangle / N$ as a function of the rescaled driving G/γ for different values of N. Middle panel: -Re$[\lambda_1/\gamma]$ (Liouvillian gap) for different values of N. Bottom panel: The error $1 - f$, where f is the fidelity between the steady state density matrix $\hat{\rho}_{ss}$ and $\hat{\xi} = (\hat{\rho}_1^+ + \hat{\rho}_1^-)/2$. The curves are shown in the region where λ_1 is purely real. Right: Liouvillian spectrum in the two-photon Kerr model for $N = 20$. Top and bottom panels: real and imaginary part of the eigenvalues of $\bar{\bar{\mathcal{L}}}$. The dots represent the 10 smallest-modulus eigenvalues obtained by numerical diagonalisation. The red lines are a guide for the eye indicating the two eigenvalues which merge into λ_1 for $G \gg \gamma$. Inset: log-log plot of $\Delta G = (G_B(N) - G_c)$ (defined in the text) as a function of the parameter N, showing the power-law behaviour $\Delta G = A\, N^{-\eta}$ with $A = 21.1 \pm 0.2$ and $\eta = 0.881 \pm 0.006$. In the thermodynamic limit, the bifurcation point $G_B(N)$ and the critical point G_c coincide. Parameters: $\Delta/\gamma = -10$, $\tilde{U}/\gamma = 10$, $\tilde{\eta}/\gamma = 1.0$. From Ref. [1].

the system in such regime. Top panel shows the emergence of a first-order phase transition in the rescaled density. In the middle panel, we plot the real part of the two eigenvalues of the Liouvillian with the smallest modulus. One presents the phenomenology we expect from a symmetry breaking: $-\mathbb{R}\mathrm{e}\,[\lambda_1] \ll \gamma$ in the symmetry-broken phase $G \geq G_c(N)$. The other is responsible for the discontinuous first-order behavior: $-\mathbb{R}\mathrm{e}\,[\lambda_2] \ll \gamma$ only for $G \simeq G_c(N)$. Indeed, we tested that $\hat{\rho}_1$ (associated to λ_1) satisfies $\mathcal{Z}_2\hat{\rho}_1 = -\hat{\rho}_1$. Moreover, $\mathcal{Z}_2\hat{\rho}_1^\pm = \hat{\rho}_1^\mp$ and $\hat{\rho}_{ss} \simeq (\hat{\rho}_1^+ + \hat{\rho}_1^-)/2$. As for $\hat{\rho}_2$, $\mathcal{Z}_2\hat{\rho}_2 = \hat{\rho}_2$ and it cannot be associated with a symmetry breaking. In the bottom panel we test the structure of $\hat{\rho}_{ss}$ in connection to the spectral decomposition of $\hat{\rho}_2$: the first-order phase transition can be interpreted as a switch between $\hat{\rho}_2^-$ and $\hat{\rho}_2^+$.

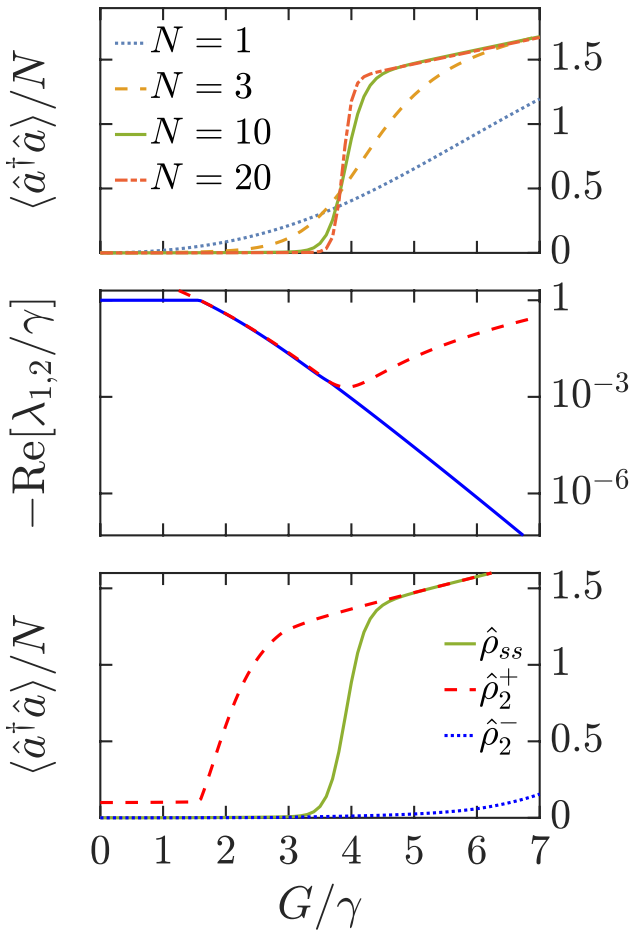

Figure 4.12 – Study of the first-order phase transition with symmetry breaking in the two-photon Kerr resonator. Top panel: rescaled number of photons $\langle \hat{a}^\dagger \hat{a} \rangle / N$ as a function of the rescaled driving G/γ for different values of N. Middle panel: real part of $\lambda_{1,2}$ rescaled by γ for $N = 10$. The two branches of Liouvillian eigevalues lead to the first-order phase transition (red) and a symmetry breaking (blue). Bottom panel: average number of photons according to $\hat{\rho}_{ss}$ and $\hat{\rho}_2^{\pm}$. Parameters: $\Delta/\gamma = 10$, $U/\gamma = 10$, $\eta/\gamma = 1.0$. From Ref. [6].

The symmetry breaking emerges in the fact that $\hat{\rho}_2^+ \simeq \left(\hat{\rho}_1^+ + \hat{\rho}_1^-\right)/2$. In conclusion, in these specific numerical examples we recover all the features predicted by our general theory.

4.4 Quantum trajectories

The previous discussion of the steady-state and spectral properties proved the emergence of a first- and second-order phase transitions in Kerr resonators. Here, we exploit quantum trajectories to characterise criticality in these driven-dissipative systems, benchmarking at the same time the theory proposed in Sec. 3.4.2. The details about the numerical protocol used to simulate the quantum trajectories can be found in App. E.4.

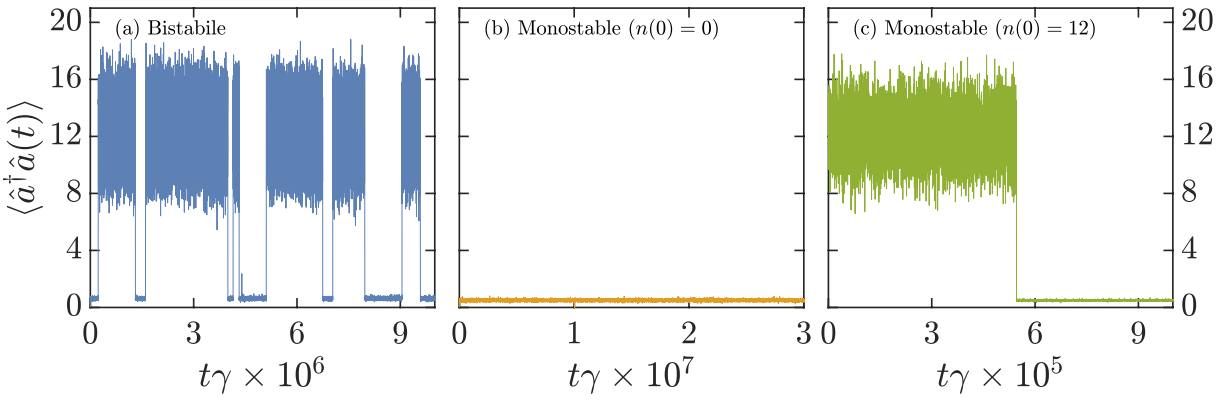

Figure 4.13 – Mean number of photon $n(t) = \langle \hat{a}^\dagger \hat{a}(t) \rangle$ for a counting trajectory as a function of time for a Kerr resonator for $N = 10$. Panel (a): Simulation for $F = 2.3 \simeq F_c$, where $\hat{\rho}_{ss}$ is an equal mixture of $\hat{\rho}_1^{\pm}$. Panel(b): We set $F = 2.1 \lesssim F_c$, where $\lambda \ll \gamma$ but $\hat{\rho}_{ss} \simeq \hat{\rho}_1^-$. The initial state is $|\Psi(0)\rangle = |0\rangle$. Panel (c): Same as in (b), but for $|\Psi(0)\rangle = |12\rangle$ Parameters as in Fig. 4.9.

4.4.1 Bistability in the Kerr resonator

Let us consider a counting quantum trajectory described in Sec. 2.2 for the one-photon Kerr resonator. As discussed in Sec. 3.4.2, we expect that, if $t \gg \tau$, the quantum trajectory should only explore the states which make $\hat{\rho}_{ss}$.

Both the general theory developed in Chapter 3 and the numerical results presented in Sec. 4.3.2 are in agree that, at the critical point F_c, the steady state is the sum of two density matrices. For finite size systems, in Fig. 4.9 we saw that this phase coexistence is present in a small region of the parameter space. Consequently, for $F \simeq F_c$, we expect that $\hat{\rho}_{ss} \simeq (\hat{\rho}_1^+ + \hat{\rho}_1^-)/2$, where $\hat{\rho}_1^{\pm}$ are a metastable state decaying towards $\hat{\rho}_{ss}$ with a timescale of order $\tau = 1/\lambda_1$. The numerical study of this regime via quantum trajectories is presented in panel (a) of Fig. 4.13, where we plot the mean number of photons as a function of time. The resonator intermittently jumps from a low-density regime [$\Psi(t) \in \{\Psi_i^-\}$, cf. Eq. (3.37)] to a high density one [$\Psi(t) \in \{\Psi_i^+\}$]. The switching time is of the order of $\tau \approx 10^5\gamma$, in agreement with $\lambda_1 \simeq 10^{-5}$ obtained by the exact diagonalisation of the Liouvillian (cf. Fig. 4.9). We stress that the wavefunction $\Psi(t) \in \{\Psi_i^-\}$ [$\Psi(t) \in \{\Psi_i^+\}$] explores all the states of $\hat{\rho}_1^-$ ($\hat{\rho}_1^+$), and therefore the trajectory is noisy.

In panel (b) of Fig. 4.13, we study the system for $F \lesssim F_c$, where $\lambda_1 \ll \gamma$ but $\hat{\rho}_{ss} \simeq \hat{\rho}_1^-$ (cf. Fig. 4.9). As discussed in Sec. 3.4.2, the system remains in a low-density state, i.e., $|\Psi(t)\rangle \in \{|\Psi_i^-\rangle\}$. Indeed, the plot shows that there are no jumps to any $\{|\Psi_i^+\rangle\}$ for a time which is much bigger than the Liouvlillian gap (notice that the simulation has been run on a time which is of the order $40/\lambda_1$). This confirm the previous analysis about the spectral structure of the Liouvillian, which tell us that the Liouvillian gap can be very small even if there is no phase coexistence.

Finally, in panel (c) of Fig. 4.13 we consider again $F \lesssim F_c$, but we choose $|\Psi(0)\rangle = |12\rangle$, so that the initial state is one of the wave function of $\{|\Psi_i^+\rangle\}$. In this case, we observe that, before reaching the low-density branch, the system remains the high branch for a very long time. Again, the quantum trajectory explores all the wavefunction which compose $\hat{\rho}_1^+$, and thus the trajectory is extremely noisy.

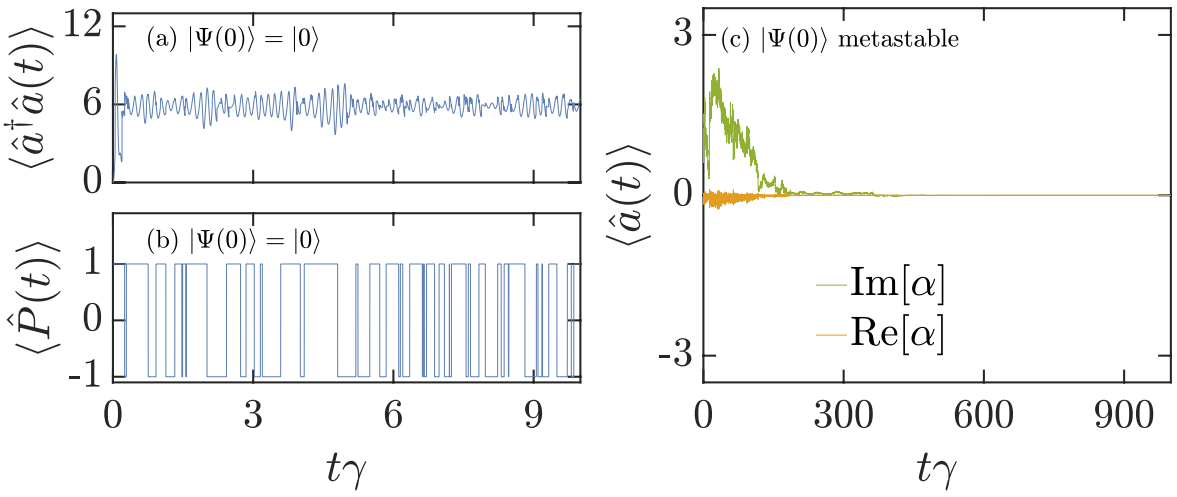

Figure 4.14 – Counting trajectory for a two-photon Kerr resonator for $N = 3$ and $G = 30$. Panel(a): Number of photons as a function of time for a state initialised in the vacuum. Panel (b): Parity as a function of time for a state initialised in the vacuum. Panel (c): Mean value of the annihilation operator as a function of time for $|\Psi(0)\rangle$ metastable. Parameters as in Fig. 4.9.

4.4.2 Bimodality of the two-photon Kerr resonator

We consider now the case of a second-order phase transition in a quadratically-driven resonator. As detailed in Sec. 4.3.3, this critical phenomenon is characterised by a spontaneous symmetry breaking of $\mathcal{Z}_2 = e^{i\pi\hat{a}^\dagger\hat{a}} \bullet e^{i\pi\hat{a}^\dagger\hat{a}}$. Therefore, in the symmetry-broken phase, we expect that $\hat{\rho}_{ss} = (\hat{\rho}_1^+ + \hat{\rho}_1^-)/2$, where $\hat{\rho}_1^+ = \mathcal{Z}_2\hat{\rho}_1^-$.

Since we are considering a second-order phase transitions, we need a order parameter to distinguish between different phases [12]. The number of photons is not a good witness since $\hat{\rho}_1^\pm = \mathcal{Z}_2\hat{\rho}_1^\mp$ and therefore $\mathrm{Tr}\left[\hat{\rho}_1^+\hat{a}^\dagger\hat{a}\right] = \mathrm{Tr}\left[\hat{\rho}_1^-\hat{a}^\dagger\hat{a}\right]$. A more suitable order parameter is the mean value of the annihilation operator $\langle\hat{a}\rangle = 0$. Indeed, since $\mathcal{Z}_2\hat{\rho}_{ss} = \hat{\rho}_{ss}$, we have that $\langle\hat{a}\rangle = 0$. That is, the emergence of a symmetry-breaking transition can be signalled by the emergence of two metastable states with opposite $\langle\hat{a}\rangle \neq 0$.

We start by studying a counting quantum trajectory. In panel (a) of Fig. 4.14, we show the time evolution of the mean number of photons, which do not present a bimodal character. As we proved in Theorem 3.5 of Sec. 3.4.2, a counting trajectory cannot observe a $\mathcal{Z}_2$ symmetry breaking, but *always* jumps between eigenstates of $\hat{Z}_2 = e^{i\pi\hat{a}^\dagger\hat{a}}$. Thus, in panel (b) we plot, as a function of time, the expectation value of the parity $\hat{P} = e^{i\pi\hat{a}^\dagger\hat{a}}$. As expected, the system switches between an even and an odd state on a timescale which is much faster than the Liouvillian gap. Moreover, we verified that, starting from a state with well-defined parity, for any t we have $\langle\hat{a}(t)\rangle = 0$. Finally, in panel (c), we show the time evolution of the real and imaginary parts of $\langle\hat{a}(t)\rangle$ if the system is initialised in a metastable state. The dynamics towards $\langle\hat{a}(t)\rangle = 0$ is very slow, and the relaxation time is consistent with the value one would obtain from the Liouvillian gap (cf. Fig. 4.11).

In order to observe the periodic switches between the two metastable states along a quantum trajectory, in Fig. 4.15 we use a homodyne protocol. In panel (a) we show that, as expected, the mean number of photons, is not a good observable to witness bimodality. In panel (b) we plot the expectation value of the parity, demonstrating that it remains always

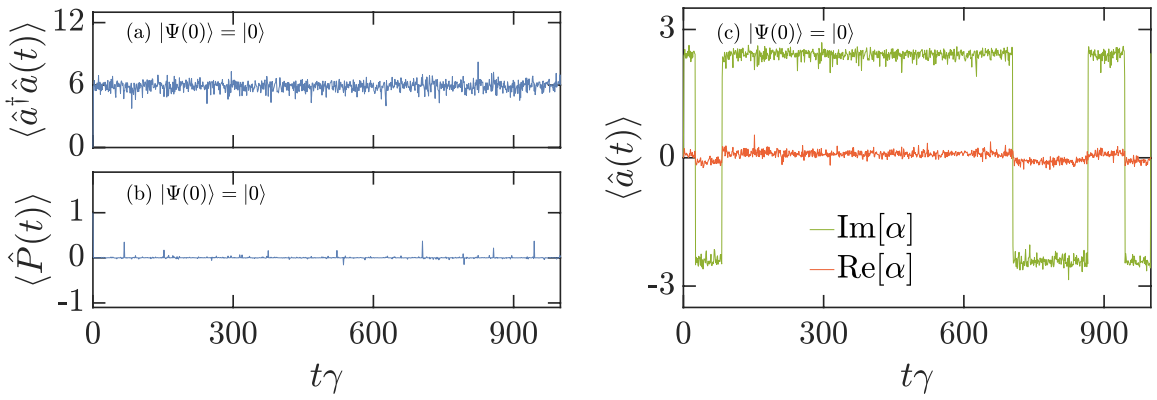

Figure 4.15 – Homodyne trajectory for a two-photon Kerr resonator for $N = 3$ and $G = 30$. Panel(a): Number of photons as a function of time for a state initialised in the vacuum Panel (b): Parity as a function of time for a state initialised in the vacuum. Panel (c): Field quadrature as a function of time for a state initialised in the vacuum. Parameters as in Fig. 4.9.

around zero, and do not present any bimodal behaviour (in sharp contrast with Fig. 4.14 (b)). Finally, in panel (c), we show that the system switches between two states with opposite $\langle \hat{a} \rangle$ on a timescale of the order of the inverse of the Liouvillian gap (cf. Fig. 4.11).

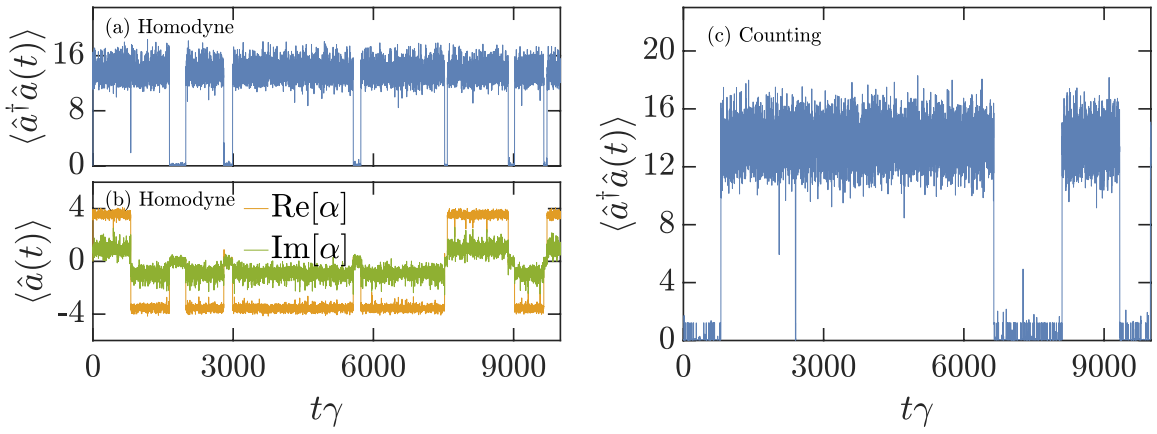

Figure 4.16 – Quantum trajectories for a two-photon Kerr resonator for $N = 10$ and $G = 4$. Panel(a): Number of photons as a function of time for a state initialised in the vacuum for a homodyne trajectory. Panel (b): Mean value of the annihilation operator as a function of time for a state initialised in the vacuum for a homodyne trajectory. Panel (c): Number of photons as a function of time for a state initialised in the vacuum for a counting trajectory. Parameters as in Fig. 4.12.

The case of a first-order phase transition in the quadratically-driven resonator is presented in Fig. 4.16. This time, there are three metastable states: one with low number of excitations, and two at high density (each one characterised by opposite value of $\langle \hat{a} \rangle$). In panel (a) we study the time evolution of $\langle \hat{a}^\dagger \hat{a} \rangle$ along a homodyne trajectory. The state intermittently jumps between a low- and high-density regimes. In order to appreciate the symmetry breaking, in panel (b) we plot the mean value of $\langle \hat{a} \rangle$. The system jumps between three values: one around zero (the low-density branch) and two characterised by opposite phases. Finally,

in panel (c), we show that a counting trajectory can capture the first-order phase transition but not the symmetry-breaking.

4.5 Conclusions

In this Chapter, we investigated two central models in quantum optics, i.e. the one- and two-photon driven-dissipative Kerr resonators. Having provided the analytic solution for the steady-state of those models, we investigate their features. In particular, we demonstrate that, in an appropriate thermodynamics limit, a phase transition might take place. We used those models as a benchmark for our general theory presented in Chapter 3.

The discussion provided in this Chapter opens many perspectives. Indeed, for the one photon pump, the exact results, combined with mean-field prediction [61, 138], will be the starting point for the study of the Driven-Dissipative Bose-Hubbard lattices presented in Chapter 5. Concerning two photon driving, the analytic solution has been used to study the mean field diagram of a two-photon Bose-Hubbard lattice in Ref. [63], while a full numerical study of this model is in progress.

CHAPTER 5

The Driven-Dissipative Bose-Hubbard Lattices

In a lattice of coupled resonators with local boson-boson interaction U, a coherent and homogeneous driving of all the sites can create a macroscopic population in the zero-wavevector mode ($k = 0$). Being delocalized in space, the latter experiences a self-interaction of strength U/N, N being the number of sites. If one retains only the $k = 0$-mode operators, the physics is the one described in Sec. 4.3 and [1, 5, 59]. An interesting and challenging problem is to understand how the presence of the other modes with $\mathbf{k} \neq \mathbf{0}$ affects the dynamics of the system. In particular, the emergence of criticality might depend on fluctuations associated to this multitude of modes and on the dimensionality of the lattice. A recent work [60] has reported calculations of the steady-state population for lattices as a function of the driving strength, suggesting the presence of a first-order discontinuity in two-dimensional lattices, but only a smooth crossover in one-dimensional arrays.

In this Chapter, we explore this paradigmatic example, performing a the finite-size scaling of the dynamical properties, to clearly signal the absence of criticality in 1D chains and emergence of a phase transition in 2D lattices. Exploiting the truncated Wigner approximation, we transform the Lindblad master equation into a set of stochastic equations for the lattice fields. We numerically solve them, and determine the presence of a critical slowing down in 2D lattices due to the emergence of a first-order phase transition between collective low-density and high-density phases. We characterize this paradigm of dissipative phase transition via a comprehensive study of the main observables.

Another interesting question is weather the phase transition is destroyed by the presence of disorder (i.e. in an inhomogeneous lattice). In this Chapter, we introduce a possible strategy relying on quantum trajectories. The advantage of the proposed method is that it only slightly increases the computational complexity of the disordered problem with respect to the homogeneous one.

This Chapter is organised as follows. In Sec. 5.1 we introduce the Driven-Dissipative Bose Hubbard (DDBH) model and we discuss the truncated Wigner approximation. In Sec. 5.2, we present our main results. In Sec. 5.3, we discuss a possible way to tackle disordered systems exploiting quantum trajectories.

Contents

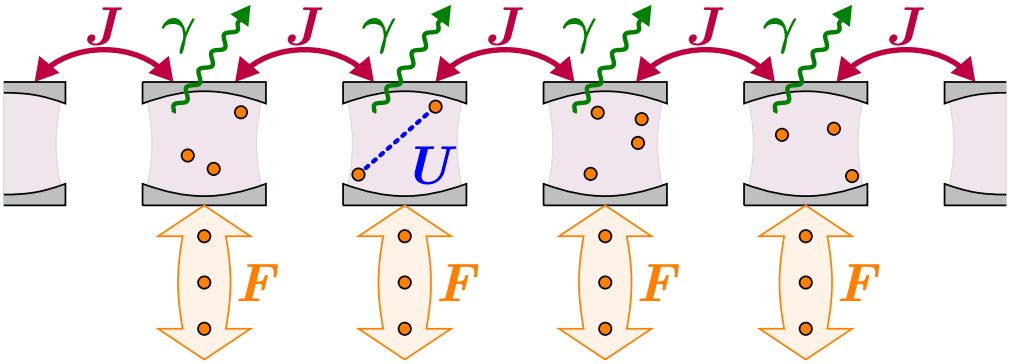

Figure 5.1 – Depiction of the considered driven-dissipative Bose-Hubbard system in the 1D case. The picture represents a lattice of photon resonators, each one subject to one-photon losses with rate γ, and coherently driven by a one-photon pump of amplitude F. The strength of the photon-photon interaction is quantified by U. Nearest neighbour sites are coupled by a tunneling of intensity J. Form Ref. [3].

5.1 The model

Here, we consider a lattice of identical one-photon Kerr resonators (described in Sec 4.1). In presence of coherent driving with frequency ω_p it is described by the following Hamiltonian (in the frame rotating with the drive):

$$\hat{H} = \sum_j -\Delta \hat{a}_j^\dagger \hat{a}_j + \frac{U}{2} \hat{a}_j^{\dagger 2} \hat{a}_j^2 + F\left(\hat{a}_j^\dagger + \hat{a}_j\right) - J \sum_{<j,j'>} \hat{a}_j^\dagger \hat{a}_{j'} \tag{5.1}$$

where, we recall, $\Delta = \omega_p - \omega_c$ is the detuning between the driving frequency and mode frequency ω_c, U the on-site interaction, F the homogeneous driving field (again, the phase is chosen in such a way that F is real). The parameter J quantifies the hopping coupling between two nearest neighboring sites (see Fig. 5.1). In the following, z will denote the number of nearest neighbors ($z = 2$ and $z = 4$ for the 1D and 2D lattices considered in this Chapter, respectively).

To describe the dissipative dynamics, we will consider that all the cavities are subject to an uniform Markovian single-boson loss rate γ. Consequently, the Lindblad master equation for $\hat{\rho}(t)$ reads:

$$\partial_t \hat{\rho}(t) = \mathcal{L}\hat{\rho}(t) = -\mathrm{i}\left[\hat{H}, \hat{\rho}(t)\right] + \gamma \sum_j \mathcal{D}[\hat{a}_j]\hat{\rho}(t). \tag{5.2}$$

We stress that, due to the presence of the one-photon pump, this model has no $\mathcal{Z}_n$ symmetry.

5.1.1 The truncated Wigner approximation

Consider, for sake of simplicity, a single Kerr resonator, whose Liouvillian has been described in Eq. (4.4). According to Eq. (2.79), we can map the time evolution of the density

matrix onto the time evolution of the Wigner function as

$$\begin{aligned}\partial_t W(\alpha) =&\partial_\alpha \left[\mathrm{i}\Delta\alpha - \mathrm{i}U(|\alpha|^2-1)\alpha + \frac{\gamma}{2}\alpha + \mathrm{i}F\right] W(\alpha) \\ &+ \partial_{\alpha^*}\left[-\mathrm{i}\Delta\alpha^* + \mathrm{i}U(|\alpha|^2-1)\alpha^* + \frac{\gamma}{2}\alpha^* - \mathrm{i}F\right] W(\alpha) \\ &+ \frac{\gamma}{2}(\partial_\alpha\partial_{\alpha^*} + \partial_{\alpha^*}\partial_\alpha)W(\alpha) + \mathrm{i}\frac{U}{4}\partial_\alpha\partial_{\alpha^*}(\partial_{\alpha^*}\alpha^* - \partial_\alpha\alpha)W(\alpha).\end{aligned} \tag{5.3}$$

In the weakly interacting limit, i.e. $U/\gamma \ll 1$, and if $W(\alpha)$ is sufficiently regular, we can discard the third-order term $\mathrm{i}U\partial_\alpha\partial_{\alpha^*}(\partial_{\alpha^*}\alpha^* - \partial_\alpha\alpha)W(\alpha)/4$.[1] In this case, one has a well-defined Fokker-Plank equation for $W(\alpha)$, which can be interpreted as a probability distribution [27, 120, 156]. To the resulting Fokker-Plank equation one can associate a stochastic Langevin equation of the form

$$\dot{\alpha} = \left[-\mathrm{i}(\Delta - U(|\alpha|^2-1) - \gamma/2)\right]\alpha + \mathrm{i}F + \sqrt{\gamma/2}\,\chi(t), \tag{5.4}$$

where $\chi(t)$ is a normalized random complex Gaussian noise such that $\langle\chi(t)\chi(t')\rangle = 0$ and $\langle\chi(t)\chi^*(t')\rangle = \delta(t-t')$. In analogy to what we did in Sec. 2.2, we call the evolution of α a (stochastic) Wigner trajectory. In the limit of an infinite number of trajectories, one retrieves all the properties of the Wigner function.

Eq. (5.4) can be easily generalised for a lattice of N cavities by considering a set of $\{\alpha_j\}$ complex numbers characterised by

$$\dot{\alpha_j} = \left[-\mathrm{i}(\Delta - U(|\alpha_j|^2-1) - \gamma/2)\right]\alpha_j - iJ\sum_{j'}\alpha_{j'} + iF + \sqrt{\gamma/2}\,\chi(t), \tag{5.5}$$

where j' runs over the nearest neighbors of j. Since we are considering a Wigner function, one can recover the expectation values for any symmetrized products of operators (see Sec. 2.3) by averaging over different stochastic trajectories through the relation

$$\langle\{(\hat{a}_i^\dagger)^n\hat{a}_j^m\}_0\rangle = \frac{1}{N_{\mathrm{traj}}}\sum_r(\alpha_{i,r}^*)^n\alpha_{j,r}^m, \tag{5.6}$$

where the index r runs over the N_{traj} random trajectories. The great advantage of this approximation is that drastically reduce the computational complexity of the problem: for an array of N cavities we need to consider a system of N complex variables. The price to pay is that, in order to obtain sufficiently precise expectation values, one may need to consider $N_{\mathrm{traj}} \gg 1$.

Finally, let us discuss which meaning can we assign to a single Wigner trajectory. In Secs. 2.2.3 and 4.4, we saw that, in the case of a quantum trajectory it is possible to study the properties of single trajectories in order to infer some relevant proprieties if the system. In case $U = 0$, we can think if $W(\alpha)$ as genuine a probability distribution of coherent states, and thus α_j represent the state of the cavity if it is forced to remain in a coherent state all along its dynamics. In this regard, a single trajectory $\{\alpha_j\}$ can recover all those "classical" properties of the system, such as time and spatial coherence in the lattice. We assume that, for small enough U, this is still the case and we can give a physical meaning to a single Wigner quantum trajectory.

1. We require a sufficiently regular Wigner function since the term which we are discarding is proportional to

$$(\partial_{\alpha^*}\alpha^* - \partial_\alpha\alpha)W(\alpha),$$

which is small if $\partial_{\alpha^*}W(\alpha) \simeq \partial_\alpha W(\alpha) \simeq 0$.

5.1.2 Benchmark of the truncated Wigner approximation

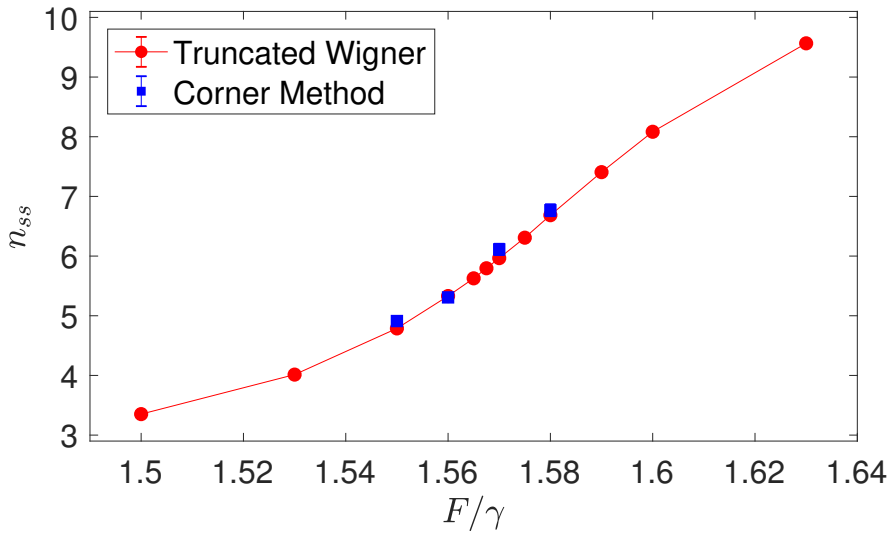

Figure 5.2 – Steady-state average boson occupation per site as a function of the driving F/γ in a 4×1 array: different symbols correspond to different numerical methods. The statistical error is of the order of the symbol size. Parameters are $U/\gamma = 0.1$, $zJ/\gamma = 0.9$, $\Delta/\gamma = 0.1$. From Ref. [3].

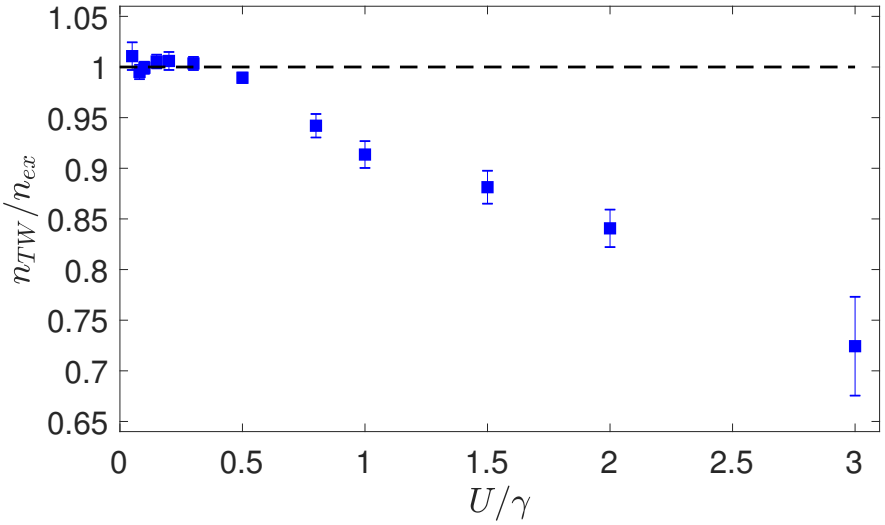

Figure 5.3 – Ratio between the steady-state average occupation obtained through the Truncated Wigner approximation n_{TW} and the exact Runge-Kutta Integration of the Lindblad Master Equation n_{ex} in a 2×1 array. The error bars refer to the statistical noise of the results associated to the stochastic Langevin simulations. F/γ has been varied so that $UF^2/\gamma^3 = 2.465$ is kept constant; $zJ/\gamma = 0.9$ and $\Delta/\gamma = 0.1$ are fixed. Note that the results for $U/\gamma \leq 0.2$ have been obtained with the corner-space renormalization. From Ref. [3].

Having detailed the truncated Wigner approximation, here we present some numerical results showing that this method is accurate in the regime which we will consider in the following. To do so, we compare the approximated results to what was obtained with numerically exact methods for small systems.

In Fig. 5.2, we present the steady-state average population in a 4×1 array for $U/\gamma = 0.1$, $zJ/\gamma = 0.9$, $\Delta/\gamma = 0.1$. The blue curve is computed with the Truncated Wigner approximation and the red one with the corner-space renormalization method (see Ref. [130] and App. E.6) finding an excellent agreement between the two. We would point out that for the considered value of $U/\gamma = 0.1$, a brute-force integration of the master equation for a one-site system requires a cutoff of $N_{max} = 40$ bosons in order to achieve adequate numerical convergence. That is, in a 4×1 lattice the dimension of such a Hilbert space would be $40^4 = 2.56 \cdot 10^6$, which cannot be handled numerically without exploiting advanced methods.

In Fig. 5.3 we present the ratio n_{TW}/n_{ex} between the steady-state average population obtained via the Truncated Wigner approximation n_{TW} and exact methods n_{ex} as a function of the nonlinearity U/γ for a 2×1 array. This quantity identifies the range of values U/γ in which the Truncated Wigner approximation is accurate. In particular, for $U/\gamma \leq 0.3$ the Truncated Wigner yields results within 1% of the exact value.

5.2 Critical behaviour in the bistable region

Here we will explore the onset of a first-order phase transition in a regime where mean-field theory predicts bistability. Within a Gross-Pitaevskii-like mean-field approach, the master equation for the lattice density matrix is replaced by a simple equation for the mean-field $\alpha_j = \langle \hat{a}_j \rangle$, which is the same as Eq. (5.5), but without the noise terms. In the homogenous case ($\alpha_j = \alpha$), the steady-state equation takes the nonlinear form $|\alpha|^2((\Delta + zJ - U|\alpha|^2)^2 + \gamma^2/4) = F^2$, which can have three non-degenerate solutions for a given F, two of which are dynamically stable. As in all mean-field theories [61, 138, 139], the effect of hopping depends only on zJ, with the lattice dimension playing no role. Hence, in the following, when comparing 1D versus 2D lattices, we will consider the same value of zJ, so that differences will only be due to effects beyond mean-field.

5.2.1 Emergence of a phase transition

In panel (a) of Fig. 5.4 we present results obtained with the truncated Wigner approximation for the steady-state site-averaged population $n_{ss} = \frac{1}{N}\sum_{i=1}^{N} \mathrm{Tr}(\hat{\rho}_{ss}\hat{a}_i^\dagger \hat{a}_i)$ for 1D arrays of different length L (up to $L = 512$). In panel (b), the same observable is reported for 2D $L \times L$ lattices (up to 14×14). Both 1D and 2D calculations have been performed with periodic boundary conditions. In both (a) and (b) the Gross-Pitaevskii-like mean-field prediction is depicted by the dashed line. While, in general, mean-field theories exhibit multistability, the density-matrix solution of the master equation is under quite general assumptions unique [135]: indeed, quantum fluctuations make the mean-field solutions metastable so that on a single trajectory the system switches back and forth from one metastable state to another on a time scale related to the inverse Liouvillian gap [1, 5, 51, 57, 120, 142] (see also Fig. 5.4 (c)). The results in Fig. 5.4 (a) show that the S-shaped multivalued curve of the mean-field theory is replaced by a single-valued function, which depends on the array size L. Remarkably, by increasing the size L of the array $n_{ss}(F)$ eventually converges to a curve with a finite slope. On the other hand, in 2D the slope of $n_{ss}(F)$ does not saturate when increasing the size L of

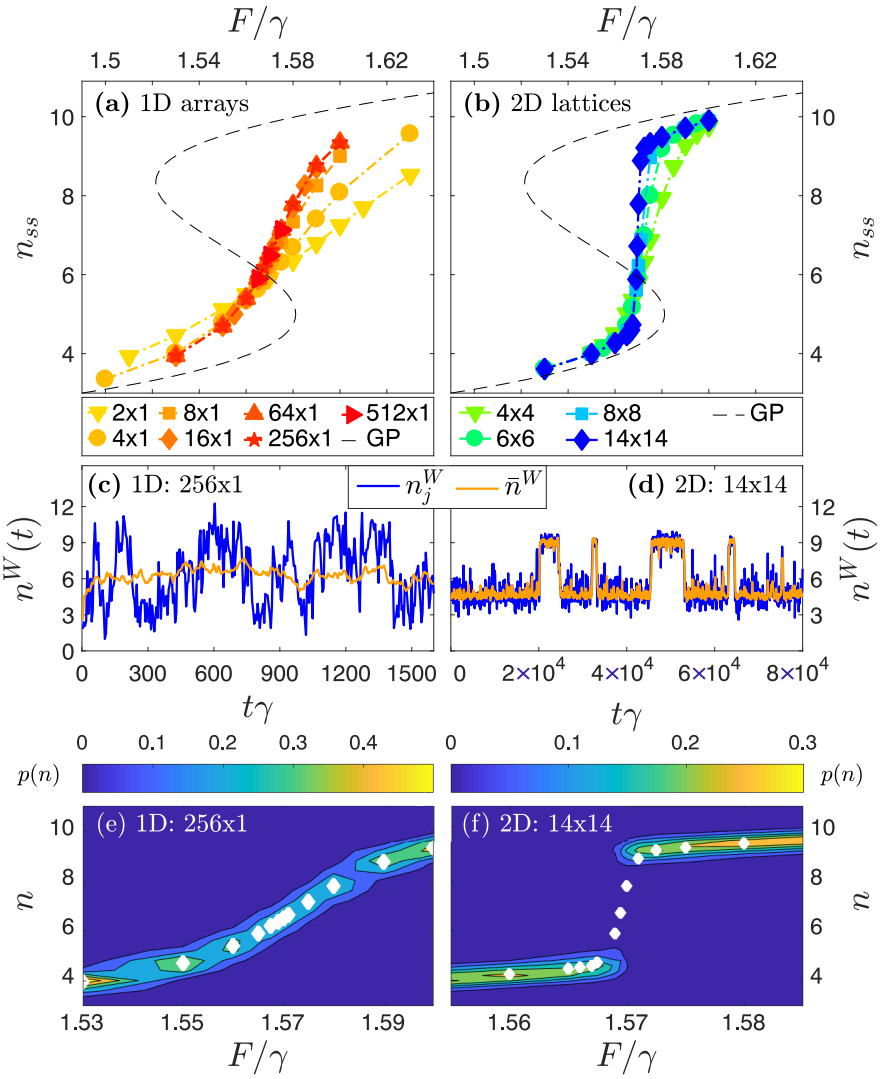

Figure 5.4 – The left panels are for 1D arrays, while the right panels refer to 2D square lattices. (a) and (b): steady-state average population per site versus driving amplitude F (in units of the dissipation rate γ) for lattices of different size. The dashed line is the prediction of the Gross-Pitaevskii mean-field theory. (c), (d): time-dependent single-trajectory population n_j^W in the j-th site (dark blue) and same quantity averaged over all sites $\bar{n}_j^W$ (light orange) for $F = 1.5695\gamma$. (e), (f): contour plot of the probability distribution $p(n)$ of the site-averaged steady-state population versus the driving. White diamonds represent the steady-state average population per site, also shown in panels (a) and (b). (c) and (e) are for a 256×1 array, while (d) and (f) are for a 14×14 lattice. Trajectories have been computed via the truncated Wigner approximation with parameters: $U = 0.1\gamma$, $\Delta = 0.1\gamma$ and $zJ = 0.9\gamma$ (hopping rate times the coordination number z). From Ref. [3].

the lattices, suggesting the emergence of a discontinuous jump in the thermodynamic limit compatible with a first-order phase transition.

In Fig. 5.4(c) and Fig. 5.4(d), we present the dynamics of the boson population in a single stochastic Wigner trajectory for the 1D and 2D lattices, respectively. In the considered regime of interaction U, Wigner trajectories have a direct correspondence to local oscillator measurements [157], such as those carried out via homodyne detection techniques [24, 111].

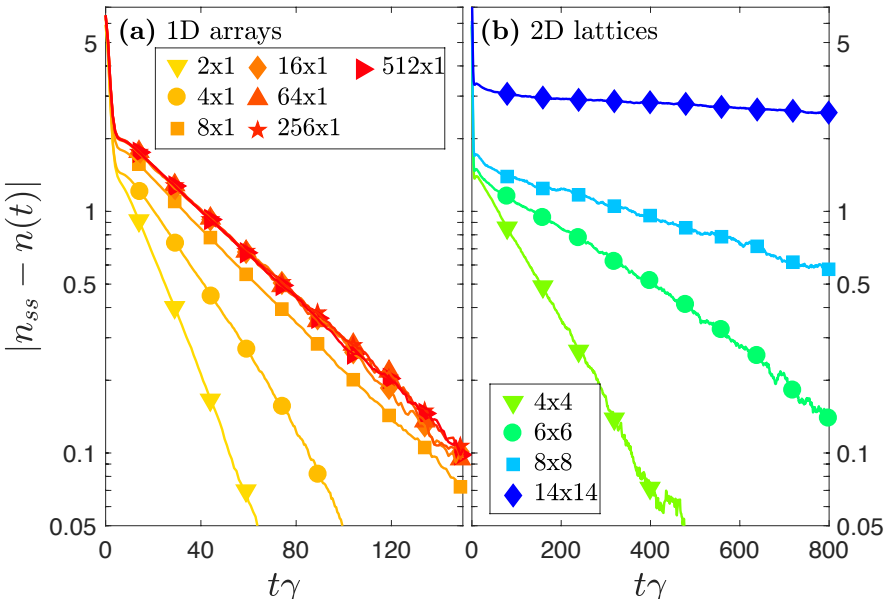

Figure 5.5 – Transient dynamics of the absolute difference between the mean occupation number $n(t)$ and its steady-state value n_{ss} for 1D arrays (a) and 2D lattices (b) of different sizes, with driving amplitude $F = 1.57\gamma$. Other parameters as in Fig. 5.4. From Ref. [3].

In 1D, switches between the two metastable mean-field solutions are barely visible in the population of the j-th site $n_j^W(t)$ (blue curve) and absent in the site-averaged population $\bar{n}^W(t) = 1/N \sum_{j=1}^{N} n_j^W(t)$ (orange curve), consistent with the formation of moving domains with low and high density inside the array [60]. On the contrary, the 2D lattice exhibits a strikingly different behavior, with a clear random switching behavior of $n_i^W(t)$ between two well definite metastable states. The populations in all sites switch collectively since $n_j^W(t)$ and $\bar{n}^W(t)$ strongly overlap. Furthermore, notice that the 2D timescales are far longer than in the 1D case, indicating a significantly slower dynamics. This result bistable behaviour along a quantum trajectory strongly suggests the presence of criticality (cf. Sec. 3.4). A particularly insightful quantity is the probability number distribution $p(n)$ defined as follows. We consider a time t_s where the system has reached the steady state and statistically collect all the values of $n = \bar{n}^W(t > t_s)$ for all the considered trajectories. Indeed, the probability distribution $p(n)$ can highlight the bimodal character of the steady-state at the critical point. The results for $p(n)$ are presented in Fig. 5.4(e,f) for different values of the driving amplitude F. We notice that, in the 1D case, this distribution is monomodal for all values of F and the steady-state mean value of the population follows the peak of this distribution. In the 2D lattice $p(n)$ exhibits a completely different behavior: it has a single peak in the limit of small and large F, while it is bimodal in proximity of the critical region. Here, for finite-size the steady-state expectation value n_{ss} falls in a region of negligible probability ($p(n_{ss}) \simeq 0$) in-between two peaks corresponding to the low and high population phases. When the 2D lattice size is increased, the crossover between the two phases becomes steeper and therefore the bistable region also becomes narrower, eventually collapsing to a single point when $L \to \infty$. This explains why in large lattices a fine scan in F is necessary to observe this feature. This phase coexistence is a clear sign of a first-order phase transition, as explained in Sec. 3.3.2.

To investigate the emergence of criticality in the dynamical properties, we calculated the time evolution towards the steady-state value n_{ss} of the site-averaged mean occupation number $n(t) = \frac{1}{N} \sum_{i=1}^{N} \mathrm{Tr}(\hat{\rho}(t)\hat{a}_i^\dagger \hat{a}_i)$, taking the vacuum as initial state. For values of F close

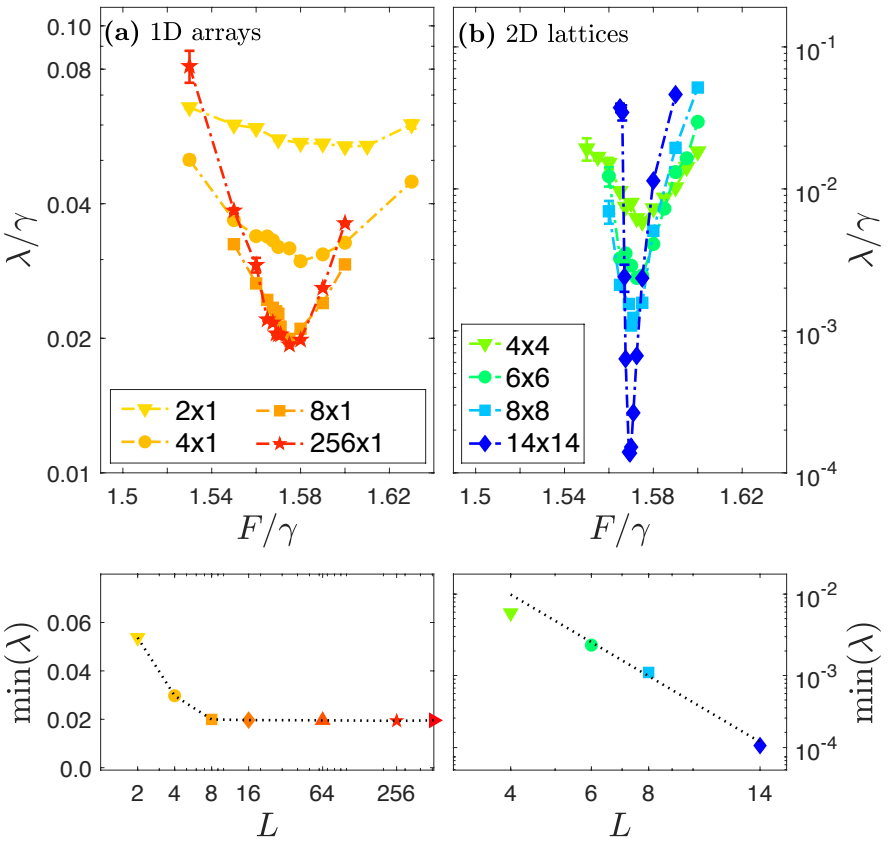

Figure 5.6 – The Liouvillian gap λ (log scale) versus the driving amplitude for several $L \times 1$ arrays (a) and $L \times L$ lattices (b). Notice the different scales used for the 1D and 2D case. The insets show the minimum of λ as a function of the size L. Error bars are within the symbol size. Parameters as in Fig. 5.4. From [3].

to the critical point, $n(t) - n_{ss}$ decays exponentially to zero at large times as reported in Fig. 5.5. In this asymptotic regime, the dynamics is dominated by the Liouvillian gap λ, which can be extracted by fitting the results with $n(t) = n_{ss} + Ae^{-\lambda t}$. Note that in order to have enough accuracy, calculations have required up to 10^6 stochastic Wigner trajectories for each data point. As discussed in Sec. 3.1.3, the asymptotic decay rate can measured using the time-dependence of the second-order correlation function [52], dynamical optical hysteresis [51] and switching statistics [45, 51]. The particular case of $F = 1.57\gamma$ is analyzed in Fig. 5.5, where we plot $|n_{ss} - n(t)|$ for 1D arrays [panel (a)] and 2D lattices [panel (b)] of different sizes. For this fixed value of F, the dynamics gets slower as the size of the simulated system is increased. While in the 1D case the exponential decay rate saturates in the thermodynamic limit, this is not the case for 2D systems. The emergence of critical slowing down is quantified in Fig. 5.6, where we provide the size-dependence of the Liouvillian gap λ versus F. Our general theory predicts that the Liouvillian gap in the thermodynamic limit is closed in one point (see Sec. 3.3.2). In Fig. 5.6(a), we report results for 1D arrays: it is apparent that, when the size L is large enough, the Liouvillian gap converges to a finite value for all the values of F, thus proving the absence of critical slowing down. The behavior is strikingly different for 2D lattices, as shown in Fig. 5.6(b): in this case, every curve $\lambda(F)$ presents a minimum, which becomes smaller and smaller when the size L of the lattice is increased. As shown in the inset of Fig. 5.6(b), the minimum of λ follows the power-law decay $\min_\lambda(L) \propto L^{-\eta}$, with exponent $\eta = 3.3 \pm 0.1$.

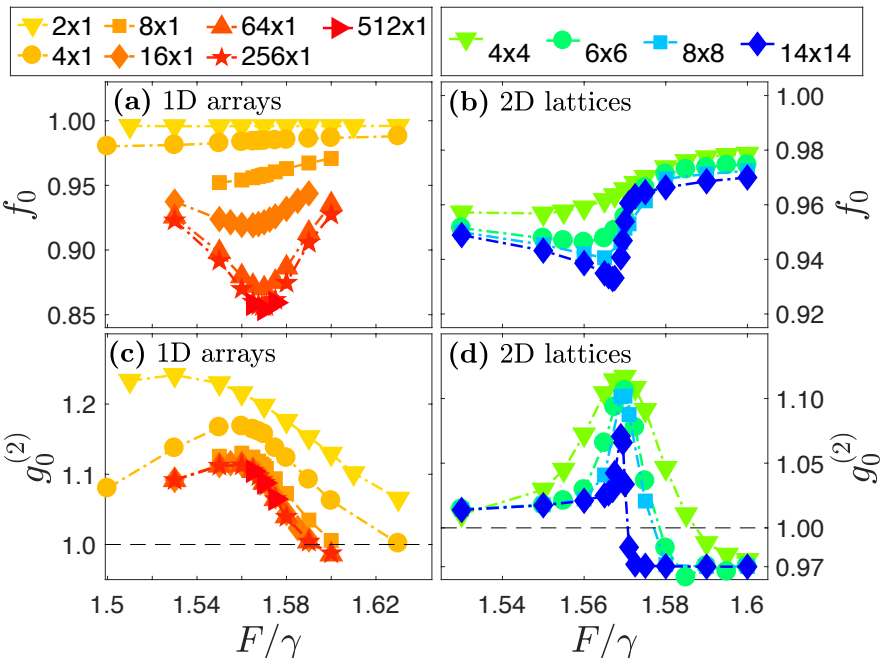

Figure 5.7 – (a) and (b): population fraction $f_0 = n_{k=0}/n_{tot}$ in the zero-momentum mode as a function of the driving amplitude. (c) and (d): zero-delay local second-order correlation $g_0^{(2)}$ versus F. Left panels are for 1D arrays, right panels for 2D lattices. Same parameters as in Fig. 5.4. From Ref. [3].

The phase transition observed here in 2D lattices is reminiscent of what predicted analytically in Sec. 4.3.2. Therefore, one may expect that a macroscopic population in the $k = 0$ mode would always give rise to a critical behavior. In this regard, we studied the fraction $f_0 = n_{k=0}/n_{tot}$ of bosons in the $k = 0$-mode, where $n_{k=0}$ is the steady-state population of the driven $k = 0$-mode and n_{tot} is the total lattice population. In Fig. 5.7(a) and (b) we report the finite-size analysis of f_0 as a function of F. In the region of mean-field bistability, f_0 presents a minimum in both 1D and 2D. In 1D this minimum saturates to a finite value as one approaches the thermodynamic limit, while in 2D f_0 exhibits a behavior consistent with a finite jump at the critical point. For the considered interaction, in both cases the population of the driven mode is dominant (f_0 close to 1), showing that the fluctuations induced by the coupling to non-zero momentum modes destroy the critical behavior in 1D.

Lastly, we present the local equal-time second-order correlation function $g_0^{(2)} = \langle \hat{a}_j^\dagger \hat{a}_j^\dagger \hat{a}_j \hat{a}_j \rangle / \langle \hat{a}_j^\dagger \hat{a}_j \rangle^2$ as a function of F. This quantity describes the amplitude of the fluctuations in the field, and has been employed extensively to investigate critical behavior in in optical systems. In 1D this quantity has a broad peak whose shape is shown to converge for large enough L (Fig. 5.7(c)), while in 2D (Fig. 5.7(d)) the finite-size results show an emerging singular behavior in its derivative at the critical point. The same qualitative behavior is also observed in the large population limit of a single-mode nonlinear resonator [5, 59], which is equivalent to the $k = 0$ approximation described above.

5.2.2 Different values of U

Since the phase transition is of first order, we expect the exponent η characterising the scaling of the Liouvillian gap not to be universal [52, 59]. To verify this, we computed

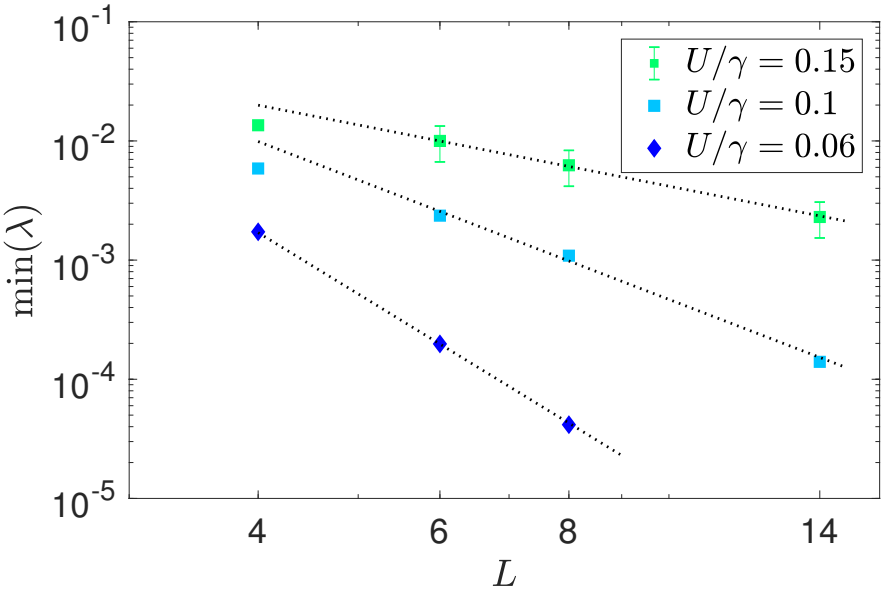

Figure 5.8 – Minimum of the Liouvillian gap λ as a function of the size L of 2D lattices, for different values of U/γ. The critical exponent is $\eta = 1.7 \pm 0.2$ for $U/\gamma = 0.15$, $\eta = 3.3 \pm 0.1$ for $U/\gamma = 0.1$ and $\eta = 5.3 \pm 0.1$ for $U/\gamma = 0.06$. Parameters: $zJ/\gamma = 0.9$ and $\Delta/\gamma = 0.1$. From Ref. [3].

the critical exponent in lattices with a different nonlinearity (the other parameters were unchanged), finding $\eta = 5.3 \pm 0.1$ for $U/\gamma = 0.06$ and $\eta = 1.7 \pm 0.2$ for $U/\gamma = 0.15$.

Moreover, we show how the power-law decay of the Liouvillian gap changes when the normalized interaction U/γ is varied. In Fig. 5.8 we present the minimum of the Liouvillian gap λ as a function of lattice size L for several 2D lattices with different nonlinearities. We find that the power-law exponent increases as U/γ is decreased.

5.3 Disordered systems: a perspective

In the previous section we made the hypothesis of a uniform lattice. In any experimental realisation, however, it is impossible to realise two sites which are exactly identical. In this regards, it is interesting to study the effects of disorder on the previously-described Bose-Hubbard lattice. When we describe disorder, we imagine that instead of having a uniform system, any parameter may have an explicit site dependency. The latter can be modelled via a set of parameters $\delta = \{\delta_i\}$ obeying to random probability distributions $p(\delta) = \prod_i p(\delta_i)$. To each distribution we associate a disordered Liouvillian

$$\mathcal{L}(\delta) = \mathcal{L}_0 + \mathcal{L}_\delta, \tag{5.7}$$

where $\mathcal{L}_0$ represent the homogeneous part of the Liouvillian and $\mathcal{L}_\delta$ the inhomogeneous one. We stress that $\mathcal{L}(\delta)$ is to all extent a legitimate Liouvillian, describing the time evolution of a physical system. Thus, to each disordered Liouvillian one associates a disordered density matrix:

$$\hat{\rho}(t, \delta) = e^{\mathcal{L}(\delta)t}\hat{\rho}(0). \tag{5.8}$$

Often one is interested in computing the mean quantities associated to the disorder. Indeed, one can think of evolving the same density matrix $\hat{\rho}(0)$ under the action of different $\mathcal{L}(\delta)$ (corresponding to different disorder configurations), and then take the average. We define the *disorder-averaged* density matrix as

$$\begin{aligned}\hat{\rho}_D(t) &= \int d\delta\, p(\delta)\, e^{\mathcal{L}(\delta)t}\hat{\rho}(0) \\ &= \int d\delta_1\, p(\delta_1) \int d\delta_2\, p(\delta_2) \ldots e^{\mathcal{L}(\delta)t}\hat{\rho}(0).\end{aligned} \tag{5.9}$$

Introducing the disorder-averaged evolution superoperator

$$e^{\mathcal{L}_D t} = \int \mathrm{d}\delta p(\delta)\, e^{\mathcal{L}_D(\delta)t} = \iint \ldots \int \prod_i \mathrm{d}\delta_i\, p(\delta_i)\, e^{\mathcal{L}_D(\delta)t}, \tag{5.10}$$

we have

$$\hat{\rho}_D(t) = e^{\mathcal{L}_D t}\hat{\rho}(0). \tag{5.11}$$

The expectation values of a disordered system can be obtained by $\langle\hat{o}\rangle_D(t) = \mathrm{Tr}[\hat{\rho}_D(t)\hat{o}]$.

In case $\mathcal{L}_0$ and $\mathcal{L}_\delta$ commute, one can separate the exponential $e^{(\mathcal{L}_0+\mathcal{L}_\delta)t}$, and the overall effect of the disorder can be easily associated to a new Liouvillian. On the other hand, if $[\mathcal{L}_0, \mathcal{L}_\delta] \neq 0$, an expansion of the exponential becomes extremely complex.

5.3.1 An efficient numerical method

If we consider a system with a high number of cavities, the integral in Eq. (5.9) can be computationally demanding. Instead of directly performing such a high-dimensional integral, one can consider a random variable r such that the configuration $\delta(r) = \{\delta_i\}_r$ is extracted with probability $p(\delta)$. Accordingly, we call $\mathcal{L}_r$ the Liouvillian associated to the set of parameters $\{\delta_i\}_r$:

$$\mathcal{L}_r = \mathcal{L}_0 + \mathcal{L}_{\delta(r)}, \tag{5.12}$$

and we have

$$\hat{\rho}_D(t) = \lim_{R\to\infty} \frac{1}{R} \sum_{r=1}^{R} e^{\mathcal{L}_r t}\hat{\rho}(0). \tag{5.13}$$

Numerically, one takes R big enough to ensure that the wanted precision is reached. One concludes that, in order to simulate a disordered system, the computational cost is R times greater that the cost of a clean system: the complexity of the disorder emerges from the sampling problem.

As we previously discussed, the time evolution of a density matrix can be obtained either by direct numerical integration of the master equation or by exploiting quantum trajectories. If one choose the latter method, one would compute T trajectories and, by averaging the obtained results, provide an estimation of the density matrix. We introduce the computational complexity parameter $\mathcal{C} = R \cdot T$ which quantifies the *total number of trajectories*, i.e. the total computational effort. Adding the disorder, naively one would compute R times the same amount T of trajectories as in the homogeneous case. However, we claim that (i) it is possible to compute an estimate of $\langle\hat{o}\rangle_D(t)$ by only simulating one trajectory per disorder realization (i.e., $T = 1$), and (ii) having fixed $\mathcal{C}$, this choice ensure the best error estimate.

This work is still in progress, but a preliminary study of a 5×1 lattice has been performed. We considered only a local Gaussian disorder in the detuning. In this system, we were able

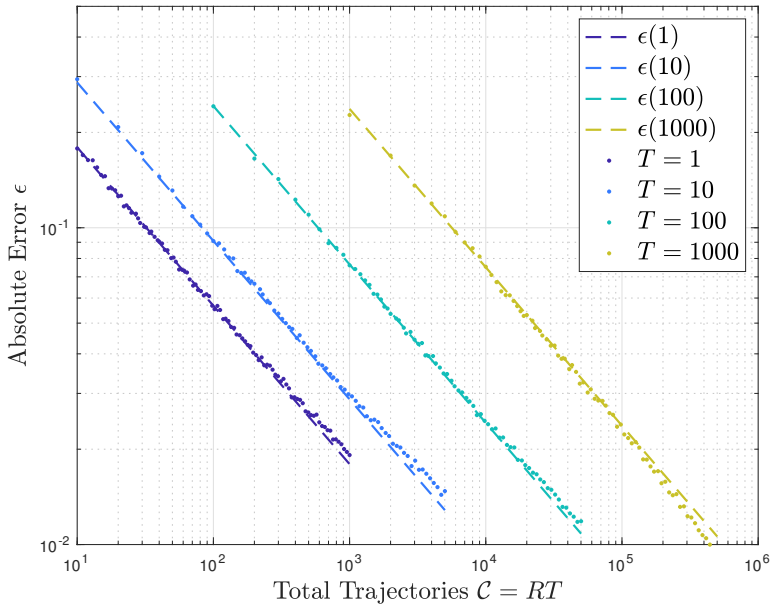

Figure 5.9 – Absolute error ϵ (defined in the main text) as a function of the computational effort $\mathcal{C}$ in a system with 5 sites. The cases presented are for $T = 1, 10, 100, 1000$ trajectories. Parameters: $U = 1.0\gamma$, $F = 2.0\gamma$, $zJ = \gamma$, $\Delta = 1.0\gamma$, and a Gaussian distributed disorder of mean 0 and variance 0.5γ.

to estimate the mean number of photons in the steady state by averaging over 10^4 different disorder realisations. For each of them, we performed a numerical evolution of the master equation. We call this result $\langle \hat{n} \rangle_D$ and we use it as reference. In Fig. 5.9 we plot the absolute error $\epsilon = |\langle \hat{n} \rangle_D (\mathcal{C}) - \langle \hat{n} \rangle_D| /2$ as a function of the computational cost. The quantity $\langle \hat{n} \rangle_D (\mathcal{C})$ is the steady-state mean number of photons obtained with a computational cost $\mathcal{C}$. Different colours represent different values of T. The dots are the results, while the dashed lines are the extrapolation of the error curve (presenting a power-law behaviour). Clearly, the smaller T the better the convergence, with the optimal choice being $T = 1$.

The presented method appears to be very powerful. For instance, let us consider the homogeneous case, where, in order to obtain an absolute error of $5 \cdot 10^{-2}$, one needs $T = 100$ trajectories (i.e., $\mathcal{C} \simeq 100$). From Fig. 5.9 we deduce that the same precision in the disordered case with $T = 1$ is attained for $\mathcal{C} \simeq 150$. Hence, the increase in the numerical cost with respect to the clean case is relatively small.

5.4 Conclusions

In this Chapter we proved the emergence of a phase transition in the driven-dissipative Bose-Hubbard model. In particular, we studied the critical slowing down associated with the closure of the Liouvillian gap. We have revealed the emergence of critical dynamics in 2D lattices via a finite-size analysis, which is instead absent in 1D arrays, indicating that the lower critical dimension for this nonequilibrium model is $d = 2$. We have shown that in 1D arrays fluctuations destroy criticality of the dynamics even if the driven mode is macroscopically occupied. The obtained result are in perfect agreement with the general theory developed in

Chapter 3.

The asymptotic decay rate associated with the Liouvillian frequency gap has been measured in nonlinear photonic systems with different techniques [45, 51, 158], hence the critical slowing down predicted here as a function of lattice size is within experimental reach and can unveil fundamental properties of dissipative phase transitions. Many intriguing studies can be foreseen on the horizon, including the role of disorder as well as the critical behavior of exotic open photonic lattices with geometric frustration [97, 159–161] or quasiperiodicity [162, 163].

CHAPTER 6

Dynamical Properties of XYZ Heisenberg Lattices

In the previous Chapter we studied phase transitions in regimes where the interaction among photons was small. When the nonlinearity of the optical cavity, however, is much larger than its dissipation rate, the presence of a single photon inside the cavity is able to effectively block the entrance of a second one. This effect, known as *photon-blockade* [164, 165], has been observed experimentally at first with optical photons using a single atom in a cavity [166] and is particularly strong in circuit quantum electrodynamics systems in the microwave domain [167]. In a lattice system, strong correlations can lead to a transition from a photonic Mott insulator to a superfluid [168–172], similar to that observed with ultracold atoms confined in optical lattices [15, 38]. Interestingly, a system of coupled resonators in the photon-blockade regime can be mapped into an effective spin model [170, 173, 174]. This class of systems can be realized nowadays using different experimental platforms, such as superconducting quantum simulators [44] or Rydberg atoms [68, 175–177].

In the context of dissipative phase transitions, the XYZ Heisenberg model [39] has attracted a considerable attention. It describes a lattice of spins interacting via an anisotropic Heisenberg Hamiltonian which are coupled to an environment forcing them to align along the z-axis. The single-site Gutzwiller mean-field theory predicts a rich phase diagram for the magnetic properties of the steady state of this model [39]. More refined calculations, based on numerical methods including many-body correlations, have confirmed the emergence of a critical behaviour in two-dimensional lattices, while the phase transition disappears when the spins are arranged according to a one-dimensional geometry [40, 62, 71, 131, 178]. All these works, however, focussed on the calculation of steady-state properties and a full description of the dynamics of the system is still lacking.

In this Chapter, we explore the dynamical properties of the dissipative XYZ model in the region where a second-order phase transition from a paramagnetic to a ferromagnetic steady state has been predicted. For finite-size 1D arrays and 2D lattices, we have performed an exact integration of the master equation using the whole Hilbert space via numerical simulation of counting quantum trajectories [115]. Moreover, for 1D arrays of infinite length we have applied the infinite Matrix Product Operator (iMPO) technique [132, 179]. We confirm the prediction about the role of dimensionality, and the study of single quantum trajectories shed new light about the nature of the phases.

This Chapter is organized as follows. In Sec. 6.1 we discuss the theoretical framework and describe the methods used for the calculations. In Sec. 6.2 we show the main results of

this Chapter.

Contents

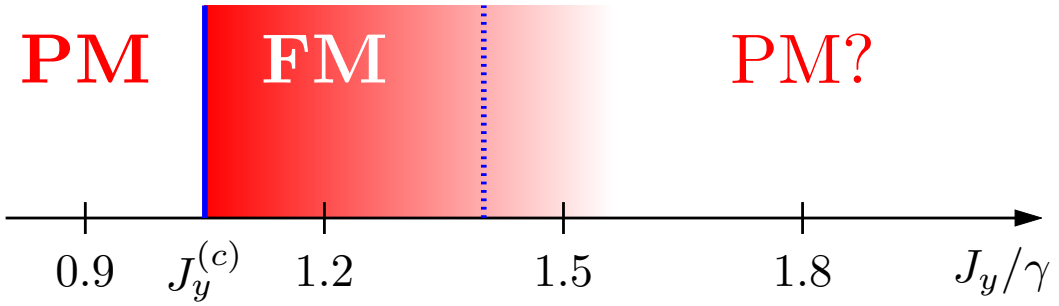

Figure 6.1 – Phase diagram of the 2D dissipative XYZ model as a function of the normalized coupling parameter J_y/γ, with fixed $J_x/\gamma = 0.9$ and $J_z/\gamma = 1$. For $J_y \simeq J_x$, the system presents a paramagnetic (PM) steady state. At the critical value $J_y^{(c)}$, the system undergoes a phase transition towards a ferromagnetic (FM) steady state. Different estimations for this critical value are: $J_y^{(c)}/\gamma = 1.039$ from Ref. [39], $J_y^{(c)}/\gamma = 1.04 \pm 0.01$ from Ref. [40], $J_y^{(c)}/\gamma = 1.07 \pm 0.02$ from Ref. [71] and $J_y^{(c)}/\gamma = 1.0665 \pm 0.0005$ from Ref. [128]. At larger values of J_y, the nature of the steady state is still under debate: Ref. [40] predicts the existence of a second critical point $J_y^{(c,2)}/\gamma = 1.40$ (dashed blue line in the figure), above which the steady state is paramagnetic, but Ref. [71] does not show any evidence of a phase transition close to this value. From Ref. [2].

6.1 The model

The dissipative XYZ model describes a lattice of spins interacting via an anisotropic Heisenberg Hamiltonian ($\hbar = 1$):

$$\hat{H} = \sum_{\langle i,j \rangle} \left(J_x \hat{\sigma}_i^x \hat{\sigma}_j^x + J_y \hat{\sigma}_i^y \hat{\sigma}_i^y + J_z \hat{\sigma}_i^z \hat{\sigma}_j^z \right), \tag{6.1}$$

where $\hat{\sigma}_i^\alpha$ ($\alpha = x, y, z$) represent the Pauli matrices acting on the i-th site. The sum runs over the nearest neighbour sites $\langle i, j \rangle$. The dissipative part describes incoherent spin-flip processes which tend to align a single spin towards the negative direction of the z-axis with a rate γ. The density matrix $\hat{\rho}(t)$ dynamics is obtained from the Lindblad master equation

$$\frac{\partial \hat{\rho}}{\partial t} = \mathcal{L}[\hat{\rho}] = -i \left[\hat{H}, \hat{\rho} \right] + \gamma \sum_j \left(\hat{\sigma}_j^- \hat{\rho} \hat{\sigma}_j^+ - \frac{1}{2} \left(\hat{\sigma}_j^+ \hat{\sigma}_j^- \hat{\rho} + \hat{\rho} \hat{\sigma}_j^+ \hat{\sigma}_j^- \right) \right), \tag{6.2}$$

where $\hat{\sigma}_j^\pm = (\hat{\sigma}_j^x \pm i\hat{\sigma}_j^y)/2$ are the spin raising and lowering operators acting on the j-th spin and $\mathcal{L}$ is the Liouvillian superoperator.

The Lindblad master equation (6.2) is invariant under a π-rotation of all the spins around the z-axis ($\hat{\sigma}_i^x \to -\hat{\sigma}_i^x$, $\hat{\sigma}_i^y \to -\hat{\sigma}_i^y$ $\forall i$). In the thermodynamic limit, the $\mathcal{Z}_2$ symmetry associated to this transformation may spontaneously break, resulting in the appearance of several magnetic phases for the steady state of the model. In this work, we will focus on a particular regime where previous calculations have predicted a transition from a paramagnetic phase with no magnetization in the xy plane ($\langle \hat{\sigma}_x \rangle = \mathrm{Tr}\left[\hat{\rho}_{ss} \hat{\sigma}_j^x\right] = 0$, $\langle \hat{\sigma}_y \rangle = \mathrm{Tr}\left[\hat{\rho}_{ss} \hat{\sigma}_j^y\right] = 0$) to a ferromagnetic phase with finite magnetization in the xy plane ($\langle \hat{\sigma}_x \rangle \neq 0$, $\langle \hat{\sigma}_y \rangle \neq 0$) [39, 40, 62, 71, 131, 178] (see Fig. 6.1).

From a computational point of view, the numerical solution of the master equation (6.2) is a formidable task when considering extended lattices. The corner-space renormalization

method [130], which has shown the criticality of several steady-state observables in 2D lattices [71], does not give access to the dynamic properties of the system. For small systems with a number $N < 10$ spins, the problem can be solved via a standard Runge-Kutta integration of Eq. (6.2). For $10 \leq N \leq 16$, instead, we have solved the master equation stochastically via counting quantum trajectories.

As we detailed in Sec. 2.2, quantum trajectories are useful not only to reduce the complexity of the integration of the Lindblad master equation (6.2), but their analysis of can also provide insightful results about the nature of the dissipative phase transition [3, 60]. To this aim, we have investigated the stochastic evolution of individual quantum trajectories for the dissipative XYZ model, obtained according to the *homodyne* protocol [cf. Eq. (2.62)], which in this case reads:

$$\begin{aligned} |\Psi_k(t+\mathrm{d}t)\rangle = \Bigg\{ & \sum_j \sqrt{\gamma} \left[\hat{\sigma}_j^- - \frac{s_j(t)}{2} \right] \mathrm{d}W_j(t) \\ & - \left[\mathrm{i}\hat{H} + \frac{\gamma}{2} \left(\hat{\sigma}_j^+ \hat{\sigma}_j^- - s_j(t) \hat{\sigma}_j^- + \frac{s_j(t)^2}{4} \right) \right] \mathrm{d}t \Bigg\} |\Psi_k(t)\rangle, \end{aligned} \tag{6.3}$$

where $s_j(t) = \langle \Psi_k(t) | \hat{\sigma}_j^x | \Psi_k(t) \rangle$ and $\mathrm{d}W_j$ are stochastic Wiener increments with zero expectation value, variance equal to $\sqrt{\mathrm{d}t}$ and uncorrelated among the different spins. As detailed in Sec. 3.4, the stochastic equation in (6.3) does not conserve the $\hat{Z}_2$ symmetry of the wave function. Therefore, by studying the time evolution of the magnetic order parameter over an individual quantum trajectory, it is possible to reveal the emergence of different magnetic phases, when we change the parameters of the system. Nevertheless, the symmetry of the Liouvillian is restored when we consider the density matrix, obtained by averaging over many trajectories.

Alternative approaches for the simulation of 1D arrays are based on tensor networks techniques [180] making use of the Matrix Product Operator (MPO) ansatz for the density matrix [40, 62, 133, 161, 181–184]. The MPO ansatz for the many-body mixed state can be controlled by changing a single parameter, i.e. the bond-link dimension χ: the more χ increases, the more non-local quantum correlations can be encoded. The dynamics of the open system is obtained via a time-evolving block decimation scheme [185, 186]. In the case of translational invariant systems, the MPO ansatz and the time evolution procedure can be further simplified leading to the infinite MPO (iMPO) representation [132, 179], which allows to directly access the thermodynamic limit of an infinite number of sites. Very recently, this technique has been extended to the case of 2D lattices [131] although with a very reduced bond dimension.

6.2 Emergence of a second-order phase transition

In the following, we will consider as an order parameter the average lattice magnetization $M^x(t) = \sum_i \mathrm{Tr}\left[\hat{\rho}(t)\hat{\sigma}_i^x\right]/N$, N being the number of spins in the lattice. For any finite size system, $M^x(t) = 0$ due to the $\mathcal{Z}_2$ symmetry of the system. However, the emergence of a phase transition may be signalled either by a critical slowing down in the time evolution of $M^x(t)$, or by the emergence of a bistable behaviour for homodyne trajectories.

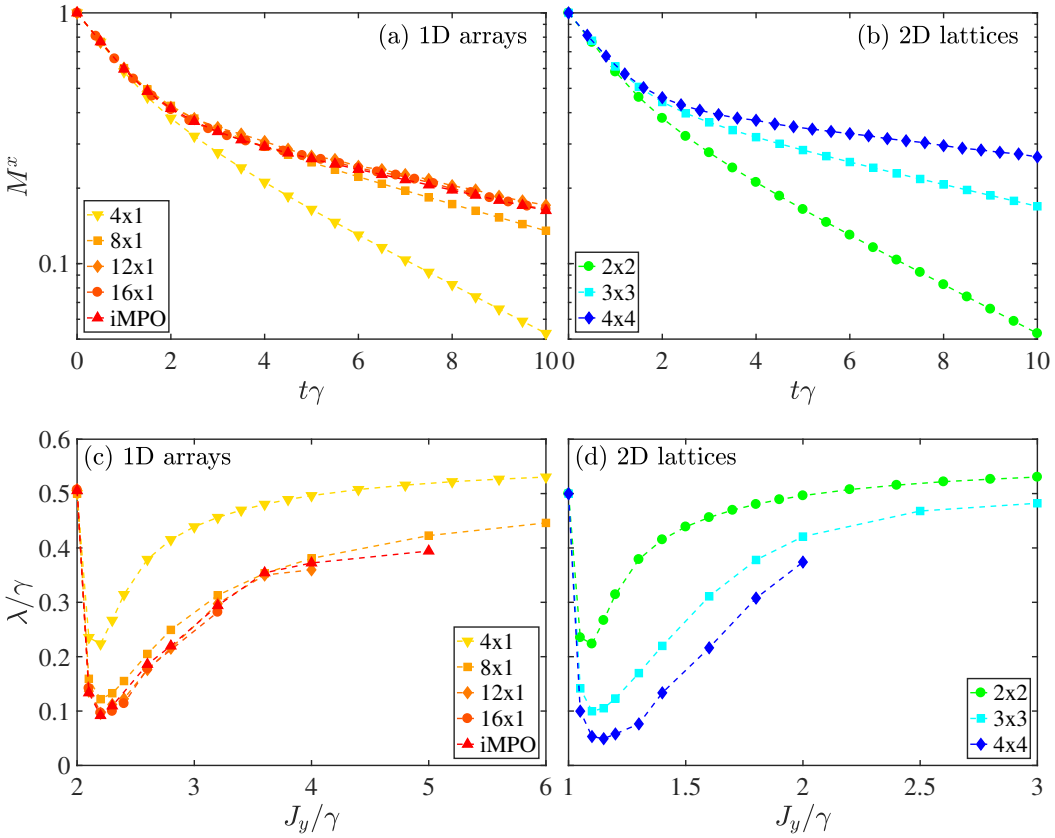

Figure 6.2 – Top panels: time dependence of the averaged magnetization $M^x(t)$ in 1D arrays (panel (a)) and in 2D lattice (panel (b)) of different size. Parameters: $J_x/\gamma = 1.8$, $J_y/\gamma = 2.2$ and $J_z/\gamma = 2$ for the 1D results in panel (a); $J_x/\gamma = 0.9$, $J_y/\gamma = 1.1$ and $J_z/\gamma = 1$ for the 2D results in panel (b). Lower panels: Liouvillian gap as a function of the coupling parameter J_y in 1D arrays (panel (c)) and 2D lattices (panel (d)). The other parameters are: $J_x/\gamma = 1.8$ and $J_z/\gamma = 2$ for the 1D results; $J_x/\gamma = 0.9$ and $J_z/\gamma = 1$ for the 2D results. From Ref. [2].

6.2.1 The Liouvillian gap

We start our discussion on the dynamics of the dissipative XYZ model by studying the time evolution of the average lattice magnetization. In Fig. 6.2, we plot $M^x(t)$ for a fixed choice of the parameters of the Hamiltonian (6.1) in vicinity of the critical point, for spin systems of different size, both with 1D (Fig. 6.2-(a)) and 2D geometry (Fig. 6.2-(b)). For small lattices (i.e. $N < 10$), the density matrix $\hat{\rho}(t)$ is computed via Runge-Kutta integration of the master equation (6.2); for larger lattices, $\hat{\rho}(t)$ is calculated averaging 2500 quantum counting trajectories (obtained with the wave function Monte Carlo protocol described in App. E.4.1). In all these calculations, the master equation has been solved assuming an initial configuration where all the spins point along the positive direction of the x-axis (therefore $M^x(t=0) = 1$) and imposing periodic boundary conditions to the finite-size lattice.

For $t \gtrsim 5\gamma$, all the curves $M^x(t)$ decay exponentially towards the steady-state expectation value $M^x_{ss} = 0$ (notice that we have $M^x_{ss} = 0$ for all the values of the parameters since we do not break explicitly the $\mathcal{Z}_2$ symmetry of the Liouvillian superoperator in our simulations). The presence of an asymptotic exponential behavior for $M^x(t)$ indicates that, at large times, the dynamics of the system can be described uniquely in terms of the eigenstate associated

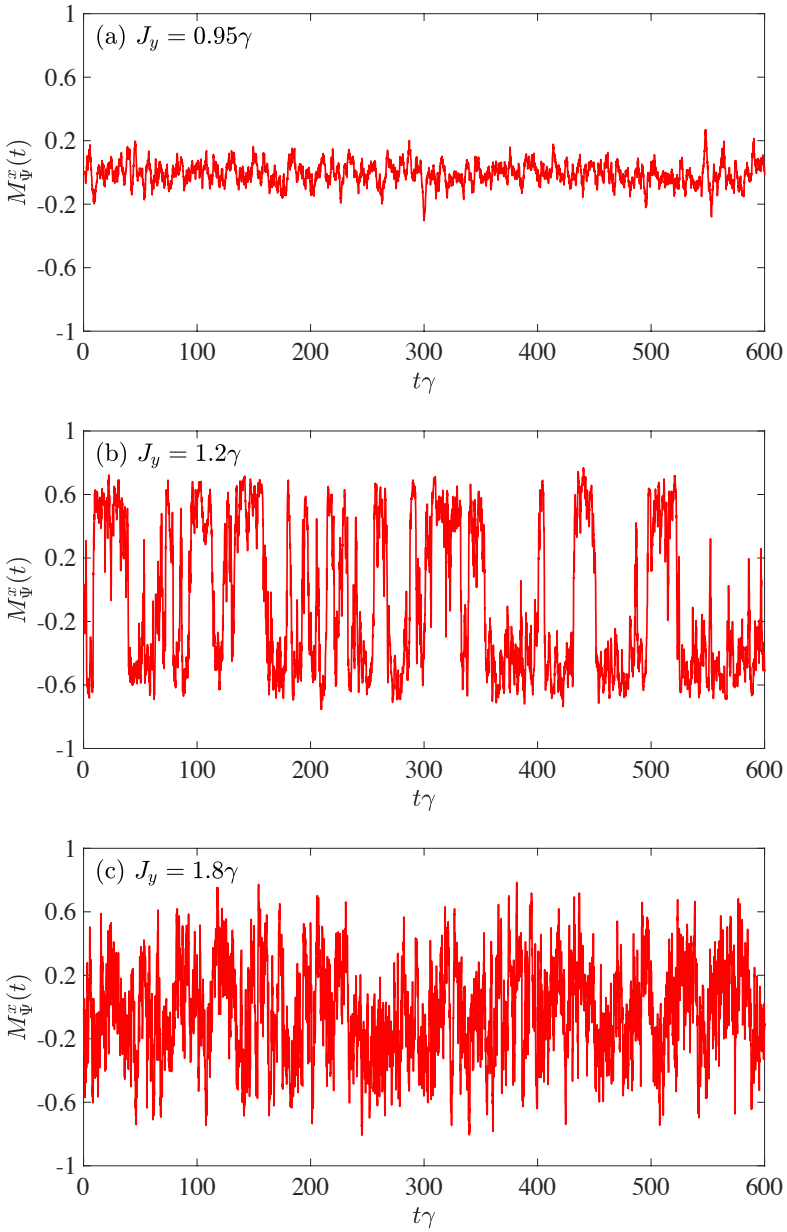

Figure 6.3 – Average magnetization M^x_Ψ calculated for a single homodyne quantum trajectory as a function of time for a 3×3 lattice. The three panels refer to different values of the coupling parameter J_y/γ (the other parameters are $J_x/\gamma = 0.9$ and $J_z/\gamma = 1$). From Ref. [2].

to the Liouvillian gap. The density matrix can be approximated as $\hat{\rho}(t) = \hat{\rho}_{ss} + A\hat{\rho}_1 e^{-\lambda t}$, where A is a real number depending on the choice of the initial configuration (c.f. Eq. (3.12)). From our results, we notice also that the dynamics gets slower when increasing the size of the system, both in 1D arrays and in 2D lattices (respectively Fig. 6.2(a) and Fig. 6.2-(b)). In 1D arrays the decay rate saturates when the size of the system increases. For an array with 16 sites the decay curve is nearly indistinguishable from what obtained for an array of infinite length (obtained via the iMPO technique). Instead, in 2D lattices no saturation of the decay rate is observed.

By fitting the curves for $M^x(t)$ at large t with a simple exponential, we can extract

the value of the Liouvillian gap λ. The results for λ obtained with this procedure have been successfully benchmarked against those calculated with an exact diagonalization of the Liouvillian superoperator in small systems (4×1 array and 2×2 lattice). In Fig. 6.2-(c,d) we plot λ as a function of the normalized coupling parameter J_y/γ (the other coupling parameters J_x/γ and J_z/γ are kept fixed). Both in the 1D and in the 2D case, all the curves $\lambda(J_y)$ present a minimum close to the critical value of J_c, indicating a slowing down in the dynamics of the system. Nevertheless, we clearly notice that this slowing down is not critical in 1D systems. Indeed, the results for $\lambda(J_y)$ in the largest 1D systems (with $N \geq 12$) overlap and are in good agreement with the prediction for the infinite array obtained with iMPO [1], showing a finite value of the Liouvillian gap. Instead, in 2D systems, the minimum of $\lambda(J_y)$ becomes smaller and smaller when the size of the lattice increases. This behavior is consistent with a Liouvillian gap closed in whole region in the thermodynamic limit.

6.2.2 Quantum trajectories

In order to better characterize the behavior of the 2D system across the critical point, we study the average magnetization of the lattice $M^x_\Psi(t) = \langle\Psi(t)|\sum_i \sigma^x_i|\Psi(t)\rangle/N$ along a single trajectory $|\Psi(t)\rangle$. To this extent, we have computed $|\Psi(t)\rangle$ following the homodyne protocol in Eq. (6.3) in 2D lattices of different sizes, for several values of the parameter J_y, starting from an initial configuration where all the spins are aligned along the z-axis. Convergence of the time integration of Eq. (6.3) has been carefully checked, requiring a time step $\mathrm{d}t \simeq (1000\gamma)^{-1}$.

In the three panels of Fig. 6.3, we show the results for $M^x_\Psi(t)$ in a 3×3 lattice for $J_y = 0.95\gamma$, $J_y = 1.25\gamma$ and $J_y = 1.8\gamma$. When the steady state presents a paramagnetic phase [$J_y = 0.95\gamma$, Fig. 6.3-(a))] the curve for $M^x_\Psi(t)$ presents only small fluctuations around the zero value for the magnetization. The behavior of the quantum trajectory is strikingly different in the ferromagnetic phase [$J_y = 1.2\gamma$, Fig. 6.3-(b)]. In this case, we can clearly distinguish intervals of time where the curve for $M^x_\Psi(t)$ fluctuates around a positive value of the magnetization and others where it fluctuates around the opposite value. The duration of these time intervals is of the order $\Delta t \sim \lambda^{-1}$. Finally, for large values of the coupling parameter J_y [$J_y = 1.8, \gamma$, Fig. 6.3-(c)], $M^x_\Psi(t)$ presents yet another different behavior. It is reminiscent of what observed in the paramagnetic phase [see Fig. 6.3-(a)], since it fluctuates around the zero value of the magnetization, but the amplitude of the fluctuations is much larger than in the regime $J_x \simeq J_y$. This peculiar behavior can be ascribed to the strongly mixed character of the steady state in this regime (see Refs. [40, 71] for a calculation of the purity and the von-Neumann entropy). In this case, the stochastic processes described by the increments $\mathrm{d}W_j$ in Eq. (6.3) would allow the quantum trajectory to explore a much larger number of quantum states with respect to the case at small anisotropy, where the trajectory fluctuates weakly around the single pure state dominating in the steady-state density matrix. As a consequence, the fluctuations of $M^x_\Psi(t)$ in the paramagnetic regime of large anisotropy are much stronger than in the regime at $J_x \simeq J_y$.

To better understand the nature of those three regimes, we studied the probability distribution of $M^x_\Psi(t)$ over many trajectories, which we will call $p(M^x)$, defined as follows. We consider a time t_s where the density matrix of the system has reached the steady state, and statistically collect all the values of $M^x_\Psi(t)$ for $t > t_s$ over many trajectories. The results for

1. The accuracy of the iMPO data is checked by increasing the bond-dimension χ until the convergence is reached (in our calculation, convergence is obtained with $\chi = 80$).

$p(M^x)$ are presented in the top panel of Fig. 6.4, as a function of the coupling J_y. We notice that for small J_y the distribution is monomodal around zero. As J_y increases, one reaches a point $J_c \simeq 1.05\gamma$ where $p(M^x)$ starts to present two distinct peaks, which are symmetric around the value $M^x = 0$. If we continue to increase J_y, the two peaks broaden and they move apart, until they reach their maximum distance for $J_y \simeq 1.2\gamma$. Above this value of J_y, the peaks continues to broaden and they start to approach one to the other, until they merge again into a single peak for $J_y \gtrsim 1.6\gamma$. The broadening, the separation and the merging of the peaks in the probability distribution is even more evident in the panels in Fig. 6.4-(a,f), where we plot the curves for $p(M_x)$ for some values of the coupling parameter J_y.

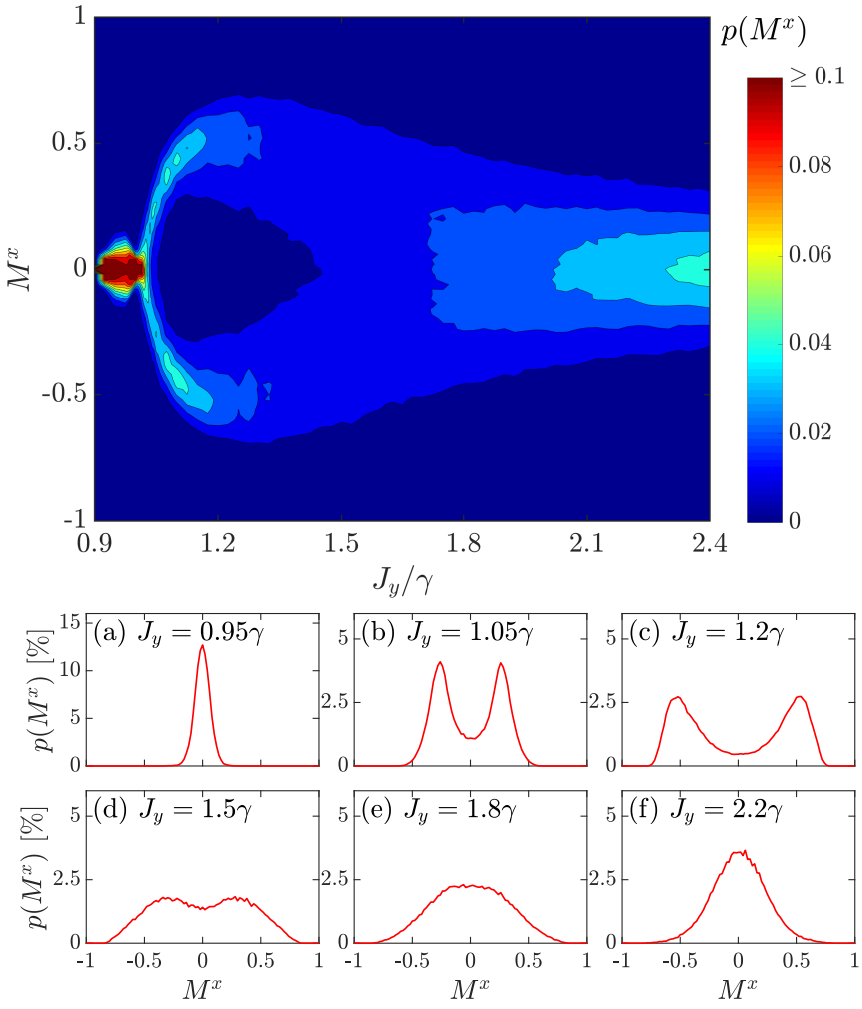

Figure 6.4 – Top panel: contour plot of the probability distribution $p(M^x)$ of the site-averaged magnetization along x versus the coupling parameter J_y for a 3×3 lattice. Lower panels: probability distribution $p(M^x)$ for different values of J_y. For each value of J_y, the distributions are obtained collecting the results of M^x from $N_T = 16$ trajectories with total time $t_T = 10^4/\gamma$. Same parameters as in Fig. 6.3. From Ref. [2].

In order to perform a more quantitative analysis of the distribution $p(M^x)$, we compute

the bimodality coefficient b [187] that for an even distribution reads:

$$b = \frac{(\int_{-1}^{1} dM_x M_x^2 p(M_x))^2}{\int_{-1}^{1} dM_x M_x^4 p(M_x)}. \tag{6.4}$$

b is an indicator of the bimodal character of the distribution, which in the present study is related to the ferromagnetic nature of the steady state. Indeed, when $p(M^x)$ presents two narrow peaks, then the quantity b approaches its maximum value $b_{max} = 1$. Instead, unimodal distributions are characterized by smaller values of b (for instance, a Gaussian distribution centered at $M_x = 0$ would have $b = 1/3$).

In Fig. 6.5, we plot the value of b as a function of J_y, for different sizes of the 2D lattice. The emergence of the phase transition at $J_y/\gamma \simeq 1.05$ is signaled by a steep increasing of the ratio b, which is almost independent of the lattice size. Furthermore, the decreasing of b for $J_y/\gamma > 1.2$ indicates the disappearance of the ferromagnetic order for large anisotropies. In this case, however, the drop of b is not particularly sharp and tends to become smoother and smoother as the size of the lattice increases.

The study of the behavior of $b(J_y)$ is interesting to address the open question about the nature of the steady state of the dissipative XYZ model for large anisotropies. Several works in literature [40, 131, 178] have predicted a ferromagnetic to paramagnetic phase transition for $J_y/\gamma > 1.5$. However, the critical value of J_y for this second transition depends strongly on the method used and on the size of the cluster considered in the calculation [40, 131, 178]. Moreover, the behavior of the magnetic susceptibility and of the von-Neumann entropy as a function of J_y do not present any feature signaling the emergence of a critical point for $J_y > 1.2\gamma$ [71]. Our results in Fig. 6.5, showing a smooth decreasing of b at large J_y, together with the absence of a slowing down for $J_y > 1.2\gamma$ (see Fig. 6.2-(d)), suggest that the disappearance of the ferromagnetic order for large anisotropies might be due to a crossover and not to another second-order phase transition.

6.3 Conclusions

In this Chapter we investigated numerically the dynamics of a dissipative spin-$\frac{1}{2}$ lattice interacting through an XYZ-Heisenberg Hamiltonian. This model is particularly relevant in the context of strongly correlated open quantum systems since it is known to support a second-order dissipative phase transition in two dimensions, associated with the breaking of the $\mathcal{Z}_2$ symmetry. By performing stochastic quantum trajectories simulations on finite-size systems, we determined the Liouvillian gap from the asymptotic decay rate of the dynamics towards the steady state. When the system is driven across the critical point, we found that the relaxation exhibits a slowing down. For 1D systems, the Liouvillian gap remains finite as the length of the chain is increased up to the thermodynamical limit, thus indicating the absence of a phase transition. Instead, results for 2D lattices do not show a saturation of the Liouvillian gap, which is consistent with the emergence of critical slowing down. By analyzing individual stochastic homodyne trajectories in 2D lattices, we characterized the emergence and disappearance of two metastable states with opposite magnetization.

Our predictions might be tested in quantum simulators based on superconducting quantum circuits or Rydberg atoms. As a perspective, the effects of disorder on the dynamics of these systems is a very interesting aspect that needs to be investigated in the future.

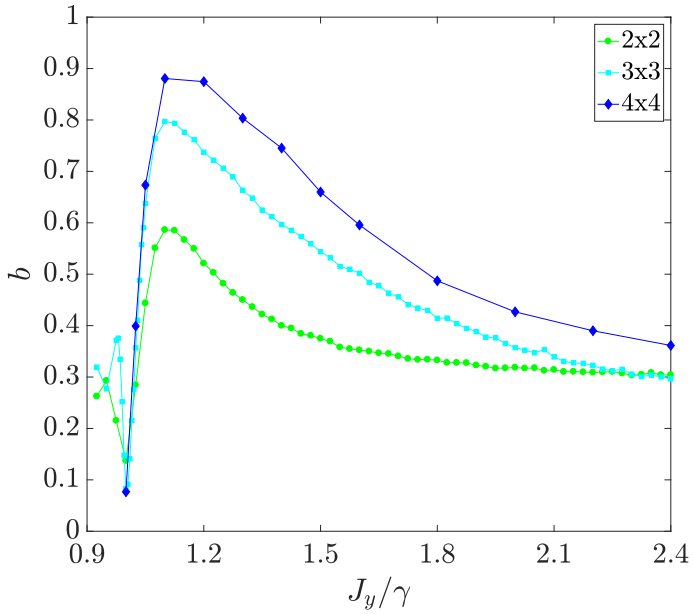

Figure 6.5 – Bimodality coefficient b (defined in the text) as a function of the coupling parameter J_y, for different sizes of the 2D lattice. The full lines are a guide for the eye. Same parameters as in Fig. 6.3. From [2].

CHAPTER 7

Schrödinger Cats and Their Feedback Stabilisation

In Chapter 4, we derived the analytic solution to the one- and two-photon driven dissipative Kerr resonator. In presence of only two-photon processes, the system steady state is a quantum superposition of coherent states $|\alpha\rangle$ and $|-\alpha\rangle$ [188, 189]:

$$|\mathcal{C}_\alpha^\pm\rangle = \frac{|\alpha\rangle \pm |-\alpha\rangle}{\sqrt{2\left(1 \pm e^{-2|\alpha|^2}\right)}}. \tag{7.1}$$

Since their theoretical conception [190], Schrödinger's cats have captured the collective imagination, because they are non-classical states at the macroscopic level. In quantum optics, the states of the electromagnetic field closest to the classical ones are the coherent states $|\alpha\rangle$ (see App. B). In this regard, the states $|\mathcal{C}_\alpha^\pm\rangle$ are known as photonic Schrödinger cats [25, 188, 189]: they are the quantum superposition of two (almost-)orthogonal (semi-)classical states. However, one-photon losses are known to destroy the quantum coherence of the cat states. As a result, the presence of both one- and two-photon dissipations makes the life of the cat states more intriguing [76, 79, 82, 189, 191, 192].

In this Chapter, exploiting the analytic solution we derived in Sec. 4.2 we demonstrate that, for a wide range of parameters around typical experimental ones [82], the unique steady-state density matrix has as eigenstates two cat-like states even for significant one-photon losses, with all the other eigenstates having negligible probability. To clarify the elusive features of quantum bimodality, we analyse this system via the quantum trajectory method both in the photon-counting and in the homodyne case.

The Chapter is organised as follows. In Sec. 7.1 we analyse the properties of the steady-state density matrix, proving that it can be written as a statistical mixture of two cat states with opposite parity or of two coherent states with opposite phases. In Sec. 7.2 we use quantum trajectories to shed light on this apparent contradiction. Finally, in Sec.7.3 we discuss a possible implementation of a feedback mechanism to protect the cat states from dissipation.

Contents

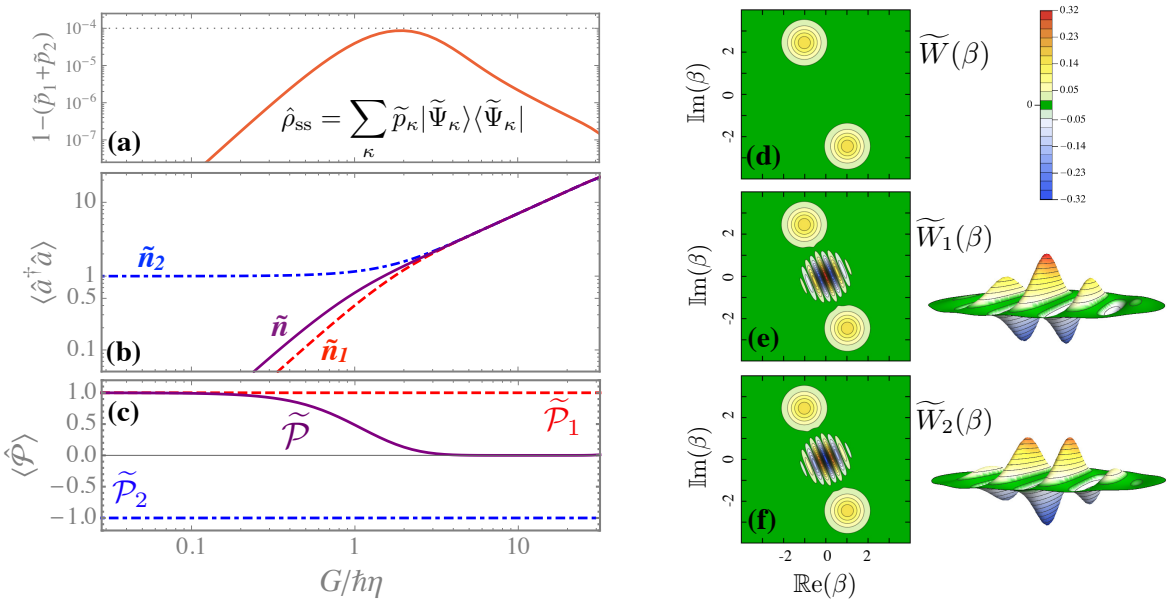

Figure 7.1 – Exact results for the steady state. The corresponding density matrix can be expressed as $\hat{\rho}_{\mathrm{ss}} = \sum_\kappa \widetilde{p}_\kappa |\widetilde{\Psi}_\kappa\rangle\langle\widetilde{\Psi}_\kappa|$, where $\widetilde{p}_1$ and $\widetilde{p}_2$ are the probabilities of the two most probable eigenstates. Parameters: $\Delta = 0$, $U = \hbar\eta$, $\gamma = 0.1\,\eta$. Panel (a): residual probability $1 - \widetilde{p}_1 - \widetilde{p}_2$ versus the two-photon drive amplitude G normalized to the two-photon loss rate η, showing that the density matrix is dominated by the first two eigenstates. Panel (b): as a function of $G/\hbar\eta$, mean number of photons $\widetilde{n}$ and its contributions $\widetilde{n}_1$ and $\widetilde{n}_2$. Panel (c): as a function of $G/\hbar\eta$, the mean parity $\widetilde{\mathcal{P}}$ and its contributions $\widetilde{\mathcal{P}}_1$ and $\widetilde{\mathcal{P}}_2$. Panel (d): for $G = 10\hbar\eta$, contour plot of the Wigner function $\widetilde{W}(\beta)$ for the density matrix $\hat{\rho}_{\mathrm{ss}}$. Panel (e) and (f): for $G = 10\hbar\eta$, Wigner functions $\widetilde{W}_1(\beta)$ and $\widetilde{W}_2(\beta)$ associated to the two most probable eigenstates. For the latter, we also show a 3D zoom of the central region $|\beta| \leq 1.6$. Note that the fringe pattern changes sign between $\widetilde{W}_1(\beta)$ and $\widetilde{W}_2(\beta)$. From [6].

7.1 Steady-state analysis

We consider the quadratically driven-dissipative Kerr resonator described in Sec. 4.2 In spite of the several parameters in the model, the solutions in Sec. 4.2.3 depends only on two dimensionless quantities, namely $c = (\Delta + \mathrm{i}\,\hbar\gamma/2)/(U - \mathrm{i}\,\hbar\eta)$ and $g = G/(U - \mathrm{i}\,\hbar\eta)$. The former can be seen as a complex single-particle detuning $\Delta + \mathrm{i}\,\hbar\gamma/2$ divided by a complex interaction energy $U - \mathrm{i}\,\hbar\eta$; g is instead the two-photon pump intensity normalized by the same quantity. Notably, Eqs. (4.54) show that, for *any* finite value of the system parameters, there will be no even-odd coherences in the steady state. In what follows following, all the quantities marked with a tilde will refer to steady-state values.

To further characterise the steady-state, we consider the spectral decomposition of the density matrix $\hat{\rho} = \sum_\kappa p_\kappa |\Psi_\kappa\rangle\langle\Psi_\kappa|$, with $|\Psi_\kappa\rangle$ the κ^{th} eigenstate of $\hat{\rho}$ with eigenvalue p_κ. The latter corresponds to the probability of finding the system in $|\Psi_\kappa\rangle$ upon an appropriate measure. The eigenstates are sorted in such a way that $p_\kappa \geq p_{\kappa+1}$. For a pure state, $p_1 = 1$ and all the other probabilities p_κ are zero. We numerically diagonalised the density matrix $\hat{\rho}_{\mathrm{ss}}$ in a truncated Fock basis, choosing a cutoff ensuring a precision of 10^{-14}. For our calculations, we chose a set of parameters around typical experimental ones [82], i.e. $\Delta \simeq 0$, $|U| \simeq \hbar\eta$, $G \gtrsim \hbar\eta$, and $\gamma \lesssim \eta$. In this regime, for the steady state only two eigenstates dominate the density

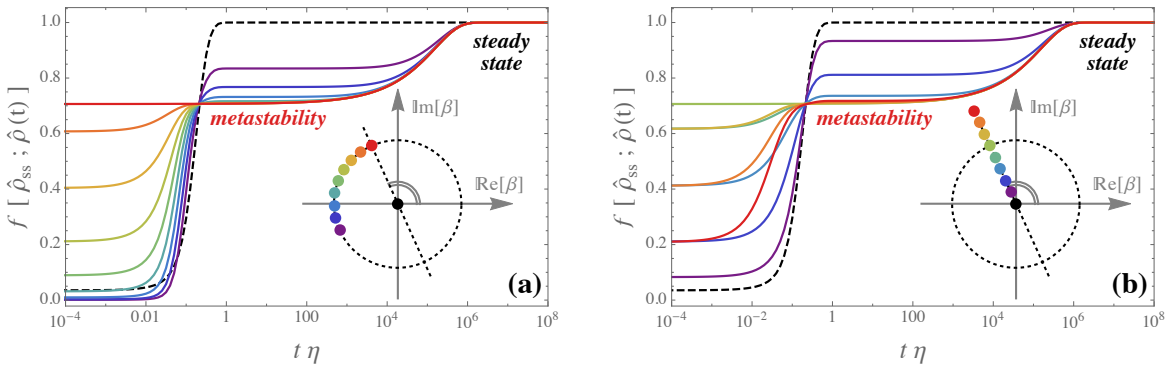

Figure 7.2 – Metastable versus steady-state regime. The curves depict the time-dependent fidelity of the density matrix $\hat{\rho}(t)$ with respect to the unique steady-state density matrix $\hat{\rho}_{\rm ss}$ by taking as initial condition a pure coherent state, i.e., $\hat{\rho}(t=0) = |\beta\rangle\langle\beta|$. The fidelity is defined as $f[\hat{\rho}_{\rm ss};\hat{\rho}(t)] = \mathrm{Tr}\left[\sqrt{\sqrt{\hat{\rho}_{\rm ss}}\,\hat{\rho}(t)\,\sqrt{\hat{\rho}_{\rm ss}}}\right]$. The values of β and the corresponding colours are indicated in the inset. Panel (a): the phase of the initial coherent state is varied (cf. inset). Panel (b): the amplitude is changed (cf. inset). The dashed lines correspond to the vacuum as initial state. Parameters: $\Delta = 0$, $U = \hbar\eta$, $G = 10\hbar\eta$, $\gamma = \eta$. From Ref. [6].

matrix. As shown in Fig. 7.1(a), typically $\tilde{p}_1 + \tilde{p}_2 \simeq 1$, and $\hat{\rho}_{\rm ss} \simeq \tilde{p}_1|\tilde{\Psi}_1\rangle\langle\tilde{\Psi}_1| + \tilde{p}_2|\tilde{\Psi}_2\rangle\langle\tilde{\Psi}_2|$. The aforementioned absence of even-odd coherences implies that $|\tilde{\Psi}_{1(2)}\rangle$ is composed of only even (odd) Fock states. Furthermore, we find that $|\tilde{\Psi}_1\rangle \simeq |\mathcal{C}_\alpha^+\rangle$ and $|\tilde{\Psi}_2\rangle \simeq |\mathcal{C}_\alpha^-\rangle$ for an appropriate choice of α. For the parameters of Fig. 7.1(d), $\langle\tilde{\Psi}_{1(2)}|\mathcal{C}_\alpha^{+(-)}\rangle \simeq (1 - 8\times10^{-6})$ for $\alpha \approx 2.7\,e^{2.0\,i}$. We have varied $\Delta/\hbar\eta$ between -0.2 and 0.2, $G/\hbar\eta$ between 0 and 15, γ/η between 0 and 5, $U/\hbar\eta$ between 1 and 10, always finding that $1 - \tilde{p}_1 - \tilde{p}_2 < 10^{-2}$. Moreover, in these ranges, we verified that there exists a value of α such that $\langle\tilde{\Psi}_{1(2)}|\mathcal{C}_\alpha^{+(-)}\rangle > 0.98$. Hence, we can conclude that for a broad range of parameters the eigenstates of $\hat{\rho}_{\rm ss}$ are two cat-like states of opposite parity. [1]

Using the linearity of the trace, for any operator $\hat{O}$ one can write $\tilde{O} = \mathrm{Tr}\left[\hat{\rho}_{\rm ss}\,\hat{O}\right] \simeq \tilde{p}_1\tilde{O}_1 + \tilde{p}_2\tilde{O}_2$, where $\tilde{O}_\kappa = \langle\tilde{\Psi}_\kappa|\hat{O}|\tilde{\Psi}_\kappa\rangle$. In Fig. 7.1(b) we plot, as a function of the pump amplitude G, the steady-state mean density $\tilde{n}$, together with its contributions $\tilde{n}_{1,2}$. For weak pumping one has $\tilde{n}_1 \simeq 0$ and $\tilde{n}_2 \simeq 1$, in agreement with what one would obtain for the even and the odd cat by taking the limit $\alpha \to 0$ of Eq. (F.15). These two contributions become equal in the limit of a very large number of photons. As shown in Fig. 7.1(c), the two contributions to the mean parity $\tilde{\mathcal{P}}_{1,2}$ always stay clearly different, being $|\mathcal{C}_\alpha^\pm\rangle$ orthogonal eigenstates of $\hat{\mathcal{P}}$ with eigenvalues ±1. To visualise the nonclassicality of the states, we use the Wigner function. Even if the Wigner function of the steady state is always positive [cf. Eq. (4.55)], the separate contributions $\widetilde{W}_1(\beta)$ and $\widetilde{W}_2(\beta)$ exhibit an interference pattern with negative regions, typical of cat states [cf. Fig. 7.1(d-f)].

We emphasize that for finite γ the considered system has always a unique steady state. However, the temporal relaxation towards the steady state depends dramatically on the initial condition. This metastable behaviour is is revealed by the time-dependent fidelity with respect to the steady state, presented in Fig. 7.2, obtained by numerical integration of the master equation. In particular, initialising the system in one of the coherent states $|\pm\alpha\rangle$

1. Let us notice that a simple method to determine the nature of the steady state in the limit $\gamma \ll U \ll G$ can be found in [88].

composing the steady-state cats, it persists nearby for a time several orders of magnitude longer than $1/\gamma$ and $1/\eta$. Hence, the "multiple stable steady states" in [82] are actually metastable.

7.2 Quantum trajectories

The density matrix $\hat{\rho}_{\rm ss}$ is well approximated by the statistical mixture of two orthogonal states:

$$\hat{\rho}_{\rm ss} \simeq p^{+} \ |\mathcal{C}_{\alpha}^{+}\rangle\langle\mathcal{C}_{\alpha}^{+}| + p^{-} \ |\mathcal{C}_{\alpha}^{-}\rangle\langle\mathcal{C}_{\alpha}^{-}| \, . \tag{7.2}$$

In Eq.(7.2), the coefficients $p^{\pm}$ can be interpreted as the probabilities of the system of being found in the corresponding cat state. For intense pumping ($G \gg U, \gamma, \eta$), one has $|\alpha| \gg 1$ and $p^{+} \simeq p^{-} \simeq 1/2$. However, in this strong-pumping regime, Eq. (7.2) can be recast as

$$\hat{\rho}_{\rm ss} \simeq \frac{1}{2} \, |\alpha\rangle\langle\alpha| + \frac{1}{2} \, |-\alpha\rangle\langle-\alpha| \, . \tag{7.3}$$

Hence, the steady state can be seen as well as a statistical mixture of two coherent states of opposite phase. Since $\hat{\rho}_{\rm ss}$ is anyhow a mixture of two (quasi-)orthogonal states, the steady state is bimodal. Now, the pivotal question is: if one monitors the evolution of the system, in which states can it be observed? The orthogonal cat states in Eq. (7.2) with $p^{\pm} = 1/2$, the two coherent states with opposite phases in Eq. (7.3), or none of them in particular? As we will show in the following, the answer dramatically depends on the type of measurement scheme employed to monitor the trajectory of the system.

7.2.1 Photon counting

As we discussed in Sec. 3.4.2 and proved in Sec. 4.4, a photon-counting trajectory for this system will always jump between eigenstates of the parity. The cat states are, indeed, orthogonal eigenstates of the parity operator $\hat{\mathcal{P}} = e^{{\rm i}\pi\hat{a}^{\dagger}\hat{a}}$ with eigenvalues ± 1. For the specific case of the Schrödinger cats, this is presented in Fig. 7.3, where in panels (a,b) we follow, respectively, the time evolution of the photon number $\langle\hat{n}\rangle$ and of the parity $\langle\hat{\mathcal{P}}\rangle$, starting from the vacuum state as initial condition. On a single trajectory, two-photon processes initially dominate, driving the system towards $|\mathcal{C}_{\alpha}^{+}\rangle$. Indeed, $\langle\hat{n}\rangle \simeq \widetilde{n}_1$ and $\langle\hat{\mathcal{P}}\rangle = \widetilde{\mathcal{P}}_1 = 1$. Two-photon losses do not affect a state parity, indeed $\hat{a}^2 \ |\mathcal{C}_{\alpha}^{\pm}\rangle = \alpha^2 \ |\mathcal{C}_{\alpha}^{\pm}\rangle$. This is why the system persists nearby the even cat until a one-photon loss occurs. At this point, the state abruptly jumps to the odd manifold [193], since $\hat{a} \ |\mathcal{C}_{\alpha}^{\pm}\rangle \propto |\mathcal{C}_{\alpha}^{\mp}\rangle$. After the jump, two-photon processes stabilise $|\mathcal{C}_{\alpha}^{-}\rangle$, so that $\langle\hat{n}\rangle \simeq \widetilde{n}_2$ and $\langle\hat{\mathcal{P}}\rangle = \widetilde{\mathcal{P}}_2 = -1$. When another one-photon jump takes place, the system is brought back to the even manifold, and so on. Hence, if the quantum trajectory is monitored via photon counting [24], the system can only be found nearby $|\mathcal{C}_{\alpha}^{+}\rangle$ or $|\mathcal{C}_{\alpha}^{-}\rangle$. The probability of being in each cat is given by the corresponding eigenvalue of $\hat{\rho}_{\rm ss}$, namely $\widetilde{p}_1$ and $\widetilde{p}_2$. Since $\widetilde{n}_{1,2} \approx \widetilde{n}$, it is impossible to discern the cats' jumps by tracking the photon density. A parity measurement, instead, would be suitable [194]. In Fig. 7.3(a) and (b) we also present the average over 100 trajectories, which, as expected, converges to the master equation solution (also shown). The latter corresponds to the full average over an infinite number of realizations [110]. The fully-averaged and single-trajectory evolutions of the Wigner function are shown in Fig. 7.3(c). In the averaged one, an even-cat transient appears, but negativities are eventually washed out for $\eta t, \gamma t \gg 1$ [82, 189, 193].

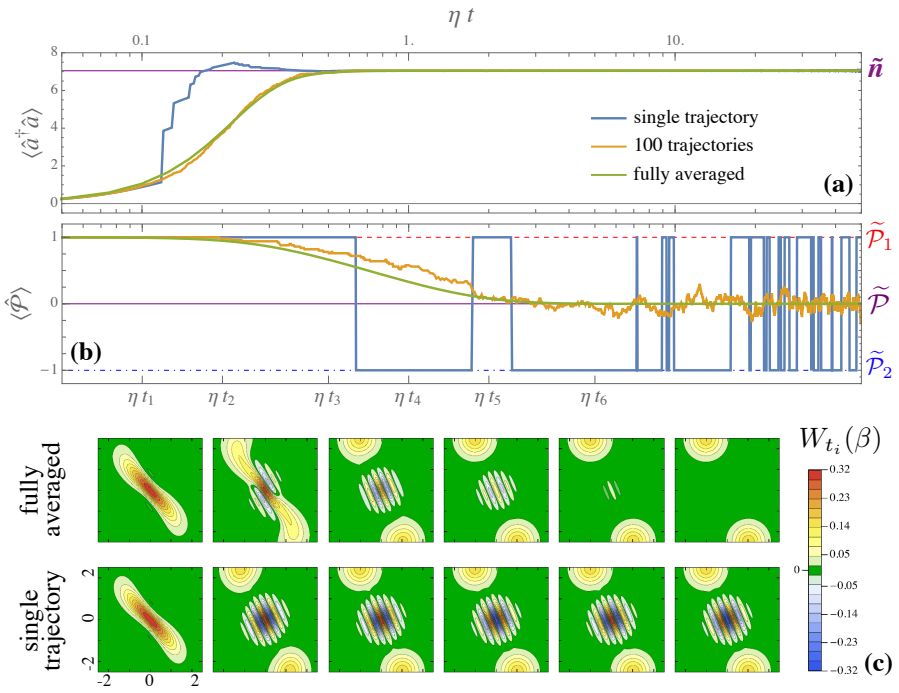

Figure 7.3 – Dynamics of averaged quantities versus single quantum trajectories. Panel (a): dynamics (time is in logarithmic scale) of the photon population for a single quantum trajectory (blue line), an average of 100 trajectories (orange line) and the fully averaged (green line) density matrix. Panel (b): same as (a) but for the expectation value of the photon parity operator. Panel (c): snapshots of the Wigner functions at different times. The system parameters are $\Delta = 0$, $U = \hbar\eta$, $G = 10\hbar\eta$, and $\gamma = 0.1\eta$. We stress that, in the single-trajectory Wigner functions, the fringe pattern changes sign after a parity jump. From Ref. [6].

By following a single quantum trajectory, instead, we see that $W_t(\beta)$ quickly tends to the one of $|\mathcal{C}_\alpha^+\rangle$. Then, it abruptly switches to that of $|\mathcal{C}_\alpha^-\rangle$, then back at each one-photon jump.

7.2.2 Schrödinger cats vs coherent states

The previous analysis seems to point in the direction of privileging Eq. (7.2) over Eq. (7.3) as the more truthful picture of the steady state. This is no more the case if we consider homodyne quantum trajectories. In Fig. 7.4(a) we present, again, the time evolution of the parity along a counting trajectories. We also show that the filed quadrature $\hat{x}$ and $\hat{p}$ have zero mean along such a trajectory. In Fig. 7.4(b), we present (in a log-linear scale) the mean parity $\langle\hat{\mathcal{P}}\rangle$ along a single homodyne trajectory, taking the vacuum as initial state. In spite of the "switching cat" picture, the parity rapidly approaches zero, and than just fluctuates around this value. These fluctuations are due to the diffusive nature of Eq.(6.3), which rules the stochastic time evolution of the system wave function under homodyne detection. The bimodal behaviour, instead, is clear in the time evolution of $\langle\hat{x}\rangle$ and $\langle\hat{p}\rangle$, shown in Fig. 7.4(c). This appears compatible with the picture given by Eq. (7.3): at the steady state the system switches between the coherent states $|\pm\alpha\rangle$. We point out that the phase switches observed for homodyne trajectories have a much smaller rate than parity switches in photon-counting trajectories. This is a consequence of the metastable nature of the coherent states $|\pm\alpha\rangle$

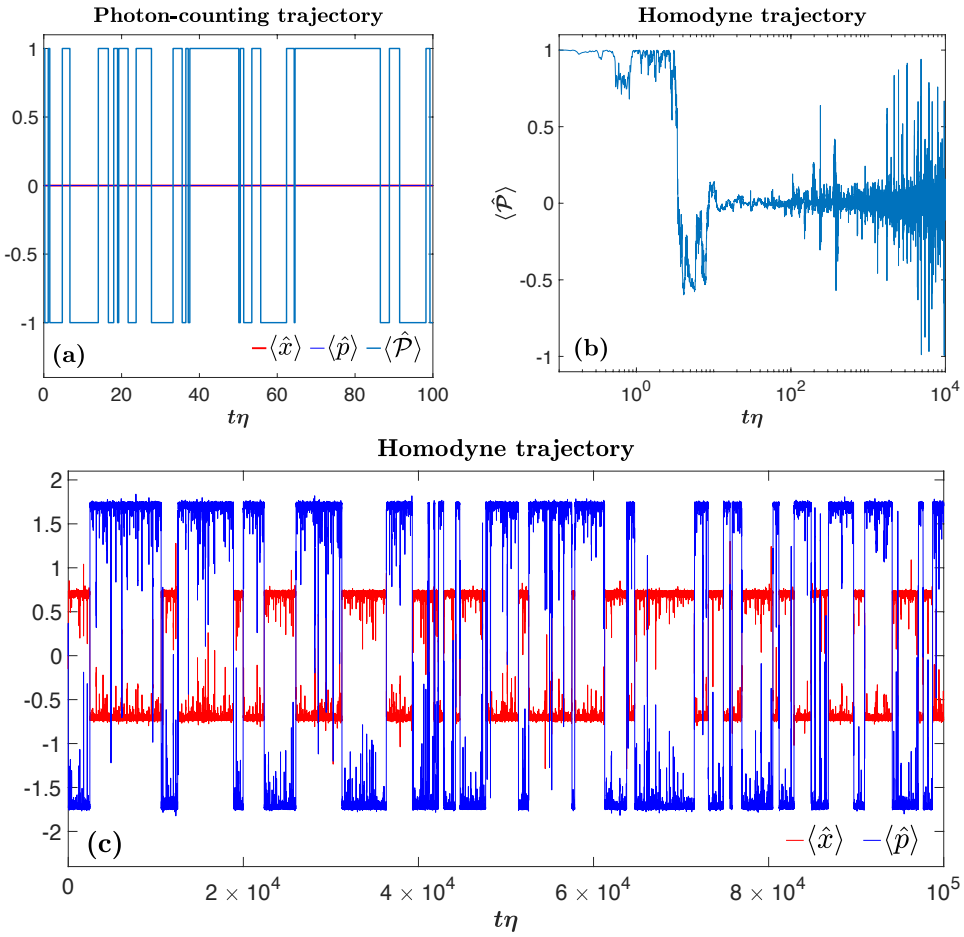

Figure 7.4 – Time evolution of $\langle\hat{x}\rangle$, $\langle\hat{p}\rangle$, and $\langle\hat{\mathcal{P}}\rangle$ along single quantum trajectories for the master equation (6.2). In (a) we show the three mean values for a photon-counting trajectory. In (b) and (c), we plot the same quantities for a homodyne protocol. Overall, we set the system parameters to $U = 1\eta$, $G = 5\eta$, and $\gamma = 0.1\eta$. Simulations were performed on a truncated Fock basis with $n_{\max} = 15$, ensuring convergence. From Ref. [4].

[6, 82], associated to the symmetry $\mathcal{Z}_2$ of the system.

Summing up, we have shown that the behaviour of the system along a single quantum trajectory dramatically depends on the measurement protocol adopted. For photon-counting measurements on the environment, the system switches between the parity-defined cat states appearing in Eq. (7.2). Under homodyne detection, the states explored along a single quantum trajectory are the coherent ones in Eq. (7.3). In other words, one may assign a physical meaning to the probabilities appearing in the mixed-state representation of $\hat{\rho}_{\rm ss}$ only upon specification of the single-trajectory protocol. However, any possible controversy at the single-trajectory level is washed out by averaging over many of them.

7.3 A feedback protocol

The results presented above suggest that, in order to have a cat-like steady state (e.g. keep interference fringes in the fully averaged Wigner function), one may try to unbalance the

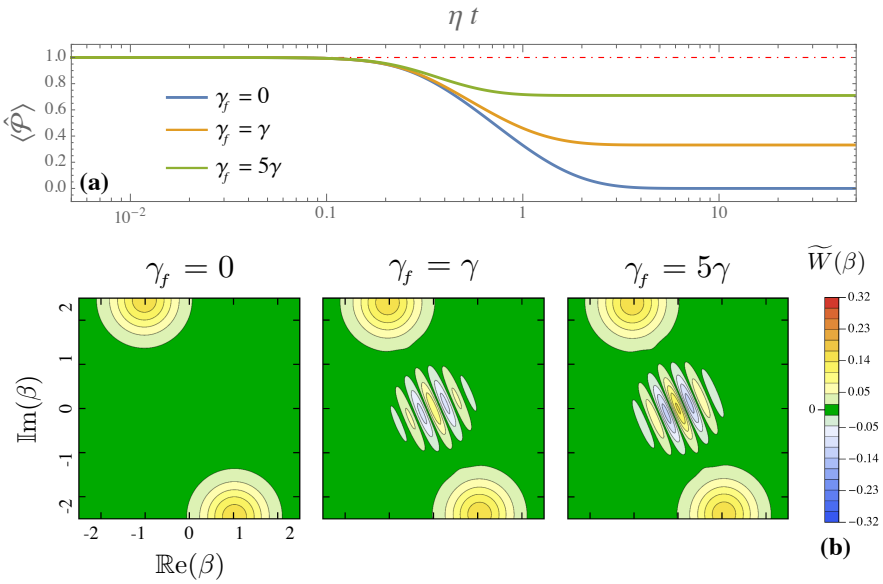

Figure 7.5 – These results are obtained by numerical integration of the Lindblad master equation, taking the vacuum as initial condition and for same system parameters as in Fig. 7.3. Panel (a): time evolution of the parity mean-value in presence of the feedback described by Eq. (7.4) for different values of γ_f (cf. legend). Panel (b): steady-state Wigner function ($t \to +\infty$) exhibiting negativities for $\gamma_f > 0$. From Ref. [6].

even and odd contributions to $\hat{\rho}_{\rm ss}$. This effect can be envisioned through a parity-triggered feedback mechanism [195–198] opening a one-photon loss channel. In practice, this can be implemented via non-destructive parity measurements [194, 199], whose rate must be larger than any other rate in the system. Note that, in general, a parity measurement projects the system into the even- or odd-parity manifold, affecting the dynamics by destroying the even-odd coherences. In the present case, however, those coherences are proven to be always zero in the steady state by the analytic solution. Thus, a high-rate and non-destructive parity measure does not alter significantly the system dynamics and allows to continuously monitor $\langle\hat{\mathcal{P}}\rangle$. When the undesired value is measured, an auxiliary qubit is put into resonance with the cavity, inducing the absorption of a photon. After the desired parity is restored, the qubit is brought out of resonance, closing the additional dissipation channel. Such a qubit acts as a non-Markovian bath for the system, and in principle its effects can not be simply assimilated to those of a Markovian environment. However, if one assumes that the excited-state lifetime of the qubit is shorter than the inverse of the qubit-cavity coupling rate, one can safely treat it as an additional Markovian dissipator [196, 200]. In other words, the coupled qubit must be engineered to easily lose the photon to the environment, which seems a reasonable task for the present experimental techniques [192, 197, 198, 201]. Under these assumptions, the proposed feedback protocol can be effectively described by the additional jump operator $\hat{a}_f = \hat{a}\,\frac{1}{2}(1-\hat{\mathcal{P}})$ and the corresponding dissipator

$$\mathcal{D}[\hat{a}_f]\hat{\rho} = \frac{\gamma_f}{2}\left(2\hat{a}_f\hat{\rho}\hat{a}_f^\dagger - \hat{a}_f^\dagger\hat{a}_f\hat{\rho} - \hat{\rho}\hat{a}_f^\dagger\hat{a}_f\right). \tag{7.4}$$

Qualitatively, $\mathcal{D}[\hat{a}_f]$ leaves the even cat undisturbed, while it enhances the dissipation for the odd one.

In Fig. 7.5(a) we show the time evolution of $\langle\hat{\mathcal{P}}\rangle$ for three different values of γ_f. These results have been obtained via numerical integration of the Lindblad master equation with

a total dissipator $\mathcal{D} = \mathcal{D}[\hat{a}] + \mathcal{D}[\hat{a}^2] + \mathcal{D}[\hat{a}_f]$. At the steady state, as γ_f increases so does $\widetilde{\mathcal{P}}$, indicating that the positive cat has a larger weight in $\hat{\rho}_{\rm ss}$. In Fig. 7.5(b) we show the corresponding steady-state Wigner functions $\widetilde{W}(\beta)$. For finite γ_f, negative fringes appear in the Wigner function. They are more pronounced as γ_f is increased, revealing a highly nonclassical state. In the limit $\gamma_f \gg \gamma$, $\hat{\rho}_{\rm ss} \simeq |\mathcal{C}_\alpha^+\rangle \langle \mathcal{C}_\alpha^+|$. By using, instead, the jump operator $\hat{a}_f = \hat{a}\,\frac{1}{2}(1+\hat{\mathcal{P}})$, one can similarly stabilize the odd cat state. Note that the Wigner-function negativities in Fig. 7.5 are those of the full steady-state density matrix. Hence, the quantum state of the system is on average nonclassical.

7.4 Conclusions

In this Chapter, we have studied the quantum many-body behaviour of interacting photons in a nonlinear resonator subject to engineered two-photon processes. The objective has been to point out and characterize the bimodal nature of the steady state, which can be seen, equivalently, as the statistical mixture of photonic Schrödinger cat states [Eq. (7.2)] or of coherent states with same amplitude and opposite phases [Eq. (7.3)]. We have also shown that the transient dynamics to the unique steady state can depend dramatically on the initial condition, revealing the existence of metastable states.

Furthermore, by monitoring the quantum trajectory of the system via photon counting (homodyne), we found that it explores the two cat states (7.2) (two coherent states (7.3)) composing the steady-state statistical mixture. On this ground, we proposed to engineer a parity-dependent dissipation which allows to stabilize a cat-like steady state.

The general nature and richness of the results predicted here paves the way to a wide variety of experimental and theoretical investigations. As a future perspective, a challenging but intriguing problem is the study of other photonic cat-like states in the transient and steady-state regime for arrays of coupled resonators. Furthermore, the components of the mixed steady state (7.2) or (7.3) can be used as (quasi-)orthogonal states in quantum computation [84–86, 88, 202].

General Conclusions

In this thesis we explored the physics of driven-dissipative systems, with a particular focus on critical phenomena. We investigated both general properties of driven-dissipative phase transitions and specific models exhibiting criticality. The generation and stabilisation of phases without an equilibrium counterpart is a timely subject, in particular for the realisation of nonclassical states which can be used for quantum simulation and computation. In this regard, we studied models characterised by a two-photon pumping mechanism, which can be obtained via reservoir engineering of the system-environment exchanges. All through the manuscript, particular attention was given to quantum trajectories, pointing out the possible use of single quantum trajectories to investigate criticality. The results presented are quite general, and several experimental platform can realise the presented models, e.g., semiconductor optical microcavities and superconducting circuits.

In particular, in Chapter 3 we unveiled the connection between phase transitions and spectral properties of the Liouvillian superoperator. Beyond the interest in the conceptual foundations of the topic of dissipative phase transitions, we found a series of general properties, which can be used to identify the onset of phase transitions: (i) A punctual closure of the Liouvillian gap indicates a first-order phase transition, while the gap closed in a whole region signals a second-order one; (ii) Around criticality, there is an intimate connection between the form of the steady-state density matrix and that of the Liouvillian eigenmatrix whose eigenvalue defines the Liouvillian spectral gap; (iii) First-order phase transition show bistable quantum trajectories only around the critical point, while to observe bimodal behaviour in second-order phase transitions is necessary to use homodyne quantum trajectories.

Using the previously derived indicators, we have then analysed the emergence of phase transitions in several models. In Chapter 4 we considered the one- and two-photon driven-dissipative Kerr resonator, for which we provided an analytic solution of the steady state density matrix. We showed that, in an appropriate thermodynamic limit, the one-photon Kerr resonator presents a first-order phase transition, while the two-photon one has a second-order phase transition. This model, for which an exact numerical diagonalisation of the Liouvillian is possible, allowed us to benchmark our general theory, both regarding the structure of the Liouvillian eigenmatrices and the use of quantum trajectories. In Chapter 5, we studied the emergence of a first-order phase transition in an extended driven-dissipative Bose-Hubbard lattice by studying the critical slowing down associated with the closure of the Liouvillian gap. Using the truncated Wigner trajectories, we demonstrated the emergence of a phase transition in 2D lattices and the lack of criticality in 1D systems, proving the role of dimensionality for dissipative phase transitions. In Chapter 6, instead, we studied the dynamical properties of dissipative XYZ Heisenberg lattices, a model presenting a second-order phase transition associated with the breaking of the $\mathcal{Z}_2$ symmetry. We also analysed the behaviour of individual homodyne quantum trajectories which, according to our general theory, well

reveal the properties of the "broken symmetry" phases.

Finally, in Chapter 7, we explored the emergence of Schrödinger cats in a two-photon driven Kerr resonators. Exploiting the exact analytical solution derived in Chapter 4, we demonstrated that the unique steady state is a statistical mixture of two cat-like states with opposite parity, in spite of significant one-photon losses. We resorted to quantum trajectories to further characterise the system. While along a single photon-counting trajectory the system intermittently switches between an odd and an even cat states, we showed that upon homodyne detection the system switches between coherent states of opposite phase. Finally, we proposed and studied a feedback protocol based on the "jumping cat" behaviour. Such a procedure can purify cat-like steady states.

The presented works open several possible prospects. First, the study of disordered systems via single quantum trajectories. Indeed, in Chapter 5 we proposed an extremely efficient protocol based on quantum trajectories, making possible to investigate such a problem. Second, the exact results derived in Chapter 3 severely constrain the nature of the steady-state around a phase transitions. One can use the conditions in the determination of a semi-analytical steady-state via variational methods. In this regard, it seems interesting to develop a variational method based on the complex P-representation. Third, one can use the symmetries of the Liouvillian superoperator to simplify the numerical cost in computing the Liouvillian spectrum in extended lattices. Finally, concerning the stabilisation of Schrödinger cats, an in-depth study of the proposed feedback is of great interest.

Appendices

APPENDIX A

Ideal Homodyne Detection Limit

To properly derive the stochastic Schrödinger equation (2.61) in the limit $\beta \to \infty$, we remark that the only non-deterministic term of Eq. (2.61) is $\mathrm{d}N(t)$. Since $\mathrm{d}N(t) = 0, 1$, one has $\mathrm{d}N(t)^2 = \mathrm{d}N(t)$. Moreover, the expectation value of $\mathrm{d}N(t)$ reads

$$E[\mathrm{d}N(t)] = \tau \left\langle (\hat{\Gamma}^\dagger + \beta)(\hat{\Gamma} + \beta) \right\rangle = \tau\beta^2 + \tau\beta \left\langle \hat{\Gamma}^\dagger + \hat{\Gamma} \right\rangle + \mathcal{O}(\beta^0), \tag{A.1}$$

where, in the limit $\beta \to \infty$ one can neglect the term due to the bare jump operator $\hat{\Gamma}$. Clearly, τ must be small enough to ensure $E[\mathrm{d}N(t)] < 1$, and therefore $\tau E[\mathrm{d}N(t)] = 0$. Consequently, $\mathrm{d}N(t)$ can be recast as

$$\mathrm{d}N(t) = \tau\beta^2 + \beta \mathrm{d}X(t), \tag{A.2}$$

where the first is a constant term, while $\mathrm{d}X(t)$ is the variable encoding the stochastic nature of the problem. We are, therefore, interested in deriving the properties of $\mathrm{d}X(t)$. By taking the expectation value of $\mathrm{d}N(t)$ we see immediately that

$$\text{Property (i): } E[\mathrm{d}X(t)] = \tau \left\langle \hat{\Gamma}^\dagger + \hat{\Gamma} \right\rangle . \tag{A.3}$$

Now, consider $(\mathrm{d}X(t))^2$. One has

$$\begin{aligned} E\left[(\mathrm{d}X(t))^2\right] &= E\left[\frac{(\mathrm{d}N(t) - \tau\beta^2)^2}{\beta^2}\right] = E\left[\frac{(\mathrm{d}N)^2}{\beta^2}\right] - 2\tau E[\mathrm{d}N(t)] - \beta^2\tau^2 \\ &= E\left[\frac{\mathrm{d}N}{\beta^2}\right] = \tau + \frac{E[\mathrm{d}X(t)]}{\beta} = \tau, \end{aligned} \tag{A.4}$$

where we remark $\tau E[\mathrm{d}N(t)] \simeq \tau^2\beta = 0$. Hence

$$\text{Property (ii)} : E\left[(\mathrm{d}X(t))^2\right] = \tau \tag{A.5}$$

Moreover, $\mathrm{d}X(t)\tau = 0$, since $\mathrm{d}N(t)\tau = 0$.

Therefore, from Property (i) and (ii) we conclude that

$$\mathrm{d}W(t) = \mathrm{d}X(t) - E[\mathrm{d}X(t)] \tag{A.6}$$

is a Wiener process, of variance $E[(\mathrm{d}W(t))^2] = \tau$ and expectation $E[\mathrm{d}W(t)] = 0$. Finally, to obtain the stochastic Schrödinger equation for a diffusive process, we have to develop the

first part of Eq. (2.61), keeping only the highest order in β. Since $\mathrm{d}N(t)$ contains terms of order β^2, the first part of Eq. (2.61) read

$$\begin{aligned}
&\left(\frac{\hat{\Gamma}+\beta}{\sqrt{\langle(\hat{\Gamma}^\dagger+\beta)(\hat{\Gamma}+\beta)\rangle}}-\mathbb{1}\right)=\mathrm{d}N(t)\left(\frac{\hat{\Gamma}+\beta}{\beta\sqrt{1+\frac{\langle\hat{\Gamma}^\dagger+\hat{\Gamma}\rangle}{\beta}+\frac{\langle\hat{\Gamma}^\dagger\hat{\Gamma}\rangle}{\beta}}}-\mathbb{1}\right)\\
&=\left[\left(1+\frac{\hat{\Gamma}}{\beta}\right)\left(1-\frac{\langle\hat{\Gamma}^\dagger+\hat{\Gamma}\rangle}{2\beta}+\frac{3\langle\hat{\Gamma}^\dagger+\hat{\Gamma}\rangle^2}{8\beta^2}-\frac{\langle\hat{\Gamma}^\dagger\hat{\Gamma}\rangle}{2\beta^2}+\mathcal{O}(\beta^{-3})\right)-\mathbb{1}\right]\\
&=\left(\frac{\hat{\Gamma}}{\beta}-\frac{\langle\hat{\Gamma}^\dagger+\hat{\Gamma}\rangle}{2\beta}+\frac{3\langle\hat{\Gamma}^\dagger+\hat{\Gamma}\rangle^2}{8\beta^2}-\hat{\Gamma}\frac{\langle\hat{\Gamma}^\dagger+\hat{\Gamma}\rangle}{2\beta^2}-\frac{\langle\hat{\Gamma}^\dagger\hat{\Gamma}\rangle}{2\beta^2}\right),
\end{aligned}\tag{A.7}$$

and therefore

$$\begin{aligned}
&\mathrm{d}N(t)\left(\frac{\hat{\Gamma}+\beta}{\sqrt{\langle(\hat{\Gamma}^\dagger+\beta)(\hat{\Gamma}+\beta)\rangle}}-\mathbb{1}\right)\\
&=\left(\beta^2\tau+\beta\mathrm{d}W(t)+\beta\tau\langle\hat{\Gamma}^\dagger+\hat{\Gamma}\rangle\right)\left(\frac{\hat{\Gamma}}{\beta}-\frac{\langle\hat{\Gamma}^\dagger+\hat{\Gamma}\rangle}{2\beta}+\frac{3\langle\hat{\Gamma}^\dagger+\hat{\Gamma}\rangle^2}{8\beta^2}-\hat{\Gamma}\frac{\langle\hat{\Gamma}^\dagger+\hat{\Gamma}\rangle}{2\beta^2}-\frac{\langle\hat{\Gamma}^\dagger\hat{\Gamma}\rangle}{2\beta^2}\right)\\
&=\tau\left[\beta\left(\hat{\Gamma}-\frac{\langle\hat{\Gamma}+\hat{\Gamma}^\dagger\rangle}{2}\right)+\hat{\Gamma}\frac{\langle\hat{\Gamma}^\dagger+\hat{\Gamma}\rangle}{2}-\frac{\langle\hat{\Gamma}^\dagger+\hat{\Gamma}\rangle^2}{8}-\frac{\langle\hat{\Gamma}^\dagger\hat{\Gamma}\rangle}{2}\right]+\mathrm{d}W(t)\left(\hat{\Gamma}-\frac{\langle\hat{\Gamma}^\dagger+\hat{\Gamma}\rangle}{2}\right).
\end{aligned}\tag{A.8}$$

Injecting the result of Eq. (A.8) into Eq. (2.61) we finally obtain

$$\mathrm{d}\left|\psi(t)\right\rangle=\left[\mathrm{d}W(t)\left(\hat{\Gamma}-\frac{\langle\hat{\Gamma}^\dagger+\hat{\Gamma}\rangle}{2}\right)+\tau\left(-\mathrm{i}\hat{H}-\frac{\hat{\Gamma}^\dagger\hat{\Gamma}}{2}+\hat{\Gamma}\frac{\langle\hat{\Gamma}^\dagger+\hat{\Gamma}\rangle}{2}-\frac{\langle\hat{\Gamma}^\dagger+\hat{\Gamma}\rangle^2}{8}\right)\right]\left|\psi(t)\right\rangle.\tag{A.9}$$

APPENDIX B

Properties of the Coherent States

B.1 Some useful properties

Expression in the Fock basis: Using the definition of the displacement operator, and noticing that

$$\hat{D}(\alpha) = e^{\alpha\hat{a}^\dagger - \alpha^*\hat{a}} = e^{-\frac{|\alpha|^2}{2}} e^{\alpha\hat{a}^\dagger} e^{-\alpha^*\hat{a}}, \tag{B.1}$$

one can express the coherent state on the Fock basis as:

$$\begin{aligned} |\alpha\rangle &= e^{-|\alpha|^2/2} e^{\alpha\hat{a}^\dagger} e^{-\alpha^*\hat{a}} |0\rangle = e^{-|\alpha|^2/2} \sum_n \alpha^n \hat{a}^{\dagger\, n} \sum_m \alpha^{*\, m} \hat{a}^m |0\rangle = e^{-|\alpha|^2/2} \sum_n \alpha^n \hat{a}^{\dagger\, n} \alpha^{*\, 0} \hat{a}^0 |0\rangle \\ &= e^{-|\alpha|^2/2} \sum_n \frac{\alpha^n}{\sqrt{n!}} |n\rangle . \end{aligned} \tag{B.2}$$

Mean number of photons: From Eq. (B.2) follows:

$$\langle \hat{n} \rangle = \langle \alpha | \hat{n} | \alpha \rangle = e^{-|\alpha|^2} \sum_{n,n'} \frac{(\alpha^*)^n \alpha^{n'}}{(n! n'!)^{1/2}} \langle n' | \hat{n} | n \rangle = e^{-|\alpha|^2} \sum_n \frac{|\alpha|^{2n}}{n!} n = |\alpha|^2. \tag{B.3}$$

Poissonian number distribution of coherent states: The probability of finding n photons in a coherent state $|\alpha\rangle$ is

$$P_\alpha(n) = |\langle n | \alpha \rangle|^2 = e^{-|\alpha|^2} \frac{|\alpha|^{2n}}{n!}, \tag{B.4}$$

from is a Poissonian distribution with mean $\langle \hat{n} \rangle = |\alpha|^2$. Moreover,

$$\langle \hat{n}^2 \rangle = \langle \alpha | \hat{n}^2 | \alpha \rangle = e^{-|\alpha|^2} \sum_n \frac{|\alpha|^{2n}}{n!} n^2 = e^{-|\alpha|^2} \sum_n \frac{|\alpha|^{2n}}{n!} [n(n-1) + n] = |\alpha|^4 + |\alpha|^2. \tag{B.5}$$

Consequently, the variance of the second momentum is

$$\langle \hat{n}^2 \rangle - \langle \hat{n} \rangle^2 = |\alpha|^2 = \langle n \rangle , \tag{B.6}$$

as required by a Poissonian distribution.

Coherent states are the only eigenstate of the annihilation operator: From Eq. (B.2), it follows that coherent states are eigenstate of the annihilation operator, i.e.,

$$\hat{a}\,|\alpha\rangle = \alpha\,|\alpha\rangle \tag{B.7}$$

We stress that this equation defines uniquely the state $|\alpha\rangle$. Indeed, suppose there exist a second state $|\Psi\rangle$ such that $\hat{a}\,|\Psi\rangle = \alpha\,|\Psi\rangle$. We would have

$$\hat{a}\,|\Psi\rangle - \alpha\,|\Psi\rangle = \sum_{n=0}^{\infty} c_n\sqrt{n}\,|n-1\rangle - \alpha c_n\,|n\rangle = \sum_{n=0}^{+\infty}\left(c_{n+1}\sqrt{n+1} - \alpha c_n\right)|n\rangle = 0. \tag{B.8}$$

This equation is true if, for every n, we have $c_{n+1}\sqrt{n+1} - \alpha c_n = 0$. We have

$$c_{n+1} = \frac{\alpha c_n}{\sqrt{n+1}} = \frac{\alpha^2 c_{n-1}}{\sqrt{(n+1)(n)}} = \ldots = \frac{\alpha^{n+1}c_0}{\sqrt{(n+1)!}} \tag{B.9}$$

By choosing $c_0 = A$, and imposing $\langle\Psi|\Psi\rangle = 1$, we obtain $A = e^{-|\alpha|^2/2}$ (up to a global phase). Thus we proven that $|\Psi\rangle$ is the coherent state $|\alpha\rangle$, since

$$|\Psi\rangle = e^{-\frac{|\alpha|^2}{2}}\sum_{n=0}^{\infty}\frac{\alpha^n\,|n\rangle}{\sqrt{n!}} = |\alpha\rangle\,. \tag{B.10}$$

Therefore, equation (B.7) can be considered as an alternative definition of a coherent state, since it uniquely identifies the state $|\alpha\rangle$.

Action of the creation operator on the coherent states: The creation operator do not admit any (right) eigenstate, since $\hat{a}^\dagger\,|\Psi\rangle = \alpha^*\,|\Psi\rangle$ would imply

$$\hat{a}^\dagger\,|\Psi\rangle - \alpha^*\,|\Psi\rangle = \sum_{n=0}^{\infty} c_n\sqrt{n+1}\,|n+1\rangle - \alpha^* c_n\,|n\rangle = c_0 + \sum_{n=1}^{+\infty}\left(c_{n-1}\sqrt{n-1} - \alpha^* c_n\right)|n\rangle = 0. \tag{B.11}$$

The only solution to this equation is $c_n = 0$ for every n. However, it is possible to obtain a compact relation for the effect of $\hat{a}^\dagger$ on $|\alpha\rangle$:

$$\begin{aligned}\hat{a}^\dagger\,|\alpha\rangle &= e^{-\frac{|\alpha|^2}{2}}\sum_n\frac{\alpha^n}{\sqrt{n!}}\sqrt{n+1}\,|n+1\rangle = e^{-\frac{|\alpha|^2}{2}}\sum_n\frac{\partial}{\partial\alpha}\frac{\alpha^{n+1}\,|n+1\rangle}{\sqrt{(n+1)!}}\\ &= e^{-\frac{|\alpha|^2}{2}}\frac{\partial}{\partial\alpha}e^{\frac{|\alpha|^2}{2}}e^{-\frac{|\alpha|^2}{2}}\sum_n\frac{\alpha^{n+1}\,|n+1\rangle}{\sqrt{(n+1)!}} = e^{-\frac{|\alpha|^2}{2}}\frac{\partial}{\partial\alpha}e^{\frac{|\alpha|^2}{2}}\,|\alpha\rangle = \left(\frac{\partial}{\partial\alpha} + \alpha^*\right)|\alpha\rangle\,.\end{aligned} \tag{B.12}$$

Composition of displacement: The composition of two displacement generates, up to a proportionality factor, a displacement operator:

$$\hat{D}(\beta)\hat{D}(\alpha) = e^{\beta\hat{a}^\dagger - \beta^*\hat{a}}e^{\alpha\hat{a}^\dagger - \alpha^*\hat{a}} = e^{(\alpha+\beta)\hat{a}^\dagger - (\beta^*+\alpha^*)\hat{a}}e^{(\alpha\beta^* - \alpha^*\beta)/2} = e^{(\alpha\beta^* - \alpha^*\beta)/2}\hat{D}(\alpha+\beta), \tag{B.13}$$

where we used the Baker-Campbell-Hausdorff formula [24]. Moreover, $\hat{D}^\dagger(\alpha) = \hat{D}(-\alpha)$.

Scalar product: Exploiting the definition of a coherent state in Eq. (B.2), one has

$$\langle\beta|\alpha\rangle = e^{-\frac{|\alpha|^2}{2}}e^{-\frac{|\beta|^2}{2}}\sum_{n,m=0}^{\infty}\frac{\alpha^n\beta^{*\,m}\,\langle m|n\rangle}{\sqrt{n!m!}} = \exp\left[-\frac{|\alpha|^2}{2} - \frac{|\beta|^2}{2} + \alpha\beta^*\right]. \tag{B.14}$$

It follows that two coherent states are never orthogonal one to each other, since

$$|\langle\beta|\alpha\rangle|^2 = \exp\left[-|\alpha-\beta|^2\right] \neq 0. \tag{B.15}$$

Indeed, $|\alpha\rangle$ and $|\beta\rangle$ are eigenstates of the annihilation operator (which is not self-adjoint), and therefore need not be orthogonal.

Overcompleteness: Coherent states form a overcomplete basis Hilbert space. In fact, one has

$$\begin{aligned}
\frac{1}{\pi}\iint \mathrm{d}^2\alpha\ |\alpha\rangle\langle\alpha| &= \sum_{n,m=0}^{\infty}\frac{|n\rangle\langle m|}{\pi\sqrt{n!m!}}\iint \mathrm{d}^2\alpha e^{-|\alpha|^2}\alpha^n\alpha^{*m} \\
&= \sum_{n,m=0}^{\infty}\frac{|n\rangle\langle m|}{\pi\sqrt{n!m!}}\int_0^{\infty} r\mathrm{d}r\int_0^{2\pi}\mathrm{d}\theta e^{-r^2}r^{n+m}e^{\mathrm{i}(n-m)\theta} \\
&= \sum_{n,m=0}^{\infty}\frac{|n\rangle\langle m|}{\pi\sqrt{n!m!}}2\pi\delta_{n,m}\int_0^{\infty}\mathrm{d}r e^{-r^2}r^{n+m+1} \\
&= \sum_{n=0}^{\infty}2\frac{|n\rangle\langle n|}{n!}\int_0^{\infty}\mathrm{d}r e^{-r^2}r^{2n+1} = \sum_{n=0}^{\infty}2\frac{|n\rangle\langle n|}{n!}\int_0^{\infty}\frac{\mathrm{d}t}{2}e^{-t}t^n \\
&= \sum_{n=0}^{\infty}\frac{|n\rangle\langle n|}{n!}\Gamma(n+1) = \sum_{n=0}^{\infty}|n\rangle\langle n|\,,
\end{aligned} \tag{B.16}$$

where $\mathrm{d}^2\alpha = \mathrm{d}\mathbb{I}\mathrm{m}\,[\alpha]\,\mathrm{d}\mathbb{R}\mathrm{e}\,[\alpha]$ is the integral over the complex plane, and $\Gamma(n+1) = \int_0^{\infty}\mathrm{d}t e^{-t}t^n$ is the integral representation of the Euler gamma function (such that $\Gamma(n+1) = n!$ for integer n). As a consequence of their nonorthogonality, any coherent state can be expanded in terms the others. Thus, the set of $|\alpha\rangle$ forms an overcomplete basis of the Hilbert space.

Trace over coherent states: The trace can be expressed as

$$\begin{aligned}
\mathrm{Tr}[\bullet] &= \sum_n\langle n|\bullet|n\rangle = \sum_n\iint\frac{\mathrm{d}^2\alpha\mathrm{d}^2\beta}{\pi^2}\langle n|\alpha\rangle\langle\alpha|\bullet|\beta\rangle\langle\beta|n\rangle \\
&= \iint\frac{\mathrm{d}^2\alpha\mathrm{d}^2\beta}{\pi^2}e^{-|\alpha|^2/2-|\beta|^2/2}\sum_n\frac{(\alpha\beta^*)^n}{n!}\langle\alpha|\bullet|\beta\rangle \\
&= \iint\frac{\mathrm{d}^2\alpha\mathrm{d}^2\beta}{\pi^2}e^{-|\alpha|^2/2-|\beta|^2/2+\alpha\beta^*}\langle\alpha|\bullet|\beta\rangle = \iint\frac{\mathrm{d}^2\alpha\mathrm{d}^2\beta}{\pi^2}\langle\alpha|\bullet|\beta\rangle\langle\beta|\alpha\rangle \\
&= \int\frac{\mathrm{d}^2\alpha}{\pi}\langle\alpha|\bullet|\alpha\rangle\,,
\end{aligned} \tag{B.17}$$

where we used $e^{-|\alpha|^2/2-|\beta|^2/2+\alpha\beta^*} = \langle\beta|\alpha\rangle$.

Bargman states and expansion of states and operators in the coherent basis: Let us introduce the Bargman states, defined as

$$|\,|\alpha\rangle = e^{\frac{|\alpha|^2}{2}}|\alpha\rangle = \sum_{n=0}^{\infty}\frac{\alpha^n}{\sqrt{n!}}. \tag{B.18}$$

The Bargman states are analytic functions of α. By using the relation derived in Eq. (B.16), any state can be expressed as

$$|\Psi\rangle = \frac{1}{\pi}\int\mathrm{d}^2\alpha\,|\alpha\rangle\langle\alpha|\Psi\rangle = \frac{1}{\pi}\int\mathrm{d}^2\alpha e^{-\frac{|\alpha|^2}{2}}\Psi(\alpha^*)\,|\alpha\rangle\,, \tag{B.19}$$

where $\Psi(\alpha^*) = \langle\Psi||\alpha\rangle$ ensures that $\Psi(\alpha^*)$ is an analytic function of α^*. We conclude that expansion (B.19) is unique.

Similarly, any operator $\hat{\xi}$ can be recast as

$$\hat{\xi} = \frac{1}{\pi^2}\int \mathrm{d}^2\alpha \int \mathrm{d}^2\beta \,|\alpha\rangle\langle\alpha|\chi|\beta\rangle\langle\beta| = \frac{1}{\pi^2}\int \mathrm{d}^2\alpha e^{-\frac{|\alpha|^2}{2}} \int \mathrm{d}^2\beta e^{-\frac{|\beta|^2}{2}} \chi(\alpha^*,\beta)\,|\alpha\rangle\langle\beta|\,, \tag{B.20}$$

where $\chi(\alpha^*,\beta) = \langle\alpha||\,\hat{\xi}\,||\beta\rangle$ is an analytic function of α^* and β.[1]

Normal product: A normal product of creation and annihilation operators is defines as an expression in which all the destruction operators are on the left of the creation operators. Such an ordering is often identified with the symbol $::$. For example $:(\hat{a}+\hat{a}^\dagger)^3: = \hat{a}^{\dagger\,3} + 3\hat{a}^{\dagger\,2}\hat{a} + 3\hat{a}^\dagger\hat{a}^2 + \hat{a}^3$. For normal ordered operators, we have

$$\langle\alpha| :(\hat{a}+\hat{a}^\dagger)^n: |\beta\rangle = (\beta+\alpha^*)^n. \tag{B.21}$$

B.2 Coherent states and the classical limit

Here we prove that $|\alpha\rangle$ is a semiclassical state state for the harmonic oscillator in Eq. (1.6), that is, at every time t, $\langle\hat{x}(t)\rangle$, $\langle\hat{p}(t)\rangle$ and $\langle\hat{H}(t)\rangle$ are the same as their classical harmonic oscillator counterparts [cf. Eqs. (1.5)]. Consider a system prepared initially in a coherent state $|\alpha, t=0\rangle = |\alpha_0\rangle$. The question is what is the form of the state $|\alpha,t\rangle = e^{-\mathrm{i}\hat{H}t}|\alpha_0\rangle$. To answer this question, let us consider the effect of the annihilation operator $\hat{a}$ on $|\alpha,t\rangle$, i.e.

$$\hat{a}\,|\alpha,t\rangle = \hat{a}e^{-\mathrm{i}\hat{H}t}|\alpha_0\rangle = e^{-\mathrm{i}\hat{H}t}e^{\mathrm{i}\hat{H}t}\hat{a}e^{-\mathrm{i}\hat{H}t}|\alpha_0\rangle\,. \tag{B.22}$$

Thus, one need to solve $e^{\mathrm{i}\hat{H}t}\hat{a}e^{-\mathrm{i}\hat{H}t}$, which is

$$\begin{aligned} e^{\mathrm{i}\hat{H}t}\hat{a}e^{-\mathrm{i}\hat{H}t} &= \sum_{j=0}^{\infty} e^{\mathrm{i}\omega\hat{n}t}\hat{a}e^{-\mathrm{i}\omega\hat{n}t}|j\rangle\langle j| = \sum_{j=0}^{\infty} e^{\mathrm{i}\omega\hat{n}t}\sqrt{j}e^{-\mathrm{i}\omega jt}|j-1\rangle\langle j| \\ &= \sum_{j=0}^{\infty}\sqrt{j}e^{-\mathrm{i}\omega t}|j-1\rangle\langle j| = e^{-\mathrm{i}\omega t}\sum_{j=0}^{\infty}\hat{a}\,|j\rangle\langle j| = \hat{a}e^{-\mathrm{i}\omega t}. \end{aligned} \tag{B.23}$$

Hence, we have

$$\hat{a}\,|\alpha,t\rangle = e^{-\mathrm{i}\hat{H}t}\hat{a}e^{-\mathrm{i}\omega t}|\alpha\rangle = \alpha e^{-\mathrm{i}\omega t}e^{-\mathrm{i}\hat{H}t}|\alpha\rangle = \alpha e^{-\mathrm{i}\omega t}|\alpha,t\rangle\,. \tag{B.24}$$

As proved in Eq. (B.7), Eq. (B.24) completely defines the coherent state. We conclude that

$$|\alpha,t\rangle = |\alpha e^{-\mathrm{i}\omega t}\rangle\,. \tag{B.25}$$

1. We notice that, equivalently, we may have written

$$|\Psi\rangle = \frac{1}{\pi}\iint \mathrm{d}^2\,\alpha e^{-|\alpha|^2}\Psi(\alpha^*)\,||\alpha\rangle\,,$$

and

$$\hat{\xi} = \frac{1}{\pi^2}\iint \mathrm{d}^2\alpha \iint \mathrm{d}^2\beta\, e^{-|\alpha|^2}e^{-|\beta|^2}\chi(\alpha^*,\beta)\,||\alpha\rangle\langle\beta||\,.$$

It follows, thanks to Eq. (1.9), that

$$\begin{cases} \langle \hat{p}(t) \rangle = -\dfrac{\mathrm{i}\sqrt{m\omega}}{\sqrt{2}} \left(\alpha_0 e^{-\mathrm{i}\omega t} - \alpha_0^* e^{\mathrm{i}\omega t} \right), \\ \langle \hat{x}(t) \rangle = \dfrac{1}{\sqrt{2\, m\omega}} \left(\alpha_0 e^{-\mathrm{i}\omega t} + \alpha_0^* e^{\mathrm{i}\omega t} \right), \end{cases} \tag{B.26}$$

which have exactly the same form as Eq. (1.5). Moreover,

$$\langle \hat{H} \rangle = \langle \alpha | \omega (\hat{n} + \frac{1}{2}) \rangle = \omega |\alpha|^2 + \frac{\omega}{2}. \tag{B.27}$$

Thus, in the limit $|\alpha|^2 = \langle \hat{n} \rangle \to \infty$, also the expectation value of the Hamiltonian correspond to the classical energy of an harmonic oscillator. We conclude that the coherent state $|\alpha\rangle$ is, indeed, the wanted state which, for a hight number of quanta, recovers the classical predictions.

APPENDIX C

The Fourier-Weil Relation

The Fourier-Weil relation allows to write any operator as a composition of displacement operators. Indeed, it constitutes the super-operatorial equivalent of the completeness relation for the coherent states derived in Eqs. (B.16) and (B.19). We start by the following:

Lemma C.1. *The displacement operators are traceless, i.e.,*

$$\mathrm{Tr}\Big[\hat{D}(\alpha)\Big] = \pi\delta^2(\alpha). \tag{C.1}$$

Proof. Exploiting the definition of trace given in terms of coherent operators (c.f. Eq. (B.17)) and Eq. (B.1):

$$\begin{aligned}\mathrm{Tr}\Big[\hat{D}(\alpha)\Big] &= \int \frac{\mathrm{d}^2\gamma}{\pi} e^{-|\alpha|^2/2} \langle\gamma| e^{\alpha\hat{a}^\dagger} e^{-\alpha^*\hat{a}} |\gamma\rangle = \int \frac{\mathrm{d}^2\gamma}{\pi} e^{-|\alpha|^2/2} e^{\alpha\gamma^*} e^{-\alpha^*\gamma} \\ &= \frac{e^{-|\alpha^2|/2}}{\pi} \int \mathrm{d}\mathbb{R}\mathrm{e}\,[\gamma]\, e^{\mathbb{R}\mathrm{e}[\gamma](\alpha-\alpha^*)} \int \mathrm{d}\mathbb{I}\mathrm{m}\,[\gamma]\, e^{-\mathrm{i}\mathbb{I}\mathrm{m}[\gamma](\alpha+\alpha^*)} \\ &= \frac{e^{-|\alpha^2|/2}}{\pi} \int \mathrm{d}\mathbb{R}\mathrm{e}\,[\gamma]\, e^{-2\mathrm{i}\mathbb{R}\mathrm{e}[\gamma]\mathbb{I}\mathrm{m}[\alpha]} \int \mathrm{d}\mathbb{I}\mathrm{m}\,[\gamma]\, e^{-2\mathrm{i}\mathbb{I}\mathrm{m}[\gamma]\mathbb{R}\mathrm{e}[\alpha]} = \pi\delta^2(\alpha),\end{aligned} \tag{C.2}$$

where with the notation $\delta^2(\alpha)$ we mean that both the real and imaginary part of α must be zero.

■

Corollary C.2. *The displacement operators are orthogonal for the Hilbert-Schmidt inner product, i.e.,*

$$\langle\hat{D}(\alpha)|\hat{D}(\beta)\rangle = \mathrm{Tr}\Big[\hat{D}^\dagger(\alpha)\hat{D}(\beta)\Big] = \pi\delta^2(\beta-\alpha). \tag{C.3}$$

Proof. One has

$$\mathrm{Tr}\Big[\hat{D}^\dagger(\alpha)\hat{D}(\beta)\Big] \propto \mathrm{Tr}\Big[\hat{D}(\beta-\alpha)\Big] = \pi\delta^2(\beta-\alpha), \tag{C.4}$$

where we used the result of the Lemma C.1.

■

Theorem C.3 (Fourier-Weyl relation)**.** *Any operator $\hat{\xi}$ can be written as*

$$\hat{\xi} = \frac{1}{\pi}\int \mathrm{d}^2\alpha \mathrm{Tr}\left[\hat{D}^\dagger(\alpha)\hat{\xi}\right]\hat{D}(\alpha). \tag{C.5}$$

Equivalently, in super-operatorial notation

$$\mathcal{I} = \frac{1}{\pi}\int \mathrm{d}^2\alpha \left|\hat{D}(\alpha)\right\rangle\!\left\langle\hat{D}(\alpha)\right| = \frac{1}{\pi}\int \mathrm{d}^2\alpha \mathrm{Tr}\left[\hat{D}^\dagger(\alpha)\bullet\right]\hat{D}(\alpha). \tag{C.6}$$

Proof. If Fourier-Weyl relation (C.5) is true, than it is also for the case $|\alpha\rangle\langle\beta|$, which would read:

$$|\alpha\rangle\langle\beta| \stackrel{?}{=} \frac{1}{\pi}\int \mathrm{d}\gamma^2 \mathrm{Tr}\left[\hat{D}^\dagger(\gamma)|\alpha\rangle\langle\beta|\right]\hat{D}(\gamma). \tag{C.7}$$

In the following, we will use the notation $\stackrel{?}{=}$ to indicate the passages which need to be proved. Exploiting the previous equation, then Eq. (B.20) becomes:

$$\begin{aligned}\hat{\xi} &= \frac{1}{\pi^2}\iint \mathrm{d}^2\alpha\mathrm{d}^2\beta\,\langle\alpha|\chi|\beta\rangle\,|\alpha\rangle\langle\beta| \stackrel{?}{=} \int\frac{\mathrm{d}\gamma^2}{\pi}\iint\frac{\mathrm{d}^2\alpha\mathrm{d}^2\beta}{\pi^2}\langle\alpha|\chi|\beta\rangle\,\mathrm{Tr}\left[\hat{D}^\dagger(\gamma)|\alpha\rangle\langle\beta|\right]\hat{D}(\gamma)\\ &= \int\frac{\mathrm{d}\gamma^2}{\pi}\mathrm{Tr}\left[\hat{D}^\dagger(\gamma)\iint\frac{\mathrm{d}^2\alpha\mathrm{d}^2\beta}{\pi^2}\langle\alpha|\chi|\beta\rangle\,|\alpha\rangle\langle\beta|\right]\hat{D}(\gamma) = \int\frac{\mathrm{d}\gamma^2}{\pi}\mathrm{Tr}\left[\hat{D}^\dagger(\gamma)\hat{\xi}\right]\hat{D}(\gamma).\end{aligned} \tag{C.8}$$

Consequently, the proof of the Fourier-Weil transform amounts to prove Eq. (C.7). We notice that, since $|\alpha\rangle\langle\beta| = \hat{D}(\alpha)|0\rangle\langle 0|\hat{D}^\dagger(\beta)$, Eq. (C.7) is equivalent to

$$\begin{aligned}|0\rangle\langle 0| &\stackrel{?}{=} \int\frac{\mathrm{d}\gamma^2}{\pi}\mathrm{Tr}\left[\hat{D}^\dagger(\gamma)|\alpha\rangle\langle\beta|\right]\hat{D}^\dagger(\alpha)\hat{D}(\gamma)\hat{D}(\beta)\\ &= \int\frac{\mathrm{d}\gamma^2}{\pi}\mathrm{Tr}\left[\hat{D}^\dagger(\gamma)\hat{D}(\alpha)|0\rangle\langle\beta|\right]\hat{D}^\dagger(\alpha)\hat{D}(\gamma)\hat{D}(\beta)\\ &= \int\frac{\mathrm{d}\gamma^2}{\pi}\mathrm{Tr}\left[e^{(\alpha^*\gamma-\alpha\gamma^*)/2}\hat{D}(\alpha-\gamma)|0\rangle\langle\beta|\right]\hat{D}^\dagger(\alpha)\hat{D}(\gamma)\hat{D}(\beta)\\ &= \int\frac{\mathrm{d}\gamma^2}{\pi}e^{(\alpha^*\gamma-\alpha\gamma^*)/2}\langle\beta|\alpha-\gamma\rangle\,e^{(\alpha\gamma^*-\alpha^*\gamma)/2}e^{[-(\alpha-\gamma)\beta^*+(\alpha^*-\gamma^*)\beta]/2}\hat{D}(\gamma+\beta-\alpha)\\ &= \int\frac{\mathrm{d}\gamma^2}{\pi}e^{-|\alpha-\beta-\gamma|^2/2}\hat{D}(\gamma+\beta-\alpha) = \int\frac{\mathrm{d}\gamma^2}{\pi}e^{-|\gamma|^2/2}\hat{D}(\gamma),\end{aligned} \tag{C.9}$$

where we used Eq. (B.13) to compose displacement operators, and $\hat{D}^\dagger(\alpha) = \hat{D}(-\alpha)$. Hence, the demonstration is

$$|0\rangle\langle 0| \stackrel{?}{=} \int\frac{\mathrm{d}\gamma^2}{\pi}e^{-|\alpha-\beta-\gamma|^2/2}\hat{D}(\gamma+\beta-\alpha) = \int\frac{\mathrm{d}\gamma^2}{\pi}e^{-|\gamma|^2/2}\hat{D}(\gamma). \tag{C.10}$$

By defining

$$\int\frac{\mathrm{d}\gamma^2}{\pi}e^{-|\gamma|^2/2}\hat{D}(\gamma) = \hat{I}, \tag{C.11}$$

we notice that,

$$\begin{aligned}\|\hat{I}\|^2 = \left\|\int\frac{\mathrm{d}\gamma^2}{\pi}e^{-|\gamma|^2/2}\hat{D}(\gamma)\right\|^2 &= \mathrm{Tr}\left[\iint\frac{\mathrm{d}\gamma^2\mathrm{d}\eta^2}{\pi^2}e^{-|\gamma|^2/2-|\eta|^2/2}\hat{D}^\dagger(\gamma)\hat{D}(\eta)\right]\\ &= \iint\frac{\mathrm{d}\gamma^2\mathrm{d}\eta^2}{\pi^2}e^{-|\gamma|^2/2-|\eta|^2/2}\mathrm{Tr}\left[\hat{D}^\dagger(\gamma)\hat{D}(\eta)\right] = 1,\end{aligned} \tag{C.12}$$

where we used the Corollary C.2, ensuring that $\mathrm{Tr}\left[\hat{D}^{\dagger}(\gamma)\hat{D}(\eta)\right] = \pi\delta^2(\eta+\gamma)$. Moreover,

$$\mathrm{Tr}\left[\hat{I}\left|0\right\rangle\left\langle 0\right|\right] = \langle 0|\int \frac{\mathrm{d}\gamma^2}{\pi} e^{-|\gamma|^2/2}\hat{D}(\gamma)|0\rangle = \int \frac{\mathrm{d}\gamma^2}{\pi} e^{-|\gamma|^2} = 1. \tag{C.13}$$

Therefore we conclude that $\hat{I} = \left|0\right\rangle\left\langle 0\right|$, ending the proof.

■

Remark: Even if the coherent states constitute an overcomplete basis of the Hilbert space, the displacement operators are a complete basis of $H \otimes H$. Moreover, given the explicit invariance of $\alpha \to -\alpha$ of Eq. (C.5), it can be rewritten as

$$\hat{\xi} = \frac{1}{\pi}\int \mathrm{d}^2\alpha \mathrm{Tr}\left[\hat{D}(\alpha)\hat{\xi}\right]\hat{D}^{\dagger}(\alpha). \tag{C.14}$$

APPENDIX D

An Example of Jordan Form of the Liouvillian

Let us consider a spin-1/2 subjected to the action of two competing decay channels, described in [203]. Its master equation is

$$\partial_t \rho(t) = \mathcal{L}\rho(t) = -\mathrm{i}[\hat{H}, \rho(t)] + \frac{\epsilon}{2}\mathcal{D}[\hat{\sigma}^-]\rho(t) + \frac{\gamma}{2}\mathcal{D}[\hat{\sigma}^x]\rho(t), \tag{D.1}$$

where $\hat{H} = \frac{\omega}{2}\sigma^z$. The steady state is

$$\hat{\rho}_{ss} = \frac{1}{2\gamma+\epsilon}\begin{pmatrix}\gamma & 0\\ 0 & \gamma+\epsilon\end{pmatrix}, \tag{D.2}$$

and the magnetizations are

$$\mathrm{Tr}[\hat{\sigma}^x\hat{\rho}_{ss}] = \mathrm{Tr}[\hat{\sigma}^y\hat{\rho}_{ss}] = 0, \tag{D.3a}$$

$$\mathrm{Tr}[\hat{\sigma}^z\hat{\rho}_{ss}] = \frac{\epsilon}{2\gamma+\epsilon}. \tag{D.3b}$$

This simple model it's particularly interesting since, according to the values of the coupling ω, can display different kind of relaxations toward the steady-state. The eigenvalues of $\mathcal{L}$ are

$$\begin{cases}\lambda_0 = 0,\\ \lambda_1 = -\gamma - \dfrac{\epsilon}{2} + \sqrt{\gamma^2-\omega^2},\\ \lambda_2 = -\gamma - \dfrac{\epsilon}{2} - \sqrt{\gamma^2-\omega^2},\\ \lambda_3 = -2\gamma - \epsilon.\end{cases} \tag{D.4}$$

which are associated to the following (unnormalized) *eigenmatrices*

$$\begin{aligned}\hat{\rho}_0 \propto \rho^{SS} &= \frac{1}{2\gamma+\epsilon}\begin{pmatrix}\gamma & 0\\ 0 & \gamma+\epsilon\end{pmatrix}, & \hat{\rho}_1 &\propto \begin{pmatrix}0 & \frac{\sqrt{\gamma^2-\omega^2}-i\omega}{\gamma}\\ 1 & 0\end{pmatrix},\\ \hat{\rho}_2 &\propto \begin{pmatrix}0 & -\frac{i\omega+\sqrt{\gamma^2-\omega^2}}{\gamma}\\ 1 & 0\end{pmatrix}, & \hat{\rho}_3 &= \begin{pmatrix}-1 & 0\\ 0 & 1\end{pmatrix}.\end{aligned} \tag{D.5}$$

The eigenmatrices $\hat{\rho}_{1,2}$ describe the decay of the $\hat{\sigma}^{x,y}$ components with rate $\lambda_{1,/,2}$, while $\hat{\rho}_3$ is associated to $\hat{\sigma}^z$ and λ_3.

According to the values of ω, we can distinguish among three different scenario:

— If $\omega < \gamma$ the the Liouvillian has 4 real distinct eigenvalues (it is diagonalizable). In this case, the decay at long times will be exponential. The asymptotic decay rate which is λ_1.

— If $\omega > \lambda$ the the Liouvillian has 4 distinct eigenvalues (it is diagonalizable), 2 of which are complex conjugate ($\lambda_1 = \lambda_2^*$). In this case, the decay at long times will be an exponential of magnitude $\mathrm{Re}[\lambda_1] = \mathrm{Re}[\lambda_2]$ multiplied by and oscillation of frequency $\mathrm{Im}[\lambda_1]$.

— If $\omega = \gamma$ we have $\lambda_1 = \lambda_2$ and $\hat{\rho}_1 = \hat{\rho}_2$: the Liouvillian is not diagonalizable but it can be written in a Jordan form.

The presence of a Jordan form has strong consequences on the long-time dynamics. Indeed, given a general initial state

$$\rho(0) = \begin{pmatrix} a & b \\ b^* & 1-a \end{pmatrix}. \tag{D.6}$$

the decay of the observables $\hat{\sigma}^{x,y}$ is given by

$$\mathrm{Tr}[\hat{\sigma}^x \rho(t)] = 2e^{-\lambda_1 t}(t\omega(\mathrm{Re}[b] + \mathrm{Im}[b]) + \mathrm{Re}[b]), \tag{D.7}$$

$$\tag{D.8}$$

$$\mathrm{Tr}[\hat{\sigma}^y \rho(t)] = 2e^{-\lambda_1 t}(t\omega(\mathrm{Re}[b] + \mathrm{Im}[b]) - \mathrm{Re}[b]), \tag{D.9}$$

hence not exponential. However, we stress that the asymptotic decay rate is anyhow λ_3 for $\hat{\sigma}^z$ (purely exponential decay).

APPENDIX E

Numerical and Analytical Techniques

In this Appendix, we provide some details about the numerical and analytical techniques which has been used in the main text.

E.1 Numerical integration of the master equation

The most natural way to tackle the solution of the Linbald Master Equation (2.24) is to introduce a so-called cutoff, i.e., consider a finite number of vectors in the Hilbert space. The idea of the procedure is that, even if the Hilbert space is infinite-dimensional, one can obtain a very good approximation of $\hat{\rho}(t)$ by studying the dynamics in a smaller space.

Consider, for simplicity, a system whose density matrix at time t is $\hat{\rho}(t) = \sum_{n,m} c_{n,m} |n\rangle \langle m|$, where $|n\rangle$ are the Fock basis vectors. Similartly, any operator is $\hat{A} = \sum_{n,m} a_{n,m} |n\rangle \langle m|$. A cutoff N is a number such that, for any operator, we define $\hat{A}_N = \sum_{n,m<N} a_{n,m} |n\rangle \langle m|$ and $\delta\hat{A} = \hat{A} - \hat{A}_N$. Choosing a cutoff N means that we impose $\delta\hat{A} = 0$ for any operator, so that $\hat{\rho}_N(t)$ obeys

$$\partial_t \hat{\rho}_N(t) = -\mathrm{i}\left[\hat{H}_N, \hat{\rho}_N(t)\right] + \hat{\Gamma}_N \hat{\rho}_N(t) \hat{\Gamma}_N^\dagger - \frac{1}{2}\hat{\Gamma}_N^\dagger \hat{\Gamma}_N \hat{\rho}_N(t) - \frac{1}{2}\hat{\rho}_N(t)\hat{\Gamma}_N^\dagger \hat{\Gamma}_N. \tag{E.1}$$

Having a finite-dimensional matrix differential equation, one can resort to standard numerical techniques to integrate it. By increasing the number N, one can verify that the quality of the approximation.

E.2 Gross-Pitaevskii mean-field approximation

A very powerful and versatile tool to study an open quantum system it the Gross-Pitaevskii (GPE) mean-field approximation. By exploiting a pure coherent-state ansatz, it allows to transform the master equation into a (set of) polynomial differential equation(s) for a (set of) complex number(s) α. For a single oscillator, one postulates $\hat{\rho}(t) = |\alpha(t)\rangle \langle \alpha(t)|$. Then, one considers

$$\begin{aligned}
\partial_t \alpha(t) &= \partial_t \langle \hat{a}(t) \rangle = \partial_t \mathrm{Tr}[\hat{a} |\alpha(t)\rangle \langle \alpha(t)|] = \partial_t \mathrm{Tr}[\hat{a}\hat{\rho}(t)] = \mathrm{Tr}[\hat{a}\partial_t \hat{\rho}(t)] \\
&= -\mathrm{i}\mathrm{Tr}\Big[\hat{\rho}(t)\left[\hat{a}, \hat{H}\right]\Big] + \mathrm{Tr}\Big[\hat{\rho}(t)\left(\hat{\Gamma}\hat{a}\hat{\Gamma}^\dagger - \frac{1}{2}\hat{\Gamma}^\dagger\hat{\Gamma}\hat{a} - \frac{1}{2}\hat{a}\hat{\Gamma}^\dagger\hat{\Gamma}\right)\Big] \\
&= -\mathrm{i}\langle \alpha(t)| \left[\hat{a}, \hat{H}\right] |\alpha(t)\rangle + \langle \alpha(t)|\hat{\Gamma}\hat{a}\hat{\Gamma}^\dagger - \frac{1}{2}\hat{\Gamma}^\dagger\hat{\Gamma}\hat{a} - \frac{1}{2}\hat{a}\hat{\Gamma}^\dagger\hat{\Gamma}|\alpha(t)\rangle\,.
\end{aligned} \tag{E.2}$$

Since any operator can be expressed as a combination of $\hat{a}$ and $\hat{a}^\dagger$, the previous expression is a polynomial function of α^* and α, which can be numerically integrated. Once $\alpha(t)$ has been obtained, the GPE allows to retrieve any correlation function, since $\langle \hat{a}^{\dagger\, m} \hat{a}^n \rangle (t) = \alpha^{*\, m}(t) \alpha^n(t)$.

The previous procedure can be generalised to extended systems, either by supposing a uniform state $\alpha(t)$ in each site, or by considering a site depend approach, in which each site is characterised by a different $\alpha_i(t)$.

E.3 Numerical diagonalisation of the Liouvillian superoperator

As shown in Sec. 2.1.1, the Liouvillian $\mathcal{L}$ is a linear superoperator, since $\mathcal{L}\left(\alpha\hat{\xi} + \beta\hat{\chi}\right) = \alpha\mathcal{L}\hat{\xi} + \beta\mathcal{L}\hat{\chi}$ for any complex number α, β and any operator $\hat{\xi}$, $\hat{\chi}$. Thus, it can be written as a matrix $\bar{\bar{\mathcal{L}}}$.

The most naive way to write the Liouvillian matrix is to compute its matrix elements. This procedure is straightforward, but it requires to explicitly write down an orthonormal basis for the density matrices and project the Liouvillian onto it. For example, using the number basis $|n\rangle$, one constructs all the basis elements $H \otimes H$, which are of the form $\hat{\xi}_{(m,n)} = |m\rangle \langle n|$. We stress that $\hat{\xi}_{(m,n)}$ constitutes an orthonormal basis of $H \otimes H$, since any operator can be written as $\hat{\chi} = \sum_{n,m} c_{n,m} \hat{\xi}_{(m,n)}$ and $\mathrm{Tr}\left[\hat{\xi}^\dagger_{(m,n)} \hat{\xi}_{(m',n')}\right] = \langle m|m'\rangle \langle n'|n\rangle = \delta_{n,n'}\delta_{m,m'}$. The matrix element of the Liouvillian are

$$\mathcal{L}_{(m,n),(p,q)} = \mathrm{Tr}\left[\hat{\xi}^\dagger_{(m,n)}\, \mathcal{L}\, \hat{\xi}_{(p,q)}\right] = \mathrm{Tr}\left[\hat{\xi}^\dagger_{(m,n)} \left(-\mathrm{i}\left[\hat{H}, \hat{\xi}_{(p,q)}\right] + \sum_\mu \mathcal{D}[\hat{\Gamma}_\mu]\hat{\xi}_{(p,q)}\right)\right]. \tag{E.3}$$

From a numerical point of view, the previously described procedure is very slow. Indeed, for a cutoff N, it requires, in principle, to compute N^4 times Eq. (E.3). A more efficient procedure passes through vectorisation of the operators, i.e. the linear transformation which converts a matrix into a column vector. Let us consider a generic operator $\hat{\xi}$. The vectorisation of this matrix is:

$$\hat{\xi} = \sum_{m,n} c_{m,n} |m\rangle \langle n| \longrightarrow \vec{\xi} = \sum_{m,n} c_{m,n} |m\rangle \otimes \langle n|^{\mathrm{TR}} = \sum_{m,n} c_{m,n} |m\rangle \otimes |n^*\rangle\,, \tag{E.4}$$

where the complex conjugate is a consequence of $|n\rangle = \langle n|^\dagger = \left(\langle n|^{\mathrm{TR}}\right)^*$. In order to convert the Lindblad superoperator into its matrix form, we have to transform the right action superoperator $R[\hat{O}]\bullet = \bullet\hat{O}$ and the left one $L[\hat{O}]\bullet = \hat{O}\bullet$ into their vectorised form $\bar{\bar{R}}[\hat{O}]$ and $\bar{\bar{L}}[\hat{O}]$. Let us start by the right action:

$$\begin{aligned} \bar{\bar{R}}[\hat{O}]\vec{\xi} = \bar{\bar{R}}[\hat{O}] \sum_{m,n} c_{m,n} |m\rangle \otimes |n^*\rangle = \overrightarrow{\xi\hat{O}} = \sum_{m,n} c_{m,n}\ |m\rangle \otimes (\langle n|\, \hat{O})^{\mathrm{TR}} \\ = \sum_{m,n} c_{m,n}\ |m\rangle \otimes (\hat{O}^{\mathrm{TR}}\, |n^*\rangle) = (\mathbb{1} \otimes \hat{O}^{\mathrm{TR}})\vec{\xi}. \end{aligned} \tag{E.5}$$

In the same way, we have:

$$\bar{\bar{L}}[\hat{O}]\vec{\xi} = (\hat{O} \otimes \mathbb{1})\vec{\xi}. \tag{E.6}$$

From the result of Eqs. (E.5) and (E.6), we can eventually write any Liouvillian $\mathcal{L} = -\mathrm{i}\left[\hat{H}, \bullet\right] + \gamma/2\, \mathcal{D}[\hat{\Gamma}]$ (for simplicity with only one jump operator $\hat{\Gamma}$) under the form

$$\begin{aligned}\bar{\bar{\mathcal{L}}} &= -\mathrm{i}\left(\bar{\bar{L}}(\hat{H}) - \bar{\bar{R}}(\hat{H})\right) + \left(2\bar{\bar{L}}(\hat{\Gamma})\bar{\bar{R}}(\hat{\Gamma}^\dagger) - \bar{\bar{L}}(\hat{\Gamma}^\dagger\hat{\Gamma}) - \bar{\bar{R}}(\hat{\Gamma}^\dagger\hat{\Gamma})\right) \\ &= -\mathrm{i}\left((\hat{H}\otimes\mathbb{1}) - (\mathbb{1}\otimes\hat{H}^{\mathrm{TR}})\right) + \frac{1}{2}\left(2\hat{\Gamma}\otimes\hat{\Gamma}^* - \hat{\Gamma}^\dagger\hat{\Gamma}\otimes\mathbb{1} - \mathbb{1}\otimes\hat{\Gamma}^{\mathrm{TR}}\hat{\Gamma}^*\right).\end{aligned} \tag{E.7}$$

E.4 Numerical resolution of the stochastic Schrödinger equation

Computing a solution to the Lindblad master equation is straightforwardly feasible for small Hilbert spaces, but it rapidly become intractable because of the N^2 scaling of the density matrix. In Sec. 2.2 we saw that it is possible to recover the results of the Lindblad master equation by considering the average ensemble over an infinite number of quantum trajectories. The advantage of such procedure is clear, since the wavefunction of an N-dimensional Hilbert space scales as N, while the density matrix has dimension N^2. Moreover, a quantum trajectory approach can exploit the parallel architecture of modern computers. The price to pay, however, is that the number of trajectories on which it is necessary to mediate to obtain good results may be extremely hight.

E.4.1 Counting trajectories (wave function Montecarlo)

The algorithm for counting trajectories (known as quantum wave function Monte Carlo [115]) follows quite directly from Eq. (2.57), and its naive implementation can be sketched as follows:

— Choose a time interval τ short on the time scale of the relaxation, but long compared to the reservoir correlation time, so to ensure that the probability of a jump $p_\mu(t) = \tau\,\langle\psi(t)|\hat{\Gamma}_\mu^\dagger\hat{\Gamma}_\mu|\psi(t)\rangle \ll 1$ for any μ and any t. Moreover, τ should be small enough to ensure a smooth integration of the deterministic part of the master equation.

— Initialize the state to the chosen $|\psi(t=0)\rangle$.

— For each time interval τ over the total evolution time, evolve the quantum state $|\psi(t)\rangle$ according to to the rules:

1. Compute $p_\mu = \tau\,\langle\psi(t)|\hat{\Gamma}_\mu^\dagger\hat{\Gamma}_\mu|\psi(t)\rangle$ for every $\mu = 1\ldots n$ and $p_0 = 1 - \sum_{\mu\neq 0} p_\mu$.
2. Construct the variables $P_{-1} = 0$, $P_0 = p_0$, $P_1 = p_0 + p_1$, …, $P_n = 1$.
3. Extract a random number $r \in [0,1]$.
4. Find the element of $\bar{\mu}$ such that $P_{\bar{\mu}-1} < r < P_{\bar{\mu}}$.
5. If $\bar{\mu} = 0$, evolve

$$|\psi(t+\tau)\rangle = \frac{1 - \mathrm{i}\hat{H}\tau - \tau\sum_\mu \hat{\Gamma}_\mu^\dagger\hat{\Gamma}_\mu/2}{\sqrt{p_0}}\,|\psi(t)\rangle\,. \tag{E.8}$$

6. Else,

$$|\psi(t+\tau)\rangle = \frac{\hat{\Gamma}_{\bar{\mu}}}{\sqrt{\langle\hat{\Gamma}_{\bar{\mu}}^\dagger\hat{\Gamma}_{\bar{\mu}}\rangle}}\,|\psi(t)\rangle\,. \tag{E.9}$$

— Create a new trajectory, and repeat until the wanted number of trajectories has been computed.

A far more efficient algorithm relies on sampling the jump time instead of checking weather at each time a jump occurs. This algorithm has the huge advantage of not introducing a characteristic time step τ. The procedure is:

— Initialize the state to its initial value.

— Evolve it until the total evolution time is reached according to the rule:

1. Take wavefunction at last simulation time t_0, i.e. $|\psi(t_0)\rangle$.
2. Extract a random number $r \in [0, 1]$.
3. Evolve the state $|\tilde{\psi}(t)\rangle$ according to

$$\frac{\mathrm{d}\,|\tilde{\psi}(t)\rangle}{\mathrm{d}t} = -\left(\mathrm{i}\hat{H} + \sum_{\mu} \frac{\hat{\Gamma}_{\mu}^{\dagger}\hat{\Gamma}_{\mu}}{2}\right)|\tilde{\psi}(t)\rangle\,, \tag{E.10}$$

until the time t_1 when $\langle\tilde{\psi}(t_1)|\tilde{\psi}(t_1)\rangle = r$. To do so, one can exploit standard adaptive-timestep algorithms. The time t_1 is the time in which the next detection occurs.

4. Compute the (unnormalised) probabilities $p_{\mu} = \tau\,\langle\tilde{\psi}(t_1)|\hat{\Gamma}_{\mu}^{\dagger}\hat{\Gamma}_{\mu}|\tilde{\psi}(t_1)\rangle$.
5. Construct the variables $P_0 = 0$, $P_1 = p_1$, $P_2 = p_1 + p_2$, $\ldots P_n = \sum_{\mu} p_{\mu}$.
6. Extract a random number $s \in [0, P_n]$.
7. Find $\bar{\mu}$ such that $P_{\bar{\mu}-1} < s < P_{\bar{\mu}}$.
8. The wave function at time t_1 is

$$|\psi(t_1)\rangle = \frac{\hat{\Gamma}_{\bar{\mu}}}{\sqrt{\langle\tilde{\psi}(t)|\hat{\Gamma}_{\bar{\mu}}^{\dagger}\hat{\Gamma}_{\bar{\mu}}|\tilde{\psi}(t)\rangle}}\,|\tilde{\psi}(t)\rangle\,. \tag{E.11}$$

— Create a new trajectory and repeat until the wanted number of trajectories is has been computed.

E.4.2 Homodyne trajectories

The homodyne trajectory algorithm amounts to an integration of a stochastic differential equation: Its steps are:

— Choose a time interval τ small enough to ensure a smooth integration of the deterministic part of the master equation and a small enough noise.

— Initialize the state to its initial value.

— For each time interval τ over the total evolution time, evolve the quantum state $|\psi(t)\rangle$ according to to the rules:

1. For each μ generate a standard normal random variable of mean zero and variance τ, corresponding to $\mathrm{d}W_{\mu}(t)$.
2. Compute $\mathrm{d}\,|\psi(t)\rangle$ as in Eq. (2.62).
3. The updated state is $|\psi(t+\tau)\rangle = |\psi(t)\rangle + \mathrm{d}\,|\psi(t)\rangle$.

— Create a new trajectory and repeat until the wanted number of trajectories is has been computed.

E.5 The complex P-Representation

In Sec. 2.3 we introduced the Glauber–Sudarshan P-representation. Although it is a very powerful instrument, such a function is often singular and can only be interpreted in a distributional sense. However, by exploiting different coherent-state base choices for the P-representation [143], it is possible to introduce the so-called complex P-representation.

E.5.1 Derivation of the complex P-representation

Consider the following generalised P-Representation

$$\hat{\rho} = \iint P(\alpha,\beta)\hat{\Lambda}(\alpha,\beta)\mathrm{d}\mu(\alpha,\beta), \tag{E.12}$$

where $\mathrm{d}\mu(\alpha,\beta)$ is the integration measure and $\hat{\Lambda}(\alpha,\beta)$ is the projector operator. In this formalism, the Glauber–Sudarshan P-representation is obtained by choosing $\mathrm{d}\mu(\alpha,\beta) = \delta^2(\alpha-\beta)\mathrm{d}^2\alpha\,\mathrm{d}^2\beta$, and consequently

$$\hat{\rho} = \int \mathrm{d}^2\alpha\, P(\alpha)\,|\alpha\rangle\langle\alpha|\,. \tag{E.13}$$

Consider now Eq. (B.20). Suppose it is possible to expand the density matrix on a bounded region of the parameter space D for α and D' for β. Using Cauchy theorem and considering two closed curves $\mathcal{C}$ and $\mathcal{C}'$, encircling D and D', respectively, we have

$$\begin{aligned}
\hat{\rho} &= \int_D d^2\alpha \int_{D'} d^2\beta\, e^{-|\alpha|^2-|\beta|^2}\,\hat{\rho}(\alpha,\beta)\,||\alpha\rangle\,\langle\beta^*||\\
&= -\int_D d^2\alpha \int_{D'} d^2\beta e^{-|\alpha|^2-|\beta|^2}\int_{\mathcal{C}}\int_{\mathcal{C}'}\frac{\mathrm{d}\alpha'\mathrm{d}\beta'}{4\pi^2}\,\frac{C(\alpha',\beta')}{(\alpha'-\alpha)(\beta'-\beta)}\,||\alpha'\rangle\,\langle\beta'||\\
&= \int_{\mathcal{C}}\int_{\mathcal{C}'}\mathrm{d}\alpha'\mathrm{d}\beta'\,||\alpha'\rangle\,\langle\beta'||\left[-\frac{C(\alpha',\beta')}{4\pi^2}\int_D d^2\alpha\int_{D'} d^2\beta\frac{e^{-|\alpha|^2-|\beta|^2}}{(\alpha'-\alpha)(\beta'-\beta)}\right]\\
&= \int_{\mathcal{C}}\int_{\mathcal{C}'}\mathrm{d}\alpha'\mathrm{d}\beta'\,\hat{\Lambda}(\alpha',\beta')P(\alpha',\beta'),
\end{aligned} \tag{E.14}$$

where we have introduced

$$\hat{\Lambda}(\alpha',\beta') = \frac{|\alpha'\rangle\langle\beta'^*|}{\langle\beta'^*|\alpha'\rangle} = \frac{|\alpha'\rangle\langle\beta'^*|}{e^{-\frac{|\alpha'|^2+|\beta'|^2}{2}+\alpha'\beta'}} = ||\alpha'\rangle\,\langle\beta'^*||\,e^{-\alpha'\beta'}, \tag{E.15}$$

and the complex P function

$$P(\alpha',\beta') = -\frac{C(\alpha',\beta')e^{-\alpha'\beta'}}{4\pi^2}\int_D d^2\alpha\int_{D'} d^2\beta\frac{e^{-|\alpha|^2-|\beta|^2}}{(\alpha'-\alpha)(\beta'-\beta)}. \tag{E.16}$$

Since $\mathrm{Tr}[\rho] = 1$, the complex P-representation can still be regarded as a complex-valued quasiprobability function. However, the semiclassical analogy which characterised the previously introduced phase-space representation cannot be extended to $P(\alpha,\beta)$, since the integral is not over all the complex plane, but only on a double closed curve in the complex plane encircling all the poles in the complex plane.

This complex-P representation is often the best candidate to find an exact solution for driven-dissipative problems [143]. Indeed, the complex P a more regular function than

Glauber–Sudarshan, all conserving the structure of Eq. (2.79), with the following "translation" rules:

$$\hat{a}\hat{\rho} \leftrightarrow \alpha\, P(\alpha,\beta), \tag{E.17a}$$
$$\hat{a}^\dagger\hat{\rho} \leftrightarrow (\beta - \partial_\alpha)\, P(\alpha,\beta), \tag{E.17b}$$
$$\hat{\rho}\hat{a} \leftrightarrow (\alpha - \partial_\beta)\, P(\alpha,\beta), \tag{E.17c}$$
$$\hat{\rho}\hat{a} \leftrightarrow \beta\, P(\alpha,\beta). \tag{E.17d}$$

E.5.2 Finding the steady-state solution for a Fokker-Plank like equation

The time evolution of the Wigner function or of the Husimi Q for interacting photons are described by third-order differential equations, as it stems from the conversion of $\hat{a}^{\dagger 2}\hat{a}^2$ according to Eqs.(2.79). On the contrary, the P-representation for interacting photons is a second-order partial differential equation. Thus, it satisfies a Fokker-Planck-like equation of the form:

$$\mathrm{i}\,\partial_t P = \sum_{i=\alpha,\beta} \partial_i \left[-A^i P + \frac{1}{2} \sum_{j=\alpha,\beta} \partial_j \left(D^{ij} P \right) \right], \tag{E.18}$$

where A^i indicates the components of the drift vector and D^{ij} is a matrix element of the diffusion tensor. If we are interested in $\hat{\rho}_{ss}$, we search a the steady-state solution of the Fokker-Planck equation (E.18), i.e., $\partial_t P_{\mathrm{ss}} = 0$. Solving the resulting differential equation is generally a hard task [114, 117], but one can simplify the problem by requiring that every term of the sum vanishes:

$$A^i P_{\mathrm{ss}} - \frac{1}{2} \sum_{j=\alpha,\beta} \partial_j \left(D^{ij} P_{\mathrm{ss}} \right) = 0, \qquad i = \alpha, \beta. \tag{E.19}$$

After some straightforward algebraic manipulation, Eq. (E.19) can be cast as

$$2A^i - \sum_{j=\alpha,\beta} \left(\partial_j\, D^{ij} \right) = \sum_{j=\alpha,\beta} D^{ij}\, \partial_j \ln(P_{\mathrm{ss}}), \quad i = \alpha, \beta, \tag{E.20}$$

which, if the matrix D is invertible, is solved by

$$\partial_j \ln(P_{\mathrm{ss}}) = \sum_{i=\alpha,\beta} \left(D^{-1} \right)^{ji} \left[2A^i - \sum_{k=\alpha,\beta} \left(\partial_k\, D^{ik} \right) \right], \tag{E.21}$$

for $j = \alpha, \beta$. Hence, we can write $P_{\mathrm{ss}} = \exp(-\phi)$ and treat ϕ as a scalar potential in the complex variables α and β. Such a potential defines a generalized force $\bar{\Phi} = -\bar{\nabla}\phi$ of components

$$\Phi_j = -\partial_j\, \phi = \sum_{i=\alpha,\beta} \left(D^{-1} \right)^{ji} \left[2A^i - \sum_{k=\alpha,\beta} \left(\partial_k\, D^{ik} \right) \right]. \tag{E.22}$$

Eq. (E.22) is valid only if ϕ is a a well-behaved scalar potential. Thus, one must require that the crossed derivatives of the force (E.22) are the same, that is

$$\partial_i \Phi_j = \partial_j \Phi_i. \tag{E.23}$$

The latter are known as the potential conditions. They also ensure that the integral of the coupled differential equations $\partial_j \phi = -\Phi_j$ $(j = \alpha, \beta)$ is independent of the integration path. Hence, it is possible to obtain ϕ as

$$\phi(\alpha, \beta) = \phi(\alpha_0, \beta_0) - \int_\Gamma \bar{\Phi}(\alpha', \beta') \cdot d\bar{s}(\alpha', \beta'), \tag{E.24}$$

where $d\bar{s}(\alpha', \beta')$ is an infinitesimal displacement element along the path Γ going from the arbitrary reference point $\{\alpha_0, \beta_0\}$ to $\{\alpha, \beta\}$. For example, one can use Eq. (E.24) for the path $\Gamma := \{0, 0\} \to \{\alpha, 0\} \to \{\alpha, \beta\}$, which formally gives

$$\phi(\alpha, \beta) = \phi(0, 0) - \int_{\{0,0\}}^{\{\alpha,0\}} \Phi_\alpha(\alpha', 0)\, \mathrm{d}\alpha' - \int_{\{\alpha,0\}}^{\{\alpha,\beta\}} \Phi_\beta(\alpha, \beta')\, d\beta'. \tag{E.25}$$

The knowledge of $P(\alpha, \beta)$ is, in theory, sufficient to fully determine the density matrix of the system. By integrating on a suitable contour, one can indeed recover all the matrix elements of $\hat{\rho}_{ss}$.

E.6 The corner-space renormalisation method

The main challenge encountered while simulating large quantum lattice systems is the complexity growing exponentially with their size. If we are, however, capable of finding a "relevant" subspace of the Hilbert space, we can extremely simplify the numerical complexity of the problem. The corner-space renormalisation method aims to find such a corner space [130].

Consider two lattices, A and B, for which the steady state density matrices $\hat{\rho}_A$ and $\hat{\rho}_B$ can be computed. We are interested in the physics resulting from the spatial merging of the lattices A and B. The ansatz of the method is that, using the most probable eigenvectors of the steady-state density matrices of smaller lattices, one can construct the good portion of the Hilbert space. To find the corner, first one diagonalises $\hat{\rho}_A$ and $\hat{\rho}_B$, obtaining

$$\begin{cases} \hat{\rho}_A = \sum_r p_r^{(A)} \left|\psi_r^{(A)}\right\rangle \left\langle\psi_r^{(A)}\right| \\ \hat{\rho}_B = \sum_r p_r^{(B)} \left|\psi_r^{(B)}\right\rangle \left\langle\psi_r^{(B)}\right| \end{cases} \tag{E.26}$$

A basis for the space $H_A \otimes H_B$ is then constituted by the tensor product $\left|\psi_i^{(A)}\right\rangle \left|\psi_j^{(B)}\right\rangle$. One order such product states as

$$\left\{ \left|\psi_{r_1}^{(A)}\right\rangle \left|\psi_{r'_1}^{(B)}\right\rangle, \left|\psi_{r_2}^{(A)}\right\rangle \left|\psi_{r'_2}^{(B)}\right\rangle, \ldots, \left|\psi_{r_N}^{(A)}\right\rangle \left|\psi_{r'_N}^{(B)}\right\rangle \right\}, \tag{E.27}$$

so that $p_{r_1}^{(A)} p_{r'_1}^{(B)} \geq p_{r_2}^{(A)} p_{r'_2}^{(B)} \geq \cdots \geq p_{r_N}^{(A)} p_{r'_N}^{(B)}$. One then imposes a "cutoff" by choosing the M states maximizing the joint probability. The accuracy of the method can be controlled by enlarging the dimension M of the corner space until convergence is reached.

More precisely, the algorithm can be decomposed into the following steps represented in Fig. E.1:

1. Determine the steady-state density matrix for two small lattices A and B.
2. Merge spatially two lattices.
3. Select the M states maximizing the joint probability.
4. Determine the steady-state solution in the corner-space.
5. Repeat until convergence in M is reached.

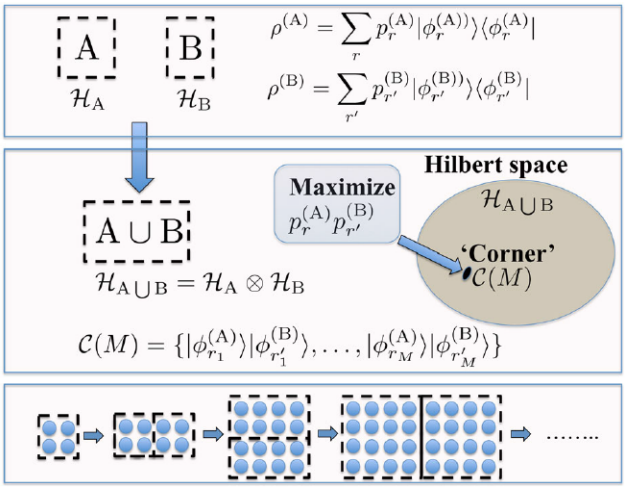

Figure E.1 – Sketch of the corner-space renormalization method, taken from Ref. [130].

APPENDIX F

Résumé substantiel

Cette thèse est une étude théorique de systèmes dissipatifs pompés, décrits par une équation maîtresse de Lindblad, focalisée sur l'émergence de phénomènes critiques. Cette équation décrit l'évolution d'une matrice densité $\hat{\rho}(t)$ sous l'action d'un super-opérateur $\mathcal{L}$, appelé le liouvillien. En particulier

$$\frac{\partial \hat{\rho}(t)}{\partial t} = -\mathrm{i}\left[\hat{H}, \hat{\rho}(t)\right] + \sum_{\mu} \mathcal{D}[\hat{\Gamma}_{\mu}] = \mathcal{L}\hat{\rho}(t), \tag{F.1}$$

o l'opérateur $\hat{H}$ est l'hamiltonien du système, et les super-opérateurs $\mathcal{D}[\hat{\Gamma}_{\mu}]$ représentent l'interaction avec l'environnent, modélisée par une série d'opérateurs de saut $\hat{\Gamma}_{\mu}$. Leur actionne est décrite mathématiquement par :

$$\mathcal{D}[\hat{\Gamma}_{\mu}]\hat{\rho}(t) = \hat{\Gamma}_{\mu}\hat{\rho}(t)\hat{\Gamma}_{\mu}^{\dagger} - \frac{1}{2}\hat{\Gamma}_{\mu}^{\dagger}\hat{\Gamma}_{\mu}\hat{\rho}(t) - \frac{1}{2}\hat{\rho}(t)\hat{\Gamma}_{\mu}^{\dagger}\hat{\Gamma}_{\mu}. \tag{F.2}$$

L'équation maîtresse de Lindblad peut être aussi transformée en une équation stochastique de Schrödinger, qui évolue de façon continue sous l'action d'une pseudo-hamiltonien et par des changements abruptes causée par les opérateurs de saut $\hat{\Gamma}_{\mu}$. Plusieurs plates-formes expérimentales obéissent cette équation, notamment les cavités optiques, les micropiliers semiconducteurs et les circuits supraconducteurs (voir la discussion dans le Chapitres 1 et 2).

Dans le Chapitre 3 nous présentons une théorie générale reliant l'émergence de transitions de phase du premier et deuxième ordres aux propriétés spectrales du superopérateur liouvillien. On considère un liouvillien $\mathcal{L}(\zeta)$ qui dépend d'un paramètre ζ. En introduisant les matrices propres de $\mathcal{L}(\zeta)$, $\hat{\rho}_i(\zeta)$, ainsi que les valeurs propres $\lambda_i(\zeta)$, on a :

$$\mathcal{L}(\zeta)\hat{\rho}_i(\zeta) = \lambda_i(\zeta)\hat{\rho}_i(\zeta). \tag{F.3}$$

Dans la région critique, nous déterminons la forme générale de l'état stationnaire $\hat{\rho}_0$ et de la matrice propre du liouvillien associée à son gap spectral $\hat{\rho}_1$. Pour les transitions de première ordre (voir Fig. 3.2, gauche), on appelle ρ^+ (ρ^-) l'état stationnaire avant (aprés) le point critique ζ_c. On trouve que à la transition $\lambda_0 = \lambda_1 = 0$ et que :

$$\hat{\rho}_1(\zeta \simeq \zeta_c) \propto \hat{\rho}^+ - \hat{\rho}^-, \tag{F.4}$$

et

$$\hat{\rho}_0(\zeta_c) \propto \hat{\rho}^+ + \hat{\rho}^-. \tag{F.5}$$

Pour les transitions d'ordre deux (voir Fig. 3.2, droite), on introduit un super-opérateur de symétrie $\mathcal{Z}_n = \hat{Z}_n \bullet \hat{Z}_n^\dagger$. Dans toute la phase où la symétrie est brisée on a $\lambda_0 = \lambda_1 = \cdots = \lambda_{n-1} = 0$ et :

$$\hat{\tilde{\rho}}_l = \mathcal{Z}_n^l \sum_{j=0}^{n-1} \frac{\hat{\rho}_j}{\mathrm{Tr}[\hat{\rho}_0]} = \sum_{j=0}^{n-1} \frac{z_j^l(i)\hat{\rho}_j}{\mathrm{Tr}[\hat{\rho}_0]}, \tag{F.6}$$

sont des matrices densité stationnaires tels que $\mathcal{Z}_n \hat{\tilde{\rho}}_i = \hat{\tilde{\rho}}_{\mathrm{mod}(i+1,n)}$. Nous discutons aussi l'utilisation de trajectoires quantiques individuelles afin de révéler l'apparition des transitions de phase. En particulier, le rôle du "unraveling" stochastique jeu un rôle primordial dans la caractérisation des états pour les transitions d'ordre deux.

Après ces résultats généraux, nous mettons en évidence l'émergence de criticaillé dans plusieurs modèles. Tout d'abord, dans le Chapitre 4 nous étudions le modèle de Kerr en présence de pompage à un photon (cohérent) et à deux photons (paramétrique) ainsi que de dissipation. Dans ce cas, l'équation de Linblad est (voir Fig. 4.1)

$$\mathcal{L}\hat{\rho}(t) = -\mathrm{i}\left[\hat{H}, \hat{\rho}(t)\right] + \frac{\gamma}{2}\mathcal{D}[\hat{a}]\hat{\rho}(t) + \frac{\eta}{2}\mathcal{D}[\hat{a}^2]\hat{\rho}(t), \tag{F.7}$$

où $\hat{a}$ et $\hat{a}^\dagger$ sont les opérateurs de création et annihilation d'un photon dans le système, et l'hamiltonien est

$$\hat{H} = -\Delta\hat{a}^\dagger\hat{a} + \frac{U}{2}\hat{a}^\dagger\hat{a}^\dagger\hat{a}\hat{a} + F\hat{a}^\dagger + F^*\hat{a} + \frac{G}{2}\hat{a}^\dagger\hat{a}^\dagger + \frac{G^*}{2}\hat{a}\hat{a}. \tag{F.8}$$

Δ est le detuning entre la fréquence propre de la cavité et les pompes, U représente l'interaction entre photons et F et G sont les intensités des pompage à un et deux photons. Nous présentons une solution analytique exacte pour l'état stationnaire de la matrice densité utilisant la représentation-P complexe, définie par

$$\hat{\rho} = \iint_{\mathcal{C},\mathcal{C}'} \mathrm{d}\alpha\, \mathrm{d}\beta\, P(\alpha,\beta)\hat{\Lambda}(\alpha,\beta), \tag{F.9}$$

où $\hat{\Lambda}(\alpha,\beta) = |\alpha\rangle\langle\beta^*| / \langle\beta^*|\alpha\rangle$ est le projecteur sur les états cohérents, $\mathcal{C}$ et $\mathcal{C}'$ sont des parcours fermés dans le plan complexe, qui encerclent les singularités de la fonctionne $P(\alpha,\beta)$. Grâce à la solution, nous pouvons atteindre la "limite thermodynamique" des hautes densités photoniques, dans laquelle des transitions de phase dissipatives ont lieu. On trouve que le résonateur pompé par un photon à la fois subit une transition de premier ordre (Figs. 4.8 et 4.9), et que celui échangeant deux photons à la fois peut avoir une transition du premier ordre au deux selon la valeur du detuning (Figs. 4.10 et 4.11).

Nous explorons les propriétés dynamiques d'une transition de phase du premier ordre dans un modèle de Bose-Hubbard dissipatif avec pompage cohérent (voir Fig. 5.1), décrivant des réseaux de résonateurs de Kerr couplés dans le Chapitre 5. L'équation maitresse pour un système de N cavités est :

$$\partial_t\hat{\rho}(t) = \mathcal{L}\hat{\rho}(t) = -\mathrm{i}\left[\hat{H}, \hat{\rho}(t)\right] + \gamma\sum_j \mathcal{D}[\hat{a}_j]\hat{\rho}(t), \tag{F.10}$$

et

$$\hat{H} = \sum_j -\Delta\hat{a}_j^\dagger\hat{a}_j + \frac{U}{2}\hat{a}_j^{\dagger 2}\hat{a}_j^2 + F\left(\hat{a}_j^\dagger + \hat{a}_j\right) - J\sum_{<j,j'>}\hat{a}_j^\dagger\hat{a}_{j'}, \tag{F.11}$$

ou les index j représente la jème cavité, et $< j, j' >$ sont premier voisins. Cette équation maitresse pour la matrice densité est équivalente à une équation différentielle pour la fonction de

Wigner du système. Dans la limite des interactions faibles ($U \ll \gamma$), on peut appliquer l'approximation dite truncated Wigner, pour associer à cette équation différentielle une équation stochastique de Langevin pour N nombres complexes (un pour chaque cavité)

$$\dot{\alpha_j} = \left[-\mathrm{i}(\Delta - U(|\alpha_j|^2 - 1) - \gamma/2)\right] \alpha_j - iJ \sum_{j'} \alpha_{j'} + iF + \sqrt{\gamma/2}\, \chi(t). \tag{F.12}$$

$\chi(t)$ c'est un bruit gaussien random et normalisé tel que $\langle \chi(t)\chi(t')\rangle = 0$ and $\langle \chi(t)\chi^*(t')\rangle = \delta(t-t')$. En prenant la moyenne sur plusieurs trajectoires on retrouve les espérances des opérateurs pour le système initial. Au moyen ce trajectoires stochastiques issues de l'approximation truncated Wigner, nous avons étudié la dynamique du système en fonction de sa taille et de sa dimensionalité dans un régime ou les théories de champ moyen prédisent un comportement bistable (Fig. 5.4). Nous montrons l'émergence d'un ralentissement critique en augmentant la taille des réseaux bidimensionnels et l'absence de criticalité dans le cas unidimensionnel (Figs. 5.5 et 5.6). Dans la région critique, les propriétés spécifiques des phases collectives ont été caractérisées (Fig. 5.7).

Dans le Chapitre 6, nous avons étudié les propriétés dynamiques d'un modèle XYZ dissipatif d'Heisenberg, où deux spin premier voisins $\langle i, j\rangle$ interagissent par un hamiltonien

$$\hat{H} = \sum_{\langle i,j\rangle} \left(J_x \hat{\sigma}_i^x \hat{\sigma}_j^x + J_y \hat{\sigma}_i^y \hat{\sigma}_i^y + J_z \hat{\sigma}_i^z \hat{\sigma}_j^z \right). \tag{F.13}$$

Ce couplage anisotrope entre spin adjacents est en compétition avec des processus incohérent d'inversion de spin, ce qui donne

$$\frac{\partial \hat{\rho}}{\partial t} = \mathcal{L}[\hat{\rho}] = -i\left[\hat{H}, \hat{\rho}\right] + \gamma \sum_j \mathcal{D}[\hat{\sigma_j}^-]. \tag{F.14}$$

Nous avons exploré une région de l'espace des paramètres où des théories de champ moyen et des simulations numériques prévoient une transition de phase magnétique du second ordre. Nous avons examiné le taux de relaxation asymptotique vers l'état stationnaire aussi bien dans une chaîne unidimensionnelle (jusqu'à la limite thermodynamique) que dans des réseaux bidimensionnels de taille finie, montrant l'absence de criticalité en géométrie unidimensionnelle et sa présence dans le cas bidimensionnel (Fig. 6.2). En utilisant des trajectoires quantiques, nous avons caractérisé la phase à symétrie brisée (Figs. 6.3, 6.4 et 6.5).

Enfin, dans le Chapitre 7 nous avons considéré la physique des cavités soumises à de la dissipation à un et deux photons ainsi qu'un pompage à deux photons, obtenu par ingénierie de réservoirs. En particulier, on s'est intéressé à l'émergence des états dit chats de Schrödinger définis par :

$$|\mathcal{C}_\alpha^\pm\rangle = \frac{|\alpha\rangle \pm |-\alpha\rangle}{\sqrt{2\left(1 \pm e^{-2|\alpha|^2}\right)}}, \tag{F.15}$$

ou $|\alpha\rangle$ et $|-\alpha\rangle$ sont dés états cohérents défini par

$$|\alpha\rangle = e^{-\frac{|\alpha|^2}{2}} \sum_{n=0}^{\infty} \frac{\alpha^n |n\rangle}{\sqrt{n!}}. \tag{F.16}$$

L'état $|\mathcal{C}_\alpha^+\rangle$ ($|\mathcal{C}_\alpha^-\rangle$) est dit chat pair (impair), vue qu'il est superposition d'états contentant un nombre pair (impair) de photons. Nous avons démontré que l'état stationnaire unique est un

mélange statistique de deux états chats de Schrödinger, malgré de fortes pertes à un photon, sous la forme :

$$\hat{\rho}_{ss} \simeq p^+ \, |\mathcal{C}_\alpha^+\rangle\langle\mathcal{C}_\alpha^+| + p^- \, |\mathcal{C}_\alpha^-\rangle\langle\mathcal{C}_\alpha^-| \, . \tag{F.17}$$

Pour un pompage intense (Fig. 7.1), on a $|\alpha| \gg 1$ et $p^+ \simeq p^- \simeq 1/2$. Par conséquence, on a aussi

$$\hat{\rho}_{ss} \simeq \frac{1}{2} \, |\alpha\rangle\langle\alpha| + \frac{1}{2} \, |-\alpha\rangle\langle-\alpha| \, . \tag{F.18}$$

On peut comprendre la différence entre les deux résultats en utilisant des trajectoires quantiques individuelles. Pour un protocole de contage de photons, le système change abruptement entre ces deux états chats, tandis que, pour un protocole de détection homodyne, la fonction d'onde de la cavité alterne entre deux états cohérents (Figs. 7.3 et 7.4). En raison de ces résultats, nous proposons et étudions un protocole de rétroaction pour la génération d'états chat purs. En fait, si on peut déséquilibre le taux de dissipation entre états pair et états impairs, on favorise un des deux chats. On peut obtenir ce résultat par l'ajout d'un dissipateur :

$$\mathcal{D}[\hat{a}_f]\hat{\rho} = \frac{\gamma_f}{2} \left(2\hat{a}_f \hat{\rho} \hat{a}_f^\dagger - \hat{a}_f^\dagger \hat{a}_f \hat{\rho} - \hat{\rho} \hat{a}_f^\dagger \hat{a}_f \right) . \tag{F.19}$$

où $\hat{a}_f = \hat{a} \, \frac{1}{2}(1 - e^{\mathrm{i}\pi \hat{a}^\dagger \hat{a}})$. Ces effets sont prouvés en Fig. 7.5.

Bibliography

[1] F. Minganti, A. Biella, N. Bartolo, and C. Ciuti, *Spectral theory of Liouvillians for dissipative phase transitions*, Phys. Rev. A **98**, 042118 (2018).

[2] R. Rota, F. Minganti, A. Biella, and C. Ciuti, *Dynamical properties of dissipative XYZ Heisenberg lattices*, New Journal of Physics **20**, 045003 (2018).

[3] F. Vicentini, F. Minganti, R. Rota, G. Orso, and C. Ciuti, *Critical slowing down in driven-dissipative Bose-Hubbard lattices*, Phys. Rev. A **97**, 013853 (2018).

[4] N. Bartolo, F. Minganti, J. Lolli, and C. Ciuti, *Homodyne versus photon-counting quantum trajectories for dissipative Kerr resonators with two-photon driving*, The European Physical Journal Special Topics **226**, 2705 (2017).

[5] N. Bartolo, F. Minganti, W. Casteels, and C. Ciuti, *Exact steady state of a Kerr resonator with one- and two-photon driving and dissipation: Controllable Wigner-function multimodality and dissipative phase transitions*, Phys. Rev. A **94**, 033841 (2016).

[6] F. Minganti, N. Bartolo, J. Lolli, W. Casteels, and C. Ciuti, *Exact results for Schrödinger cats in driven-dissipative systems and their feedback control*, Scientific Reports **6**, 26987 EP (2016).

[7] M. Planck, *Zur Theorie des Gesetzes der Energieverteilung im Normalspektrum*, Verhandlungen der Deutschen Physikalischen Gesellschaft **2**, 237 (1900).

[8] E. Einstein, *Über einen die Erzeugung und Verwandlung des Lichtes betreffenden heuristischen Gesichtspunkt*, j-ANN-PHYS-1900-4 **322**, 132 (1905).

[9] C. Cohen-Tannoudji, B. Diu, and F. Laloe, *Quantum Mechanics Volume 1* (Wiley, New York, 1991).

[10] L. Landau and E. Lifshitz, *Quantum Mechanics: Non-Relativistic Theory*, Course of Theoretical Physics, Vol. 3 (Elsevier Science, 1981).

[11] L. Pítajevskíj and S. Stringari, *Bose-Einstein Condensation*, International Series of Monographs on Physics (Oxford University Press, 2003).

[12] L. D. Landau and E. M. Lifshitz, *Statistical Physics*, Course of Theoretical Physics, Vol. 5 (Elsevier Science, 2013).

[13] C. J. Pethick and H. Smith, *Bose–Einstein Condensation in Dilute Gases*, 2nd ed. (Cambridge University Press, 2008).

[14] F. Dalfovo, S. Giorgini, L. P. Pitaevskii, and S. Stringari, *Theory of Bose-Einstein condensation in trapped gases*, Rev. Mod. Phys. **71**, 463 (1999).

[15] I. Bloch, J. Dalibard, and W. Zwerger, *Many-body physics with ultracold gases*, Rev. Mod. Phys. **80**, 885 (2008).

[16] N. Ashcroft and N. Mermin, *Solid State Physics* (Holt, Rinehart and Winston, 1976).

[17] C. Kittel, *Introduction to Solid State Physics* (Wiley, 2004).

[18] R. P. Feynman, *Superfluidity and Superconductivity*, Rev. Mod. Phys. **29**, 205 (1957).

[19] M. Tinkham, *Introduction to Superconductivity* (Dover Publications, 2004).

[20] A. J. Leggett, *Superfluidity*, Rev. Mod. Phys. **71**, S318 (1999).

[21] P. Rossi, *The Birth of Modern Science* (Wiley, 2001).

[22] Á. Rivas and S. F. Huelga, *Open Quantum Systems: An Introduction* (Springer Berlin Heidelberg, 2011).

[23] H. Breuer and F. Petruccione, *The Theory of Open Quantum Systems* (OUP Oxford, 2007).

[24] C. Gardiner and P. Zoller, *Quantum Noise: A Handbook of Markovian and Non-Markovian Quantum Stochastic Methods with Applications to Quantum Optics* (Springer, 2004).

[25] S. Haroche and J. M. Raimond, *Exploring the Quantum: Atoms, Cavities, and Photons* (Oxford University Press, 2006).

[26] H. J. Carmichael, *Statistical Methods in Quantum Optics 1: Master Equations and Fokker-Planck Equations* (Springer-Verlag).

[27] I. Carusotto and C. Ciuti, *Quantum fluids of light*, **85**, 299.

[28] R. J. Schoelkopf and S. M. Girvin, *Wiring up quantum systems*, Nature **451**, 664 EP (2008).

[29] J. Q. You and F. Nori, *Atomic physics and quantum optics using superconducting circuits*, Nature **474**, 589 (2011).

[30] B. Deveaud, *The Physics of Semiconductor Microcavities: From Fundamentals to Nanoscale Devices* (Wiley, 2007).

[31] M. Aspelmeyer, T. J. Kippenberg, and F. Marquardt, *Cavity optomechanics*, Rev. Mod. Phys. **86**, 1391 (2014).

[32] J. J. Hopfield, *Theory of the Contribution of Excitons to the Complex Dielectric Constant of Crystals*, Phys. Rev. **112**, 1555 (1958).

[33] C. Ciuti, P. Schwendimann, and A. Quattropani, *Theory of polariton parametric interactions in semiconductor microcavities*, Semiconductor Science and Technology **18**, S279 (2003).

[34] A. Polkovnikov, K. Sengupta, A. Silva, and M. Vengalattore, *Colloquium: Nonequilibrium dynamics of closed interacting quantum systems*, Rev. Mod. Phys. **83**, 863 (2011).

[35] J. Eisert, M. Friesdorf, and C. Gogolin, *Quantum many-body systems out of equilibrium*, Nature Physics **11**, 124 EP (2015), review Article.

[36] S. Sachdev, *Quantum Phase Transitions* (Cambridge University Press, 2001).

[37] M. P. A. Fisher, P. B. Weichman, G. Grinstein, and D. S. Fisher, *Boson localization and the superfluid-insulator transition*, Phys. Rev. B **40**, 546 (1989).

[38] M. Greiner, O. Mandel, T. Esslinger, T. W. Hänsch, and I. Bloch, *Quantum phase transition from a superfluid to a Mott insulator in a gas of ultracold atoms*, Nature **415**, 39 (2002).

[39] T. E. Lee, S. Gopalakrishnan, and M. D. Lukin, *Unconventional Magnetism via Optical Pumping of Interacting Spin Systems*, Phys. Rev. Lett. **110**, 257204 (2013).

[40] J. Jin, A. Biella, O. Viyuela, L. Mazza, J. Keeling, R. Fazio, and D. Rossini, *Cluster Mean-Field Approach to the Steady-State Phase Diagram of Dissipative Spin Systems*, Phys. Rev. X **6**, 031011 (2016).

[41] S. Diehl, A. Micheli, A. Kantian, B. Kraus, H. P. Büchler, and P. Zoller, *Quantum states and phases in driven open quantum systems with cold atoms*, Nat. Phys. **4**, 878 (2008).

[42] F. Verstraete, M. M. Wolf, and J. I. Cirac, *Quantum computation and quantum-state engineering driven by dissipation*, Nat. Phys. **5**, 633 (2009).

[43] E. M. Kessler, G. Giedke, A. , S. F. Yelin, M. D. Lukin, and J. I. Cirac, *Dissipative phase transition in a central spin system*, Phys. Rev. A **86**, 012116 (2012).

[44] A. A. Houck, H. E. Tureci, and J. Koch, *On-chip quantum simulation with superconducting circuits*, Nat Phys **8**, 292 (2012).

[45] M. Fitzpatrick, N. M. Sundaresan, A. C. Y. Li, J. Koch, and A. A. Houck, *Observation of a Dissipative Phase Transition in a One-Dimensional Circuit QED Lattice*, Phys. Rev. X **7**, 011016 (2017).

[46] M. Müller, S. Diehl, G. Pupillo, and P. Zoller, *Engineered Open Systems and Quantum Simulations with Atoms and Ions*, Adv. At. Mol. Opt. Phys. **61**, 1 (2012).

[47] H. Bernien, S. Schwartz, A. Keesling, H. Levine, A. Omran, H. Pichler, S. Choi, A. S. Zibrov, M. Endres, M. Greiner, V. Vuletić, and M. D. Lukin, *Probing many-body dynamics on a 51-atom quantum simulator*, Nature **551**, 579 EP (2017).

[48] E. Gil-Santos, M. Labousse, C. Baker, A. Goetschy, W. Hease, C. Gomez, A. Lemaître, G. Leo, C. Ciuti, and I. Favero, *Light-Mediated Cascaded Locking of Multiple Nano-Optomechanical Oscillators*, Phys. Rev. Lett. **118**, 063605 (2017).

[49] J. Kasprzak, M. Richard, S. Kundermann, A. Baas, P. Jeambrun, J. M. J. Keeling, F. M. Marchetti, M. H. Szymanska, R. Andre, J. L. Staehli, V. Savona, P. B. Littlewood, B. Deveaud, and L. S. Dang, *Bose-Einstein condensation of exciton polaritons*, Nature **443**, 409 (2006).

[50] J. M. Fink, A. Dombi, A. Vukics, A. Wallraff, and P. Domokos, *Observation of the Photon-Blockade Breakdown Phase Transition*, Phys. Rev. X **7**, 011012 (2017).

[51] S. R. K. Rodriguez, W. Casteels, F. Storme, N. Carlon Zambon, I. Sagnes, L. Le Gratiet, E. Galopin, A. Lemaître, A. Amo, C. Ciuti, and J. Bloch, *Probing a Dissipative Phase Transition via Dynamical Optical Hysteresis*, Phys. Rev. Lett. **118**, 247402 (2017).

[52] T. Fink, A. Schade, S. Höfling, C. Schneider, and A. Imamoglu, *Signatures of a dissipative phase transition in photon correlation measurements*, Nature Physics **14**, 365 (2018).

[53] H. J. Carmichael, *Breakdown of Photon Blockade: A Dissipative Quantum Phase Transition in Zero Dimensions*, Phys. Rev. X **5**, 031028 (2015).

[54] H. Weimer, *Variational Principle for Steady States of Dissipative Quantum Many-Body Systems*, Phys. Rev. Lett. **114**, 040402 (2015).

[55] M. Benito, C. Sánchez Muñoz, and C. Navarrete-Benlloch, *Degenerate parametric oscillation in quantum membrane optomechanics*, Phys. Rev. A **93**, 023846 (2016).

[56] J. J. Mendoza-Arenas, S. R. Clark, S. Felicetti, G. Romero, E. Solano, D. G. Angelakis, and D. Jaksch, *Beyond mean-field bistability in driven-dissipative lattices: Bunching-antibunching transition and quantum simulation*, Phys. Rev. A **93**, 023821 (2016).

[57] W. Casteels, F. Storme, A. Le Boité, and C. Ciuti, *Power laws in the dynamic hysteresis of quantum nonlinear photonic resonators*, Phys. Rev. A **93**, 033824 (2016).

[58] W. Casteels and C. Ciuti, *Quantum entanglement in the spatial-symmetry-breaking phase transition of a driven-dissipative Bose-Hubbard dimer*, Phys. Rev. A **95**, 013812 (2017).

[59] W. Casteels, R. Fazio, and C. Ciuti, *Critical dynamical properties of a first-order dissipative phase transition*, Phys. Rev. A **95**, 012128 (2017).

[60] M. Foss-Feig, P. Niroula, J. T. Young, M. Hafezi, A. V. Gorshkov, R. M. Wilson, and M. F. Maghrebi, *Emergent equilibrium in many-body optical bistability*, Phys. Rev. A **95**, 043826 (2017).

[61] M. Biondi, G. Blatter, H. E. Türeci, and S. Schmidt, *Nonequilibrium gas-liquid transition in the driven-dissipative photonic lattice*, Phys. Rev. A **96**, 043809 (2017).

[62] A. Biella, F. Storme, J. Lebreuilly, D. Rossini, R. Fazio, I. Carusotto, and C. Ciuti, *Phase diagram of incoherently driven strongly correlated photonic lattices*, Phys. Rev. A **96**, 023839 (2017).

[63] V. Savona, *Spontaneous symmetry breaking in a quadratically driven nonlinear photonic lattice*, Phys. Rev. A **96**, 033826 (2017).

[64] C. Sánchez Muñoz, A. Lara, J. Puebla, and F. Nori, *Hybrid systems for the dissipative preparation of mechanical Schrödinger cats*, (2018), arXiv:1802.01306 .

[65] L. M. Sieberer, S. D. Huber, E. Altman, and S. Diehl, *Dynamical Critical Phenomena in Driven-Dissipative Systems*, Phys. Rev. Lett. **110**, 195301 (2013).

[66] L. M. Sieberer, S. D. Huber, E. Altman, and S. Diehl, *Nonequilibrium functional renormalization for driven-dissipative Bose-Einstein condensation*, Phys. Rev. B **89**, 134310 (2014).

[67] E. Altman, L. M. Sieberer, L. Chen, S. Diehl, and J. Toner, *Two-Dimensional Superfluidity of Exciton Polaritons Requires Strong Anisotropy*, Phys. Rev. X **5**, 011017 (2015).

[68] T. E. Lee, H. Häffner, and M. C. Cross, *Antiferromagnetic phase transition in a nonequilibrium lattice of Rydberg atoms*, Phys. Rev. A **84**, 031402 (2011).

[69] C. Chan, T. E. Lee, and S. Gopalakrishnan, *Limit-cycle phase in driven-dissipative spin systems*, Phys. Rev. A **91**, 051601 (2015).

[70] M. F. Maghrebi and A. V. Gorshkov, *Nonequilibrium many-body steady states via Keldysh formalism*, Phys. Rev. B **93**, 014307 (2016).

[71] R. Rota, F. Storme, N. Bartolo, R. Fazio, and C. Ciuti, *Critical behavior of dissipative two-dimensional spin lattices*, Phys. Rev. B **95**, 134431 (2017).

[72] V. R. Overbeck, M. F. Maghrebi, A. V. Gorshkov, and H. Weimer, *Multicritical behavior in dissipative Ising models*, Phys. Rev. A **95**, 042133 (2017).

[73] D. Roscher, S. Diehl, and M. Buchhold, *Phenomenology of a First Order Dark State Phase Transition*, (2018), arXiv:1803.08514 .

[74] E. G. Dalla Torre, E. Demler, T. Giamarchi, and E. Altman, *Dynamics and universality in noise-driven dissipative systems*, Phys. Rev. B **85**, 184302 (2012).

[75] J. Marino and S. Diehl, *Driven Markovian Quantum Criticality*, Phys. Rev. Lett. **116**, 070407 (2016).

[76] W. H. Zurek, *Decoherence, einselection, and the quantum origins of the classical*, Rev. Mod. Phys. **75**, 715 (2003).

[77] J. F. Poyatos, J. I. Cirac, and P. Zoller, *Quantum Reservoir Engineering with Laser Cooled Trapped Ions*, Phys. Rev. Lett. **77**, 4728 (1996).

[78] H. Tan, G. Li, and P. Meystre, *Dissipation-driven two-mode mechanical squeezed states in optomechanical systems*, Phys. Rev. A **87**, 033829 (2013).

[79] C. Arenz, C. Cormick, D. Vitali, and G. Morigi, *Generation of two-mode entangled states by quantum reservoir engineering*, Journal of Physics B: Atomic, Molecular and Optical Physics **46**, 224001 (2013).

[80] M. Asjad and D. Vitali, *Reservoir engineering of a mechanical resonator: generating a macroscopic superposition state and monitoring its decoherence*, Journal of Physics B: Atomic, Molecular and Optical Physics **47**, 045502 (2014).

[81] A. Roy, Z. Leghtas, A. D. Stone, M. Devoret, and M. Mirrahimi, *Continuous generation and stabilization of mesoscopic field superposition states in a quantum circuit*, Phys. Rev. A **91**, 013810 (2015).

[82] Z. Leghtas, S. Touzard, I. M. Pop, A. Kou, B. Vlastakis, A. Petrenko, K. M. Sliwa, A. Narla, S. Shankar, M. J. Hatridge, M. Reagor, L. Frunzio, R. J. Schoelkopf, M. Mirrahimi, and M. H. Devoret, *Confining the state of light to a quantum manifold by engineered two-photon loss*, Science **347**, 853 (2015).

[83] J. Kerckhoff, M. A. Armen, and H. Mabuchi, *Remnants of semiclassical bistability in the few-photon regime of cavity QED*, Opt. Express **19**, 24468 (2011).

[84] A. Gilchrist, K. Nemoto, W. J. Munro, T. C. Ralph, S. Glancy, S. L. Braunstein, and G. J. Milburn, *Schrödinger cats and their power for quantum information processing*, Journal of Optics B: Quantum and Semiclassical Optics **6**, S828 (2004).

[85] A. Ourjoumtsev, R. Tualle-Brouri, J. Laurat, and P. Grangier, *Generating Optical Schrödinger Kittens for Quantum Information Processing*, Science **312**, 83 (2006).

[86] M. Mirrahimi, M. Leghtas, V. Albert, S. Touzard, R. Schoelkopf, L. Jiang, and M. Devoret, *Dynamically protected cat-qubits: a new paradigm for universal quantum computation*, New Journal of Physics **16**, 045014 (2014).

[87] H. Goto, *Universal quantum computation with a nonlinear oscillator network*, Phys. Rev. A **93**, 050301 (2016).

[88] S. Puri, S. Boutin, and A. Blais, *Engineering the quantum states of light in a Kerr-nonlinear resonator by two-photon driving*, npj Quantum Information **3**, 18 (2017).

[89] L. Landau and E. Lifshitz, *Mechanics*, Course of Theoretical Physics, Vol. 1 (Elsevier Science, 1982).

[90] H. Goldstein, C. Poole, and J. Safko, *Classical Mechanics* (Addison Wesley, 2002).

[91] M. Maggiore, *A Modern Introduction to Quantum Field Theory* (Oxford University Press, 2005).

[92] M. Hillery, *An introduction to the quantum theory of nonlinear optics*, Acta Physica Slovaca. Reviews and Tutorials **59**, 1 (2010).

[93] R. W. Boyd and D. Prato, *Nonlinear Optics*, 3rd ed. (Academic Press).

[94] V. G. Sala, D. D. Solnyshkov, I. Carusotto, T. Jacqmin, A. Lemaître, H. Terças, A. Nalitov, M. Abbarchi, E. Galopin, I. Sagnes, J. Bloch, G. Malpuech, and A. Amo, *Spin-Orbit Coupling for Photons and Polaritons in Microstructures*, Phys. Rev. X **5**, 011034 (2015).

[95] A. Verger, C. Ciuti, and I. Carusotto, *Polariton quantum blockade in a photonic dot*, Phys. Rev. B **73**, 193306 (2006).

[96] A. Le Boité, *Strongly correlated photons in arrays of nonlinear cavities*, Theses, Université Paris Diderot - Paris 7 (2015).

[97] F. Baboux, L. Ge, T. Jacqmin, M. Biondi, E. Galopin, A. Lemaître, L. Le Gratiet, I. Sagnes, S. Schmidt, H. E. Türeci, A. Amo, and J. Bloch, *Bosonic Condensation and Disorder-Induced Localization in a Flat Band*, Phys. Rev. Lett. **116**, 066402 (2016).

[98] F. Baboux, E. Levy, A. Lemaître, C. Gómez, E. Galopin, L. Le Gratiet, I. Sagnes, A. Amo, J. Bloch, and E. Akkermans, *Measuring topological invariants from generalized edge states in polaritonic quasicrystals*, Phys. Rev. B **95**, 161114 (2017).

[99] M. Milićević, T. Ozawa, G. Montambaux, I. Carusotto, E. Galopin, A. Lemaître, L. Le Gratiet, I. Sagnes, J. Bloch, and A. Amo, *Orbital Edge States in a Photonic Honeycomb Lattice*, Phys. Rev. Lett. **118**, 107403 (2017).

[100] U. Vool and M. Devoret, *Introduction to quantum electromagnetic circuits*, International Journal of Circuit Theory and Applications **45**, 897.

[101] B. D. Josephson, *The discovery of tunnelling supercurrents*, Rev. Mod. Phys. **46**, 251 (1974).

[102] F. R. Ong, M. Boissonneault, F. Mallet, A. Palacios-Laloy, A. Dewes, A. C. Doherty, A. Blais, P. Bertet, D. Vion, and D. Esteve, *Circuit QED with a Nonlinear Resonator: ac-Stark Shift and Dephasing*, Phys. Rev. Lett. **106**, 167002 (2011).

[103] S. Schmidt and J. Koch, *Circuit QED lattices: Towards quantum simulation with superconducting circuits*, Annalen der Physik **525**, 395 (2013).

[104] Y. Makhlin, G. Schön, and A. Shnirman, *Quantum-state engineering with Josephson-junction devices*, Rev. Mod. Phys. **73**, 357 (2001).

[105] J. Koch, T. M. Yu, J. Gambetta, A. A. Houck, D. I. Schuster, J. Majer, A. Blais, M. H. Devoret, S. M. Girvin, and R. J. Schoelkopf, *Charge-insensitive qubit design derived from the Cooper pair box*, Phys. Rev. A **76**, 042319 (2007).

[106] J. A. Schreier, A. A. Houck, J. Koch, D. I. Schuster, B. R. Johnson, J. M. Chow, J. M. Gambetta, J. Majer, L. Frunzio, M. H. Devoret, S. M. Girvin, and R. J. Schoelkopf, *Suppressing charge noise decoherence in superconducting charge qubits*, Phys. Rev. B **77**, 180502 (2008).

[107] E. T. Jaynes and F. W. Cummings, *Comparison of quantum and semiclassical radiation theories with application to the beam maser*, Proceedings of the IEEE **51**, 89 (1963).

[108] V. Gorini, A. Kossakowski, and E. C. G. Sudarshan, *Completely positive dynamical semigroups of N-level systems*, Journal of Mathematical Physics **17**, 821 (1976).

[109] G. Lindblad, *On the generators of quantum dynamical semigroups*, Communications in Mathematical Physics **48**, 119 (1976).

[110] H. Carmichael, *Statistical Methods in Quantum Optics 2: Non-Classical Fields* (Springer Berlin Heidelberg, 2007).

[111] H. Wiseman and G. Milburn, *Quantum Measurement and Control* (Cambridge University Press, 2010).

[112] M. G. A. Paris, *The modern tools of quantum mechanics*, The European Physical Journal Special Topics **203**, 61 (2012).

[113] S. Barnett, *Quantum Information* (OUP Oxford, 2009).

[114] D. F. Walls and G. J. Milburn, *Quantum Optics* (Springer Science & Business Media).

[115] K. Mølmer, Y. Castin, and J. Dalibard, *Monte Carlo wave-function method in quantum optics*, J. Opt. Soc. Am. B **10**, 524 (1993).

[116] A. J. Daley, *Quantum trajectories and open many-body quantum systems*, Advances in Physics **63**, 77 (2014).

[117] C. Gardiner, *Stochastic Methods: A Handbook for the Natural and Social Sciences*, 4th ed. (Springer-Verlag).

[118] G. S. Agarwal and E. Wolf, *Calculus for Functions of Noncommuting Operators and General Phase-Space Methods in Quantum Mechanics. I. Mapping Theorems and Ordering of Functions of Noncommuting Operators*, Phys. Rev. D **2**, 2161 (1970).

[119] G. S. Agarwal and E. Wolf, *Calculus for Functions of Noncommuting Operators and General Phase-Space Methods in Quantum Mechanics. II. Quantum Mechanics in Phase Space*, Phys. Rev. D **2**, 2187 (1970).

[120] K. Vogel and H. Risken, *Quasiprobability distributions in dispersive optical bistability*, **39**, 4675.

[121] A. Serafini, *Quantum Continuous Variables: A Primer of Theoretical Methods* (Taylor & Francis Group, 2017).

[122] W. Greiner, D. Rischke, L. Neise, and H. Stöcker, *Thermodynamics and Statistical Mechanics*, Classical Theoretical Physics (Springer New York, 2012).

[123] T. Kato, *Perturbation theory for linear operators*, Classics in Mathematics (Springer, 1995).

[124] K. Macieszczak, M. Gută, I. Lesanovsky, and J. P. Garrahan, *Towards a Theory of Metastability in Open Quantum Dynamics*, Phys. Rev. Lett. **116**, 240404 (2016).

[125] B. Horstmann, J. I. Cirac, and G. Giedke, *Noise-driven dynamics and phase transitions in fermionic systems*, Phys. Rev. A **87**, 012108 (2013).

[126] B. Baumgartner and H. N., *Analysis of quantum semigroups with GKS-Lindblad generators: II. General*, Journal of Physics A: Mathematical and Theoretical **41**, 395303 (2008).

[127] A. Nagy and V. Savona, *Driven-dissipative quantum Monte Carlo method for open quantum systems*, Phys. Rev. A **97**, 052129 (2018).

[128] A. Biella, J. Jin, O. Viyuela, C. Ciuti, R. Fazio, and D. Rossini, *Linked cluster expansions for open quantum systems on a lattice*, Phys. Rev. B **97**, 035103 (2018).

[129] M. Biondi, S. Lienhard, G. Blatter, H. E. Türeci, and S. Schmidt, *Spatial correlations in driven-dissipative photonic lattices*, New Journal of Physics **19**, 125016 (2017).

[130] S. Finazzi, A. Le Boité, F. Storme, A. Baksic, and C. Ciuti, *Corner-Space Renormalization Method for Driven-Dissipative Two-Dimensional Correlated Systems*, Phys. Rev. Lett. **115**, 080604 (2015).

[131] A. Kshetrimayum, H. Weimer, and R. Orús, *A simple tensor network algorithm for two-dimensional steady states*, Nature Communications **8**, 1291 (2017).

[132] G. Vidal, *Classical Simulation of Infinite-Size Quantum Lattice Systems in One Spatial Dimension*, Phys. Rev. Lett. **98**, 070201 (2007).

[133] M. Zwolak and G. Vidal, *Mixed-State Dynamics in One-Dimensional Quantum Lattice Systems: A Time-Dependent Superoperator Renormalization Algorithm*, Phys. Rev. Lett. **93**, 207205 (2004).

[134] J. Cui, J. I. Cirac, and M. C. Bañuls, *Variational Matrix Product Operators for the Steady State of Dissipative Quantum Systems*, Phys. Rev. Lett. **114**, 220601 (2015).

[135] P. D. Drummond and D. F. Walls, *Quantum theory of optical bistability. I. Nonlinear polarisability model*, **13**, 725.

[136] S. Diehl, A. Tomadin, A. Micheli, R. Fazio, and P. Zoller, *Dynamical Phase Transitions and Instabilities in Open Atomic Many-Body Systems*, Phys. Rev. Lett. **105**, 015702 (2010).

[137] A. Tomadin, S. Diehl, and P. Zoller, *Nonequilibrium phase diagram of a driven and dissipative many-body system*, Phys. Rev. A **83**, 013611 (2011).

[138] A. Le Boité, G. Orso, and C. Ciuti, *Steady-State Phases and Tunneling-Induced Instabilities in the Driven Dissipative Bose-Hubbard Model*, Phys. Rev. Lett. **110**, 233601 (2013).

[139] A. Le Boité, G. Orso, and C. Ciuti, *Bose-Hubbard model: Relation between driven-dissipative steady states and equilibrium quantum phases*, Phys. Rev. A **90**, 063821 (2014).

[140] J. Jin, D. Rossini, R. Fazio, M. Leib, and M. J. Hartmann, *Photon Solid Phases in Driven Arrays of Nonlinearly Coupled Cavities*, Phys. Rev. Lett. **110**, 163605 (2013).

[141] J. Jin, D. Rossini, M. Leib, M. J. Hartmann, and R. Fazio, *Steady-state phase diagram of a driven QED-cavity array with cross-Kerr nonlinearities*, Phys. Rev. A **90**, 023827 (2014).

[142] R. M. Wilson, K. W. Mahmud, A. Hu, A. V. Gorshkov, M. Hafezi, and M. Foss-Feig, *Collective phases of strongly interacting cavity photons*, Phys. Rev. A **94**, 033801 (2016).

[143] P. D. Drummond and C. W. Gardiner, *Generalised P-representations in quantum optics*, **13**, 2353.

[144] W. Bailey, *Generalized Hypergeometric Series*, Cambridge tracts in mathematics and mathematical physics (Hafner, 1972).

[145] M. Abramowitz and I. Stegun, *Handbook of Mathematical Functions: With Formulas, Graphs, and Mathematical Tables* (Dover Publications, 1964).

[146] T. MacRobert, *Functions of a Complex Variable* (MacMillan, 1954).

[147] G. Kryuchkyan and K. Kheruntsyan, *Exact quantum theory of a parametrically driven dissipative anharmonic oscillator*, Optics Communications **127**, 230 (1996).

[148] C. H. Meaney, H. Nha, T. Duty, and G. J. Milburn, *Quantum and classical nonlinear dynamics in a microwave cavity*, EPJ Quantum Technology **1**, 1 (2014).

[149] M. Elliott and E. Ginossar, *Applications of the Fokker-Planck equation in circuit quantum electrodynamics*, Phys. Rev. A **94**, 043840 (2016).

[150] H. M. Gibbs, S. L. McCall, and T. N. C. Venkatesan, *Differential Gain and Bistability Using a Sodium-Filled Fabry-Perot Interferometer*, Phys. Rev. Lett. **36**, 1135 (1976).

[151] A. Dorsel, J. D. McCullen, P. Meystre, E. Vignes, and H. Walther, *Optical Bistability and Mirror Confinement Induced by Radiation Pressure*, Phys. Rev. Lett. **51**, 1550 (1983).

[152] G. Rempe, R. J. Thompson, R. J. Brecha, W. D. Lee, and H. J. Kimble, *Optical bistability and photon statistics in cavity quantum electrodynamics*, Phys. Rev. Lett. **67**, 1727 (1991).

[153] V. R. Almeida and M. Lipson, *Optical bistability on a silicon chip*, Opt. Lett. **29**, 2387 (2004).

[154] A. Baas, J. P. Karr, H. Eleuch, and E. Giacobino, *Optical bistability in semiconductor microcavities*, Phys. Rev. A **69**, 023809 (2004).

[155] T. Boulier, M. Bamba, A. Amo, C. Adrados, A. Lemaitre, E. Galopin, I. Sagnes, J. Bloch, C. Ciuti, E. Giacobino, and A. Bramati, *Polariton-generated intensity squeezing in semiconductor micropillars*, Nature Communications **5**, 3260 EP (2014), article.

[156] I. Carusotto and C. Ciuti, *Spontaneous microcavity-polariton coherence across the parametric threshold: Quantum Monte Carlo studies*, Phys. Rev. B **72**, 125335 (2005).

[157] P. D. Drummond and M. Hillery, *The Quantum Theory of Nonlinear Optics* (Cambridge University Press).

[158] R. Labouvie, B. Santra, S. Heun, and H. Ott, *Bistability in a Driven-Dissipative Superfluid*, Phys. Rev. Lett. **116**, 235302 (2016).

[159] S. Mukherjee, A. Spracklen, D. Choudhury, N. Goldman, P. Öhberg, E. Andersson, and R. R. Thomson, *Observation of a Localized Flat-Band State in a Photonic Lieb Lattice*, Phys. Rev. Lett. **114**, 245504 (2015).

[160] W. Casteels, R. Rota, F. Storme, and C. Ciuti, *Probing photon correlations in the dark sites of geometrically frustrated cavity lattices*, Phys. Rev. A **93**, 043833 (2016).

[161] M. Biondi, E. P. L. van Nieuwenburg, G. Blatter, S. D. Huber, and S. Schmidt, *Incompressible Polaritons in a Flat Band*, Phys. Rev. Lett. **115**, 143601 (2015).

[162] A. Amo and J. Bloch, *Exciton-polaritons in lattices: A non-linear photonic simulator*, Comptes Rendus Physique **17**, 934 (2016), polariton physics / Physique des polaritons.

[163] D. Tanese, E. Gurevich, F. Baboux, T. Jacqmin, A. Lemaître, E. Galopin, I. Sagnes, A. Amo, J. Bloch, and E. Akkermans, *Fractal Energy Spectrum of a Polariton Gas in a Fibonacci Quasiperiodic Potential*, Phys. Rev. Lett. **112**, 146404 (2014).

[164] H. J. Carmichael, *Photon Antibunching and Squeezing for a Single Atom in a Resonant Cavity*, Phys. Rev. Lett. **55**, 2790 (1985).

[165] A. Imamoglu, H. Schmidt, G. Woods, and M. Deutsch, *Strongly Interacting Photons in a Nonlinear Cavity*, Phys. Rev. Lett. **79**, 1467 (1997).

[166] K. M. Birnbaum, A. Boca, R. Miller, A. D. Boozer, T. E. Northup, and H. J. Kimble, *Photon blockade in an optical cavity with one trapped atom*, Nature **436**, 87 (2005).

[167] C. Lang, D. Bozyigit, C. Eichler, L. Steffen, J. M. Fink, A. A. Abdumalikov, M. Baur, S. Filipp, M. P. da Silva, A. Blais, and A. Wallraff, *Observation of Resonant Photon Blockade at Microwave Frequencies Using Correlation Function Measurements*, Phys. Rev. Lett. **106**, 243601 (2011).

[168] A. D. Greentree, C. Tahan, J. H. Cole, and L. C. L. Hollenberg, *Quantum phase transitions of light*, Nature Physics **2**, 856 (2006).

[169] M. J. Hartmann, F. G. S. L. Brandão, and M. B. Plenio, *Strongly interacting polaritons in coupled arrays of cavities*, Nature Physics **2**, 849 (2006).

[170] D. G. Angelakis, M. F. Santos, and S. Bose, *Photon-blockade-induced Mott transitions and XY spin models in coupled cavity arrays*, Phys. Rev. A **76**, 031805 (2007).

[171] M. J. Hartmann, F. G. S. L. Brandão, and M. B. Plenio, *Quantum many-body phenomena in coupled cavity arrays*, Laser and Photonics Reviews **2**, 527 (2008).

[172] J. Lebreuilly, A. Biella, F. Storme, D. Rossini, R. Fazio, C. Ciuti, and I. Carusotto, *Stabilizing strongly correlated photon fluids with non-Markovian reservoirs*, Phys. Rev. A **96**, 033828 (2017).

[173] M. J. Hartmann, F. G. S. L. Brandão, and M. B. Plenio, *Effective Spin Systems in Coupled Microcavities*, Phys. Rev. Lett. **99**, 160501 (2007).

[174] A. Kay and D. G. Angelakis, *Reproducing spin lattice models in strongly coupled atom-cavity systems*, EPL (Europhysics Letters) **84**, 20001 (2008).

[175] J. Qian, G. Dong, L. Zhou, and W. Zhang, *Phase diagram of Rydberg atoms in a nonequilibrium optical lattice*, Phys. Rev. A **85**, 065401 (2012).

[176] M. Viteau, P. Huillery, M. G. Bason, N. Malossi, D. Ciampini, O. Morsch, E. Arimondo, D. Comparat, and P. Pillet, *Cooperative Excitation and Many-Body Interactions in a Cold Rydberg Gas*, Phys. Rev. Lett. **109**, 053002 (2012).

[177] J. Qian, L. Zhang, J. Zhai, and W. Zhang, *Dynamical phases in a one-dimensional chain of heterospecies Rydberg atoms with next-nearest-neighbor interactions*, Phys. Rev. A **92**, 063407 (2015).

[178] W. Casteels, R. M. Wilson, and M. Wouters, *Gutzwiller Monte Carlo approach for a critical dissipative spin model*, Phys. Rev. A **97**, 062107 (2018).

[179] R. Orús and G. Vidal, *Infinite time-evolving block decimation algorithm beyond unitary evolution*, Phys. Rev. B **78**, 155117 (2008).

[180] R. Orús, *A practical introduction to tensor networks: Matrix product states and projected entangled pair states*, Annals of Physics **349**, 117 (2014).

[181] F. Verstraete, J. J. García-Ripoll, and J. I. Cirac, *Matrix Product Density Operators: Simulation of Finite-Temperature and Dissipative Systems*, Phys. Rev. Lett. **93**, 207204 (2004).

[182] C. Joshi, F. Nissen, and J. Keeling, *Quantum correlations in the one-dimensional driven dissipative XY model*, Phys. Rev. A **88**, 063835 (2013).

[183] L. Bonnes, D. Charrier, and A. M. Läuchli, *Dynamical and steady-state properties of a Bose-Hubbard chain with bond dissipation: A study based on matrix product operators*, Phys. Rev. A **90**, 033612 (2014).

[184] A. Biella, L. Mazza, I. Carusotto, D. Rossini, and R. Fazio, *Photon transport in a dissipative chain of nonlinear cavities*, Phys. Rev. A **91**, 053815 (2015).

[185] G. Vidal, *Efficient Classical Simulation of Slightly Entangled Quantum Computations*, Phys. Rev. Lett. **91**, 147902 (2003).

[186] G. Vidal, *Efficient Simulation of One-Dimensional Quantum Many-Body Systems*, Phys. Rev. Lett. **93**, 040502 (2004).

[187] B. S. Chissom, *Interpretation of the Kurtosis Statistic*, The American Statistician **24**, 19 (1970).

[188] C. C. Gerry, *Non-classical Properties of Even and Odd Coherent States*, Journal of Modern Optics **40**, 1053 (1993).

[189] L. Gilles, B. M. Garraway, and P. L. Knight, *Generation of nonclassical light by dissipative two-photon processes*, Phys. Rev. A **49**, 2785 (1994).

[190] E. Schrödinger, *Die gegenwärtige Situation in der Quantenmechanik*, Naturwissenschaften **23**, 807 (1935).

[191] M. Wolinsky and H. J. Carmichael, *Quantum noise in the parametric oscillator: From squeezed states to coherent-state superpositions*, Phys. Rev. Lett. **60**, 1836 (1988).

[192] M. Everitt, T. Spiller, G. G. Milburn, R. D. Wilson, and A. M. Zagoskin, *Engineering Dissipative Channels for Realising Schrödinger Cats in SQUIDs*, Frontiers in ICT **1** (2014), 10.3389/fict.2014.00001.

[193] L. Krippner, W. J. Munro, and M. D. Reid, *Transient macroscopic quantum superposition states in degenerate parametric oscillation: Calculations in the large-quantum-noise limit using the positive P representation*, Phys. Rev. A **50**, 4330 (1994).

[194] L. Sun, A. Petrenko, Z. Leghtas, B. Vlastakis, G. Kirchmair, K. M. Sliwa, A. Narla, M. Hatridge, S. Shankar, J. Blumoff, L. Frunzio, M. Mirrahimi, M. H. Devoret, and R. J. Schoelkopf, *Tracking photon jumps with repeated quantum non-demolition parity measurements*, Nature **511**, 444 (2014).

[195] D. Vitali, S. Zippilli, P. Tombesi, and J.-M. Raimond, *Decoherence control with fully quantum feedback schemes*, Journal of Modern Optics **51**, 799 (2004).

[196] S. Zippilli, D. Vitali, P. Tombesi, and J. M. Raimond, *Scheme for decoherence control in microwave cavities*, Phys. Rev. A **67**, 052101 (2003).

[197] C. Sayrin, I. Dotsenko, X. Zhou, B. Peaudecerf, T. Rybarczyk, S. Gleyzes, P. Rouchon, M. Mirrahimi, H. Amini, M. Brune, J.-M. Raimond, and S. Haroche, *Real-time quantum feedback prepares and stabilizes photon number states*, Nature **477**, 73 (2011).

[198] X. Zhou, I. Dotsenko, B. Peaudecerf, T. Rybarczyk, C. Sayrin, S. Gleyzes, J.-M. Raimond, M. Brune, and S. Haroche, *Field Locked to a Fock State by Quantum Feedback with Single Photon Corrections*, Phys. Rev. Lett. **108**, 243602 (2012).

[199] P. Campagne-Ibarcq, E. Flurin, N. Roch, D. Darson, P. Morfin, M. Mirrahimi, M. H. Devoret, F. Mallet, and B. Huard, *Persistent Control of a Superconducting Qubit by Stroboscopic Measurement Feedback*, Phys. Rev. X **3**, 021008 (2013).

[200] P. Goetsch, P. Tombesi, and D. Vitali, *Effect of feedback on the decoherence of a Schrödinger-cat state: A quantum trajectory description*, Phys. Rev. A **54**, 4519 (1996).

[201] M. Brune, S. Haroche, J. M. Raimond, L. Davidovich, and N. Zagury, *Manipulation of photons in a cavity by dispersive atom-field coupling: Quantum-nondemolition measurements and generation of "Schrödinger cat" states*, Phys. Rev. A **45**, 5193 (1992).

[202] T. C. Ralph, A. Gilchrist, G. J. Milburn, W. J. Munro, and S. Glancy, *Quantum computation with optical coherent states*, Phys. Rev. A **68**, 042319 (2003).

[203] M. S. Sarandy and D. A. Lidar, *Adiabatic approximation in open quantum systems*, Phys. Rev. A **71**, 012331 (2005).

Title: Out-of-Equilibrium Phase Transitions in Nonlinear Optical Systems

Abstract: In this thesis we theoretically study driven-dissipative nonlinear systems, whose dynamics is capture by a Lindblad master equation. In particular, we investigate the emergence of criticality in out-of-equilibrium dissipative systems. We present a general and model-independent spectral theory relating first- and second-order dissipative phase transitions to the spectral properties of the Liouvillian superoperator. In the critical region, we determine the general form of the steady-state density matrix and of the Liouvillian eigenmatrix whose eigenvalue defines the Liouvillian spectral gap. We discuss the relevance of individual quantum trajectories to unveil phase transitions. After these general results, we analyse the inset of criticality in several models. First, a nonlinear Kerr resonator in the presence of both coherent (one-photon) and parametric (two-photon) driving and dissipation. We then explore the dynamical properties of the coherently-driven Bose-Hubbard and of the dissipative XYZ Heisenberg model presenting a first-order and a second-order dissipative phase transition, respectively. Finally, we investigate the physics of photonic Schrödinger cat states in driven-dissipative resonators subject to engineered two-photon processes and one-photon losses. We propose and study a feedback protocol to generate a pure cat-like steady state.

Keywords: Open quantum systems, Phase transitions, Quantum optics, Many-body physics, Optical Cavities, Circuit QED, Semiconductors micropillars, Reservoir engineering, Schrödinger cats.

Titre : Transitions de Phase Hors Équilibre dans les Systèmes Optiques Non Linéaires

Résumé : Dans cette thèse nous étudions théoriquement de systèmes dissipatifs pompés, décrits par une équation maîtresse de Lindblad. En particulier, nous addressons les problematiques liés à l'émergence de phénomènes critiques. Nous présentons une théorie générale reliant les transitions de phase du premier et deuxième ordres aux propriétés spectrales du superopérateur liouvillien. Dans la région critique, nous déterminons la forme générale de l'état stationnaire et de la matrice propre du liouvillien associée à son gap spectral. Nous discutons aussi l'utilisation de trajectoires quantiques individuelles afin de révéler l'apparition des transitions de phase. En ayant dérivé une thèorie génerale, nous étudions le modèle de Kerr en présence de pompage à un photon (cohérent) et à deux photons (paramétrique) ainsi que de dissipation. Nous explorons les propriétés dynamiques d'une transition de phase du premier ordre dans un modèle de Bose-Hubbard dissipatif et d'une de second ordre dans un modèle XYZ dissipatif d'Heisenberg. Enfin, nous avons considéré la physique des cavités soumises à de la dissipation à un et deux photons ainsi qu'un pompage à deux photons, obtenu par ingénierie de réservoirs. Nous avons démontré que l'état stationnaire unique est un mélange statistique de deux états chats de Schrödinger, malgré de fortes pertes à un photon. Nous proposons et étudions un protocole de rétroaction pour la génération d'états chat purs.

Mots clefs : Systèmes quantiques ouvertes, Transitions de phases, Optique quantique, Physique à N corps, Cavités optiques, Circuits supraconducteurs, Micropiliers semi-conducteurs, Ingénierie du réservoir, Chats de Schrödinger.